PHD

Chemical reaction fouling.

Hout, S. A.

Award date:
1983

Awarding institution:
University of Bath

CHEMICAL REACTION FOULING

submitted by S. A. Hout

for the degree of Ph.D.

of the University of Bath

1983

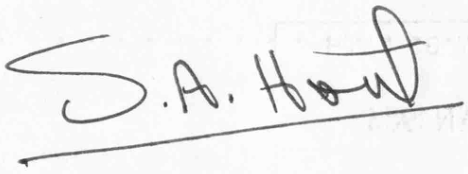

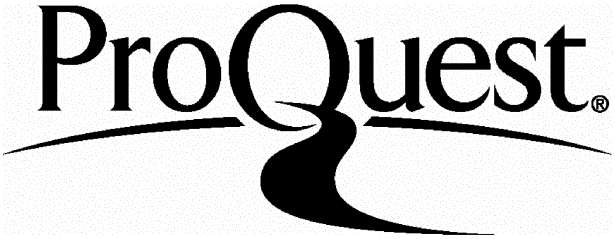

Aknowledgement

My deepest respect and gratefulness is due to my supervisor Dr. B. D. Crittenden for his friendship, care, support and continuous constructive criticism which made this work presentable.

I am indebted to Professor W. J. Thomas for giving the opportunity to conduct this work through the supply of equipment, material and finance.

Also my thanks are due to the British Council for part of the finance to cover the needs of the project. The continuous advice and help that came from different departments at Bath University was indispensable. My thanks are due to the technicians in the school of Chemical Engineering and to Mr. Denis Davis for his continuous help and advice on the programming and presentation of the results. Finally, my thanks are due to my friends and colleagues at Bath for their continuous discussion and communication without which this work would be incomplete.

Summary

The initial rate of chemical reaction fouling of the surface of a furnace tube by polymerisation of styrene in an otherwise non-fouling kerosene feedstock was studied as a function of mass flow rate over the range 336 to 1620 $^{lb}/hr$ and wall temperature between 556 and 909°R. The investigation was carried out by conducting experiments at constant heat flux with continuous circulation of the liquid in a single horizontal tube. The change in fouling resistance with time was measured over the initial twelve hours of operation. In all runs the fouling resistance increased steadily with time. At the highest temperatures, the fouling resistance increased almost linearly with time, and for a given surface temperature the initial fouling rate increased with increasing mass flow rate indicating that mass transfer effects were important. At the lowest temperatures studied, the initial fouling rate decreased with increasing mass flow rate indicating again that mass transfer effects were important. At intermediate temperatures, the initial fouling rate passed through a maximum with respect to mass flow rate showing that mass transfer and kinetic effects could be both effective and competitive simultaneously.

The initial fouling rates were compared with the experimental results of the kinetics of polymerisation of 1% styrene in kerosene in a batch vessel. At low temperatures the initial fouling rate was slightly higher than the initial rate of polymerisation of 1% styrene indicating that the fouling rate may be kinetically controlled. At higher temperatures, the initial

fouling rate became progressively lower than the initial rate of polymerisation of 1% styrene indicating the additional resistance of mass transfer to the fouling process.

A mathematical model based on a chemical reaction and mass transfer mechanism is applied to describe the deposition process and incorporates physical properties of the system, geometry, chemical reaction kinetics and mass transfer. The mathematical expression that describes the initial fouling rate is given by

$$\dot{R}_f\ (0) = \frac{1}{\rho_f\ Tk_f}\ \left(Np - \frac{0.607\lambda\mu^{0.2}G^{0.8}C_{fi}}{\rho\ d^{1.8}Sc_f^{0.67}}\right)$$

(See section 5.4)

The model predicts the mass flow rate and temperature dependence of the initial fouling rate in agreement with the experimental results. It is believed that it can also be applied more generally to other chemical reaction fouling systems.

TABLE OF CONTENTS

1. Introduction

Estimates of the costs to industry of the effects of fouling of heat transfer equipment vary enormously, but are in the order of thousands of millions of pounds[198,203]. (Section 2.1). Fouling in general consists of the build-up of deposits on the surfaces of process plant and is a problem common to many industries[115]. It affects heat exchangers and boilers with particular severity, causing a marked reduction in their heat transfer capabilities because of the insulating nature of the deposits[21,115,145]. It is therefore necessary for the designer to provide additional heat transfer surface area to take account of this expected loss of thermal performance[72,115,119,208].

There have been several recent reviews of fouling in general[208,205,183,72,73]. It has been recognized that a better understanding of fouling would be achieved by paying particular attention to the physics and chemistry of the deposition of foulants, to the way in which they adhere to surfaces and to the means by which deposits may be removed. In turn this understanding would lead to the development of improved methods for the prevention and control of fouling and to the removal of deposits.

Fouling is a transient phenomenon[115,117]. Data scatter and induction periods are common in fouling[208,209]; resistance-time curves may be of linear, falling rate or asymptotic form[72] (Figure 1.1). The ultimate value of R_f sometimes exceeds the TEMA value within relatively short periods of time[21].

where:

R_f fouling resistance

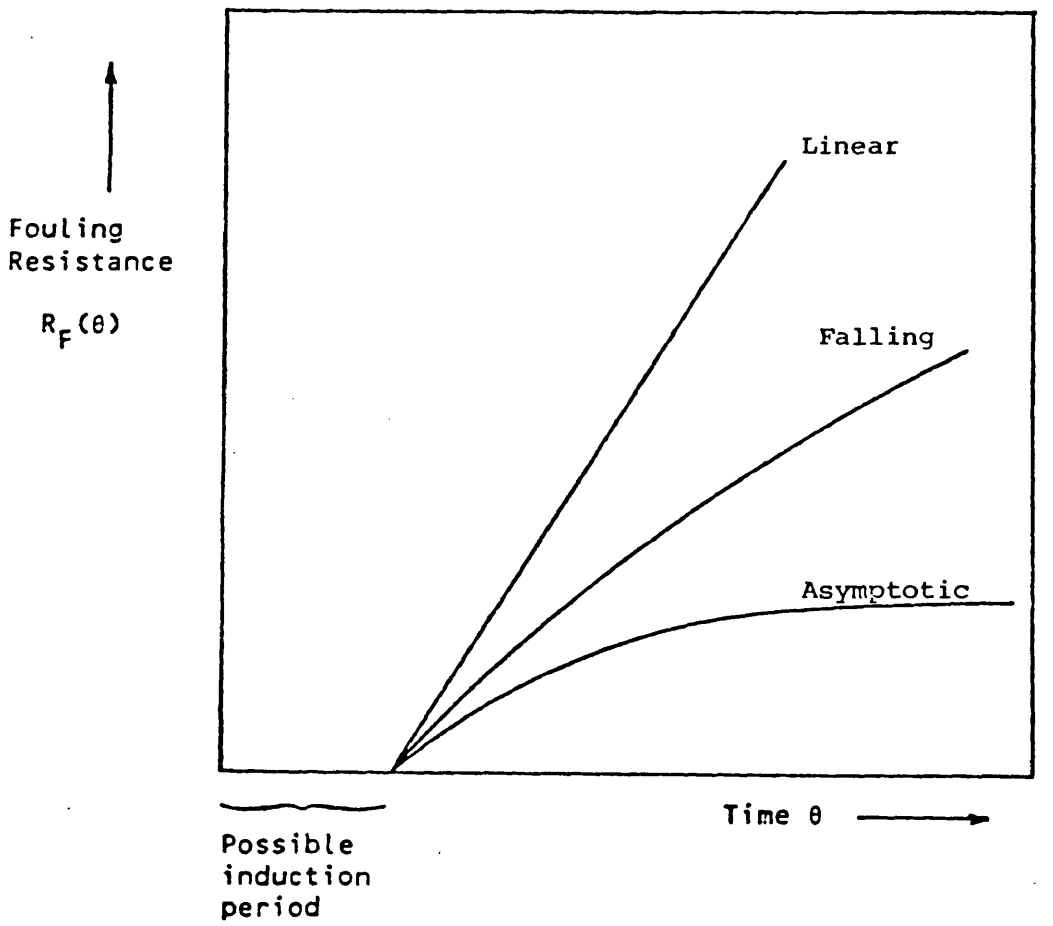

Figure 1.1 General Fouling transients

A fouling rate is a function of process operating conditions, such as time, temperature, heat flux, pressure, feed composition, etc.[59]. Irrespective of this designers continue to use the fouling factor implicitly assuming that a fouling resistance is independent of the process parameters[21]. Some factors do take velocity and temperature into account (Table 1.1); but rarely time[10].

It is emphasized that various types of fouling can occur in heat transfer equipment[21,72] and that more often a combination of two or more of these may occur simultaneously[72,73]. For example, crystallization, particulate and chemical reaction mechanisms are all expected to be important in fouling from hydrocarbon streams. It is possible to classify thermal fouling according to the mechanism which controls the deposition rate. Epstein and other investigators[72,205,208] made their classification according to the immediate cause of fouling; or the dominant fouling mechanism (See Table 1.2).

1.1 Chemical Reaction Fouling

Chemical reaction fouling involves the build up of thermally insulating deposits on a heat transfer surface which is not a reactant in the complex sequence of autoxidation, polymerisation, cracking or coking reactions[59,72]. The surface may catalyze or inhibit the initial stages of the process[72,135]. Process streams prone to fouling occur in the oil refining, petrochemical and food stuff industries and may be in either liquid, vapour or multi-phase forms[59].

The appearance of a hydrocarbon deposit, strongly depend-

Table 1.1 TEMA values of fouling resistance for oil refinery systems[196].

	$(Btu/hr\ ft^2\ {}^{0}F)^{-1}$
Crude and vacuum unit gases and vapours	
Atmospheric tower overhead vapours	·001
Light naphthas	·001
Vacuum overhead vapours	·002
Crude and vacuum liquids	
Gasoline	·001
Naphtha and light distillates	·001
Kerosene	·001
Light gas oil	·002
Heavy gas oil	·003
Heavy fuel oils	·005
Asphalt and residuum	·010
Cracking and coking unit streams	
Overhead vapours	·002
Light cycle oil	·002
Heavy cycle oil	·003
Light coker gas oil	·003
Heavy coker gas oil	·004
Bottoms slurry oil (4½ ft/sec min.)	·003
Light liquid products	·002

(Btu/hr ft^2 °F)$^{-1}$

Catalytic reforming, hydrocracking and hydrodesulphurization streams

Reformer charge	•002
Reformer effluent	•001
Hydrocracker charge and effluent	•002
Recycle gas	•001
Hydrodesulphurization charge and effluent	•002
Overhead vapours	•001
Liquid product over 50° A.P.I.	•001
Liquid product 30° - 50° A.P.I.	•002

Light ends processing streams

Overhead vapours and gases	•001
Liquid products	•001
Absorption oils	•002
Alkylation trace acid streams	•002
Reboiler streams	•003

Lube oil processing streams

Feedstock	•002
Solvent feed mix	•002
Solvent	•001
Extract	•003
Raffinate	•001
Asphalt	•005
Wax slurries	•003
Refined lube oil	•001

ent upon processing conditions, is not necessarily uniform throughout the deposit thickness[10]. A gradation from dense deposit close to the heat transfer surface to a more porous material near the fluid-solid interface is likely[10]. Trapped fluid, which reduces the thermal conductivity of the porous material, may thermally degrade to form further dense coke[10] and create crevices and pores by the release of gaseous products[58,59]. Atkins[10] considered that the resistance of the porous layer could be evaluated from standard sources, e.g. TEMA tables[195] (Table 1.1). The increase in thermal resistance of the denser coke layer could be obtained from Figure 1.2. Inevitably such an analysis predicts a linear dependence of fouling resistance on time.

In addition to carbon and hydrogen, deposits may contain significant amounts of inorganic matter[44,195] which may aid further deposition either by catalysing degradation reactions[194] or by participating in corrosion reactions[72,153]. Inorganic material may be present in the fluid[59] as:

(a) Salts dissolved in the aqueous fraction.

(b) Organic molecules containing hetero-atoms.

(c) Organo-metallic compounds.

(d) Corrosion products detached from upstream processing units.

Table 1.2 Categories of Fouling[72,73]

Type	Definition
Precipitation	The precipitation of dissolved substances on the heat transfer surface. Where the dissolved substances have inverse rather than normal solubility versus temperature characteristics, the precipitation occurs on superheated rather than subcooled surfaces and the process is often referred to as scaling.
Particulate	The accumulation of finely divided solids suspended in the process fluid onto the heat transfer surface. In a minority of instances settling by gravity prevails, and the process may then be referred to as sedimentation fouling.
Chemical reaction	Deposits formed at the heat transfer surface by chemical reactions in which the surface material itself is not a reactant.

Corrosion	The heat transfer surface itself reacts to produce corrosion products which foul the surface and may promote the attachment of other foulants.
Biological	The attachment of macro-organisms (macro-biofouling) and/or micro-organisms (micro-biofouling or microbial fouling) to a heat transfer surface, along with the adherent slimes often generated by the latter.
Freezing	Solidfication of a liquid or some of its higher melting constituents onto a subcooled heat transfer surface.

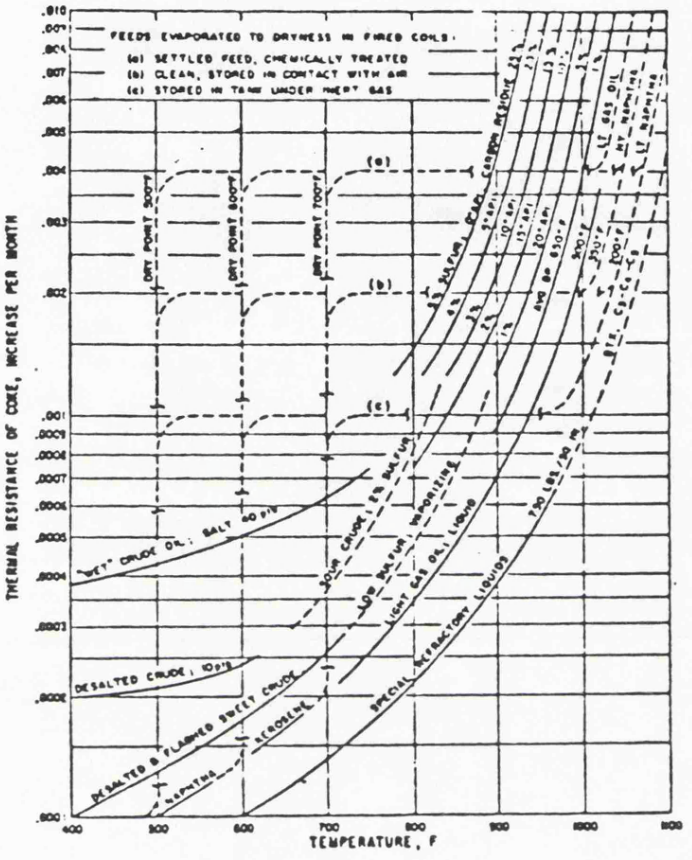

Figure 1.2 Increase per month in thermal resistance (Btu/hr ft^2 ^oF) $^{-1}$ vs temperature of coke at isotherm in porous layer wetted by oil (reproduced from Atkins ref. 10).

1.2 Exchanger Design

The designer generally assigns fixed values of the fouling resistances to an unsteady state problem[21]. The effect of fouling on the design and operation is expressed in the fundamental equation for heat transfer:

$$Q = U_o \, A \, \Delta T_m \tag{1}$$

where:

Q	rate of heat transfer
U_o	overall heat transfer coefficient
A	heat transfer surface area
ΔT_m	log-mean temperature difference

U_o is given by the summation of film and other resistances to heat transfer:

$$\frac{1}{U_o} = \frac{1}{h_o} + \frac{Ao}{Ai}\frac{1}{hi} + R_{f_o} + \frac{Ao}{Ai} R_{f_i} + R_w \tag{2}$$

where:

h	heat transfer coefficient
A	surface area
R_f	fouling resistance
R_w	Wall resistance
i	inside
o	outside

The heat transfer coefficients ho and hi may be determined from well established correlations[66,70,178]. However, the fouling resistances R_{f_o} and R_{f_i} may be experience proven or may be selected from tables of values which neglect the peculiarities of feedstocks and operating environments e.g. TEMA[196].

1.2.1 Fouling Resistances

The fouling resistance at a heat transfer surface depends upon time, and a number of other parameters[20,28,148]:

* The geometry and lay-out of the heat exchanger.
* The material and finish (smooth or rough tube) of the heat transfer surface.
* The wall temperature and the temperature of the interface between the fluid and the surface.
* The velocity of the fluid over the surface.
* The chemical and physical properties of the fouling fluid.

The use of fouling resistances does not by itself solve the fouling problem. The adoption of a large design fouling resistance leads to a much larger and more expensive heat exchanger. This extra heat exchange surface may even cool the fluid more and cause more fouling[53], thereby reducing the heat transfer rate below the figure which would have been achieved with a smaller surface area. Selection of the fouling resistance is often arbitrary and there are very few data available to make an accurate assessment of the likely degree of fouling for a given design with a given fluid. For sensible heat exchange in single phase circulated fluids, a normal provision for 10-30% excess surface corresponds to $1.0 - 1.9 \times 10^{-3}$ h $ft^2{}^\circ F/Btu$[53].

1.3 Purpose of Study

This study is concerned with the chemical reaction fouling from a liquid feedstock flowing inside a heated round tube. The aim of the project is to understand further the manner in which key operating parameters affect fouling rates and fouling

resistances. This is to be done by simulating the dynamic coking phenomenon by the addition of a reactive monomer (styrene) to a non-fouling hydrocarbon feedstock (kerosene). The principal variables to be studied are surface temperature and mass flow rate. The initial rates of deposition are to be compared with those predicted by a general fouling model.

2. Literature Study of Chemical Reaction Fouling

2.1 Economics

It is not possible to provide a formula for calculating the true costs associated with fouling in any specific situation[198]. However, some overview of the economics of fouling with particular reference to chemical reaction fouling may help with regard to plant design, purchase and maintenance. Thackery estimated the cost of all types of fouling in heat exchange plant and with reference to the United Kingdom market[198]. Based largely on statistics, market information and some specific studies relating to the period 1977-79 he reported that the overall cost of fouling in the UK lay in the range £ 360-600 million p.a.(1978 prices) i.e. equivalent to approximately 0.5% of the UK Gross National Product[198]. For subsequent years due allowance should be given for inflation and relative increases in energy costs. This overall cost includes additional capital costs, energy wastage, maintenance costs and loss of production. (Table 2.1).

2.1.1 Capital Cost of Process Side Fouling (Refinery and Chemical Plant)

Oversurfacing of heat exchangers incurs on average an extra delivered capital cost of 20-25%[198]. Extra capital is also required for larger pumps and motors to cope with higher back pressures[198].

2.1.2 Energy Wastage

Loss of thermal efficiency through increased fouling and even heat exchanger failure may incur massive financial penalties. Van Nostrand et al[203] monitored and reviewed refinery process side fouling and extrapolated their data to cover both the U.S. and the known non-Communist world refining capacities. (Table 2.2). Their analysis included fouling in the pre-heat crude distillation,

Table 2.1[198] Overall annual cost of fouling of industrial heat exchanger plant in the UK - (1978 values)

Aspect	Approx annual cost £M
Extra Capital Costs	60- 80
Maintenance, etc	
. direct maintenance	30- 50
. anti-fouling chemicals etc	20- 25
Wasted Energy	150-250
Lost production, opportunity etc	100-200
Total	360-600

Tables 2.2 (203)

Fouling Related Expenses For The United States[1]

	Capacity K Bbl/SD	Fouling Related Expenses (Millions of dollars) Energy	Throughput	Maintenance & Cleaning	Total
Crude Distillation	18,000	183.6	671.4	6.3	861.3
Hydrotreating	7,500	89.2	85.0	4.2	178.4
Visbreaking	220	37.3	9.2	2.6	49.1
Reforming	3,800	162.6	106.4	2.3	271.3
Total		427.7	872.0	15.4	1,360.1

(1) Including Puerto Rico and the Virgin Islands

Fouling Related Expenses For The Non-Communist World

	Capacity K Bbl/SD	Fouling Related Expenses (Millions of dollars) Energy	Throughput	Maintenance & Cleaning	Total
Crude Distillation	62,000	632.4	2312.6	21.7	2966.7
Hydrotreating	21,500	255.6	243.7	11.9	511.2
Visbreaking	1,500	254.3	63.0	18.0	335.3
Reforming	8,400	359.5	235.2	5.0	599.7
Total		1,501.8	2,854.5	56.6	4,412.9

reforming, cracking, hydrotreating , visbreaking and coking units as being the most representative of oil processing equipment which can foul. The energy debits are due to higher consumptions of process fuel. In the crude unit, Figure 2.1, thermal fouling in exchangers upstream of the desalter is generally low[128]. However, fouling and plugging (due to solids and salts deposition) can cause inefficient desalter operation which in turn can lead to fouling of the pre-heat exchanger train immediately downstream of the desalter[128,203]. As the crude oil becomes progressively hotter flowing through the preheat exchanger train, thermal fouling on the crude side of these exchangers becomes increasingly more of a problem. The fouling deposits cause a decrease in exchanger heat transfer efficiency, and therefore a decline in the furnace inlet temperature[203]. For a typical crude unit this decay rate can be 4-10 $^{\circ}$F/month[203], and must be compensated for by increasing the firing rate of the furnace. (Figure 2.1). Further losses of energy are caused by the increased back pressure due to the restricted flow channels.

Many oil refining and petrochemical processes occur at high temperature and much of the heat input must be recovered for economic operation. As more attention is paid to energy recovery systems, an increasing number of heat exchangers will be incorporated into integrated energy schemes. Fouling may then become the major limiting technical factor affecting the entire economic viability of a waste heat recovery system[198].

2.1.3 Maintenance Debits (including antifoulants)

Additional operating costs due to fouling arise in stripping, cleaning and refitting heat transfer equipment. The costs of treatment by anti-fouling additives and the operation of any on-line

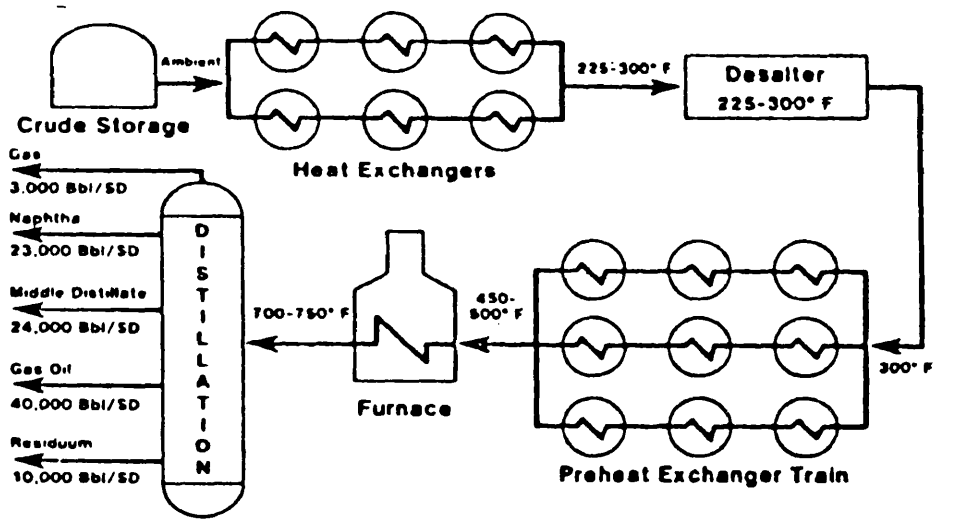

Schematic Of Crude Unit

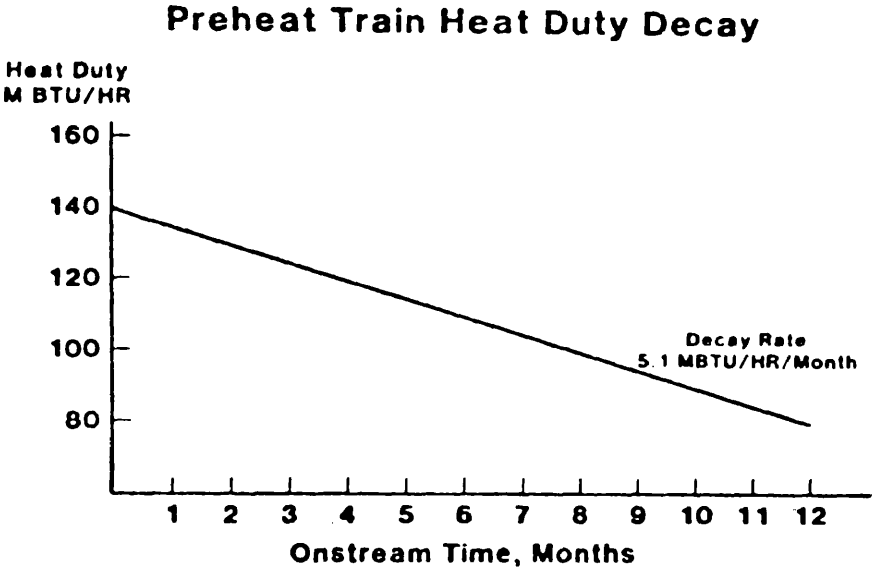

Figure 2.1[203] Crude unit and preheat train heat duty decay

anti-fouling procedures add to these debits. The U.K. expenditure on antifouling chemicals and additives is estimated to be about £20-25M p.a. (1978 prices)[198] for all types of fouling. The economic savings generated by the chemicals, on average, considerably exceed their additional costs[203]. The total expenditure on anti-fouling chemicals in oil refineries appears to be rather less than 10% of the overall cost of fouling[203]. (Table 2.3).

2.1.4 Reduced Throughput and Loss of Production

Lawler[128] reported heavy fouling of exchangers in the preheat trains of crude oil distillation plants due to a mixture of chemical reaction fouling (coking and polymerisation) and deposition of crystalline particulates which were present in the crude. The Exxon study[203] considered the reduced throughput, since the total refinery production is based on uniform operation of the crude unit at constant temperatures and balanced flow rates. A decline in the furnace temperature leads to a decrease in the crude unit throughput.

The financial penalties associated with lost production in oil refining depend on market demand[198]. The value of lost production will be relatively low during a period of slack demand, and very high when plants are operating at full capacity.

2.1.5 Implications of the Economic Balance Analysis

A global approach can be criticised for being too far removed from individual situations[198]. However, relating the overall cost of fouling to the heat transfer area of the heat exchanger in service, suggests an average cost of fouling. In the U.K., the cost is estimated to be about £25 per m^2 of surface[198] (1978). The annual cost of fouling of a particular heat exchanger

Tables 2.3 (203)

Economic Effects Of Antifoulant Use On Crude Unit

	Fouling Related Expenses (Thousands of Dollars)				
	Energy	Throughput	Cleaning	Antifoulant*	Total
Without Antifoulant	1,020	3,730	35	-	4,785
With Antifoulant	265	2,050	15	155	2,485
Savings	+755	+1,680	+20	-155	+2,300

*Cost Of Antifoulant:
$5.20/Gallon
20 vppm
100,000 Bbl/SD Charge

Economic Effects Of Antifoulant Use On Hydrotreater

	Fouling Related Expenses (Thousands of Dollars)				
	Energy	Throughput	Cleaning	Antifoulant*	Total
Without Antifoulant	297	282	14	-	593
With Antifoulant	74	132	7	40	253
Savings	+223	+150	+7	-40	+340

*Cost Of Antifoulant:
$5.35/Gallon
20 vppm
25,000 Bbl/SD Charge

Tables2.4 (198)

Fouling Related Expenses for a Hypothetical, Typical 100,000 Bbl/SD Refinery (Annual)

	Fouling Related Expenses in $K				
	Capacity Bbl/SD	Energy	Throughput	Maintenance & Cleaning	Total
Crude Unit	100,000	1,020	3,730	35	4,785
Hydrotreaters	45,000	535	510	25	1,070
Visbreaker	10,000	1,695	420	120	2,235
Reformer	25,000	1,070	700	15	1,785
Total ($K)		4,320	5,360	195	9,875

Equivalent Annual Fouling Related Costs in UK Oil Refineries

	Approx Capacity (1000 Bbl/Day)	Approx UK Refinery Fouling Costs* (£M)			
		Energy	Throughput	Maintenance	
Crude Distillation	3000	13	48	0.5	
Hydrotrating	1250	6.5	6	0.3	
Visbreaking	40	2.5	0.5	0.2	Overall Total
Reforming	600	12	7.5	0.2	
Total		£34M	£62M	£1.2M	£97M

* At early 1979 oil prices

in refinery service may be far in excess of its original cost[198]. In this situation an increase in capital expenditure on heat exchanger design, material, size, maintenance aids, etc. could make economic sense in order to reduce the fouling-induced costs during service. Thackery[198] presented a scale to correlate the probable annual cost of fouling per m^2 of exchanger surface with the fouling severity. The main difficulty of using the suggested scale is the problem of ascribing the correct rating to a particular situation.

2.2 Chemical Reaction Fouling

In chemical reaction fouling deposits are likely to be formed via a complex sequence of parallel and series reactions. Thus the overall rate of the deposition process may be controlled by the kinetics of these reactions and/or by the rates of physical processes such as the diffusion of reactants, the sticking of deposits and the removal or release of deposits.

Chemical reaction deposits vary from soft, loose and soot-like material[10] often found at relatively low temperatures, to hard coke[77,175,184] formed at much higher temperatures in, for example, hydrocarbon thermal cracking furnaces.

Deposits found in refinery service have been categorized by Nelson[154] as:

(1) Hard deposits whose thickness and resistance to heat transfer increase approximately linearly with time; such deposits are tenacious and their removal cannot be effected by the use of a high fluid velocity alone.

(2) Porous deposits, essentially the same material but containing trapped hydrocarbons whose thermal conductivity is generally lower than that of the hard structure.

(3) Loose deoposits whose resistance to heat transfer depends largely upon the properties of the trapped fluid; it may be possible to remove such material by the use of a high fluid velocity.

Deposits may consist of a wide variety of substances ranging from corrosion products, inorganic salts to coke and other high molecular weight organic material. Individual components in the deposits may vary by weight according to feedstock composition. For example, naphtha processing deposits include[44] lead, sulphur, iron, and trace quantities of copper, nickel, zinc, sodium, silicon, manganese, calcium and magnesium in the ash content and also up to 20% by weight water. (Table 2.2.1).

The diversity of feedstocks and thermal processing environments makes it difficult to generalize about the bounds of chemical reaction fouling. However, deposition may be severe enough to cause significant reductions in throughput or frequent shut-downs for cleaning not only at high temperatures (~ 1700 °F) in the gas phase, as in thermal cracking but also at much lower temperatures (~260 °F) in the liquid phase, as in crude oil preheat exchangers[128]. Cooling of a process stream may also lead to fouling through the condensation of high molecular weight material formed in upstream processing units. For this reason the run length of olefin plants is sometimes controlled by the fouling of the transfer line exchanger[37].

From these observations it is unlikely that any one chemical or physical mechanism can be used to account generally for chemical reaction fouling. Since the thermal cracking of

Table 2.2.1 Weight variations of the main constituents detected in deposits from naphtha vaporizers[44].

	% wt.		
Carbon	4·65	-	80·78
Hydrogen	0·39	-	6·62
Ash	3·18	-	86·5
Sulphur	1·65	-	27·45
Iron	0·09	-	55·8
Lead	0·005	-	4·65
Zinc	0·00	-	0·09
Nickel	0·04	-	0·30

hydrocarbons does not occur at temperatures much below 800°F[79], it is generally accepted in the literature[22] that fouling at lower temperatures in the liquid phase is due to free-radical reactions involving trace species. Oxygen and other trace elements and organo-sulphur compounds are known to have a profound effect on deposit formation rates[188,192,193].

2.2.1 Time Dependency

Fouling resistance-time curves may take a number of forms[72]. (Figure 2.2.0). Fouling resistances may increase exponentially[208], linearly or otherwise with time[27,212]. Some workers[208] have observed an induction period during which the increase in fouling resistance is negligible. This period of time is thought to correspond to a nucleation time, or the deposit initially roughening the heat transfer surface[208], thereby perhaps increasing the heat transfer coefficient before the actual insulating deposit thickness causes the resistance to rise. (See Figure 2.2.0).

$R_f(\theta)$ is often correlated with time, θ, by the transient originally proposed by Kern and Seaton[115]:

$$R_f(\theta) = R_f(\infty)[1-\exp(-\beta\theta)] \qquad (3)$$

It can be shown that for short times, i.e. small $\beta\theta$ that

$R_f(\theta) \propto \theta$ for small $\beta\theta$

The Kern and Seaton equation can be used for predictive purposes only if prior knowledge of the physico-chemical mechanisms and the effects of pertinent parameters on the asymptotic fouling resistance, $R_f(\infty)$, and the time parameter β are available.

In some cases, after long periods of operation the net rate of fouling approaches zero, implying a competitive deposit-release mechanism which accounts for the asymptotic nature of the fouling process[29,209]. In this dynamic balance between deposition

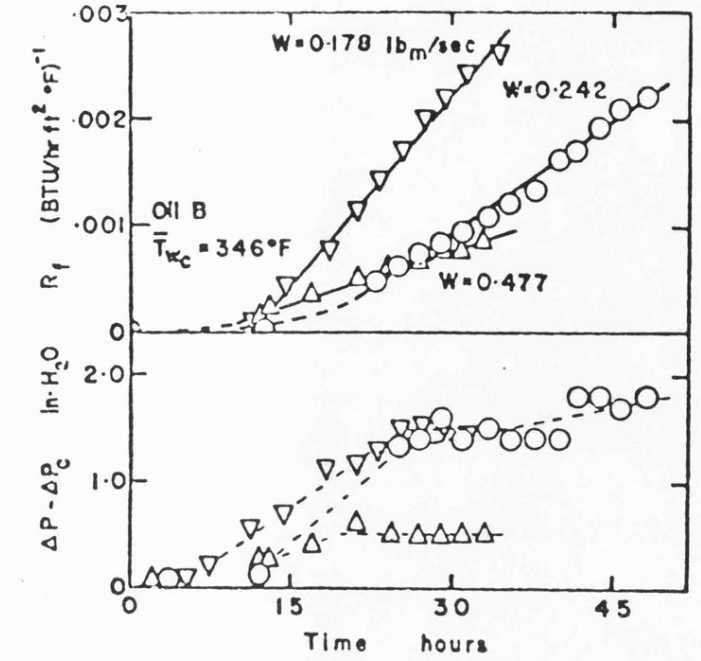

Fouling resistance and pressure drop increase vs. time for $\bar{T}_{w_c} = 346°F$.

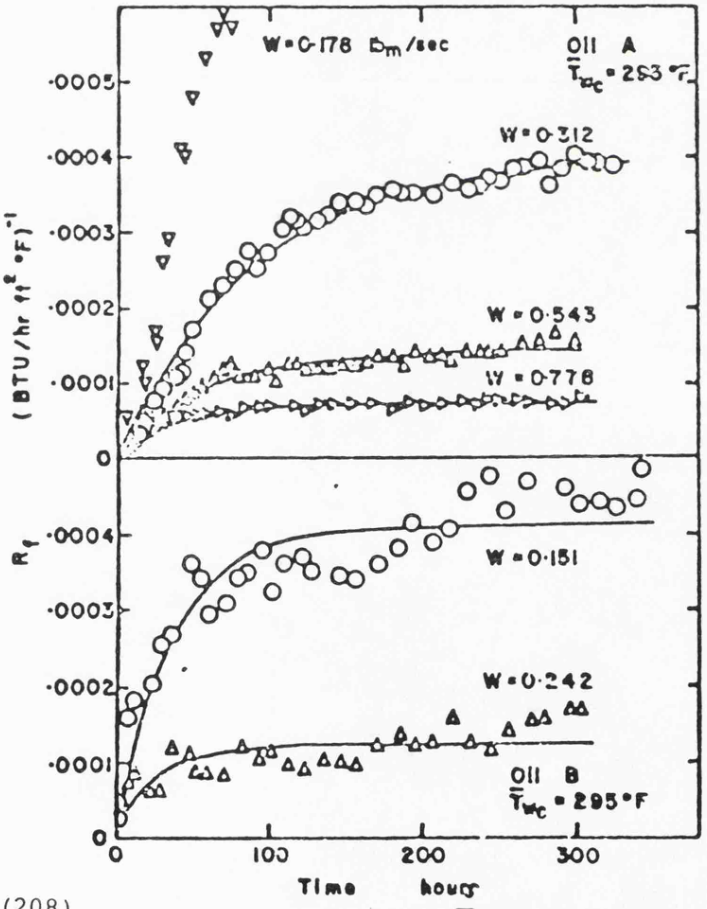

Figure 2.2.0 (208)

Fouling resistance vs. time for $\bar{T}_{w_c} \simeq 295°F$. [solid lines are least squares fit]

and removal mechanisms, deposition rates may be controlled by mass transfer, hydrodynamics or interface-surface kinetics; while the removal rate may be governed by fluid shear[117,187] and/or back diffusion of relatively mobile species.

Atkins[10] has proposed a method for predicting the increase in fouling resistance with time. For fired heaters he assumed that the thermal resistances between the bulk oil and the outside tube wall surface were lying in the oil film layer, porous coke layer, crust coke layer and the tube wall. (Figure 2.2.1). The oil film resistance can be calculated as the inverse of the local film heat transfer coefficient. The porous coke resistance could be determined from standard sources, e.g. Tubular Exchanger Manufacturers Association[196]. The hard coke layer is formed from the porous layer as it is subjected to the higher temperatures adjacent to the tube wall over a long period of time. The temperature gradient across the hard coke layer defines the coking rate, and the thermal resistance of the hard coke layer can be determined from a series of curves based on empirical observations of heaters operating under the indicated conditions[10]. (Figure 1.1). The thermal resistance of the wall can be determined if the wall thickness and the thermal conductivity of the material of the transfer surface are known. Atkins' method did not include a removal or release term and thus predicts an ultimate linear dependence of fouling resistance on time.

2.2.2 Effect of Process Variables

Data from plant and laboratory experiments illustrate the effects of process variables on chemical reaction fouling. Chemical reaction rates are strongly dependent upon temperature,

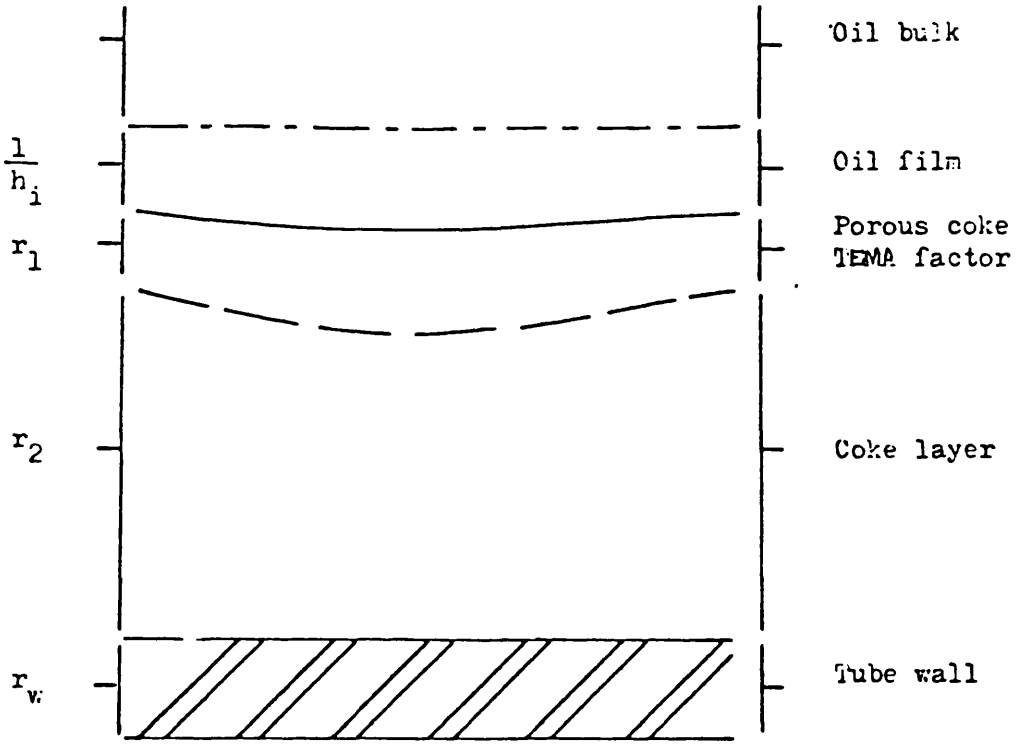

Figure 2.2.1 Four thermal resistances to heat transfer considered by Atkins[10].

pressure, composition and the presence of catalysts, but the overall rate of a deposition process may in addition be dependent upon the rates of physical processes such as mass and heat transfer and surface phenomena[59,72,85]. Thus many variables can affect, and in turn can be affected by the deposition process.

2.2.2.1 Effect of Temperature

Individual chemical reaction rate constants increase exponentially with absolute temperature, T, according to the Arrhenius relationship

$$\text{rate constant} \propto \exp\left(-E/RT\right) \qquad (4)$$

where E - activation energy, R - universal gas constant.

Watkinson and Epstein[209] found that the initial fouling rate of a sour gas oil (0.7%S) in a sensible heat exchanger operated at constant heat flux showed such a dependency. (Figure 2.2.2). Over the wall temperature range, $293 < T_w < 401\,^{\circ}F$ the results were well correlated by[208]:

$$\text{initial fouling rate} \propto \exp\left(-E/RT_w\right)/W^{1.07} \qquad (5)$$

in which, E = 121 KJ/mol., Tw = initial surface temperature, and W = mass flow rate.

For moderate conditions and relatively low temperatures (350-408 °F), deposition rates from pure hydrocarbon jet fuels (major aliphatic, paraffinic and naphthenic content) are well correlated by the above expression[190] with E = 42 KJ/mol. Taylor and coworkers[194] measured the rate of deposit formation in a kinetic unit. The main section of the unit consisted of a glass tubular reactor 1.496 inches in diameter and 39.37 inches in length. The unit had five separate reactor heaters, each independently regulated by its own temperature control. The liquid fuel flow rate was fixed and the total run time employed was 4 hours. The liquid

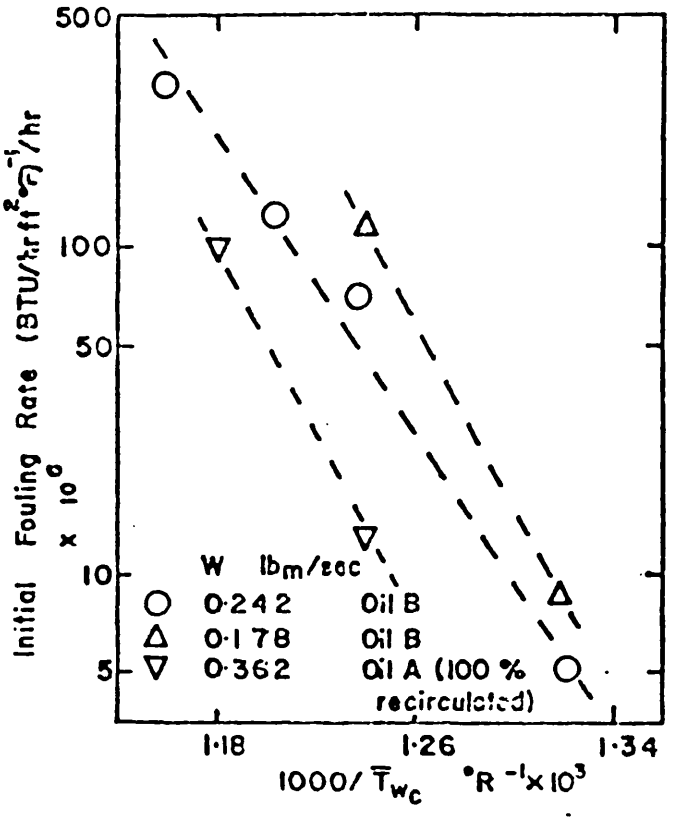

Initial fouling rate vs. reciprocal of clean tube wall temperature.

Figure 2.2.2 (209)

fuel was presaturated with air or an air-nitrogen mixture prior to admission to the reactor section. At the conclusion of a run, hydrocarbon fuel was shut off and a full vacuum was applied to the unit while the temperature was maintained, to remove any physical or chemisorbed jet fuel range hydrocarbon species. Nitrogen was passed down the reactor as the unit was cooled to room temperature.

In the range 300-1000°F, Taylor et al[194] observed that the deposit formation rate from jet fuels increased with temperature until a "deposit formation cut-off temperature" was reached. The fouling rates below the cut-off temperature produced excellent Arrhenius plots[193]. (Figure 2.2.3). Taylor accounted for the drop in the deposit formation rate in the temperature range 660-795°F by assuming that a reduction in the autoxidation reaction rate was caused by the decrease in the concentration of reactive specie through reaction. He postulated that the deposition rate then increases again with temperature, since the autoxidation rate constants continue to rise with temperature and ultimately overcome the concentration effect.

Although high temperatures and low residence times are generally favoured for olefins production[35], the operating periods of naphtha-gas oil cracking heaters tend to decrease with increasing tube wall temperatures. The units are usually shut down periodically for cleaning because coking of the cracking coils results in high tube wall temperatures and high pressure drops[36], or the transfer line exchanger fouls as a result of reaction products being transferred and deposited down stream on cooler surfaces.

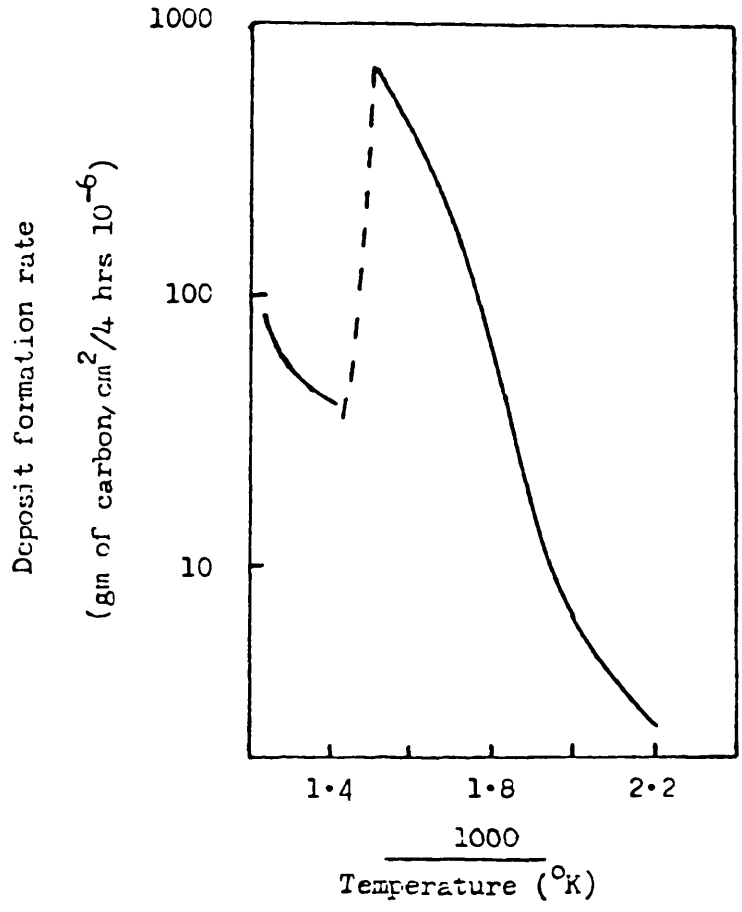

Figure 2.2.3 Deposit formation rate of an air-saturated jet fuel (64ppm of O_2) at 69 atm[194].

Braun and Hausler[23] measured fouling rates of hydrocarbon liquids with a hot wire test apparatus and reported apparently inconsistent and varying behaviours of fouling rates with temperature. In two cases Hausler[99] reports a decrease in the fouling rate with increasing temperature in the range 220-300°C (Figure 2.2.4) after an initial increase below 220°C. In another case beyond 160°C, the fouling rate increases so sharply that it appears that if such a situation existed in heat exchangers, blockage of the tubes would take place at temperatures little above 200°C.

Butler et al[27] observed that in refinery exchangers the overall fouling resistance increases with temperature. At the lower temperatures (275-354°F), deposition occurs primarily as a result of vaporization of the salt fraction in crude oil. Below the inorganic phase bubble point, deposition was found to be minimal. At higher temperatures (350-449°F), degradation of the organic phase can occur. Thus flashing the crude dries out the salt fraction so that deposition at ascending temperatures can be minimized, provided that the temperature is not too high. Lawler[128] reports that prior to the desalter (<241°F) in crude oil processing, deposits were essentially salt and corrosion products. After the desalter not much fouling occurred until the temperature was in the range 323 to 419°F when the exchanger became blocked with thick waxy deposits on the tube sheets and hard shiny deposits within the tubes. Subsequent thermal processing (419-485°F) caused waxy deposits to completely block the last exchanger before the furnace. About 5% of the crude is vaporized in this exchanger.

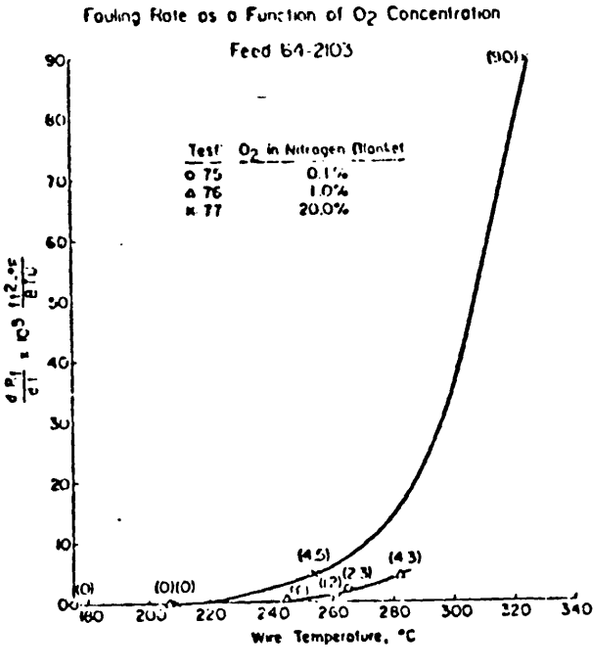

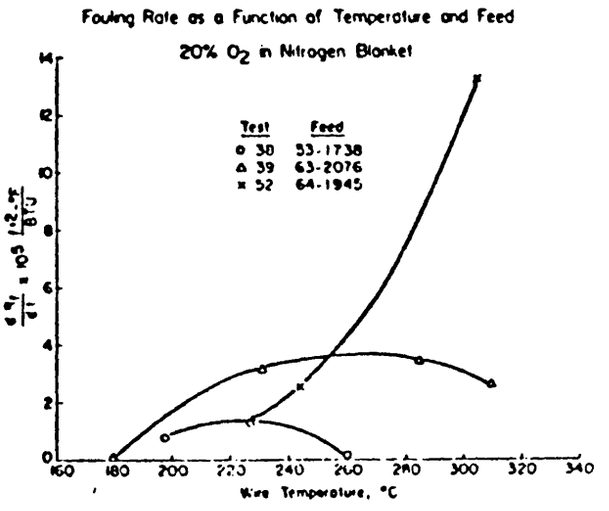

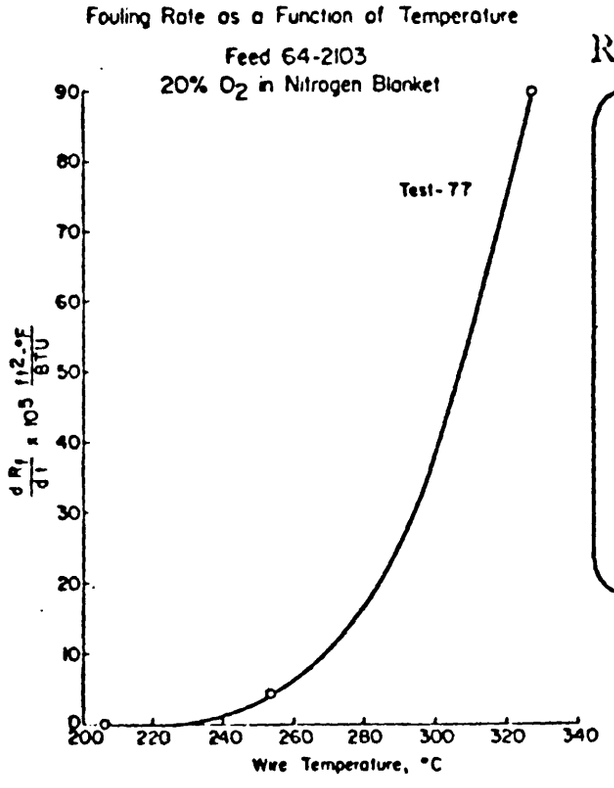

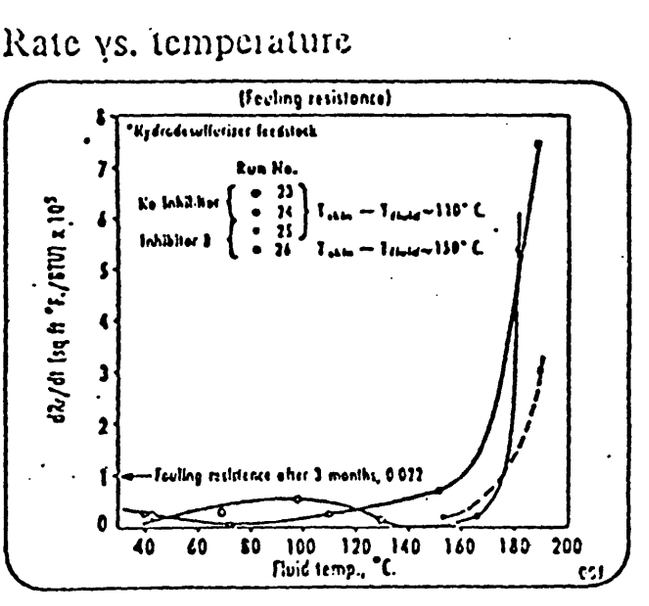

Figure 2.2.4[23,99] | Effect of temperature

Shah et al[174] have studied coking rates from n-octane in small scale tubular flow reactors in the temperature range of 1382 to 1472°F and with space times up to one second. Starting with a fresh tube, several runs were repeated under identical conditions. The amount of coke formed increased with each successive air treatment. The coke being burned off in air at the end of the run. However, when the surface was treated with hydrogen sulphide at 1292°F, the amount of coking was found to be extremely low. It was believed that this was due to the metal surface condition influencing the coking reactions, since it was known[174] also to affect the thermal cracking reactions. Reproducible coking rates were obtained after the metal had been cleaned to provide a fresh steel surface. After a certain period of operation the coking rate became independent of time (for all space times). Shah et al[175] suggested that the higher initial and unsteady coking rate was probably due to the tube surface effect. Both the initial and steady rates of coking exhibited maxima with respect to space time for a given surface to volume ratio and temperature. (Figure 2.2.5). The initial coking rate increased with an increase in surface to volume ratio (decrease in tube diameter) for a given space time and temperature. At a higher run temperature (1652°F) the amount of coke deposited was much smaller. The coke itself was much fluffier and the effluent liquid products were of a dark colour rather than clear. It was suggested that the low deposition on the surface in this case was a consequence of a large amount of carbon material being carried by the fluid bulk. This material can foul downstream equipment by depositing on the

surfaces of transfer line exchangers to thereby control the run time of cracking units[37].

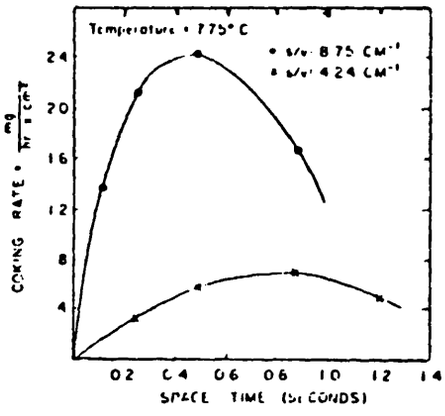

Figure 2.2.5[175] Initial coking rate *vs* space time

2.2.2.2 Effect of Flow Rate

Generally, when temperatures are moderate increasing the mass flow rate tends to reduce the rate of fouling from liquid feeds. Much of the reduction in fouling rate may arise from the increase in film heat transfer coefficient h causing a reduction in the surface temperature Tw for an exchanger operated at constant heat flux Φ and bulk temperature T_b.

i.e. $Tw = T_b + \Phi/h$ (6)

Higher mass flow rates also reduce the volume of fluid exposed to temperatures in excess of T_b. Nelson[154] believed this to be responsible for a reduction in the fouling rate.

In addition, deposit removal, release or re-entrainment rates are likely to increase with increasing flow rates[16,208].

A practical application of the use of high velocities to reduce fouling is described by Chantry and Church[32]. By increasing velocities to 3-10 m/s, forced circulation reboilers originally requiring cleaning every 6 to 180 days, did not require cleaning more than twice a year. They worked out a sample design by economic balance, since operating costs increase with velocity, but commented that a knowledge of the relationship between flow velocity and fouling rates is essential.

Watkinson and Epstein[209] observed in their tests (Figure 2.2.6), with a gas oil that the initial fouling rate decreased with an increase in mass flow rate, W thus:

$\dot{R}_f(0) \propto 1/W \quad 9800 < Re < 41900$ (7)

They believe that the advantage of going to higher velocities lies in the reduction of the tube wall temperature, on which the chemical reaction fouling rate is strongly dependent, rather than shear or removal effects. From their results[209] the asymptotic fouling

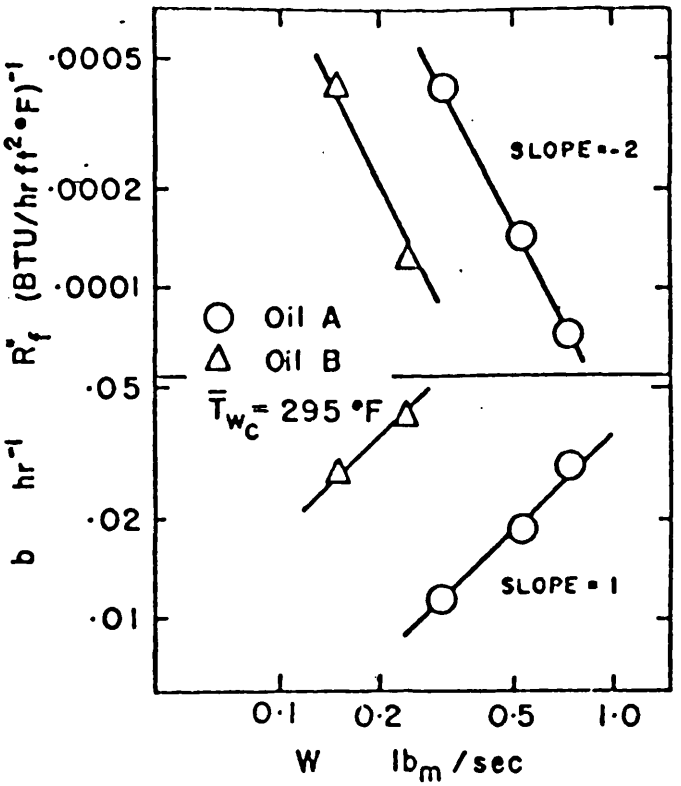

Variation of parameters of Equation (3) with mass flow rate (log – log).

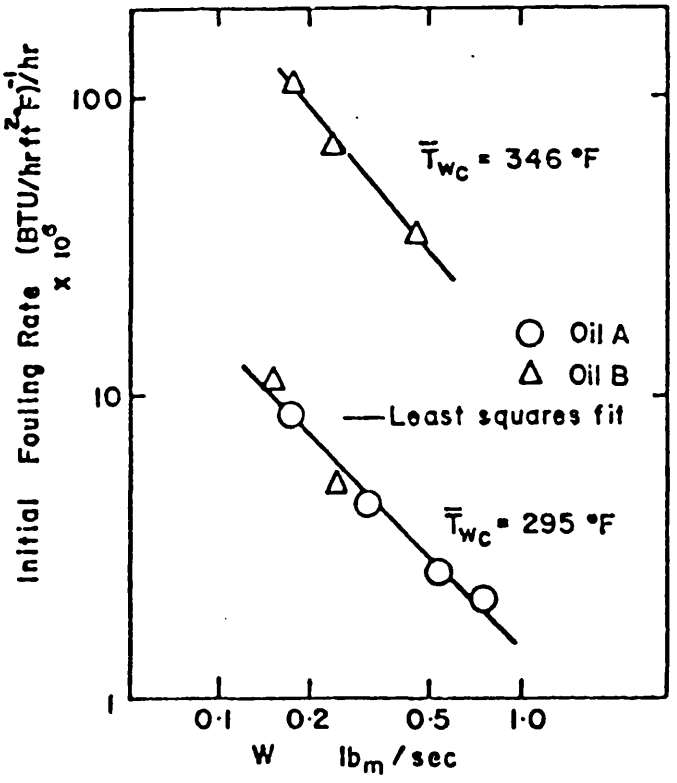

Figure 2.2.6 (209) Initial fouling rate vs. mass flow rate (log – log).

resistance was found to be inversely proportional to the square of flow rate.

$$R_f(\infty) \propto 1/W^2 \qquad (8)$$

The time constant in the Kern and Seaton transient (equation 3), which was used to fit their experimental data, was found to be directly proportional to W, i.e.

$$\beta \propto W \qquad (9)$$

However, there are exceptions to the fouling rate reducing with increasing flow rate. For example Smith[179], working with aviation fuel, found that the higher the flow rate the higher the thermal resistance of the deposit became. (See Figure 2.2.7).

Smith accounted for his results by suggesting that the deposits formed on the walls of smooth-bore tubes disturb the major resistance to heat transfer in the laminar sublayer, and cause turbulence adjacent to the wall. The insulating tendency of the low thermal conductivity deposit only becomes effective when the thickness of the deposit exceeds that of laminar sublayer[179].

Vranos et al [204] have reported a similar increase in the fouling rate with an increase in the Reynolds number for a jet fuel with temperatures in the range 450 to 500 °F.

At much higher temperatures, vapour phase coking rates are often increased with increasing flowrate. Fernandez-Baujin and Solomon [77] found that a model which assumed that the rate of coking was proportional to the mass flowrate raised to the power 0.8 accounted well for plant operating data.

In the relatively high temperature range (1380-1470 °F) of octane cracking, Shah et al found that the coking rate passes through a maximum as a function of space time[175].

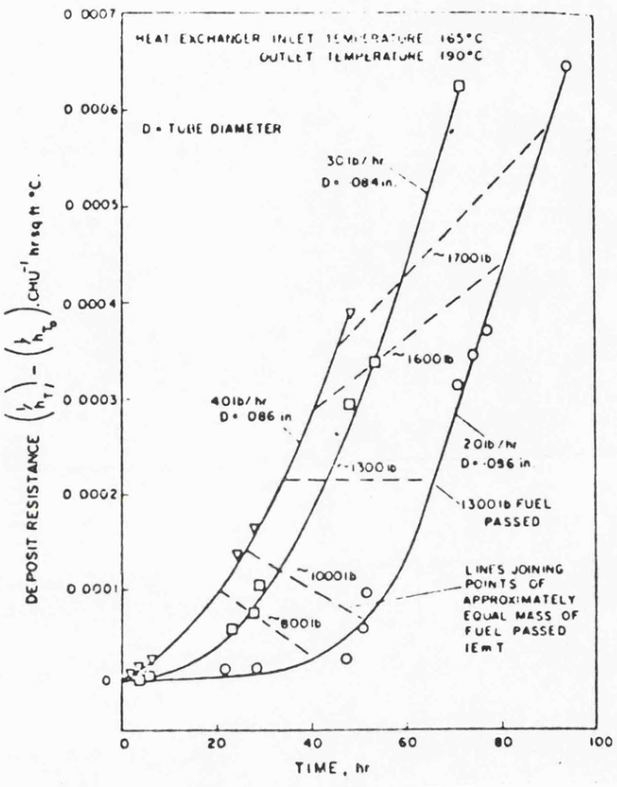

Figure 2.2.7[179] Thermal resistances of deposits from aviation turbine fuels, at mass flow rates of 20, 30 and 40 pounds per hour

2.2.2.3 Effect of Pressure

Pressure can have a complex effect on fouling rates. Taylor and Wallace[194] observed in their fuel studies that at lower temperatures (less than 300°F) and lower pressures (less than 261 psig) and with the exclusion of Oxygen the rate of deposition in jet fuels was very low. On the other hand, keeping a fixed oxygen partial pressure and increasing the total pressure of the system increased the fouling rate.

High pressure can increase the solubility of undesirable gaseous impurities such as air or oxygen in liquid feed stocks. Gas phase polymerisation reactions are favoured thermodynamically by higher pressures. Gas phase reactant partial pressures are also increased by increasing the pressure.

2.2.2.4 Effect of Feedstock Composition

The fouling of feedstocks in refineries may be related to the concentration of trace materials as well as to bulk fluid properties. It is well known that the presence of trace quantities of compounds can play important roles in the deterioration of hydrocarbon feedstocks under storage[101,193]. The susceptibility to gum formation, deposit formation or discoloration varies with the kinds of hydrocarbons present, but feedstocks which have undergone some degree of thermal cracking can be particularly unstable[56,99,189]. Deposition is believed to be initiated by air oxidation which is catalysed by trace material contaminants (sulphur, nitrogen, metals, etc.)[29,190,208].

However, it is not just the concentration of these species, but also their chemical structure which can have pronounced effects on deposition rates.

Table 2.2.2 Composition variation in crude oils[114]

Location	Middle East	Venezuela	U.S.S.R.	Trinidad
Type	Paraffinic	Naphthenic	Aromatic	Asphaltic
		(% wt.)		
Paraffins	76	12	13	5
Naphthenes	16	75	15	15
Aromatics	6	10	40	20
Asphaltenes	2	3	32	60

2.2.2.4.1 Structure

Coggins[44] has surveyed the blockage of naphtha vaporizers used in the gas industry. Out of 55 blocked vaporizers 7% used naphtha with a final boiling point less than 250°F. It was suggested that the greater tendency for heavier distillates to block equipment was due not only to heavier components undergoing decomposition more easily, but also to the presence of unsaturates and aromatics. (See Table 2.2.3 and 2.2.4).

For a given temperature, Taylor[189] found that the deposition rate from n-paraffins decreased with increasing carbon number, from 10 to 16. This is somewhat in variance with what might be expected from an autoxidation mechanism. For a given temperature and carbon number, chain branching of paraffins increased the deposition rate[190]. Also Taylor[193] observed that the addition of aromatics or naphthenes (at 10% by weight) in general inhibited the rate of deposition from n-decane in the temperature range 200-350°F. At higher temperatures the inhibition was less pronounced. The magnitude of the inhibition was found to be function of the aromatic or naphthene structure.

Taylor found that olefins increased the deposition rate from n-decane at a given temperature[193], the magnitude of the increase being a function of olefin structure.

Mekler and Brooks[147] identified the fouling rate increase with characterization factor which in turn increases with carbon number. (Figure 2.2.8).

Table 2.2.3[128]

Physical properties and characteristics of typical crude oils

Crude Type	Arab Light	Arab Heavy	Russian
API Gravity	34.5	27.0	31.9
SG 60/60°F	0.8524	0.8927	0.8660
Viscosity 100°F CS	4	20	7.3
Pour Point °F	-15	-15	0
Sulphur % wt	1.7	3.1	1.6

Table 2.2.4: Stability of Hydrocarbons[79]

Paraffins < Olefins < Aromatics

Stability increase (1520°F < Temperature)

Paraffins carbon number decreases

Stability increases

Olefins carbon number decreases

Stability increases (higher temperature)

Alkylated aromatic <corresponding unsubstituted Aromatics

Stability increases

Aromatics decreasing length of side chain

Stability increases

Aromatics number of rings increases

Stability increases

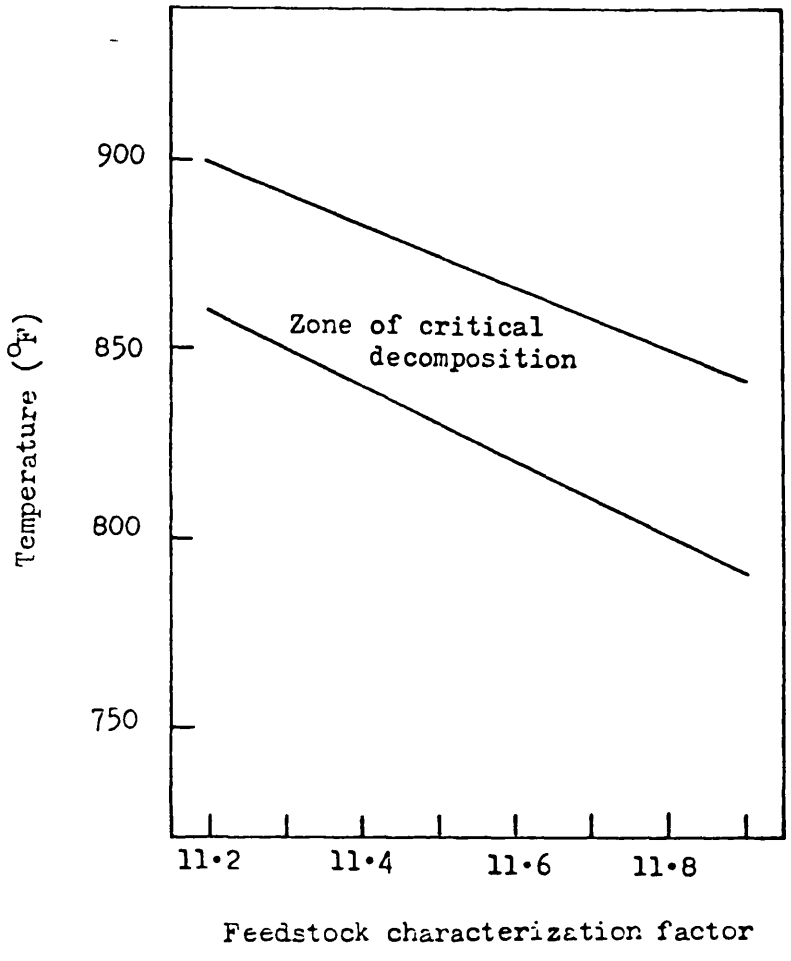

Figure 2.2.8 Prediction of undesirable temperature zones[147].

2.2.2.4.2 Oxygen

Oxygen stripping and inert gas blanketting of storage tanks generally reduces deposition and fouling rates[27,29].

Watt el al [211] have studied the formation of deposits from jet fuels on the walls of an electrically heated Nichrome tube. The fuel temperature and pressure ranges were 70-700 °F and 2.5-609 psig, respectively. The deposits were thin and not easily wiped off the surface and a filter located downstream of the heated tube became blackened. Both pressure and oxygen concentration strongly affected the amount of the deposits. When saturated with air (~45 ppm) the poorest quality fuels formed deposits at two local positions but when deoxygenated (<0.3 ppm) the peak associated with the lower temperature position was not observed. The second peak did not coincide with the tube outlet where the surface temperature was highest. The presence of oxygen increased the total amount of deposition by three to tenfold. For air saturated fuels it was noted that the wall temperature necessary for the incipience of deposition was 103-200 °F lower than that required for deoxygenated fuels. For deoxygenated fuels an increase in fuel pressure from 14.5 to 319 psig resulted in lower total and local deposit accumulations and caused peaks to occur at higher temperature localities. No further improvement was found for pressures in excess of 319 psig.

The deleterious effect of air or oxygen in chemical reaction fouling has been observed by many other workers[100,193]. (Figure 2.2.9). Taylor[193] observed a square root relationship between the fouling rate and the oxygen content of a jet fuel. Taylor and Wallace[194], in studying the effect of oxygen in a jet fuel tank enviornment, have reported that the rigorous ex-

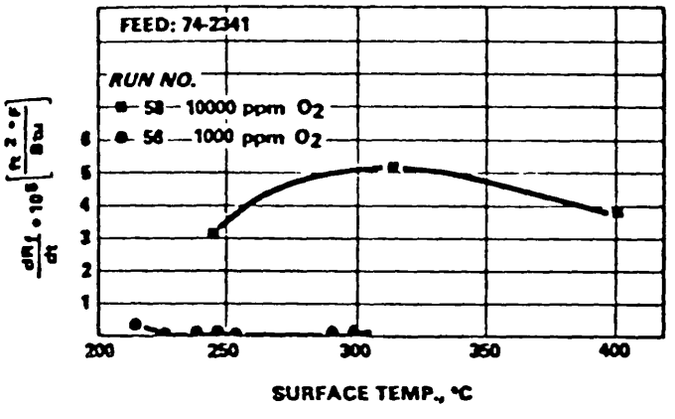

Figure 2.2.9[100] Fouling rate *vs* surface temperature

clusion of oxygen reduced the deposit formation rate greatly up to 599°F, even at pressures as high as 1014 psi. In the range 300-599°F the apparent activation energies for the air saturated fuels ranged from 5 to 15 kcal/mol. The activation energies for deoxygenated fuels were less than 5 kcal/mol. Even at temperatures up to 1112°F, deoxygenated fuels continued to exhibit relatively low deposit formation rates. They concluded that the largest effect of oxygen concentration on the deposit formation rate occurs at the lower temperatures, just before the "transition" zone observed in Figure 2.2.3 (See Section 2.2.2.1). At higher temperatures, Taylor et al [194] suggested that new hydrocarbon reactions begin to assume importance and the effect of deoxygenation is not as pronounced.

Braun and Hausler[23] found that one feed fouled very little at 0.1% O_2, but fouled heavily when aerated. (See figures 2.2.4 and 2.2.9).

Canapary[29], working on a laboratory scale single tube exchanger concluded that fouling can be reduced considerably by complete removal of oxygen from the naphtha charge to hydrosulphurizers. Overall heat transfer coefficients were improved by up to 85% by sparging the naphtha charge stock with nitrogen.

Butler et al [27] used natural gas stripping to reduce the oxygen content of light gas oil and hence obtain a reduction in the rate of fouling.

2.2.2.4.3 Sulphur

Taylor[188] studied the effect of various trace sulphur compounds on the kinetics of deposit formation from hydrocarbons and jet fuels. In the temperature range of 200-450°F the addition of thiols, sulphides, disulphides and thiophenes to a jet fuel in

the presence of oxygen increased the rate of deposition by up to twenty times. (Figure 2.2.10). Similar results were obtained for deoxygenated hydrocarbon fuels.

Taylor[192] also found that there was a good correlation between the cut-off temperature and the square root of the sulphur content. An interesting and consistent observation was a square root dependence of the deposit formation rate on the relative sulphur level. (Figure 2.2.11). He postulated that if a sulphur compound decomposed to produce a single active free radical, and deposits were produced via a radical-radical recombination reaction, then a square root dependence of formation rate on sulphur level could be expected. Taylor suggested that rigorous deoxygenation by itself to suppress deposition depends upon the type and level of trace impurity sulphur compounds which are present in the fuel.

Fabuss et al [75] found that the hydrocarbon structure, to which sulphur compounds were added was also of significance. The thermal decomposition rates of several normal paraffins and naphthenes were actually reduced whilst the decomposition of branched chain paraffins was accelerated.

Thompson et al [199] observed that free sulphur, disulphides, polysulphides and in particular thiophenol promote sludge formation from fuel oils in storage, whilst thiophenes, aliphatic mercaptans and aliphatic sulphides have little effect. These observations are generally in agreement with those made by Johnson et al [113].

Chemical analysis of the soft, powdery soot-like material found by Watkinson and Epstein[209] in their experiments with sour gas oils (0.7% S) revealed relatively high ash (~10%) and sulphur (~5.5%) contents.

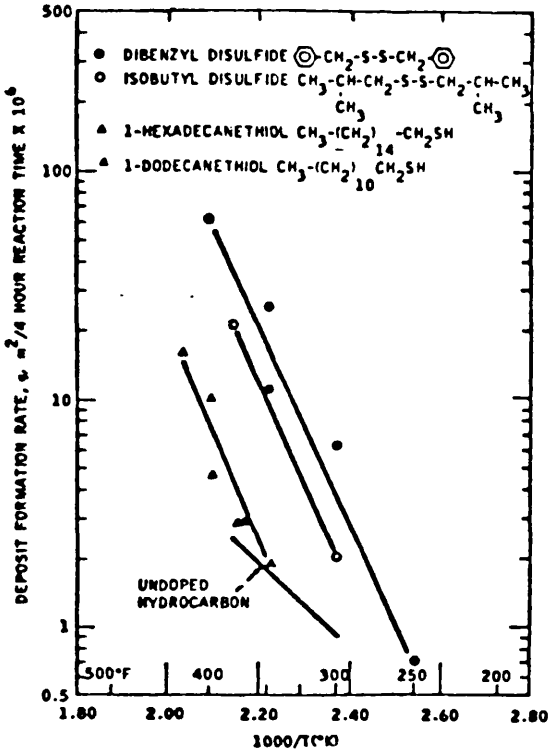

Effect on deposit formation rate of addition of 1000 ppm S to hydrocarbons using: ●, dibenzyl disulfide; ○, isobutyl disulfide; △, 1-hexadecanethiol; ▲, 1-dodecanethiol

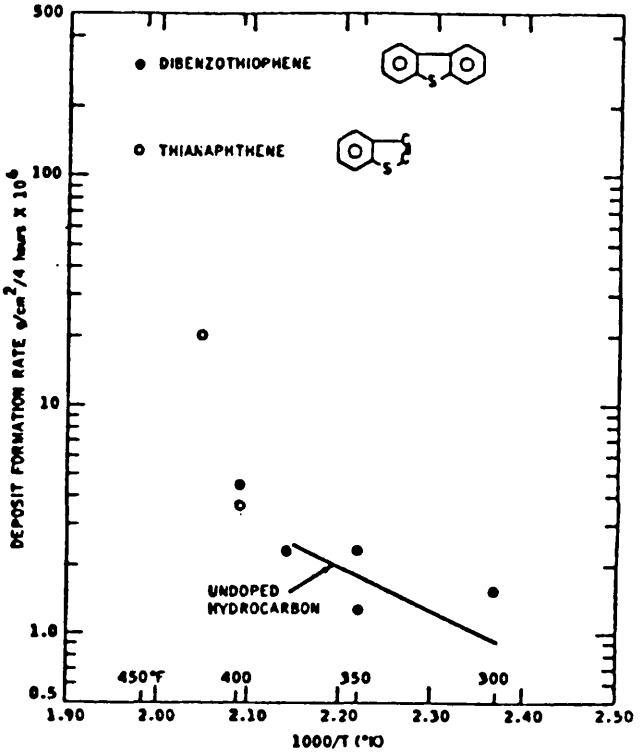

Effect on deposit formation rate of addition of 1000 ppm S to hydrocarbons using: ●, dibenzothiophene; ○, thianaphthene

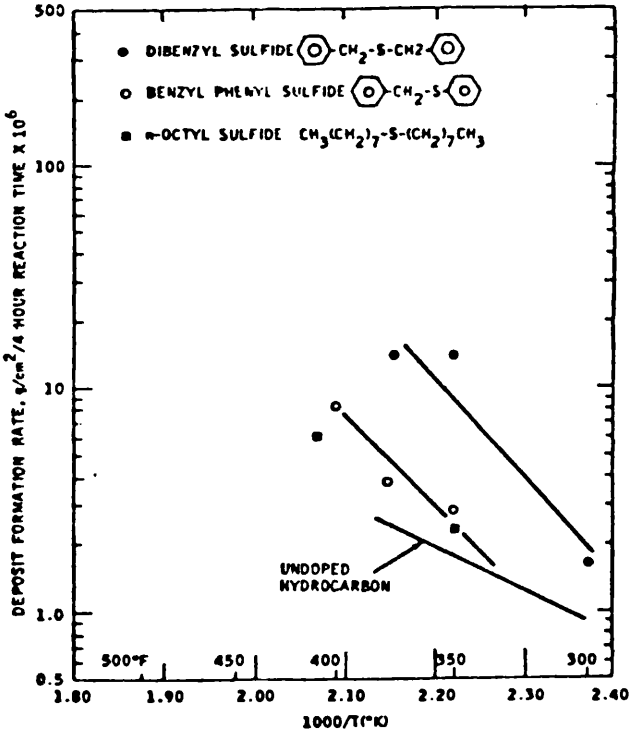

Effect on deposit formation rate of addition of 1000 ppm S to hydrocarbons using: ●, dibenzyl sulfide; ○, benzyl phenyl sulfide; and ■, di-n-octyl sulfide

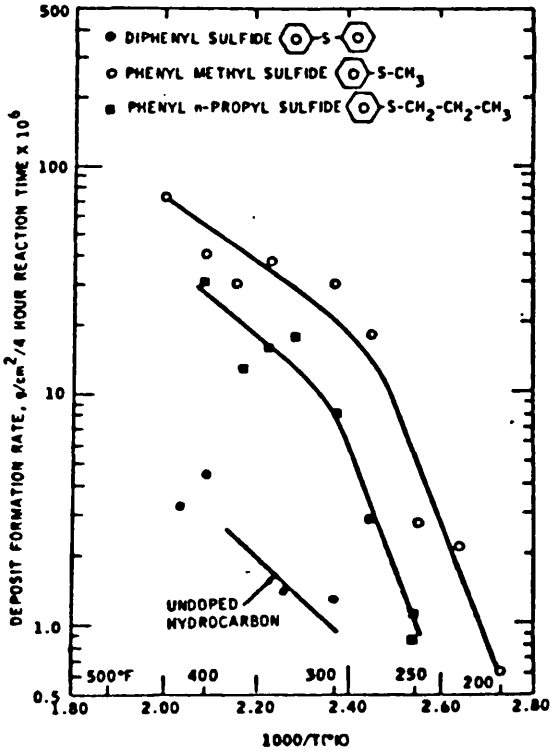

Effect on deposit formation rate of addition of 1000 ppm S to hydrocarbons using: ●, diphenyl sulfide; ○, phenyl methyl sulfide; and ■, phenyl-n-propyl sulfide

Figure 2.2.10 (188,192) | Effect of sulphur

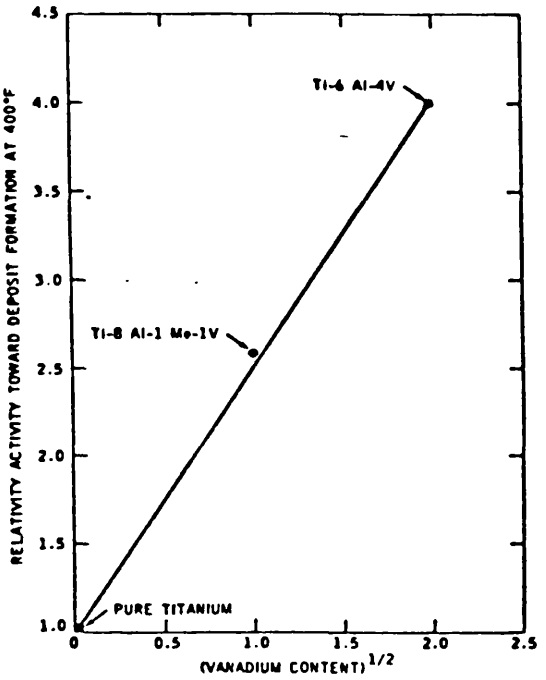

Effect of vanadium content of titanium alloys on relative activity toward deposit formation

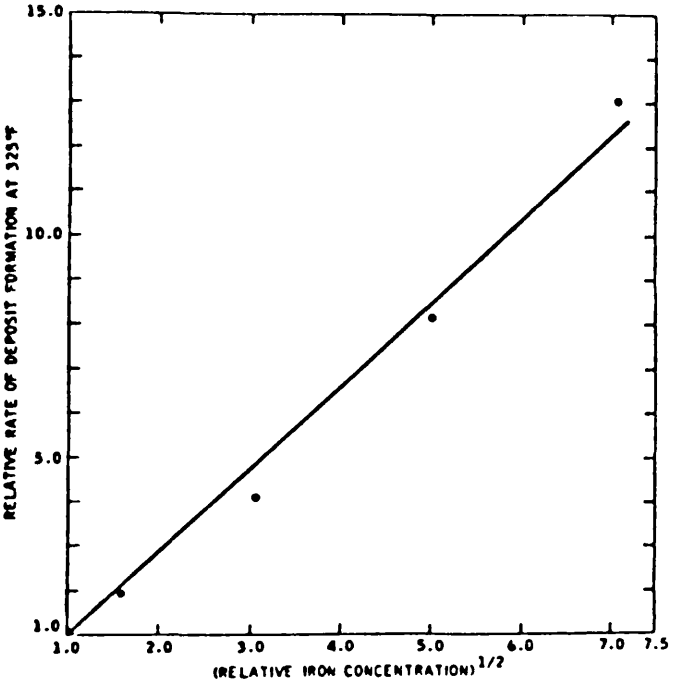

Effect of ferric acetylacetonate concentration on relative rate of deposit formation

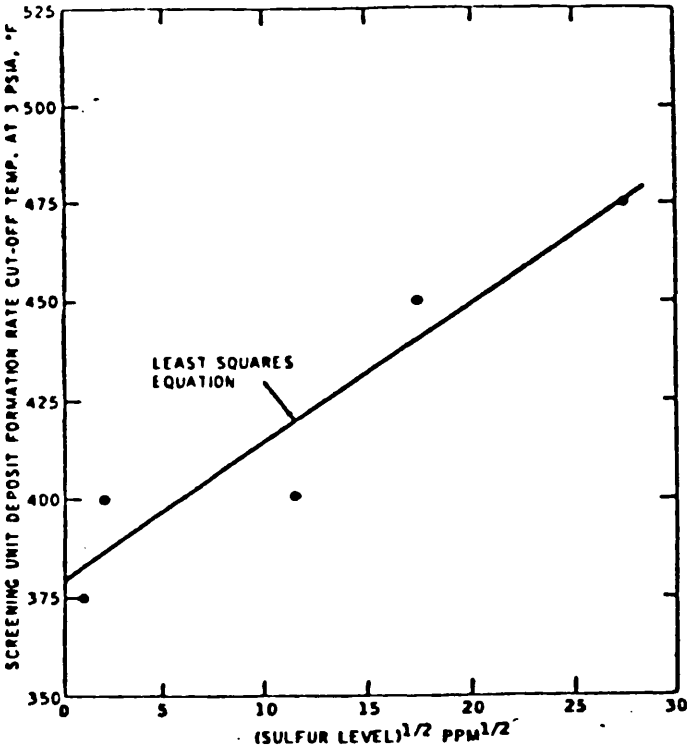

Cutoff temperature as a function of the total sulfur content of jet fuels

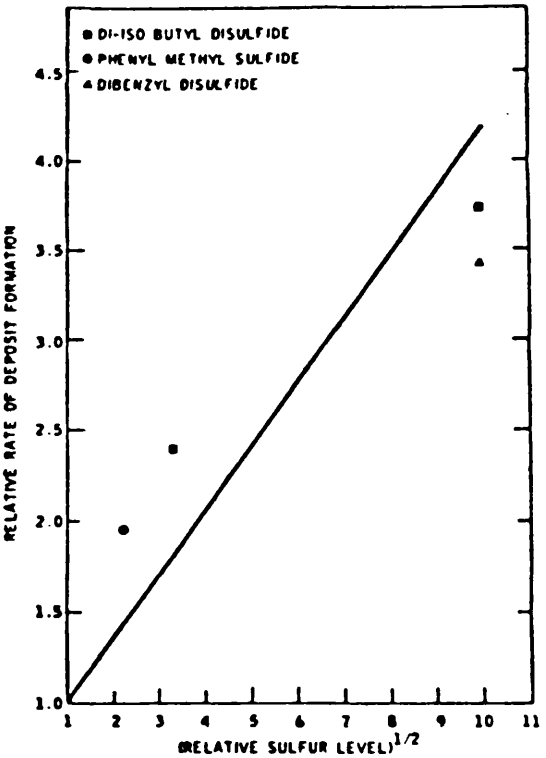

Effect of relative sulfur level on relative rate of deposit formation

Figure 2.2.11 (192,195) Square root dependencies of fouling rate

2.2.2.4.4 Nitrogen Compounds

Pyrroles, pyridines and in general trace levels of nitrogen heterocyclic compounds increase the rate of deposition. Thompson et al [200] studied the effects of small amounts of nitrogen compounds on the stability in storage of fuel oils. Pyridines and pyrroles both caused deposits to be formed, the latter being the most deleterious.

Taylor [193] carried out experiments in the presence of dissolved oxygen in the hydrocarbon. (Figure 2.2.12). The addition of nitrogen compounds markedly increased the rate of deposit formation and once more a square root dependence of the rate of deposit formation on the relative nitrogen concentration was found, suggesting that nitrogen compounds also contribute to the initiation step of a fouling process.

2.2.2.4.5 Trace Metals

Metal elements or metallic compounds not only add to the foulant itself but also enhance fouling by catalyzing some reactions. The addition of 50 ppm of metal in the form of acetylacetonates (Figure 2.2.13), increased the deposition rate from a jet fuel at 300 °F by a factor of between 40 and 120 [195]. The complex of copper resulted in a higher rate than that of iron, nickel or cobalt [195]. Taylor [195] observed that the rate of deposit formation depended on the square root of the relative iron concentration when the ferric complex was added to the fuel. (See Figure 2.2.11). It was suggested that trace metals can enter the reaction mechanism by catalyzing or initiating the chain reactions.

Apart from catalyzing polymer formation, trace metals may be trapped by the polymer binder and provide a new surface

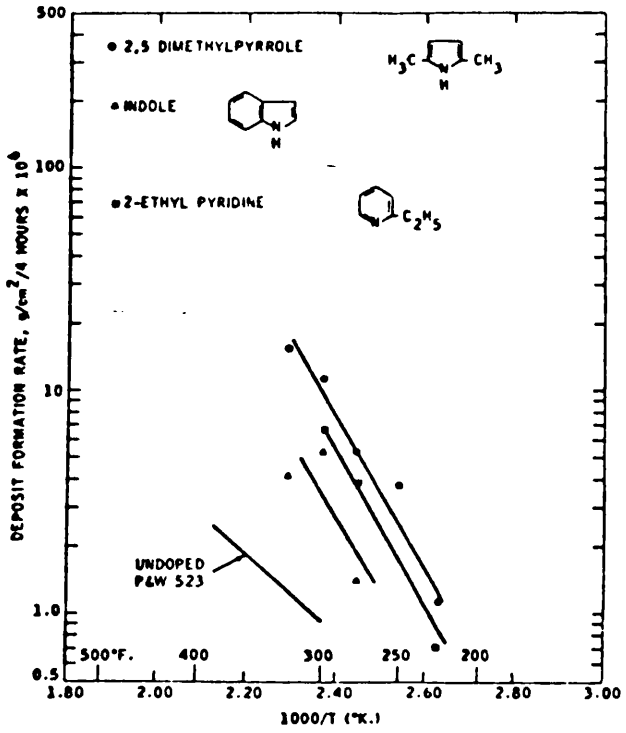

Effect on deposit formation of addition of 1000 ppm N to hydrocarbons using: o, 2,5 dimethylpyrrole; ▲, indole; ■ 2-ethyl pyridine

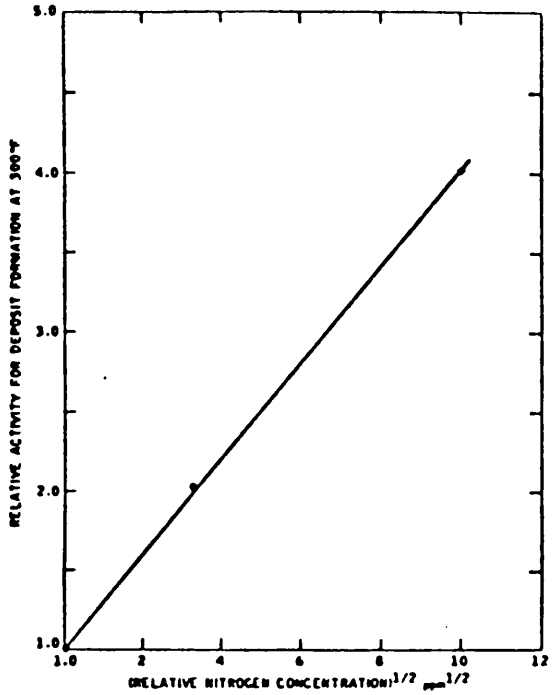

Effect of relative nitrogen level on relative rat of deposit formation

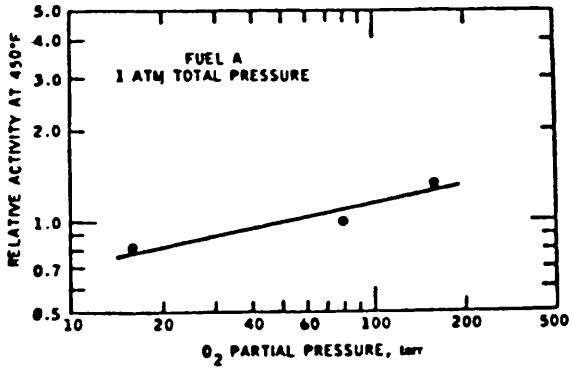

Relative activity for deposit formation as function of oxygen partial pressure

Figure 2.2.12 (193,194) Effect of oxygen and nitrogen

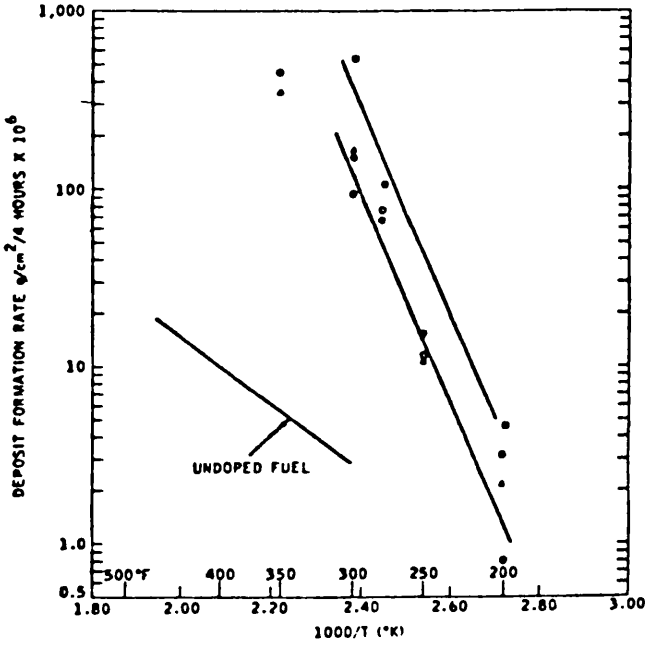

Arrhenius plot of rate of deposit formation of fuels containing 50 ppm added metal: ●, FeIII $(AcAc)_3$; 0, NiII $(AcAc)_2$; □, CuII $(AcAc)_2$, ▲, CoII $(AcAc)_2$

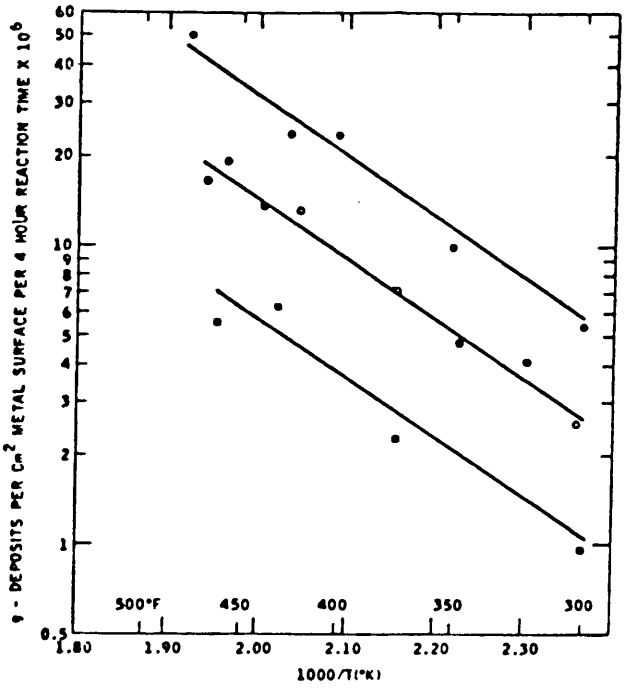

Arrhenius plot of rate of deposit formation as function of temperature: ●, copper; 0, Ti-8A1-1Mo-1V; ■, stainless steel 304

Figure 2.2.13 (195) | Effect of metals

to which more organic polymer can adhere. Crawford et al [56] studied the effects of metals on deposit formation from refinery process liquid streams by adding different metals as oxides or salts to the hydrocarbon stream. In the presence of sulphur, nitrogen, oxygen, and olefinic compounds the deposition rate was increased. For six different metals (iron, chromium, vanadium, copper, nickel and manganese) tested at a fluid temperature of 600°F, iron resulted in the greatest increase in fouling in a naphtha comprising 25% cracked and 75% straight-run material; however nickel was the most effective in a 100% straight-run feedstock. In both cases, the deposition tendency was increased as the temperature was increased. In the presence of trace metals Crawford noticed that the hydrocarbon fuel uptake of oxygen was also increased.

2.2.2.4.6 Surface Effect

Besides homogeneous trace metals, i.e. those dissolved in the process stream, the metal of the heat transfer surface may also catalyze fouling reactions. Copper has a pronounced effect on the stability of feedstocks under storage [112,161], Taylor [191] also noticed that the nature of the metal surface influenced the deposition rate. Copper and a titanium alloy (containing vanadium) were particularly deleterious. (Figure 2.2.13).

2.2.2.4.7 Additives, Surface Coatings and Antifoulants

While the addition of various antioxidants, including alkylsubstituted phenols and a phenylenediamine, reduced the deposition rate from a jet fuel at temperatures between 250 and 425°F [191], the use of rust preventives and metal deactivators

increased the rate of deposition at temperatures above 350°F. The fact that deposit formation is a function of the previous time and temperature history of a process stream and various characteristics of the existing components in the fuel makes the choice of an effective antifoulant difficult[94]. Additives or surface coatings work effectively only in the temperature range that they have been developed for[99,191]. Canapary[29] and Frazier et al [83] stress that additives can be efficient only if applied in the right concentrations.

Taylor[191] found in most of his tests that additives or surface coatings were not effective in reducing fouling; on the contrary, some of them increased the deposition rate. At higher temperatures, they decomposed forming radicals which could initiate chemical reactions and hence deposition.

Lawler[128] found that an antifoulant was not effective in improving the heat transfer in an already fouled industrial refinery preheat exchanger. A water soluble antifoulant was injected at a level of 25 ppm into the wash water which was mixed with the crude, before the preheat exchangers and desalter. The results were not satisfactory.

2.2.2.5 Effect of Equipment Geometry

The surface to volume ratio of a tube becomes of greater relative importance when this ratio is high, i.e. when the tube diameter is small. The size and number density of protuberances and cavities may affect reaction initiation through the provision of active and nucleation sites, participate catalytically in the reactions, affect the bonding of the deposit to the wall, and affect the shear stress at the clean wall. The deposition rate onto

a clean surface also is often different from that onto a fouled surface[128,208]. Changes in the surface roughness may also enhance the heat transfer coefficient by increasing the turbulence at the tube wall[21,58,59], possibly giving rise to apparently negative values of R_f[20,21].

Rankin and Adamson[166] have discussed the importance of wall surface energy as a factor determining the adherence of the initial foulant layers. High surface energy rough metal walls should give rise to a greater adherence than low surface energy smooth "Teflon" walls[125,158]. Lund[135] argues that the mechanical strength of the scale layer can be reduced by the simultaneous deposition on the metal surface of artificially introduced polymers which have a low surface energy; they create a zone of mechanical weakness. High energy surfaces (or wettable surfaces), such as metal surfaces, are very susceptible to fouling and the adhesion strength increases with an increase in roughness[135].

Chemical treatment of the tube surfaces in thermal cracking furnaces affects coking rates. For example, the oxidation of stainless steel reactor surfaces results in increased rates of coking whilst treatment with hydrogen sulphide passivates the surface[175].

2.2.2.6 Effect of Vaporization

Vaporization of a liquid stream may exacerbate fouling through the concentration of the least volatile components and therefore the least stable material at the hot surface. Coggins' data[44] show that it is undesirable to operate a vaporizer close to the temperature at which the last trace of liquid is vaporized since high boiling fractions become concentrated in the liquid

phase where catalytic metal impurities are present and temperatures are high.

In forced convective vaporization[46] drying out of liquid on the tube wall may occur at quite low vapour qualities because the high velocity vapor core can entrain a large amount of liquid in mist form[46]. Boiling can occur also when the bulk temperature is below its bubble point because bubbles form at the hotter heat transfer surface. A certain amount of superheat (above the bubble point) is required, however, for the onset of nucleation[46]. The temperature at which dry-out on the wall occurs is a function of pressure.

Chantry and Church[32] have suggested that deposition caused by evaporation of feedstocks on reboiler tube walls can be eliminated by controlling the pressure so that heat is introduced only in the sensible form. Vapor formation at the walls exerts an insulating effect resulting in a lower heat transfer coefficient and a higher tube surface temperature. Higher fouling rates in the liquid deficient region were caused by exposure to higher temperatures[32] resulting in cracking and increased polymerisation reactions. These degradations enhance the formation of foulant particles.

Khater recently studied chemical reaction fouling in a Hydrocarbon vaporizer[120]. Working on Kerosene in the laminar region at various pressures between 16 and 36 psia and a surface temperature range of 60 to 1200 °F, he found a complex plot of the logarithm of the initial fouling rate versus the reciprocal absolute temperature for all the air saturated runs. (Figure 2.2.14). With increasing temperature the initial fouling rate increased in the all liquid phase flow region, decreased during the vaporization region

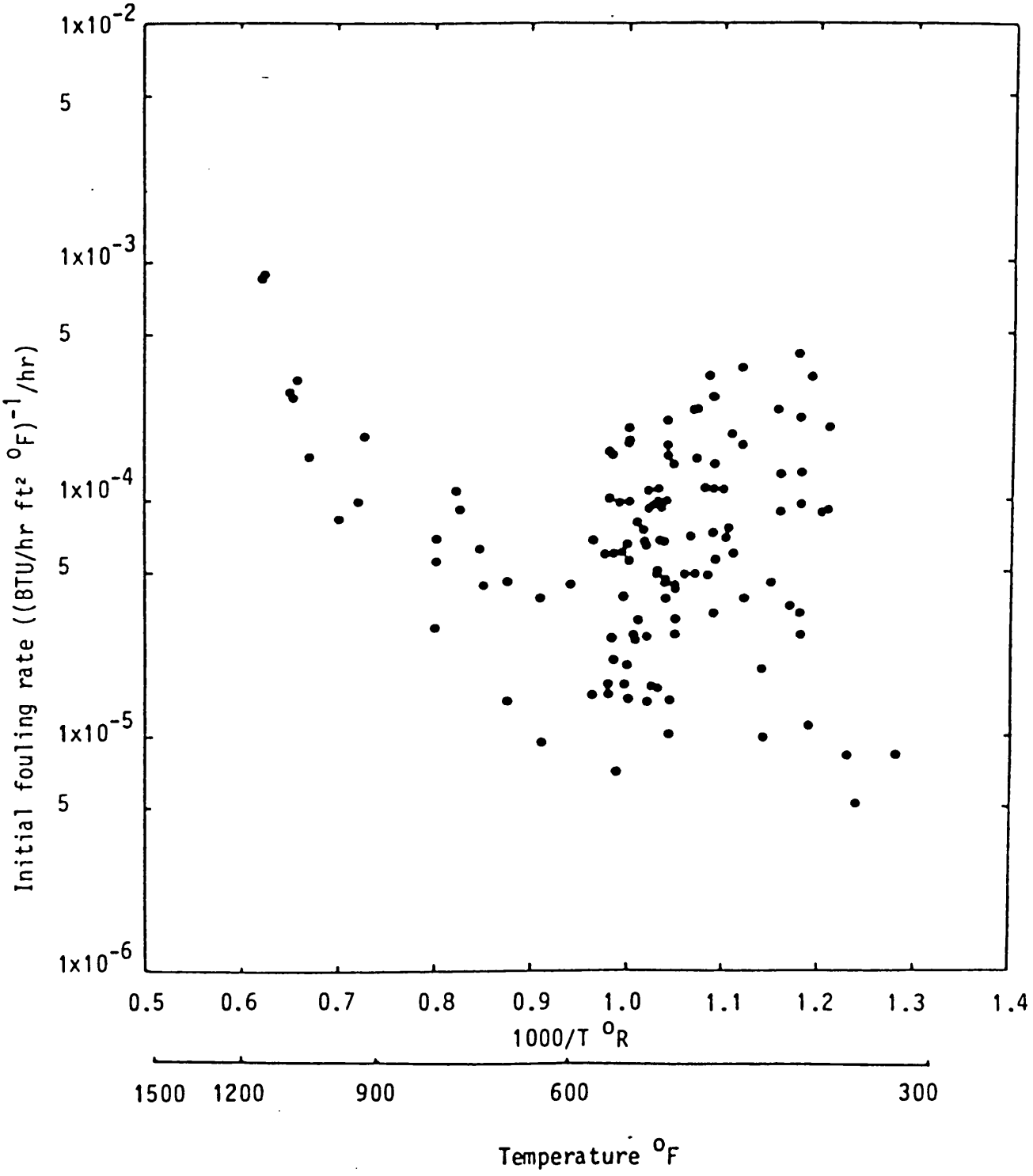

Figure 2.2.14[120] Logarithm of initial fouling rate versus reciprocal absolute temperature.

and increased again in the all vapour phase flow region. Decreasing the oxygen content from 100% saturation to 15% saturation caused a decrease in the initial fouling rate by between three and sixty times. The critical dependence of the initial fouling rate on air or oxygen content during subcooled heating and vaporization was suggested to be due to the formation of bubbles of oxygen rich gas on the heat transfer surface. The formation of such bubbles required the transport of oxygen to the heat transfer surface thus leading to an increase in the rate of the autoxidation fouling process with increasing oxygen content.

During vaporization the initial fouling rate varied circumferentially around the tube. The highest rate was obtained at the bottom of the tube where the liquid tended to flow. The lowest rate was obtained at the top of the tube where the vapour tended to flow.

It was concluded that the complex plot was a result of a change in the dominant chemical mechanism from free-radical autoxidation in the liquid phase to thermal cracking in the vapour phase.

2.2.3 Mechanisms

Chemical reaction fouling involves a complex physico-chemical mechanism within the boundary layer of heating surfaces[135]. It is likely to be interrelated with both particulate and crystallization fouling. When material of increasing molecular weight and structural complexity exceeds its solubility in the fluid it forms a deposit which, initially, may not be a rigid solid. This process occurs not necessarily at the heat transfer surface, but rather in a reaction zone where the local conditions are favourable[59]. The foulant may have to be transported, adsorbed, or otherwise

attached to the surface. Deposit formation from hydrocarbon streams may be the end result of a complex sequence of cracking, autoxidation and polymerisation reactions. Adhesion is necessary and release may also occur. Once formed deposits may also degrade with time and temperature to form hard coke[10].

2.2.3.1 Chemical Mechanisms

It is believed[194,208] that deposits in air saturated hydrocarbons form as a result of free radical chain reactions involving molecular oxygen. Apart from autoxidation, there may be other polymerisation mechanisms going on simultaneously[101,208], depending on the process conditions.

2.2.3.1.1 Autoxidation/Polymerisation

Since thermal cracking reactions do not occur at temperatures much below 650°K[64,85,174,184], it is widely accepted that low temperature thermal degradation is due to free radical autoxidation[26,29]. Different substances have been shown[101] to be able to produce free radicals which could initiate chain reactions. Trace levels of compounds of oxygen, nitrogen, sulphur or metal ions[188, 193,195], either from the surface in contact with the process stream or dissolved in it, can either by themselves act as reactive radicals[56] or help to form reactive radical peroxides[22,193].

Autoxidation reactions are initiated by hydrogen abstraction from the substrate molecule (R-H), by a free radical Z. .

Initiation

$$R\text{-}H + Z\cdot \rightarrow R\cdot + HZ \qquad (10)$$

Chain propagation then proceeds via a peroxy radical

$$R\cdot + O_2 \rightarrow ROO\cdot \qquad (11)$$

$$ROO\cdot + RH \rightarrow ROOH + R\cdot \qquad (12)$$

Termination can occur via the following reactions:

$$R\cdot + R\cdot \rightarrow R\text{-}R \quad (13)$$

$$ROO\cdot + R\cdot \rightarrow ROOR \quad (14)$$

$$ROO\cdot + ROO\cdot \rightarrow ROOR + O_2 \quad (15)$$

where:

RH is a hydrocarbon molecule,

ROOH is a hydroperoxide,

ROOR is an acid, aldehyde, alcohol, ketone, or ester

Z· is a free radical having sufficient reactivity to abstract a hydrogen atom.

R· substrate radical

ROO· peroxyl radical

Reaction (11) is rapid with sufficient oxygen. In this case most of R· would be used up and it is generally considered that reaction (15) is then the most important termination reaction. In the progress of the reaction chain, homolysis of the O–O bond in the hydroperoxide leads to the formation of more radicals, which can initiate further hydrogen abstraction from the substrate molecule.

$$RO\text{-}OH \rightarrow RO\cdot + \cdot OH \quad (16)$$

Breeding, where one free-radical generates three may take place via reactions (11), (12) and (16). With dissolved trace metals (or surface interaction) free-radicals may be generated by the following oxidation-reduction reactions:

$$ROOH + M^{++} \text{ (metal ion)} \rightarrow RO\cdot + OH^{-} + M^{+++} \quad (17)$$

$$ROOH + M^{+++} \rightarrow ROO\cdot + H^{+} + M^{++} \quad (18)$$

$$R\text{-}H + M^{+++} \rightarrow R\cdot + H^{+} + M^{++} \quad (19)$$

How the above reactions proceed is determined by the strengths of the bonds broken (see bond energies in Table 2.2.5) and the stabilities of the free radicals formed. A considerable

Table 2.2.5[68]

C-H Bond Energies in Hydrocarbons

Hydrocarbon	Bond	Bond Energy $kJgmole^{-1}$
benzene	C_6H_5-H	426
ethane	C_2H_5-H	410
n-propane	nC_3H_7-H	397
i-propane	iC_3H_7-H	393
n-butane	nC_4H_9-H	393
t-butane	tC_4H_9-H	389
toluene	$C_6H_5CH_2-H$	347
propylene	$CH_2=CH-CH_2-H$	322

increase in the rate of oxidation is found when there is a double bond or an aromatic group in the position α to the group undergoing oxidation, e.g. Olefins and alkyl substituted aromatic hydrocarbons[68,152]. Oxidation of unsubstituted aromatic hydrocarbons and of primary C-H bonds in paraffins is difficult, but becomes increasingly easier for secondary and tertiary C-H bonds[152]. It is believed that at relatively low temperatures, radical intermediates can react with olefins (unsaturates) from the hydrocarbon stream leading to oxidative polymerisation, the end product having a gum-like appearance[193]. At higher temperatures, oxidative dehydrogenation of paraffins (saturates) generates additional olefins which can sustain the oxidative polymerisation reactions.

2.2.3.1.2 Vapour Phase Thermal Cracking

In a cracking furnace coke is formed via secondary or synthesis reactions of the products of the primary or degradation reactions (cracking and dehydrogenation)[79]. The secondary reactions involve firstly cyclization of hydrocarbon chains to form aromatics and secondly condensation of aromatics to form high molecular weight polycyclic aromatic systems. Primary cracking reactions are relatively fast in the gas phase and take place at temperatures in excess of about 650 °K[79]. Aromatization occurs preferentially at temperatures in excess of 950 °K, while chemical condensation of aromatics in the liquid phase can occur at temperatures in the range 650 to 800 °K[79]. Cross linking between polycyclic systems can occur at temperatures below 650 °K[79]. Synthesis reactions are relatively slow and therefore coke deposition can be minimised in a thermal cracking furnace by operation at low residence times[79].

In general, the chemical mechanisms of the primary cracking reactions are reasonably well understood[213]. On the

contrary the secondary reactions are poorly accounted for. Both Diels-Alder and radical pyrocondensation mechanisms have been proposed[79].

2.2.3.2 Physical Mechanisms

Adhesion of foulant particles to the heat transfer surface may occur only after the reactants (precursors and/or particulates) have been transferred by convective mechanisms to the reaction zone. Release or removal by, for example dissolution, spalling, fluid shear, etc., of reaction products from the surface back to the fluid bulk may lead either to further fouling reactions or to deposition on cooler surfaces in downstream units[37].

2.2.3.2.1 Adhesion

Studies in adsorption have shown that the wettability and heat of immersion of solid surfaces increase as the difference between the surface free energy of the solid and that of the adjacent liquid increases[135,218]. The surface free energies of all liquids (excluding liquid metals) are less than 100 erg/Cm^2 at ordinary temperatures[218]. The surface energies for conventional metallic heat transfer surfaces, e.g. stainless steel, 70-30 CrNi, 90-40 CrNi, and titanium are in the range 1800 to 1300 erg/Cm^2[166]. Roughness increases the contact surface areas so that the true contact area is much larger than the apparent surface area[166,218]. Wenzel's equation[166,218] predicts very important behaviours of rough surfaces:

The wettability of wettable rough surfaces is larger than that of the corresponding smooth surfaces; it follows therefore that stronger adsorption should occur on rough surfaces since there would exist a greater difference between the surface free energies of the solid surface and the adjacent fluid phase[166].

Adhesion strength is markedly influenced by the roughness of metal surfaces; this is due to the penetration of the fouling products into the interstices created by the roughness, followed by hardening of the deposits[166]. It is generally accepted also that the effective viscosity of a fluid near a solid surface increases considerably as the surface is approached[108]; the arguments for this phenomenon are based on molecular adsorption on surfaces. The first molecular monolayer of fluid is retarded in flow by this adsorption or adhesion on solid surfaces[218]. The slowing down of fluid velocity in subsequent monolayers is caused by cohesion between molecules in the fluid[135]. Nevertheless, a very rough surface supplementally adds to the effect of adhesion by introducing a retarding effect caused by the roughness peaks penetrating into the fluid boundary layer[135].

Charlesworth[34], working with a very pure organic nuclear coolant found a tightly bonded organic deposit which he postulated must be formed by the pyrolytic binding of submicron particulates present in the coolant to the wall. For these particulates it was assumed that Brownian movement is a likely transfer mechanism to the wall and for bonding to take place, the contact time and position would be important. This mechanism also explains why Charlesworth found that organic fouling only set in after an entry length and that the nature of the deposit changed along the tube; presumably a significant contact time is needed to bring about the chemical changes to form an organic deposit. Similar results are reported by Trilling[202].

After Parkins[159]; Watkinson and Epstein[210] incorporated a sticking probability,S in their model to account for

deposition from gas oil. They argued that S was dependent upon Kinetics and hydrodynamics to give:

$$S = C_1 e^{-E/RT_W}/(U^*)^2 \quad (20)$$

For deposition of particles, C_1 may be taken as the minimum friction velocity squared, i.e. $C_1=(U^*min)^2$.

where:

$$U^*=(\tau_S/\rho)^{\frac{1}{2}} \quad (21)$$

τ_S =fluid shear stress at surface

ρ=fluid density

E- activation energy

R- universal gas constant

T_W- surface temperature

Their model is discussed more fully in Section 2.2.5.1.4.

2.2.3.2.2 Removal and Release

Ruckenstein and Prieve[169] and others[41-43,72] have recognized that a particle in the vicinity of the wall would be under the influence of several forces which can profoundly affect whether or not it will remain there. The most important of these forces are the London-Van der Waals forces, which are always attractive; the electrical double layer interaction forces, which are attractive if the particle and the wall have Zeta potentials of opposite sign[72], and repulsive if these charges are of the same sign; and a hydrodynamic viscous interaction force whereby the fluid friction on the particle increases greatly as it moves normal to the plane surface.

A re-entrainment process can be expressed in terms of a local release flux, Φ_r; most mathematical models of fouling[72] show the release flux increasing with the mass of deposited foulant.

One exception is that of Bartlett[14] who assumed that Φ_r is a function of the deposition flux, Φ_d. Taborek et al [187] proposed a general dependence of the release flux on mass, i.e.

$$\Phi_r \propto m^x \tag{22}$$

where:

m = mass of foulant

x = order of m

In practice however, they assumed that x=1, on the basis of the Kern-Seaton assumption[115] (equation 3) which gave a good rectification of their fouling data.

Beal's[16] latest model distinguishes between the loose deposit which is assumed to be removable by the circulating liquid and the more adherent interior deposit, which is not subject to such removal. This distinction was noted qualitatively by Atkins, and Perera and Rafique[10,162]. Beal[16] assumed that the loose deposit was sintered into the adherent deposit at the interface between the two. The deposition-sintering-removal model was unique in its allowance for a variation of density and thermal conductivity of deposit with the mass of deposit. Such variations have been reported by Meetor et al [146].

Re-entrainment is built explicitly into the models of Kern-Seaton[115] and of Taborek et al [187] in terms of the fluid shear stress. (See Section 2.2.1). Gutman[93] derived a re-entrainment equation based on the turbulent burst theory of Cleaver and Yates[41]. The fraction of surface covered by turbulent bursts was derived from the Kern-Seaton model[115] as a function of β, the rate of approach to the asymptote.

Crittenden and Kolaczkawski[59] proposed that diffusion

of foulant back into the bulk fluid may be important when the deposit contains relatively mobile species. The solubility of such species in the bulk fluid is likely to reduce as the molecular weight increases but increase with increasing temperature[59]. However, higher interfacial temperatures generally tend to further degradation to form higher molecular weight deposits[208].

2.2.4 Chemical Reaction Fouling Evaluations, Tests and Measurement Techniques

Dynamic test techniques should take into consideration the geometry of the industrial surface which is subject to fouling[189] whether it be the inside of a tube, circular cylinder, sphere, outside of U-tube, metallic strip or plate, porous plug, wire, or a more complex geometry such as the shell side of an exchanger.

Residence times in batch or circulating continuous flows must be considered when building a rig to monitor fouling. Usually a continuous technique is preferable as it simulates industrial situations better. The choice of the type of heating, whether sensible fluid, condensing vapour, electrical resistance of the test section itself, or indirect electrical heating should preferably simulate industrial experience.

Deposit formation may be monitored visually, morphologically, by direct weighing, microscopically, by pressure drop, thermally, by radiation (x-ray)[92], electrolytically and chemically. Chemical analysis can be carried out quantitatively by determining the composition of the elements and compounds in the deposit material. Solubility and spectroscopic methods (e.g. IR, UV, Mass Spectrometry, NMR, ESR, and X-Ray diffraction) could aid in identifying the deposit chemically and help to determine the

mechanism of formation and aging of the deposit.

2.2.4.1 Hot Wire Test[22,99]

A preheated petroleum stream contacts a hot metal wire in a test cell. The feed stream is recirculated and the coiled metal wire probe is electrically heated. Knowing the fluid temperature and the wire temperature the heat transfer coefficient can be calculated. The variation in the heat transfer coefficient reflects the rate of deposit formation.

2.2.4.2 Kinetic Unit[194]

Liquid hydrocarbon and air are introduced in a tubular reactor having several separate reactor heaters. Carefully weighed metal strips are positioned in the centre section of each heater zone. A thermowell extends down the length of the tubular reactor, and an individual thermocouple is positioned in each zone. At the end of each time run (4 hr.)[194], the metal strips are removed carefully and weighed on a precision balance. The deposit formation rate is calculated as grams of deposit per square centimeter of metal surface per unit reaction time.

2.2.4.3 Heat Exchanger Loop[29,179,208]

A batch of the test liquid is continuously circulated through the heated section. The test section is heated by passing a current through the tube wall or by use of a heat transfer fluid. The heat transfer calculations are based on the outside tube wall temperature and the power dissipated in the tube. This technique is noted as being the most representative of actual exchanger situations.

2.2.4.4 Fuel Coker Test[83] (ASTM - CRL or Erdco CFR)

This test makes use of the increase in pressure drop

due to deposition on a heated metal filter (ASTM approved for measuring thermal stability of aviation turbine fuel). The hydrocarbon is preheated in an exchanger to 400°F and then allowed to flow through an electrically heated metal filter which is held about 100°F higher than the sample temperature. The fouling resistance is determined from the increase in pressure drop with time. If the pressure drop-time curve is plotted on a semilog scale, then the ratio of the test slope to the slope for a low fouling tendency stock gives a fouling index.

2.2.5 Predictive Fouling Models

Steady and unsteady state models of fouling have been reviewed by Epstein[72], Bott and others[21,114,205]. It is very unlikely that any single model will be generally applicable since chemical reaction fouling is both chemically and physically complex. Chemical reaction fouling models are summarized chronologically in Table 2.2.6). Reflecting the general observation that organic deposits are often tenacious, some models do not include removal or release terms. All models relate to in-tube fouling only.

2.2.5.1 Chemical Reaction Fouling Models

Exhaustive knowledge of the chemical and physical mechanisms is important in determining the rate of deposition in chemical reaction fouling. Even for surface reactions of simple mechanism and kinetics the solutions to the heat, mass and momentum transfer equations are difficult to obtain without invoking further assumptions[59,156]. For example, for turbulent flow in a tube with reaction at the surface, several authors[165,214] have demonstrated that even with simplifying assumptions about the reaction kinetics the mathematical analysis is complex.

Table 2.2.6 Chemical Reaction Fouling Models

Authors	Application	Deposition Term	Removal Term	Remarks
Nelson[154] (1934)	hydrocarbon streams in petroleum refining	deposition depends on the film volume at surface	increase fluid velocity reduce the film volume	fouling decreased by higher velocity optimal flow rate
Parkins[159] (1961)	nuclear coolant systems, particulate fouling	deposition is composed of a mass particle flux to the wall, and a sticking probability. suspended solids. deposition in terms of drag force on particle, wall and activation energy	none considered	single process of transport of suspended particles to the wall. Brownian motion, electrostatic forces and chemical bonds stick them.
Nijsing[156] (1964)	organic coolant in nuclear reactor	hydrodynamic boundary layer and diffusion partial differential equations (1) instantaneous first order reaction in zone (2) very rapid crystallization at hot surface	product diffusion back to the fluid bulk is an integral part of the differential equations	(1) solution with diffusion control fits plant data i.e. fouling increases with velocity (2) extended to consider colloidal transfer to the hot surface.
Watkinson & Epstein[209] (1969)	liquid phase fouling from gas oils	mass transfer and adhesion of suspended particles (1) sticking probability proportional to exp(-E/RT) (2) sticking probability	first order Kern & Seaton release term	(1) correct prediction of initial fouling rate dependence on velocity

Table 2.2.6 Continued

		inversely proportional to hydrodynamic forces on the particle as it reaches wall.		(2) incorrect prediction of asympotic resistance on velocity.
Jackman & Aris (1971)[110]	vapour phase pyrolysis	kinetics control - two reactions: (1) first order dissociation of A into products (2) zeroth order coke formation	none considered	(1) quasi-steady state assumption invoked (2) untested
Fernandez-Baujin & Solomon (1976)[77]	vapour phase pyrolysis	kinetics and/or mass transfer control with first order reaction	none considered	solution with mass transfer control fits plant run-time data i.e. fouling increases with velocity
Sundaram & Froment (1979)[184]	vapour phase pyrolysis of ethane	kinetics control (1) at surface temperature (2) first order in propylene concentration (product of primary cracking reactions).	none considered	(1) quasi-steady state assumption invoked (2) good agreement between industrial and numerically simulated data
Crittenden & Kolaczkowski (1979)[59]	unspecified	kinetics and/or mass transfer control with first order reaction	(1) diffusion of foulant back into fluid bulk (2) first order Kern & Seaton release term	(1) untested (2) complex - many parameters (3) extended to a two layer model

2.2.5.1.1 Nelson

Of the many correlations available, the Dittus-Boelter[66] equation can be used to describe the heat transfer coefficient on the inside of a tube:

$$h = 0.023 \times \frac{K_f}{d} \times (Re)^{0.8} (Pr)^n \quad (23)$$

where:

K_f = fluid thermal conductivity

d = inside diameter of the tube

Pr = Prandtl number

Re = Reynolds number

n = 0.4 for heating

Equation (23) applies only for single phase turbulent flow. The heat transfer film thickness, δ_h providing the resistance to heat transfer may be obtained from this equation as:

$$\delta_h = \frac{K_f}{h} = \frac{43.5\ d^{1.8}}{(4G/\pi\mu)^{0.8} (Pr)^{0.4}} \quad (24)$$

in which μ = fluid viscosity G = mass flow rate

Nelson[154] suggested that the rate of coking in petroleum refining equipment is directly dependent upon the volume of fluid in the film at the heat transfer surface. The volume of this film which is exposed to high temperatures is proportional to δ_h. He proposed therefore that by increasing the fluid velocity a reduction in the coking rate could be achieved by reducing the volume of fluid exposed to a high temperature. Nelson[154] considered that there was little advantage in using velocities in excess of 4m/s, since the pressure drop was greatly increased for only slightly further reductions in the coking rate.

2.2.5.1.2 Parkins[159] (See Sections 2.2.3.2.1 and 2.2.6)

2.2.5.1.3 Nijsing

Nijsing[156] assumed that fouling from an organic coolant in a nuclear reactor was caused by the instantaneous, irreversible reaction of a precursor to a product which crystallized rapidly when compared with its diffusion rate to the reaction zone. This molecular process was described as:

$$\text{Fluid + Solute } [A]_0 \xrightarrow{T_C} \text{Fluid + Insoluble } [B], \quad T_S > T_C \qquad (25)$$

The assumptions made were as follows:

(a) The fluid contains a solute A of initial concentration $[A]_0$, which above a critical temperature, T_C (less than the surface temperature T_S) becomes unstable and decomposes into an insoluble compound B.

(b) The fluid passes in turbulent flow through a channel of hydraulic diameter, d.

(c) The reaction product B crystallizes at the heating surface without forming particles in the fluid.

(d) The physical process involving the change of phase at surface-fluid interface is very rapid compared with the diffusion rate of reaction products towards the heating surface.

(e) The reaction is first order, instantaneous and irreversible.

(f) All physical properties are independent of temperature.

(g) The diffusivities of A and B are equal, i.e. $D_A = D_B$.

Solving the hydrodynamic and diffusion equations within the boundary layer limitations gave the average rate of deposition of product, q_m as:

$$q_m = 0.0136\ M_B[A]_0\ \frac{D_A}{d}\ (Re)^{0.875}\ (Sc)^{0.33},\ \mu g/m^2 s \qquad (26)$$

in which:

M_B = molecular weight of B

$Sc = \frac{\mu}{\rho D_A}$ = Schmidt number (27)

ρ = fluid density

μ = fluid viscosity

The experimental fouling rate of 303 $\mu g/m^2 s$ compared reasonably well with the predicted value of 500 $\mu g/m^2 s$. Consequently, Nijsing concluded that the rate of deposition is controlled by the diffusion of the solute A.

Nijsing also considered that the decomposition of thermally unstable components in the bulk could give rise to the formation of colloidal particles which could then migrate towards the wall. For a given impurity level "molecular fouling" was predicted to be much more rapid than "particle fouling".

2.2.5.1.4 Watkinson and Epstein

The fouling of a single tube sensible heat exchanger by a sour petroleum gas oil was studied by Watkinson and Epstein[209]. (Figure 2.2.15). The results were compared firstly with the predictions of a mathematical model proposed originally by Kern and Seaton[115], and then with the predictions of a transfer-adhesion-release model developed by themselves. Their model was based on the premises that, (1) deposition is caused by mass transfer of suspended particles to the wall followed by adhesion of some particles on the surface, (2) removal is a first order function of deposit thickness as proposed by Kern and Seaton[115].

The net rate of fouling, that is the difference between the deposit-adhesion rate and the release rate was given by:

$$\dot{R}_f(\theta) = a_1 NS - a_2 \tau X \quad (28)$$

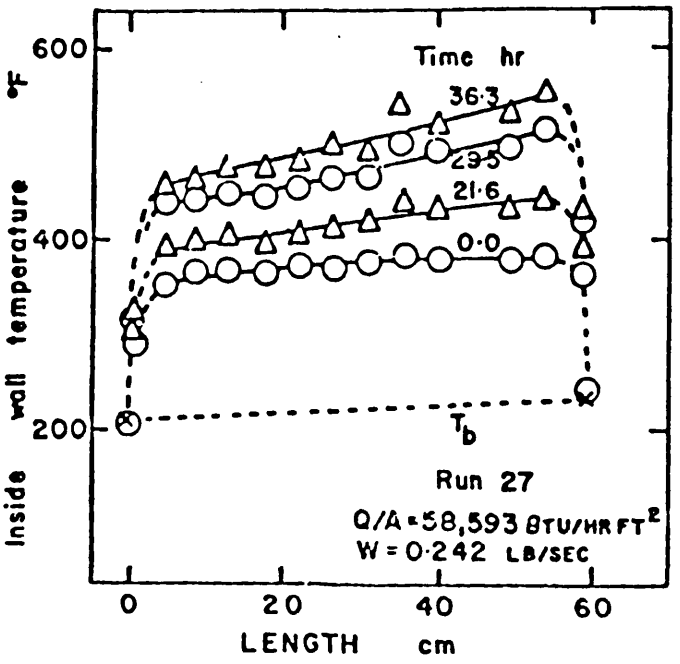

Tube wall temperature profiles and terminal fluid temperatures.

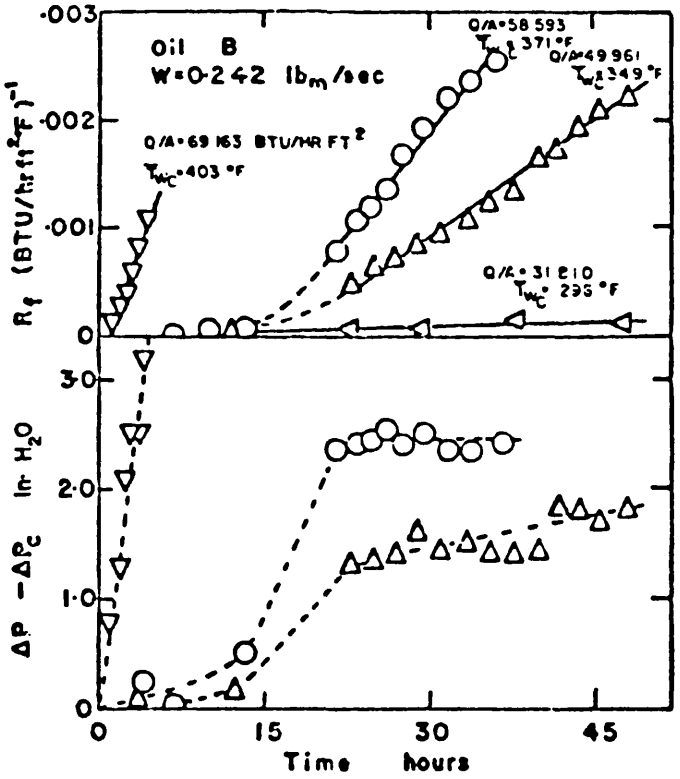

Effect of heat flux on fouling resistance and pressure drop increase.

Figure 2.2.15 (209) Results of Watkinson and Epstein

where:

a_1, a_2 = constants

$\bar{N}$ = mass flux of particulate material

S = a sticking probability

τ = shear stress at the wall

X = deposit thickness

The mass flux was assumed to be proportional to the difference in particulate concentrations in the bulk, C_b, and at the surface, C_w. The sticking probability was assumed to be proportional to the physico-chemical adhesive forces binding a particle to the wall. S is dependent on T_s according to the Arrhenius equation, and inversely proportional to the hydrodynamic forces on the particle as it reaches the wall. Hence, the fouling rate was given by:

$$\dot{R}_f\ (\theta) = \frac{a_3 (C_b - C_w) \exp(-E/RT_s)}{uf^{0.5}} - a_4 u^2 f X \qquad (29)$$

in which:

f = friction factor and u = average fluid velocity

a_3, a_4 = constants

Equation (29) correctly predicts the experimental dependency of the initial fouling rate (i.e. when x=0) on temperature and flow rate. However, it does not give the correct dependency of the asymptotic fouling resistance on the flow rate (i.e. when $\dot{R}_f\ (\theta) = 0$).

2.2.5.1.5 Jackman and Aris

Jackman and Aris[110] considered that production in a thermal cracking furnace may be maximised by correct control of temperature, thus preventing coke from building up too rapidly. The kinetics of pyrolysis were simplified to include only two

reactions whose rates were dependent upon temperature. Again, they assumed a quasi-steady state, i.e. the reactor was regarded as being in the steady state condition corresponding to the current coke thickness. The rate of coke formation was assumed to be relatively slow and the two reactions considered were:

(1) First order endothermic dissociation of the hydrocarbon into products.

(2) A zero order formation of coke per unit surface area.

They reported that if the temperature of the furnace is kept at its maximum value right from the start of the reactor service, this may promote so rapid a formation of the coke layer that the useful life of the reactor is shortened. The computations performed with a two segment reactor employing parameter values suitable for methane pyrolysis showed that an intermediate controller guides the reactor through 80% of its period of service. This control results in an initial conversion of 0·79 which decreases very slightly before the control variables attain their maximum permissible value. The two isothermal segments are constrained by the requirement that the wall temperatures should not exceed 2690°F and that the conversion should not drop below 70%.

2.2.5.1.6 Fernandez-Baujin and Solomon

Fernandez-Baujin and Solomon[77] have incorporated the film theory for mass transfer into the deposition rate expression for coking in a steam cracking furnace. They realized that whereas the rate of the coke formation reaction is greatest at the tube wall the precursors of the coke must diffuse to the surface from the fluid bulk. They proposed a two step mechanism as follows:

(1) Mass transfer of coke precursors from the gas bulk to the tube wall.

(2) Chemical reaction of the precursors at the wall.

The mass transfer flux, N, of reactants to the reaction zone (surface) was given in terms of a partial pressure driving force and a mass transfer coefficient, Kp.

$$Np = Kp\ (Cp_B - Cp_i) \tag{30}$$

where:

p = precursors

B = bulk conditions

i = interface conditions

The chemical reaction rate, r, was assumed to be first order with respect to precursor concentration.

$$r = k\ Cp_i \tag{31}$$

where:

k = reaction rate constant

At steady state, the reaction rate was assumed to be balanced by the mass transfer flux. Hence by eliminating Cp_i from equations (30) and (31):

$$r = \frac{C_{PB}}{1/Kp + 1/k} \tag{32}$$

In view of the fact that the tube wall temperature in cracking furnaces is very high, Fernandez-Baujin et al[77] concluded that the reaction rate constant is very much greater than the mass transfer coefficient i.e. $k >> Kp$

Equation (32) therefore was reduced to:

$$r = Kp\ Cp_B \tag{33}$$

The mass transfer coefficient was expressed in terms of fluid physical properties. The Chilton and Colburn analogy[40] for

mass transfer gives:

$$St = \frac{Kp}{Uav} = \frac{f}{2} (Sc)^{-0.67} \qquad (34)$$

$$St = \text{stanton number} = \frac{h}{\rho u Cp}$$

where:

Kp = mass transfer coefficient

Uav = average fluid velocity

f = friction factor

Sc = Schnidt number

h = heat transfer coefficient

ρ = fluid density

u = fluid velocity

Cp = heat capacity

The friction factor is a function of roughness and Reynolds number. For a given roughness it is well correlated[151,163] by:

$$f = \lambda Re^{-0.2} \qquad 5x10^3 < Re < 2x10^5 \qquad (35)$$

Re = Reynold number

λ = a function of roughness

Substitution of equations (34) and (35) in equation (33) gave the coking rate as:

$$r = \frac{K^* G^{0.8}}{(d-2x)^{1.8}} \qquad (36)$$

in which:

G = mass flow rate

K* = a function of feedstock, cracking severity and selectivity, dilution steam ratio and other system properties

x = coke deposit thickness

d = inside tube diameter

The furnace run length, θ_{RL} was then given by:

$$\theta_{RL} = \frac{Xmax}{r} \qquad (37)$$

in which:

Xmax = coke thickness which coincides with the maximum allowable tube temperature or pressure drop.

In agreement, Chen and Maddock[36] reported that the coking rate in high temperature olefin furnaces was dependent upon mass transfer and not surface kinetics whilst for lower temperature operation, the reverse applied.

2.2.5.1.7 Sundaram and Froment

Sundaram and Froment[184] invoked a quasi-steady state assumption in their study of the kinetics of coke deposition in the thermal cracking of propane over the temperature range 1328-1598°F. (See Figure 2.2.16). They said that since the coking rate is much less than the precursor throughput rate, the energy, continuity, and pressure drop equations need not contain explicit time dependencies, but are updated periodically for changes in tube diameter as a result of deposition. By taking incremental steps along the tube, they numerically integrated the equations to give results which compared well with plant data. In general agreement with Shah et al[175], Sundaram and Froment[184] found that the initial coking rate in a stirred reactor vessel decreased in a short time to an asymptotic value. The asymptotic rate increased with propane conversion and temperature. By comparing the kinetic results with various reaction schemes to account for coke formation, Sundaram and Froment[184] concluded that coke is formed from propylene which is a primary product of the cracking reactions.

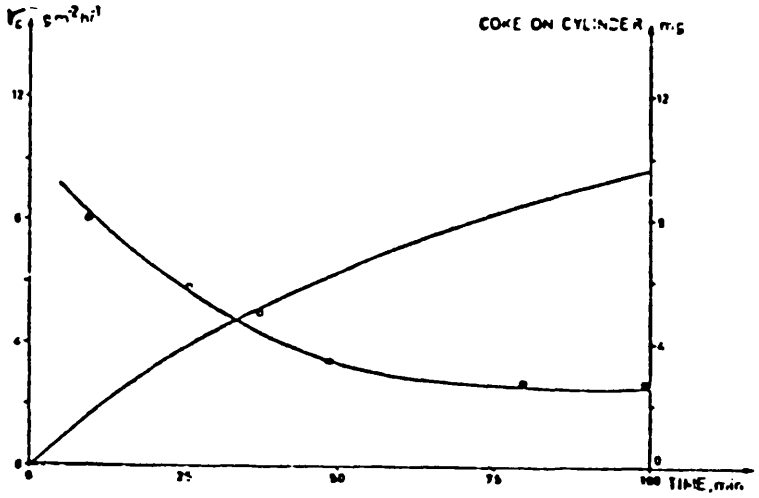

Rate of coke formation and coke content on cylinder as a function of time.

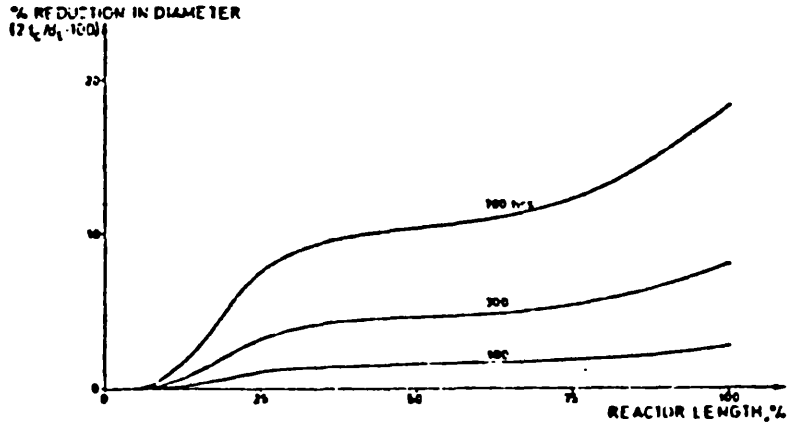

Coke profiles in an industrial reactor, Model II for coking.

Figure 2.2.16[184] (Reproduced from Sundaram and Froment)

For the tubular reactor, it was assumed that the coke formation rate depended in first order on propylene concentration and that the reaction occurred at the tube surface at a temperature, T_S. From elementary kinetics

$$\text{rate} \propto A \exp(-E/RT_S) \quad (38)$$

The increase in coke thickness Δx in a time interval $\Delta\theta$ in any increment was given by:

$$\Delta x = A \exp(-E/RT_S)\ C.\Delta\theta/\rho_C \quad (39)$$

where:

C = average propylene concentration in an increment

ρ_C = coke density

In the simulation, the outlet pressure was held constant whilst the inlet pressure was raised to maintain the gas flowrate. The temperature profile for clean tube conditions was retained because of the uncertainty of the heat flux profile with time. The simulation was run for a furnace operating period of 700 hr. and the final predicted coke layer thickness was in good agreement with the value found in practice. (Figure 2.2.17). The amount of coke deposition, when expressed per unit reactor volume rather than per unit surface area, was found to be much higher than the industrial value. It is not possible to determine from their model the effect that the fluid flow rate has on the deposition rate.

2.2.5.1.8 Crittenden and Kolaczkowski

Crittenden and Kolaczkowski[58] have extended the two step model (kinetics and diffusion) proposed by Fernandez-Baujin et al[77]. They considered that the foulant, whilst still mobile, could be transferred back to the fluid bulk (where its concentration was assumed to be relatively low) to be deposited else-

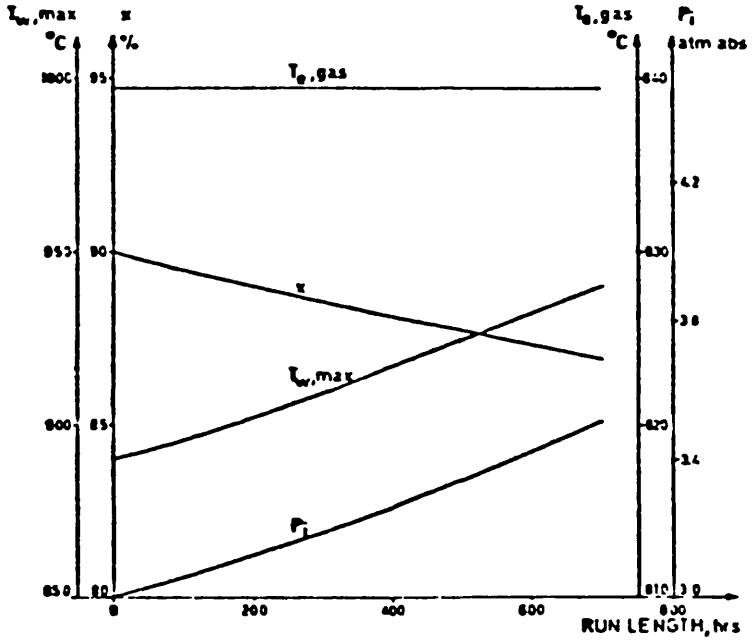

Maximum tube skin temperature, outlet gas temperature, conversion and inlet pressure as a function of run length.

Figure 2.2.17 (184) (Reproduced from Sundaram and Fromant)

where. The back diffusion flux of foulant N_f was given by

$$N_f = K_f(C_{fi} - C_{fB}) \tag{40}$$

where:

K_f = mass transfer coefficient for the foulant

C_{fi} = foulant concentration at the deposit-fluid interface, i.e. its solubility

C_{fB} = concentration of the foulant in the bulk, assumed to be zero

Subtraction of equation (40) from equation (32) gave

$$r = \frac{C_{PB}}{\frac{1}{Kp} + \frac{1}{k}} - K_f C_{fi} \tag{41}$$

In obtaining the rate of increase in fouling resistance, Crittenden and Kolaczkowski[59] assumed

(1) The deposition reaction was first order.

(2) Friction factors were a function of Reynolds number only.

(3) Application of the Chilton and Colburn analogy. Thus mass transfer coefficients were expressed in terms of mass flow rate, friction factor, and fluid properties.

(4) Elementary kinetics apply, and the dependency of the rate constant on temperature is described by the Arrhenius equation.

Substitution of equations (34), (35), and (38) into equation (41), the rate of fouling incorporating back diffusion was given by:

$$\dot{R}_f(\theta) = \pi_1 = \frac{1}{\mu_f K_f}\left[\frac{C_{PB}}{\frac{\rho(d-2x)^{1.8}(Sc_p)^{0.67}}{1.213\lambda\mu^{0.2}G^{0.8}} + \frac{1}{A\exp(-E/RT_s)}} - \frac{1.213\lambda\mu^{0.2}G^{0.8}C_{fi}}{\rho(d-2x)^{1.8}(Sc_f)^{0.67}}\right] \tag{42}$$

in which:

ρ_f = density of foulant

K_f = effective thermal conductivity of foulant

Sc = Schmidt number

P = precursor conditions

f = foulant conditions

Equation (42) predicts a critical dependency of the fouling rate on mass flowrate. For example, at lower temperatures, with small tube diameters and higher mass flowrates deposition is likely to be controlled by reaction kinetics (i.e. $k << Kp$) and therefore according to equation (42) the rate of fouling decreases with increasing mass flowrate. At much higher temperatures, according to equation (42), it is predicted that mass transfer controls (i.e. $k >> Kp$), and the rate of fouling increases with increasing mass flow rate. Equation (42) was reduced to:

$$\dot{R}_f(\theta) = \frac{1.213\lambda\mu^{0.2}G^{0.8}}{\rho(d-2x)^{1.8}\rho_f K_f}\left[\frac{C_{PB}}{Sc_p^{0.67}} - \frac{C_{fi}}{Sc_f^{0.67}}\right] \quad (43)$$

At much higher temperatures, it was assumed that severe degradation of the foulant would occur and thus its mobility in the bulk fluid would be reduced. Crittenden and Kolaczkowski[59] therefore assumed that the interfacial foulant concentration was minimal, i.e. $C_{fi} \rightarrow 0$. Hence equation (43) became

$$\dot{R}_f(\theta) = \frac{1.213\lambda\mu^{0.2}G^{0.8} \cdot C_{PB}}{K_f\rho_f \quad \rho(d-2x)^{1.8} \cdot Sc_p^{0.67}} \quad (44)$$

The deposition rate dependence in this case, on mass flowrate, tube diameter and diffusion coefficient is virtually identical to the predictions of Nijsing[155] (Equation 26). After Kern and

Seaton[115] the rate of decrease of fouling (i.e. the removal or release term) was assumed to be proportional to both the shear stress at the wall τ and the deposit thickness, x. A first order dependence of foulant removal rate on thickness gave

$$\dot{R}_f(\theta) = - \frac{\tau x}{\psi K_f} \tag{45}$$

in which ψ = a function of deposit structure (or deposit-surface structure). Considering the shear stress in terms of fluid and system properties, i.e.

$$\tau = \rho U_{av}^2 \frac{f}{2} \quad \text{and,} \tag{46}$$

$$U_{av} = \frac{\mu \cdot Re}{\rho (d-2x)} \tag{47}$$

Substitute (46), (47) and equation (35) in equation (45), hence

$$\dot{R}_f(\theta) = - \frac{0.607\lambda\mu^{0.2} G^{1.8}}{\rho\psi K_s (d-2x)^{3.8}} \cdot \frac{X}{K_f} \quad \text{and,} \tag{48}$$

$$\dot{R}_f(\theta) = - \pi_2 R_f \tag{49}$$

Addition of equation (49) to the right hand side of equation (42) results in a first order differential equation of the form

$$\dot{R}_f(\theta) = \pi_1 - \pi_2 R_f \quad \text{for } 2x \ll d \tag{50}$$

where π_1 and π_2 are defined in equations (42) and (49) respectively. Integrating equation (50) gives an asymptotic fouling equation of the Kern-Seaton[115] form

$$R_f(\theta) = \frac{\pi_1}{\pi_2} (1-\exp(- \pi_2\theta)) \tag{51}$$

where $R_f(\infty) = \frac{\pi_1}{\pi_2}$ and $\beta = \pi_2$ (52)

Crittenden and Kolaczkowski[58] extended their analysis to consider a twin-layer model by assuming the build up of two layers of deposit on the wall in the manner described originally by Atkins[10]. It was assumed that thermal degradation of a mobile tarry layer adjacent to the fluid bulk results in

the formation of hard coke.

2.2.6 Interaction with Other Types of Fouling

Of the various types of fouling (See Table 1.2), particulate and crystallization mechanisms can interact with chemical reaction fouling. The accumulation of particles and/or the precipitation of salts onto a heat transfer surface may act as potential reactants, active sites, catalysts, or binders for further fouling by chemical reaction. Particulate and crystallization fouling mechanisms and examples will be briefly discussed.

For example, Epstein[73] reported a case of fouling in a crude oil preheater, in which a carry-over of inorganic salts in a small amount of water from the desalter occurred leading to vaporization of the water at the temperature and pressure in the preheater. The crystallized inorganic salts were therefore left behind to trap and hold hydrocarbons against the hot heat transfer surface until coke was formed. This is an example of precipitation promoting chemical reaction fouling. Coking itself is usually categorized as an example of chemical reaction fouling at the hot surface[162], though it could at times conceivably involve transfer of suspended particles from the bulk stream to the surface[210], i.e. particulate fouling.

Particulate fouling involves the accumulation of particles suspended in a liquid onto a heat transfer surface[73]. This includes gravitational settling of relatively large particles onto a horizontal heat transfer surface (sedimentation fouling), as well as deposition of colloidal particles by other mechanisms onto a heat transfer surface at any inclination[72]. Parkins[159] working on particulate mechanisms of surface film formation in

reactor systems proposed that the gross deposition rate, Φ_d was composed of a mass particle flux to the wall, N, and a sticking probability S:

$$\Phi_d = N\ S \tag{53}$$

The particle flux N was expressed in terms of a general mass transfer coefficient. The sticking probability S, defined as the probability that any particle reaching the wall would be held in contact with it, was expressed in terms of the drag force on a particle at the wall and an activation energy term (See Equations 20, 21 and 28). Therefore,

$$\Phi_d = N\ c\ e^{-E/RT} \tag{54}$$

in which C = sticking probability constant.

The observations on film formation in organic cooled reactor systems[33,34,159] indicated that, from the stand point of the detailed mechanisms involved, a single basic process, dependent upon the presence of suspended solids in the coolant, involved transport of these particles to the surface, and attachment there through the establishment of chemical bonds. Brownian motion appeared to be the principal mechanism which brought the particles in contact with the surface. However it was also considered that transport of particles by electrostatic forces and the probability of permanent attachment due to the nuclear radiation field and conventional thermal effects would occur.

Cleaver and Yates[41-43] derived a theory for predicting the net deposition rate of particulate material from a turbulently flowing suspension based on boundary layer analysis. This was based on suggestions by several authors of flow in the laminar sub-layer adjacent to the wall[16,135], extending from

the early work of Fage and Townsend[76], to the recent comprehensive flow visualisation of the wall region on a flat-plate boundary layer by Kline et al[121], and by Corino and Brodkey[49] in pipe flow. These studies showed that the sub-layer was disturbed by sudden random eruptions of fluid normal to the wall, so-called "turbulent bursts". A model for deposition rates due to inertia forces in the fluid, Φ_{di}, was developed[41] based on the idea that particles are convected to the wall by "down sweeps" within the flowing fluid. In addition to the inertial deposition process there is always a flux of particles to the wall due to natural diffusion processes[41-43]. This diffusional deposition rate, Φ_D, is added to the inertial deposition rate to give the total deposition rate, Φ_d, thus

$$\Phi_d = \Phi_{di} + \Phi_D \tag{55}$$

Crystallization fouling (due to sensible heat or boiling) may arise if the concentration of ions in a solution is such that the solution becomes supersaturated with respect to some solid crystalline form[24]. Supersaturation may arise whenever there is a change in temperature or concentration in a liquid. Many systems[95-97] involve inverse solubility salts; the solubility falling as the temperature rises, and in these cases supersaturation will be greatest at a heated surface. Supersaturation may also arise due to changes in bulk concentration due to evaporation or mixing[24]. Mixing streams may change the ionic strength, I, and this will affect solubility and hence the supersaturation

$$I = \tfrac{1}{2} \sum_i m_i Z_i^2 \tag{56}$$

in which m_i is the molality of ionic species i and Z_i is the

charge on it[65]. The Gibb's function of a crystal, comparising two terms due to both its size and its surface area (and the associated interfacial energy) decreases with increasing crystal size[24]. Nucleation sites are provided by suspended particles as well as by bounding solid surfaces. Nucleation is aided by high supersaturation and by low fluid velocities and turbulence intensities[24].

McCabe and Robinson[145] proposed the first mathematical model to be known in the literature involving surface fouling. Considering scaling of evaporators at constant temperature gradient, they proposed a transient equation for the build up of scale inside evaporator tubes; where fouling predominantly occurred as a result of the crystallization of inverse solubility salts. They assumed that the thickness of scale deposited was proportional to the total heat flow, then

$$X_f = a\ Q \tag{57}$$

in which X_f = deposit thickness

a = deposition constant

Q = quantity of heat

The Fourier equation[18] of heat flow defined the overall heat transfer coefficient, U

$$\frac{dQ}{d\theta} = U.A.\Delta T \tag{58}$$

in which A = surface area

ΔT = temperature driving force

and

$$U = \frac{1}{\alpha + B.Q} \tag{59}$$

dQ is the differential heat flow, α is the combined scale free resistance of the heating surface, and B.Q is the resistance proportional to the scale thickness.

Integrating the Fourier equation, the following expression was derived for the overall resistance as a function of time

$$\frac{1}{U^2} = C_1\theta + C_2 \qquad (60)$$

in which θ = time

C_1, C_2 = constants

A linear relationship was found when $\frac{1}{U^2}$ was plotted against θ.

3. Polymerisation of Styrene

Styrene polymerises spontaneously on heating in a vacuum or an atmosphere from which oxygen has been excluded[69]. Very few other vinyl monomers possess this property. Figure 3.1 shows the extent of polymerisation of styrene as a function of time and temperature[69]. Collectively, the polymerisation reactions of styrene may be represented by

$$n \quad \underset{\underset{C_6H_5}{|}}{CH = CH_2} \rightarrow \quad \underset{\underset{C_6H_5}{|}}{\{CH - CH_2\}_n} \qquad (61)$$

Equation (61) is a simple representation of styrene polymerisation for which the heat of polymerisation is 17.4 ± 0.2 Kcal/mol at 26.9°C[62].

The presence of the tertiary carbon atom in the polymer may lead to stereoisomers depending on the mechanism of polymerisation (i.e. free radical or ionic) at the reaction conditions[152].

Although the basic polymerisation reaction is, in every case, the stepwise addition of monomer units, the properties of the polymer depend to a remarkable extent on the mechanism of initiation[106]. Commercially, ionic methods of initiating styrene polymerisation are far less important than the free radical method[168].

Styrene can be polymerised by the four common polymerisation processes used in industry (See Table 3.1). These are, in the order of decreasing commercial importance[69]:

(1) Bulk polymerisation

(2) Solution polymerisation

(3) Suspension polymerisation

(4) Emulsion polymerisation

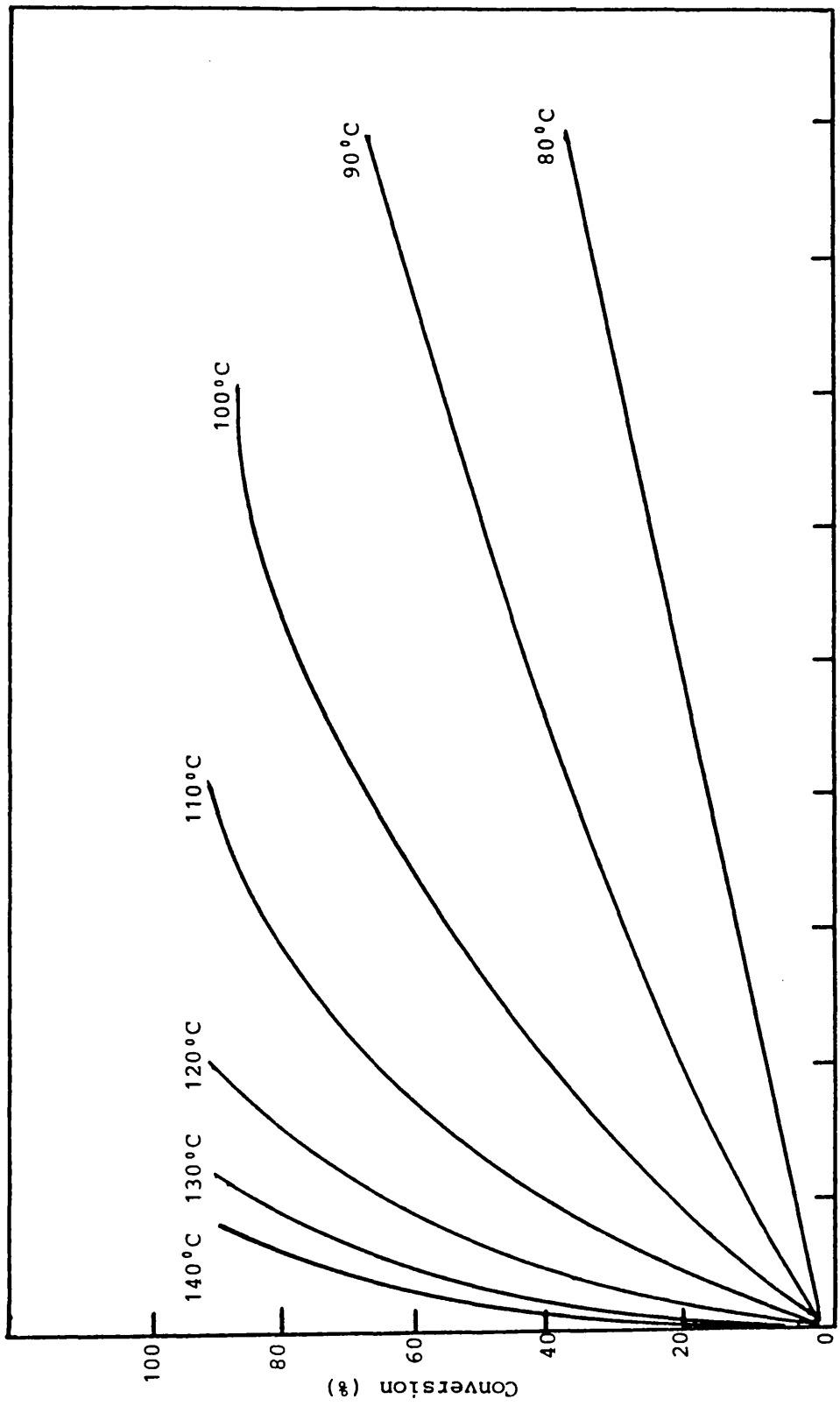

Figure 3.1[69] The Polymerisation of Styrene as a Function of Time and Temperature.

Table 3.1[69] Polymerisation Techniques for Producing Polystyrene

Method	Polymerizing system	Advantages	Disadvantages	Cost factors
Bulk polymerization	Pure styrene monomer	Simplicity High clarity Excellent electrical properties	Poor heat control Broad mol wt distribution	Polymerization cans Handling and grinding equipment
Solution polymerization	Styrene diluted with solvent	Much better temperature control	Solvent reduces mol wt and rate	Drying of polymer Solvent recovery Polymerization cans
Suspension polymerization	Water used as a carrier with stabilizing agents to keep material in suspension, and one or more catalysts to speed polymerization	No difficulty with heat of polymerization Simple kettles for polymerization Volatile materials can be reduced to low level by suitable choice of catalysts and of temperature schedules	Possible contamination from water and stabilizing agent Batch operation	Catalysts Stabilizers Washing and drying of polymer
Emulsion polymerization	Water used as carrier with emulsifying agent to give extremely small particles	Rapid reaction and no difficulty with heat of polymerization Many copolymerizations not possible by other techniques proceed readily in emulsion Adaptable to continuous polymerization Usefulness of latexes Simple kettles for polymerization Polymer has higher heat distortion temperature (by 10°C) than from mass polymerization	Contamination of polymer with water and emulsifying agents Color and clarity of polymer deficient Broad mol wt distribution	Catalysts Emulsifiers and stabilizers Coagulants Washing and drying of polymer Pelleting of dried polymer
Continuous bulk solution polymerization	Styrene monomer fed continuously to reactor	More uniform product High clarity Excellent color	Mechanical problem in moving highly viscous finished polymer Slow rate of production per unit volume of equipment	Expensive equipment
Solution polymerization, ionic	Styrene and other monomers diluted with solvent	Can produce copolymers that cannot be produced readily by other polymerization methods, eg. styrene–butadiene block copolymer Rapid polymerization rate	Difficulty in maintaining good color Solvent and catalyst residue removal High sensitivity to impurities	Expensive equipment Recovery of solvent and recycle Catalyst Purification

By most methods high molecular weight polymer is obtained at all conversions. Under isothermal conditions and at temperatures above 100°C the molecular weight of the polymer produced is independent of conversion except at very low conversions[69]. Figure 3.2 is a plot of the initial rate of polymerisation against molecular weight.

Added compounds can seriously effect the rate of polymerisation and/or the molecular weight of the polymer[2]. These compounds can be classified as follows:

(1) Initiators

Compounds which undergo homolytic bond cleavage by heat, light and other forms of radiation to form reactive free radicals. The effect of an initiator on the polymerisation of styrene is to increase the rate of polymerisation and to decrease the molecular weight of the polymer[104]. Examples are Benzoyl peroxide and 2-2- Azobisisobutyronitrile (AIBN)[69].

(2) Chain transfer agents

A chain transfer agent decreases the molecular[69,141] weight of the styrene polymer with no effect on the rate of polymerisation. Examples are Alkyl Mercaptans, ethyl benzene, and non-polymerisable olefins[69].

(3) Inhibitors

The effect of an inhibitor on the polymerisation of styrene is to retard the rate or to suppress completely the polymerisation[168]. Examples are tert-Butyl pyrocatechol (TBC), Benzoquinone, sulphur, and Ferric salts. Commercially, styrene is supplied with ~10 ppm of an inhibitor to suppress thermal polymerisation during storage[69].

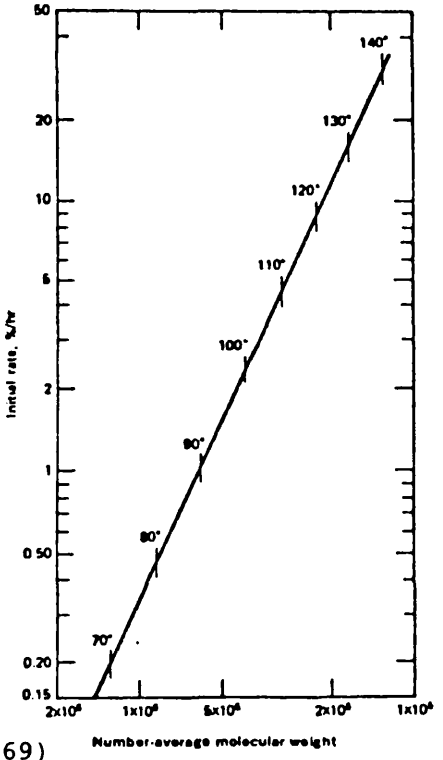

Figure 3.2 (69) Relationship between rate of styrene polymerisation and molecular weight at various temperatures.

3.1 Mechanisms

There are two dissimilar chemical mechanisms for the polymerisation of styrene; free radical polymerisation which is initiated by free radicals generated thermally or chemically[170], and ionic polymerisation initiated by an ionic reaction[69].

3.1.1 Free Radical Polymerisation[69,106]

The sequence of reactions by which styrene is converted into high molecular weight polymer by free radical polymerisation can be divided into four distinct steps.

(1) Generation of free radicals

(2) Initiation of polymer chains

(3) Propagation of polymer chains

(4) Termination of polymer chains

3.1.1.1 Polymerisation of Styrene Initiated by Thermally Generated Free Radicals

The accepted[69,106] initiation mechanism for the polymerisation of styrene by thermally generated free radicals is given below

Initiation

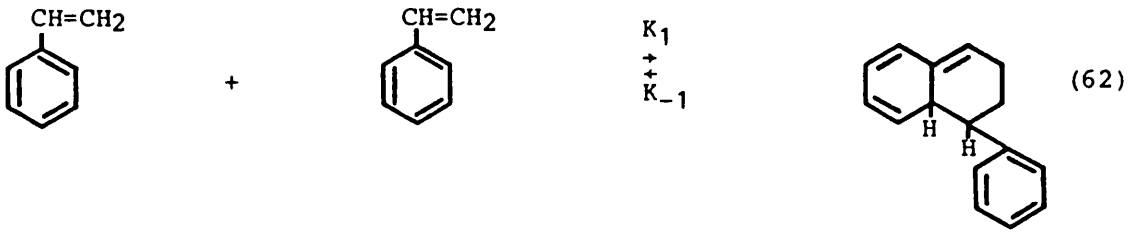

(62)

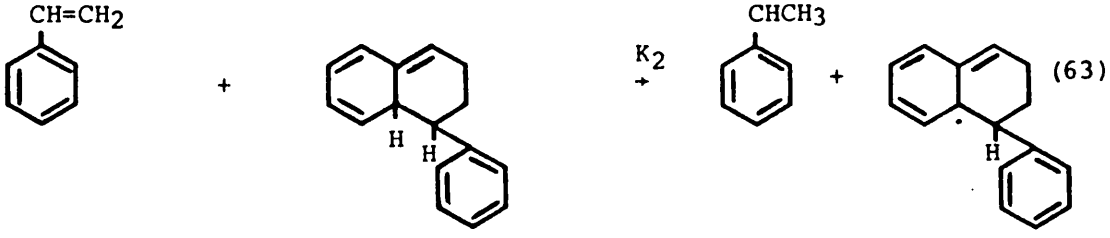

(63)

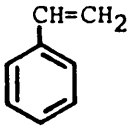

+

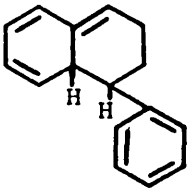

$\xrightarrow{K_3}$ Trimer (64)

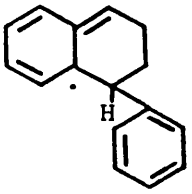

+

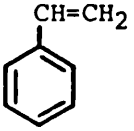

$\xrightarrow{K_4}$ $\dot{R}_1$ (65)

in which $\dot{R}_1$ = free radical

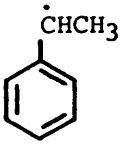

+

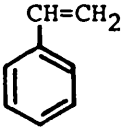

$\xrightarrow{K_5}$ $\dot{R}_1$ (66)

Propagation

$\dot{R}_n$ + 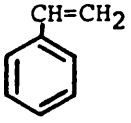

$\xrightarrow{K_p}$ $\dot{R}_{n+1}$ (67)

Termination

(1) By combination

$$\dot{R}_n + \dot{R}_M \xrightarrow{K_{tc}} P_{n+m} \quad (68)$$

(2) By disproportionation

$$\dot{R}_n + \dot{R}_M \xrightarrow{K_{td}} P_n + P_M \quad (69)$$

Chain transfer

$$\dot{R}_n + \text{ 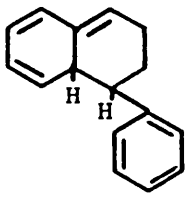 } \xrightarrow{K_{AH}} P_n + \dot{R}_1 \qquad (70)$$

$$\dot{R}_n + \text{ 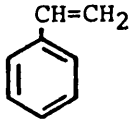 } \xrightarrow{K_M} P_n + \dot{R}_1 \qquad (71)$$

in which $\dot{R}$ = free radical and P = 'dead' polymer molecule.

3.1.1.2 Polymerisation of Styrene Initiated by Chemically Generated Free Radicals

The accepted chemical mechanism[106] for the polymerisation of styrene initiated by chemically generated free radicals is outlined below

Initiation

$$X \xrightarrow{K_I} \dot{R}_C \qquad (72)$$

In which X = initiator and $\dot{R}_C$ = initiator radical

$$\dot{R}_C + \text{ 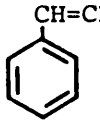 } \rightarrow \dot{R}_1 \qquad (73)$$

Propagation

$$\dot{R}_n + \text{ 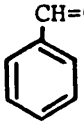 } \xrightarrow{K_p} \dot{R}_{n+1} \qquad (74)$$

Termination

(1) By combination

$$\dot{R}_n + \dot{R}_M \xrightarrow{K_{tc}} P_{n+m} \qquad (75)$$

(2) By disproportionation

$$\dot{R}_n + \dot{R}_m \xrightarrow{K_{td}} P_n + P_m \qquad (76)$$

Chain transfer

$$\dot{R}_n + \text{ 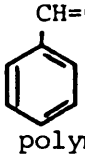 } \xrightarrow{K_m} P_n + \dot{R}_1 \qquad (77)$$

in which P = 'dead' polymer molecule.

3.1.2 Ionic Polymerisation

Ionic polymerisation proceeds through a species which aquires a partial negative or positive charge. The two cases are:

(1) Anionic polymerisation in which the active site is a carbanion.

(2) Cationic polymerisation in which the active site is a carbonium ion.

3.1.2.1 Anionic Polymerisation

Initiation takes place by the generation of the anionic active site. Then propagation follows by the rapid addition of the monomer to the anionic active site. In anionic polymerisation, there is no termination step. If the polymerisation reaction of styrene is carried out with highly purified anionic initiators and in an inert solvent, the polystyryl anions remain active even after all the styrene monomer has been consumed. The term 'living' polymer was suggested by Szwarc et al[185] for such polymeric anions. The absence of the termination step in anionic polymerisation has two important effects.

(i) A much higher concentration of active sites can be maintained in anionic polymerisation than in free radical polymerisation for the same molecular weight polymer. This permits much higher polymerisation rates in anionic polymerisation than in free radical polymerisation.

(ii) As the rate of initiation is very fast compared with the rate of propagation, virtually all the polymer chains are growing simultaneously,

and the molecular weight distribution of the polymer is thus very narrow. This is in marked contrast with free radical polymerisation where the termination of polymer chains result in a much wider molecular weight distribution[69,106].

The initiation of anionic polymerisation of styrene can be induced by organometallic compounds such as Ethyl Lithium, Butyl Lithium, Amyl Sodium, and Benzyl Sodium or alkali metals. The exact mechanism of initiation is dependent upon the metal-cation bond strength, the polarity of the solvent, the size of the metal cation and the temperature.

3.1.2.2 Cationic Polymerisation

Initiation of cationic polymerisation can be induced by proton-donating acids e.g. Perchloric, Hydrochloric and Sulphuric acid, or compounds which generate a carbonium ion by the Friedel-Crafts reaction e.g. $AlCl_3$, $TiCl_4$ and BF_3. Trace quantities of water are required as a co-catalyst to activate the compounds. However, unlike anionic polymerisation, an inherent termination step is the rule rather than the exception[69]. The solvent again plays an important role in the effectiveness of the initiator[69]. The polarity and the solvating power of the solvent are crucial; generally, the reaction rate and the molecular weight both increase with the dielectric constant of the solvent[103].

The mechanism of initiation for cationic polymerisation, as for anionic polymerisation, is dependent on the physical properties of the system.

3.2 Kinetics

The overall polymerisation reaction of styrene does

not correspond to a simple kinetic order with respect to the styrene monomer. At temperatures of ~170°C and above, the reaction is close to second order with respect to the monomer for at least 70% of the polymerisation. At lower temperatures, (~127°C) the reaction is close to first order with respect to the monomer for 85% of the polymerisation. At 75°C, the reaction is zero order with respect to the monomer for 65% of the polymerisation[69]. And at temperatures between 25-50°C, the order with respect to the monomer is negative[69].

3.2.1 Kinetics of Styrene Initiated by Thermally Generated Free Radicals

The initial rate of the thermal polymerisation of pure styrene (in the absence of solvent and added initiator) is given by[69]:

$$\text{Initial rate of polymerisation} = 10^{11.55} \times 10^{-\frac{4170}{T}} \qquad (78)$$

in which T = absolute temperature in °K, and the initial rate of polymerisation is in the units %/hr. This dependence of the rate upon temperature is given in Figure 3.3[168].

Let M = 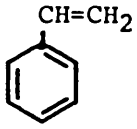 , styrene monomer

AH = 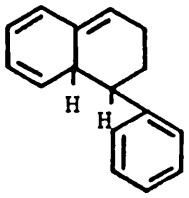 , Diels-Alder adduct

$\dot{M}$ = 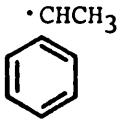 , styrene monomer radical

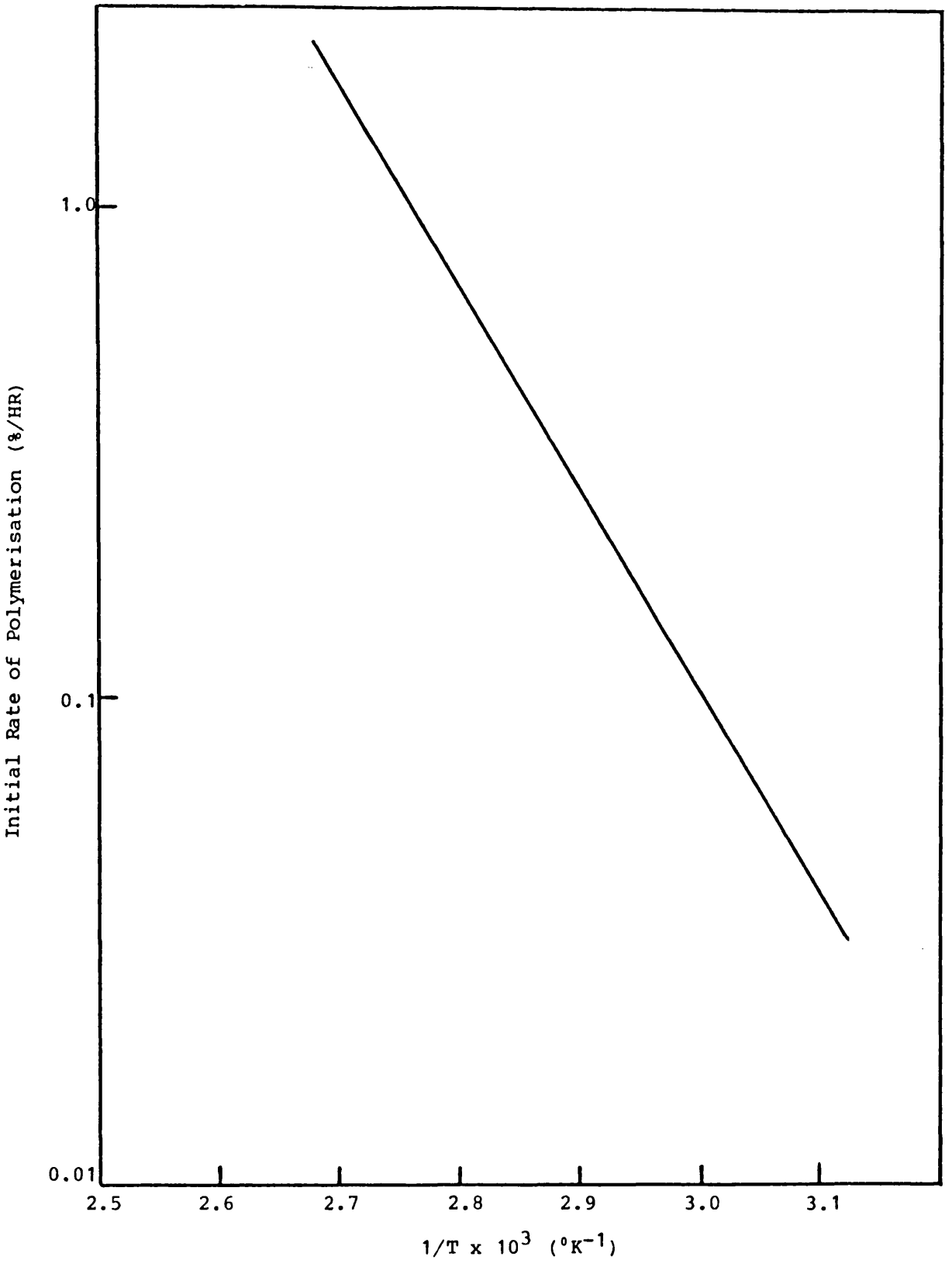

Figure 3.3[168] Variation of the Initial Rate of Polymerisation Against Reciprocal Absolute Temperature. Pure Styrene.

$\dot{A}$ = 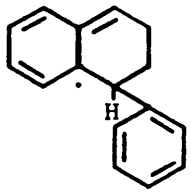 , Diels-Alder adduct radical

The rate of initiation r_I is given by (See Section 3.1.1.1)

$$r_I = K_4[\dot{A}][M] + K_5[\dot{M}][M] \tag{79}$$

Apply the steady state hypothesis[31] to $\dot{M}$

$$\frac{d[\dot{M}]}{dt} = 0 = K_2[M][AH] - K_5[\dot{M}][M] \tag{80}$$

and $$[\dot{M}] = \frac{K_2}{K_5}[AH] \tag{81}$$

Apply the steady-state to $\dot{A}$

$$\frac{d[\dot{A}]}{dt} = 0 = K_2[M][AH] - K_4[\dot{A}][M] \tag{82}$$

and $$[\dot{A}] = \frac{K_2}{K_4}[AH] \tag{83}$$

Substituting equations (81) and (83) into (79) gives

$$r_I = 2K_2[AH][M] \tag{84}$$

Apply steady-state to AH

$$\frac{d[AH]}{dt} = 0 = K_1[M]^2 - K_{-1}[AH] - K_2[M][AH] - K_3[M][AH] - K_{AH}[\dot{R}][AH] \tag{85}$$

and $$[AH] = \frac{K_1[M]^2}{K_{-1} + (K_2+K_3)[M] + K_{AH}[\dot{R}]} \tag{86}$$

Apply steady-state to $\dot{R}$

$$\frac{d[\dot{R}]}{dt} = 0 = K_4[\dot{A}][M] + K_5[\dot{M}][M] - K_{tc}[\dot{R}]^2 - K_{td}[\dot{R}]^2 \tag{87}$$

and $$[\dot{R}] = \left(\frac{K_4[\dot{A}][\dot{M}] + K_5[\dot{M}][M]}{K_{tc}+K_{td}}\right)^{\frac{1}{2}} \tag{88}$$

Substitute equation (79) into (88) gives

$$[\dot{R}] = \left(\frac{r_I}{K_{tc}+K_{td}}\right)^{\frac{1}{2}} \tag{89}$$

Substitute equations (86) and (89) into (84) gives

$$r_I = \frac{2K_1K_2[M]^3}{K_{-1}+(K_2+K_3)[M]+K_{AH}\left(\frac{r_I}{K_{tc}+K_{td}}\right)^{\frac{1}{2}}} \tag{90}$$

The rate of propagation is given by

$$r_p = K_p[\dot{R}][M] \tag{91}$$

Substitute equation (89) into (91)

$$r_p = K_p\left(\frac{r_I}{K_{tc}+K_{td}}\right)^{\frac{1}{2}}[M] \tag{92}$$

Schulz et al[69] found that for styrene polymerisation in most solvents, r_p is second order with respect to the styrene monomer. It can be seen that from equation (92) that this requires r_I to be of second order with respect to the styrene monomer.

Consider equation (90) when $(K_2+K_3)[M] >> K_{-1}+K_{AH}\left(\frac{r_I}{K_{tc}+K_{td}}\right)^{\frac{1}{2}}$

Therefore,

$$r_I = \frac{2K_1K_2}{K_2+K_3}[M]^2 \tag{93}$$

i.e. $$r_I = 2K_{I_1}[M]^2 \tag{94}$$

Substitute equation (94) into (92) gives

$$r_p = K_p\left(\frac{2K_{I_1}}{K_{tc}+K_{td}}\right)^{\frac{1}{2}}[M]^2 \tag{95}$$

Mayo[141] found that for styrene polymerisation in bromobenzene, r_p is of $^5/_2$ order with respect to the styrene monomer. It can be seen from equation (92) that this requires r_I to be of third order with respect to the styrene monomer.

Consider equation (90) when

$$K_{-1} >> (K_2+K_3)[M]+K_{AH}\left(\frac{r_I}{K_{tc}+K_{td}}\right)^{\frac{1}{2}}$$

Therefore,

$$r_I = \frac{2K_1K_2}{K_{-1}}[M]^3 \qquad (96)$$

i.e. $$r_I = 2K_{I_2}[M]^3 \qquad (97)$$

Substitute equation (97) into (92) gives

$$r_p = K_p\left(\frac{2KI_2}{K_{tc}+K_{td}}\right)^{\frac{1}{2}}[M]^{5/2} \qquad (98)$$

3.2.2 Kinetics of Styrene Initiated by Chemically Generated Free Radicals

Let M = 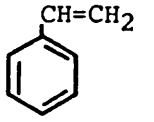 , styrene monomer

X = initiator

The rate of initiation r_I is given by (See Section 3.1.1.2)

$$r_I = K_I[X] \qquad (99)$$

The rate of propagation r_p is given by (See Section 3.1.1.2)

$$r_p = K_p[\dot{R}][M] \qquad (100)$$

Apply steady-state to $\dot{R}$

$$\frac{d[\dot{R}]}{dt} = 0 = K_I[X]-K_{tc}[\dot{R}]^2-K_{td}[\dot{R}]^2 \qquad (101)$$

and $$[\dot{R}] = \left(\frac{K_I[X]}{K_{tc}+K_{td}}\right)^{\frac{1}{2}} \qquad (102)$$

Substitute equation (99) into (102)

$$[\dot{R}] = \left(\frac{r_I}{K_{tc}+K_{td}}\right)^{\frac{1}{2}} \qquad (103)$$

Substitute equation (103) into (100)

$$r_p = K_p\left(\frac{r_I}{K_{tc}+K_{td}}\right)^{\frac{1}{2}}[M] \qquad (104)$$

The two most widely used initiators[69] for the initiation of styrene polymerisation are

(i) Benzoyl peroxide[69]

(ii) 2,2 - Azobisibobutyronitrile (AIBN)[69]

Benzoyl peroxide decomposes by an approximately first order process[69]

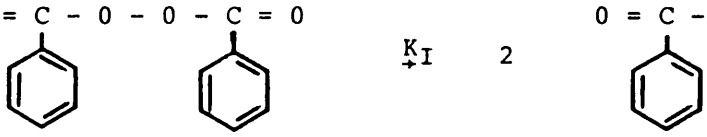

(105)

The rate of decomposition depends on the solvent[103].

The Arrhenius relationship for the rate of decomposition of benzoyl peroxide in benzene is given by[69]

$$K_I = 3.0 \times 10^{13} \exp\left(-\frac{29600}{RT}\right) \qquad (106)$$

R = universal gas constant

T = absolute temperature

It has been found[103] that K_I varied only by a factor of two in various solvents; being slowest in benzene and fastest in ethyl acetate.

2,2 - azobisisobutyronitrile also decomposes by an approximately first order process[69]

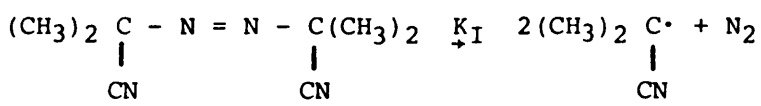

(107)

The rate of decomposition depends on the solvent[103].

The Arrhenius relationship for the rate of decomposition of AIBN in benzene[69] is given by

$$K_I = 10^{15} \exp\left(-\frac{30700}{RT}\right) \qquad (108)$$

3.2.3 Kinetics of n^{th} Order Forward Reaction

There is no simple direct method of determining the rate of a reaction. The experimental results obtained in a kinetic study of a reaction are normally values of concentration of a reactant or product determined at various times[104]. The slope of the concentration transient at anytime is the rate of reaction at that time. If the forward reaction of n^{th} order is represented by

$$n\,M \xrightarrow{K_n} P$$

then the rate equation is given by[181]

$$-\frac{dC_M}{dt} = K_n\, C_M^n \qquad (109)$$

in which C_M = concentration of M at time t.

with the boundary conditions,

$$C_M = C_{M_O} \text{ at } t = 0$$

and, $C_M = C_M$ at $t = t$

then on integration

$$-\int_{C_{M_O}}^{C_M} \frac{dC_M}{C_M^n} = K_n \int_o^t dt \qquad (110)$$

Table 3.2 shows the integration of equation (110) for various values of n.

3.2.4 Determination of the Order of Reaction

The order of the reaction may be determined by either

(1) The integral method; or

(2) The differential method

3.2.4.1 The Integral Method

If a particular differential rate equation is applied

Table 3.2 Differential and Integrated Rate Expressions

Order	Rate Equation		Units of Rate Constant
	Differential Form	Integrated Form	
0	$-\frac{dc_M}{dt} = k_o$	$k_o = \frac{C_{Mo} - C_M}{t}$	Moles litre^{-1} sec^{-1}
1/2	$-\frac{dc_M}{dt} = k_{1/2}\, C_M^{1/2}$	$k_{1/2} = \frac{2}{t}\,[C_{Mo}^{1/2} - C_M^{1/2}]$	Moles$^{1/2}$ litre$^{-1/2}$ sec^{-1}
1	$-\frac{dc_M}{dt} = k_1\, C_M$	$k_1 = \frac{1}{t} \ln \frac{C_{Mo}}{C_M}$	Sec^{-1}
3/2	$-\frac{dc_M}{dt} = k_{3/2}\, C_M^{3/2}$	$k_{3/2} = \frac{2}{t}\,[\frac{1}{C_M^{1/2}} - \frac{1}{C_{Mo}^{1/2}}]$	Litres$^{1/2}$ mole$^{-1/2}$ sec^{-1}
2	$-\frac{dc_M}{dt} = k_2\, C_M^2$	$k_2 = \frac{1}{t}\,[\frac{1}{C_M} - \frac{1}{C_{Mo}}]$	Litres mole^{-1} sec^{-1}
5/2	$-\frac{dc_M}{dt} = k_{5/2}\, C_M^{5/2}$	$k_{5/2} = \frac{2}{3t}[\frac{1}{C_M^{3/2}} - \frac{1}{C_{Mo}^{3/2}}]$	Litres$^{3/2}$ mole$^{-3/2}$ sec^{-1}
3	$-\frac{dc_M}{dt} = k_3\, C_M^3$	$k_3 = \frac{1}{2t}[\frac{1}{C_M^2} - \frac{1}{C_{Mo}^2}]$	Litres^2 mole^2 sec^{-1}

to the reaction under consideration then the integrated form of the differential rate equation is applied to the experimental results. If a good fit is obtained, then it can be concluded that the differential rate equation is applicable to the reaction under consideration. The rate constant for the reaction can then be obtained. However, if a poor fit is obtained, the procedure is repeated with another differential rate equation until the fit is satisfactory. The methods used for applying the integrated form of the differential rate equations to the experimental results are given in appendix A.

The integration method is a trial and error procedure. As it is highly dependent on the accuracy of the experimental results, the conclusions drawn from a particular method of application of the integrated form of the differential rate equation to the experimental results should be confirmed with those of another method.

3.2.4.2 The Differential Method

Experiments are carried out with different initial concentrations of reactant, and the resulting initial rates of reaction are evaluated by the measurement of the initial slopes of the plots of concentration against time. Figure 3.4 shows schematically experimental results for various initial concentrations of reactants and the initial slopes at each initial concentration of reactant.

The rate equation for the n^{th} order reaction can be written as

$$r = -\frac{dC_M}{dt} = K_n C_M^n \qquad (111)$$

Taking the logarithm of equation (111)

$$\ln r = \ln K_n + n \ln C_M \qquad (112)$$

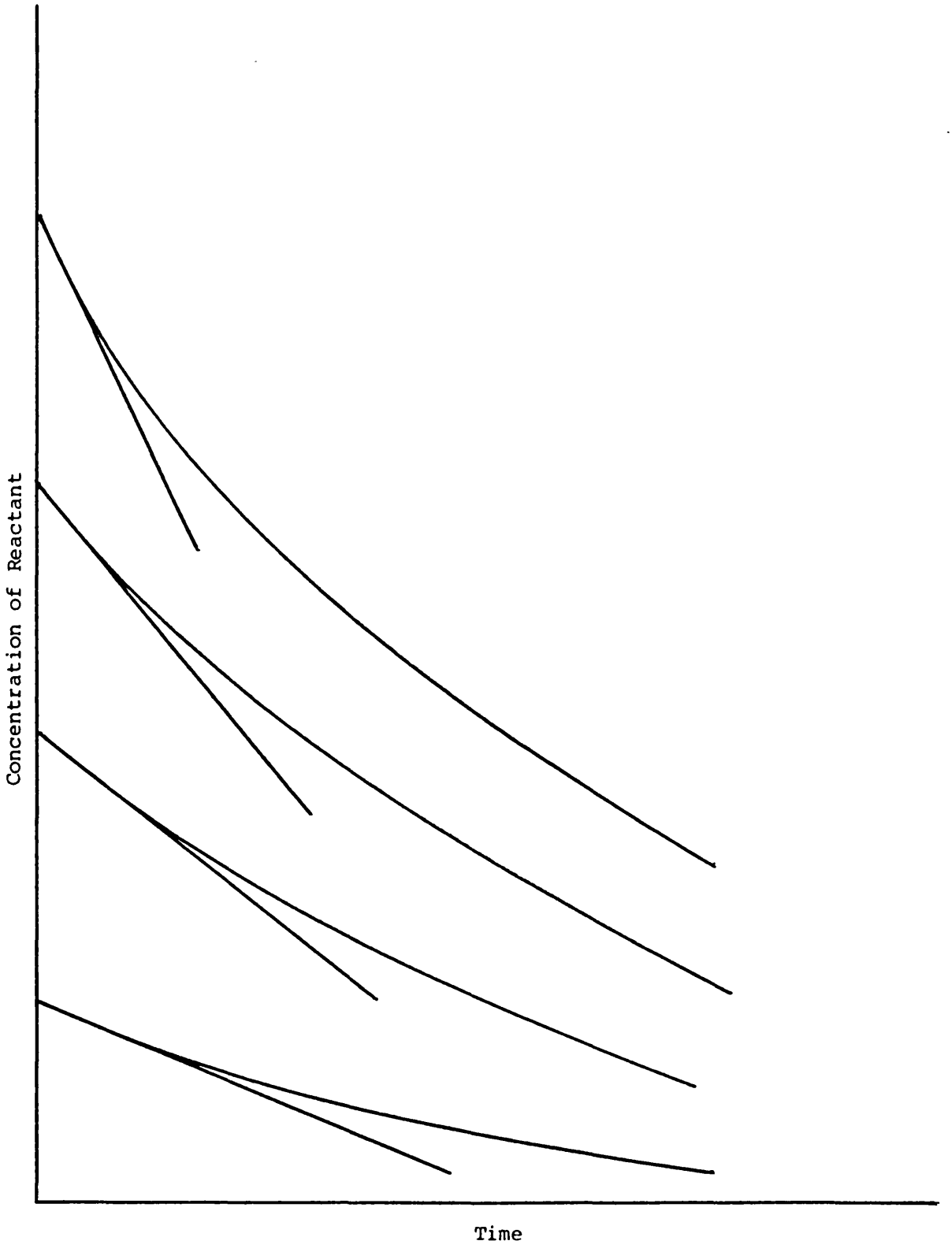

Figure 3.4 Concentration transients

It can be seen from equation (112) that a plot of the initial rate of reaction against the corresponding initial concentration of reactant on a logarithmic scale should give a straight line of slope n and intercept $\ln K_n$ on the ln r axis. Alternatively, the results of two experiments can be expressed as

$$\frac{r_1}{r_2} = \frac{K_n (C_M^n)_1}{K_n (C_M^n)_2} \tag{113}$$

from which,

$$n = \frac{\ln r_1 - \ln r_2}{\ln (C_M)_1 - \ln (C_M)_2} \tag{114}$$

The serious restriction of the differential method is the limited accuracy of measurement of the initial slopes.

4. Equipment Design and Operation

4.1 Apparatus

A detailed description of the apparatus which was used to study fouling has been presented by Kolaczkowski[114]. The flow diagram from this reference is shown in Figure 4.1.

In summary the closed loop heat transfer circuit consisted of

(1) a radiantly heated horizontal furnace tube

(2) a water coded double pipe heat exchanger to cool the fouling stream after the furnace

(3) a feedstock reservoir

(4) a feed pump (See Table 4.3)

(5) a closed loop cooling water circuit

(6) instrumentation for process analysis and safety

To determine the fouling rate in the furnace tube as a function of the operating conditions the change in overall heat transfer coefficient (from outside tube surface temperature to bulk fluid temperature) was followed with time. The feedstock was circulated around the loop at a constant flowrate and the furnace was operated at a constant heat flux for the duration of each run.

Key to Figure 4.1

Hydrocarbon Flow Loop

V_1, V_2, V_4	stop/control valves
V_3	needle valve
V_p	pressure relief valve
R_1	Rotameter 18 (alarm fitted)
R_2	Rotameter 24
P_1	pump suction pressure
P_2	furnace inlet pressure
P_3	furnace outlet pressure
T_1	furnace inlet temperature
T_2	furnace outlet temperature
T_3	condenser outlet temperature (alarm fitted)
F_1, F_2	line filters
V.S.	visual section

Cooling Water Circuit

V_5, V_6, V_7	stop/control valves
R_3	Rotameter (alarm fitted)
F_3, F_4	line filters
T_4	condenser outlet temperature

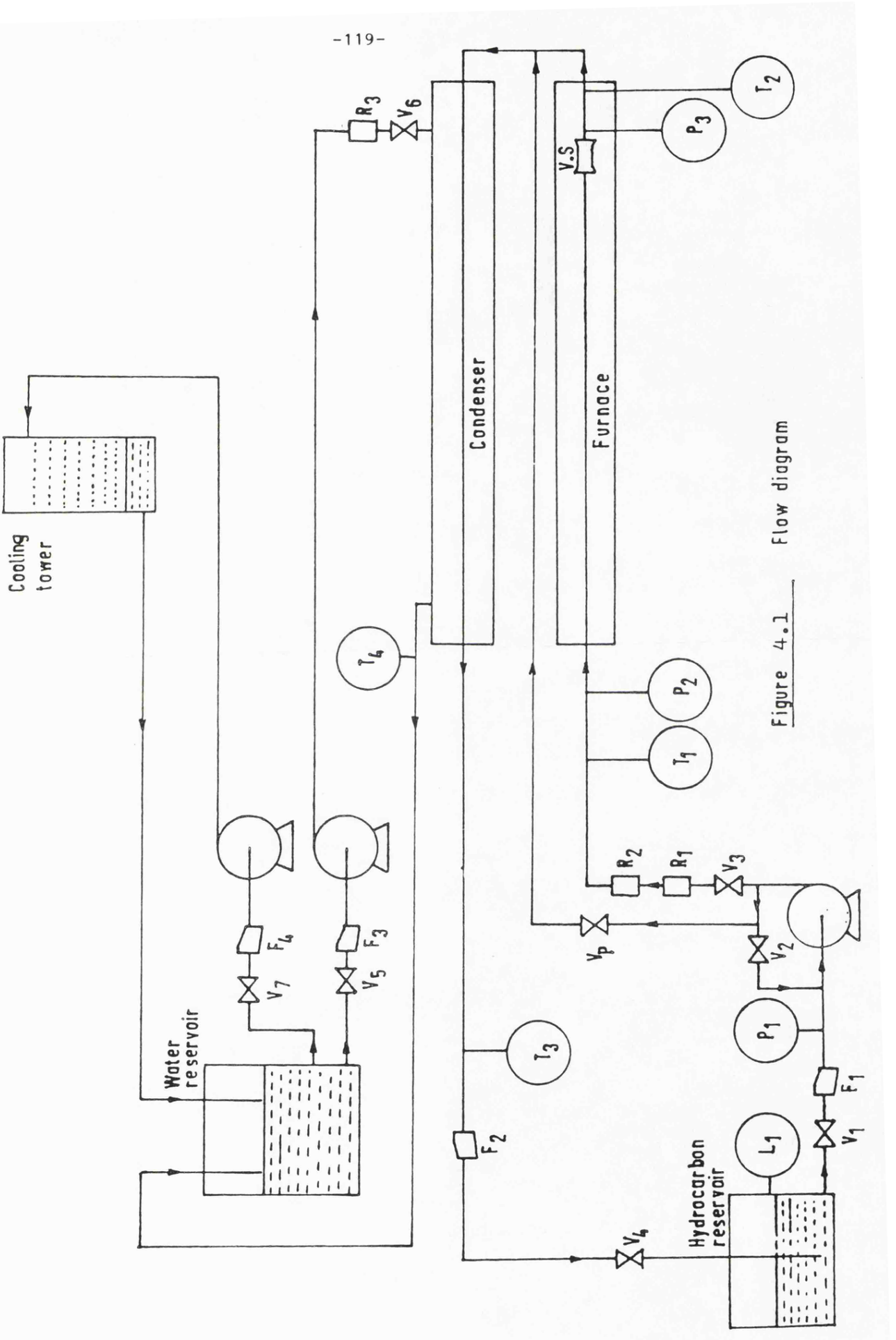

Figure 4.1 Flow diagram

4.1.1 Furnace Tube

The furnace tube was mounted horizontally[114] with the following specifications

I.D. = 0.792 ins. O.D. = 1.0 ins.

length = 15 ft. type = 321 stainless steel seamless tube

The maximum safe tube wall operating temperature = 732°C

The tube was supported to allow for horizontal movement caused by thermal expansion. At the tube outlet an expansion bellows permitted a horizontal movement of 7/8 ins.

Seventy six Chromel-Alumel thermocouples (T/C) were brazed onto the surface of the tube[114] at the positions shown in Figure 4.2. The thermocouple wires were insulated with Refrasil sleeving.

Fifteen heating elements[114], each 1 ft. long, were supplied independently with power by Triac regulators. Each element consisted of an 80/20 nickel-chromium alloy wire, 60.75 ft. x 0.0492 in. O.D. coiled on a mandrell (which was 3 times the diameter of the wire). The coil was then wound onto a ceramic tube and set in refractory cement. (See Figure 4.3).

At the tube inlet the following properties of the feedstock could be sampled or measured:

(1) Composition: sampling point being located at the pump outlet.

(2) Flow rate: by means of 2 Rotameters.

(3) Temperature: by means of a vapour pressure thermometer.

(4) Pressure: by means of a piezometer ring consisting of four 3/32 in. pressure tappings.

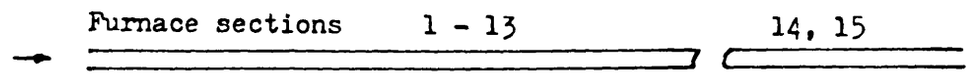

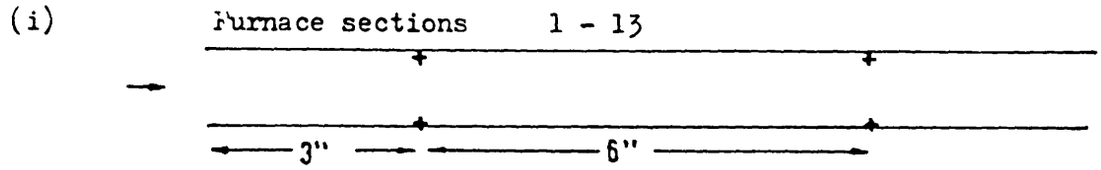

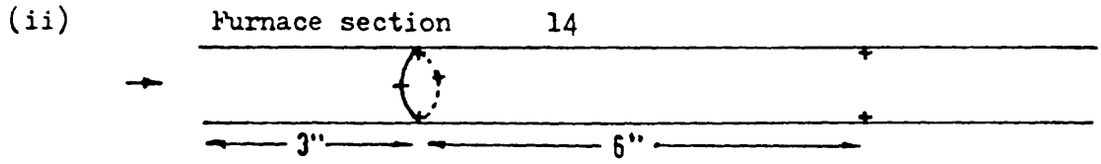

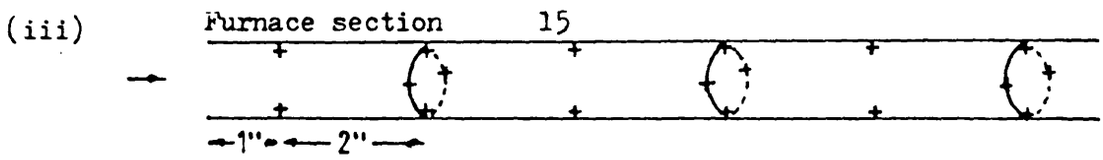

Figure 4.2 The location of thermocouples on the surface of the furnace tube.

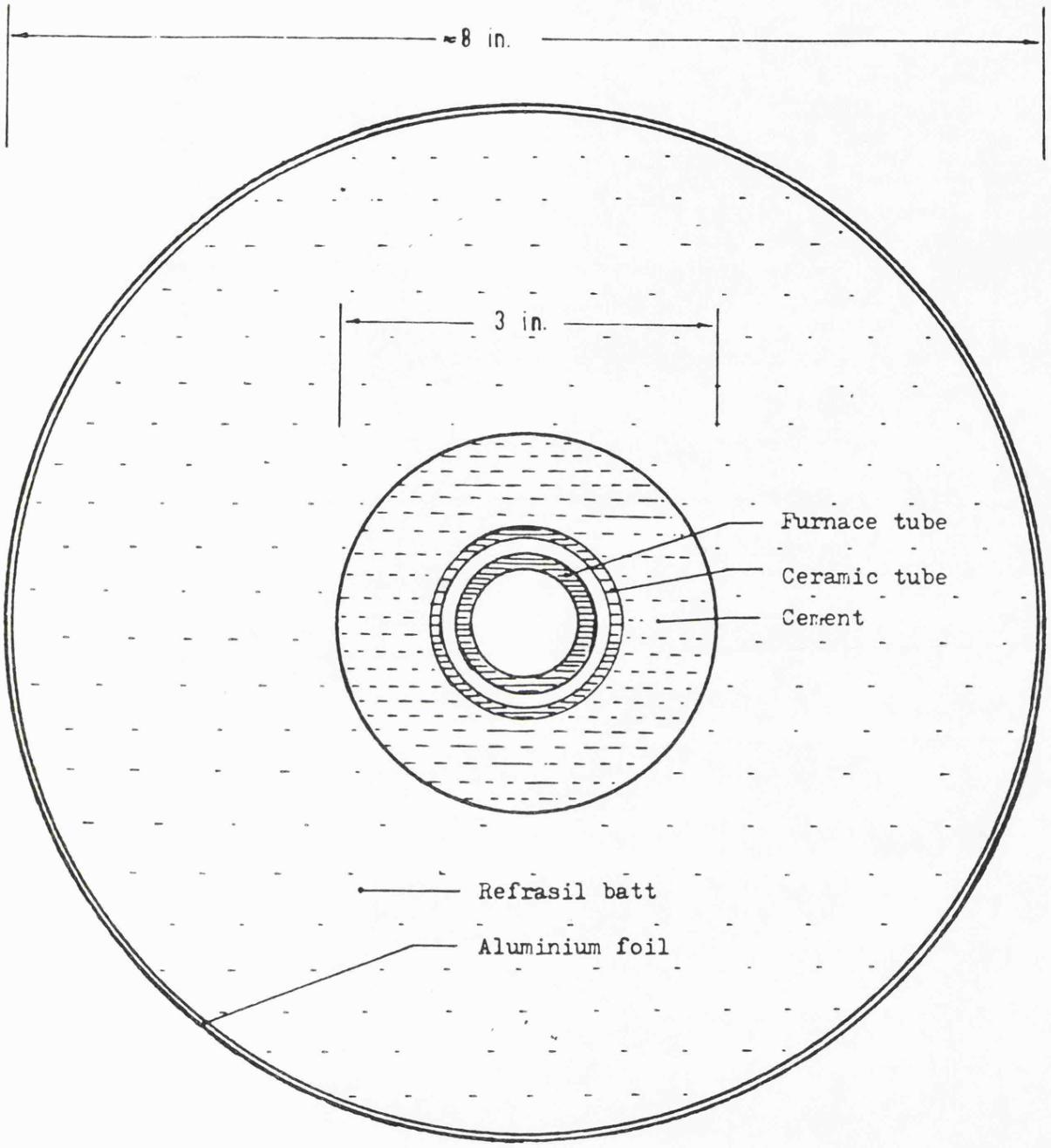

Figure 4.3 Cross-section of a heating element (not to scale).

This particular size of pressure tapping was found to be most suitable to avoid blockage by foulants.

At the tube outlet the following properties of the feedstock could be sampled or measured:

(1) Composition: sampling point.

(2) Flow pattern: a 2 in. long glass section at the tube outlet facilitated visual and photographic examination. (See Figure 4.4).

(3) Temperature: a Chromel-Alumel T/C in a 1/16 in. O.D. stainless steel sheath was situated in the exit stream.

(4) Pressure: a piezometer ring consisting of three 3/32 in. pressure tappings.

The tube was enclosed in a box (17 ins. x 14 ins. x 17 ft.)[114] of Aluminium panels bolted onto a steel frame. A gas tight seal was maintained between the panels during operation. For safety reasons, the box was filled with nitrogen. (See Figure 4.5).

4.1.2 Double Pipe Heat Exchanger

A three section double pipe heat exchanger was designed[114] to be easily dismantled for the purpose of cleaning. Water was used in the annuli as the cooling medium and was available at about 20°C to be returned to the water reservoir at less than 50°C. The contents of the water reservoir were circulated to an external induced draft cooling tower.

Each of the three double pipe heat exchanger sections have the following specifications:

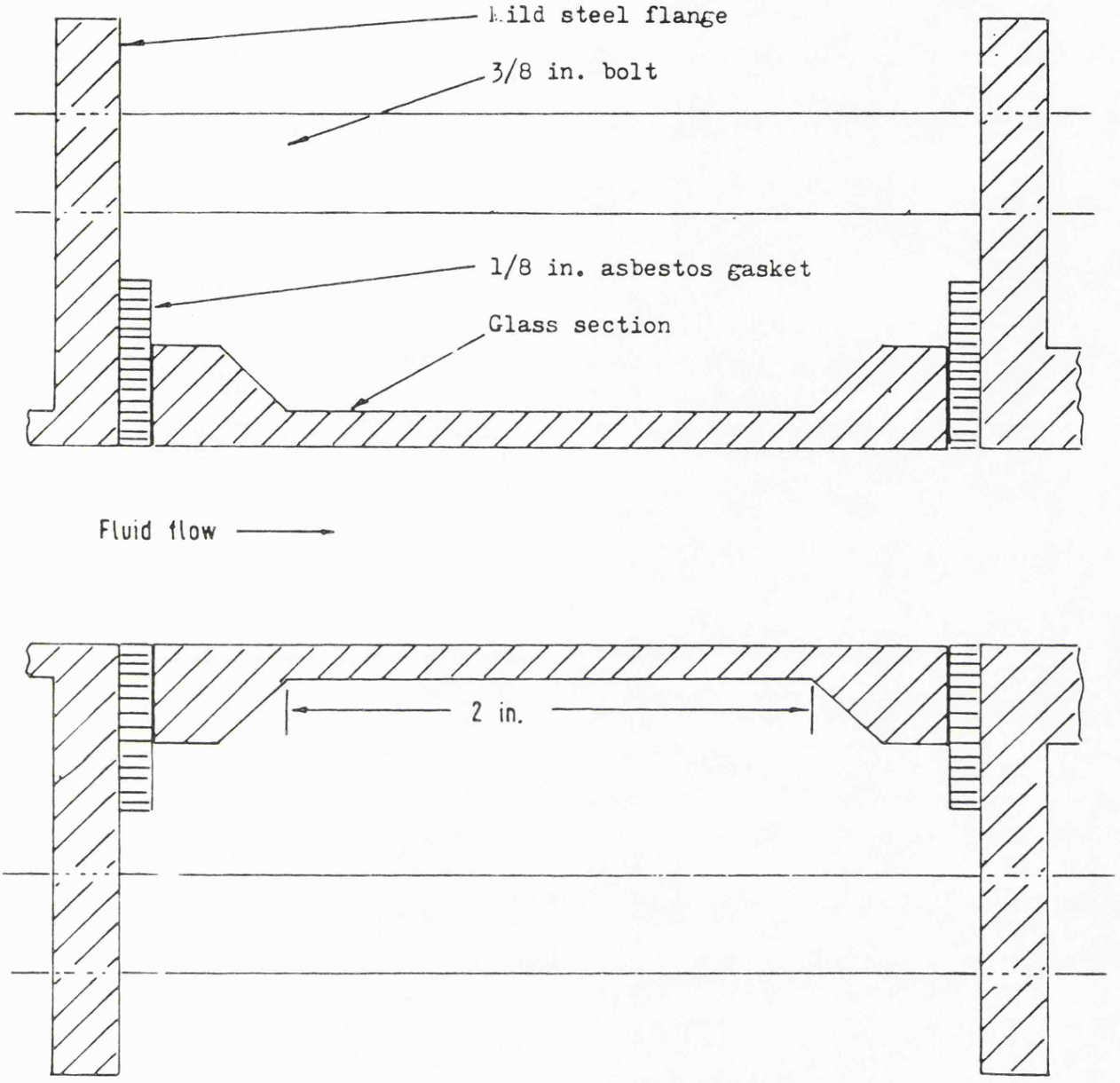

Figure 4.4 Diagram of visual section.

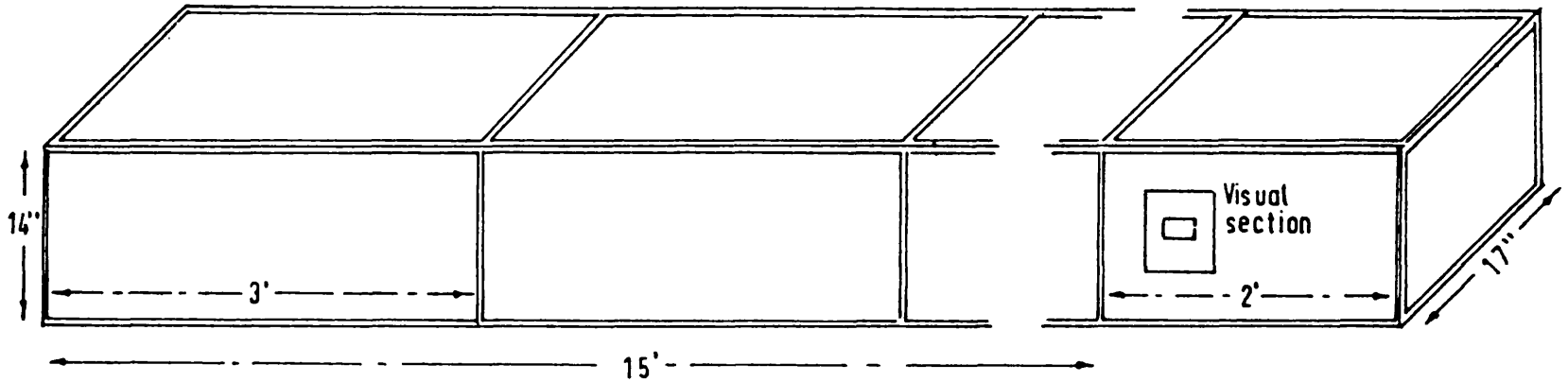

Figure 4.5 Furnace tube housing

Length = 14.75 ft.

Inside tube diameters: I.D. = 0.792 in. O.D. = 1.0 in.

Outside tube diameters: I.D. = 2.75 ins. O.D. = 3.0 in.

To allow for thermal expansion, bellows were fitted at two locations on each of the sections. (See Figure 4.6). The unit was fabricated from mild steel with neoprene rubber gaskets and each section was supported on rollers to allow for thermal expansion.

4.1.3 Process Variable Measurement/Instrumentation

The emf outputs from the thermocouples were displayed on a digital panel meter[114]. Temperatures of selected thermocouples could be recorded also on a twelve point single range chart recorder[114]. Vapour pressure thermometers were used to measure the temperatures of the furnace tube aluminium housing atmosphere, the hydrocarbon inlet to the tube, the hydrocarbon outlet from the condenser, and the cooling water outlet from the condenser.

The hydrocarbon flow rate through the furnace tube was measured by either

(1) Rotameter 18 x E stainless steel float (0-8 l/min. water at 20°C).

or (2) Rotameter 24 x E stainless steel float (0-20 l/min. water at 20°C).

The hydrocarbon purge flow to the pressure tappings was measured by a series 1100 Rotameter (0.6 - 6 ml/min. water at 20°C).

A relay switching arrangement permitted the selection of an individual heating element for power measurement on a

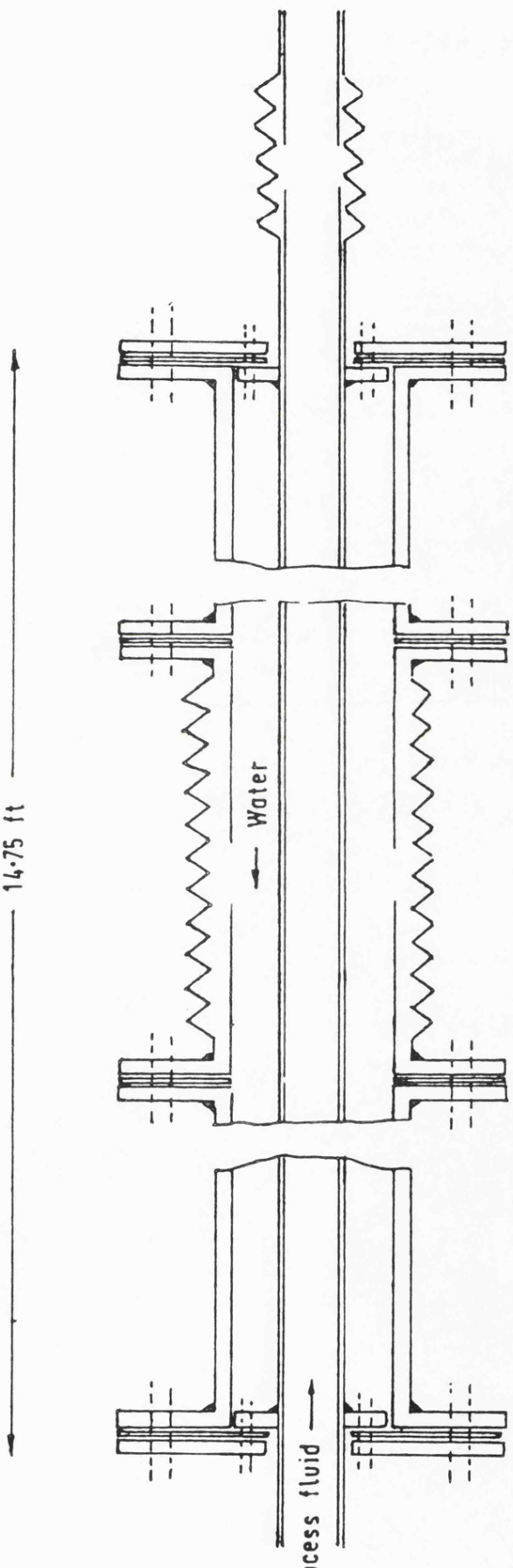

Figure 4.6 Condenser

0 - 4.8 KW wattmeter. (See Figure 4.7). The pressure drop along the tube was measured by an inverted U-tube manometer. A special feature of the unit was the ability to maintain a nitrogen atmosphere above the liquid levels in the manometer. In the event of a pressure surge the flow of a nitorgen atmosphere into the tube would not constitute a hazard, but rather suppress any existing hazard.

Chemical analysis of hydrocarbon feedstocks were carried out by means of a Pye 104 gas/liquid chromatograph fitted with heated dual flame ionisation detectors. A programmer controller facilitated linear temperature programming with initial and final periods of isothermal operation over any part of the analyser-oven temperature range. The output from the amplifier was recorded on a chart recorder and connected to a digital integrator.

4.1.4 Selection of Working Fluids

To study chemical reaction fouling at relatively low temperatures, the polymerisation of styrene dissolved at a concentration of 1% in odourless kerosene (supplied by Tenneco Organics) was chosen as the feedstock. Advantages of this system are

(1) Polymerisation of styrene is generally of known mechanism and kinetics. The kinetics of polymerisation in odourless kerosene could also be studied in laboratory.

(2) Relatively high rates of polymerisation at relatively low temperatures, thus enabling the possibility of studying the effects of mass trans-

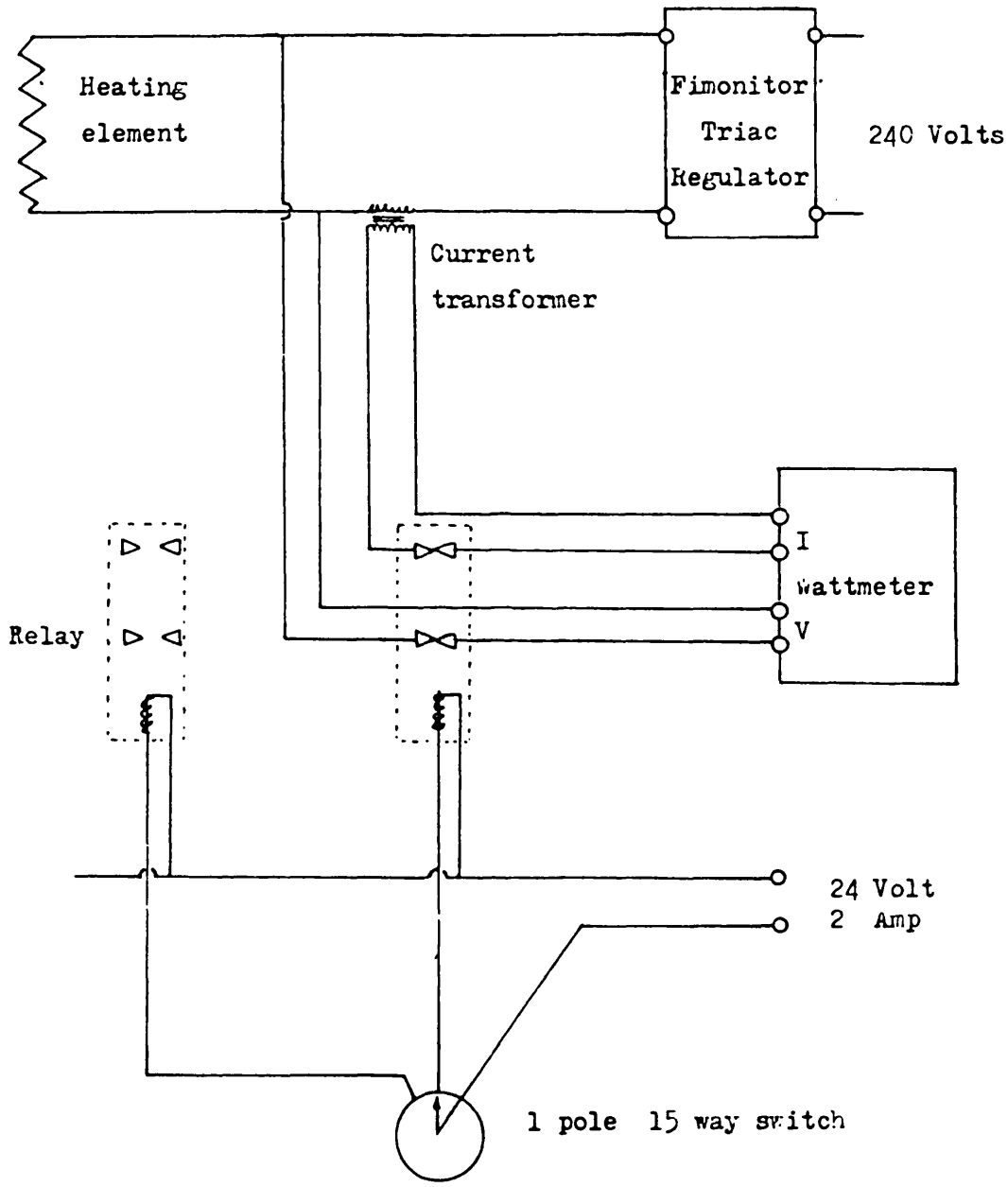

Figure 4.7 Power measuring circuit illustrated for one heating element.

fer in the fouling process.

(3) Close control on concentration of foulant precursor (styrene). Easy to check concentration by gas/liquid chromatography.

(4) Cheap, readily available feedstock.

(5) Foulant (polystyrene) can be removed easily from inside the furnace tube by washing and brushing out with an aromatic solvent.

(6) Odourless kerosene has a relatively high boiling point (200-240°C) ensuring a good range of temperatures for sensible heating. (See Table 4.1).

(7) Odourless kerosene is thermally stable up to its initial boiling point (201°C).

(a) high flash point for safety (79°C)

(b) kerosene is multi-component (potential for vaporization)

Disadvantages of this system are

(1) Chemical simulation, styrene only one of many possible foulant precursors in chemical reaction fouling. (See Table 4.2).

4.1.5 Safety and Loss Prevention

The flammable nature of the feedstock and the applied temperatures necessitated a very careful consideration of safety and loss prevention. As reported earlier[114] a large section of the hydrocarbon flow loop (water cooled heat exchanger and the storage tank) was sited outside the laboratory in a specially constructed housing.

An inert atmosphere of nitrogen was used in the furnace

Table 4.1 Properties of Odourless Kerosene Petroleum Fraction.

Typical Inspections Exsol	200/240
Initial Boiling Point (^{o}C)	201
5%	210
10%	214
50%	222
90%	236
95%	239
Final Boiling Point (^{o}C)	--
Dry Point (^{o}C)	243
S.G. at 60^{o}F	0.790
Flash Point (^{o}F)*	174
K-B Value	29
Aniline Point (^{o}C)	76
Total Aromatics (Vol. %)	0.5
Benzene (Vol. p.p.m.)	<20
Bromine No.	0.09
Colour (Saybolt)	+30
Sulphur (p.p.m.)	3
Comp. Evaporation Rate**	0.5
Viscosity @ 25^{o}C (Cps)	1.52
Refractive Index @ 20^{o}C	1.446
Litres/Tonne	1246

*Below 120^{o}F ABEL
Above 120^{o}F Pensky-Martens (closed)

**Comparative Evaporation Rate
for nButyl Acetate = 100

Table 4.2 Styrene Properties

Styrene (Phenylethylene)	M.Wt. = 104.15
$C_6H_5CH:CH_2$	99.5%
Wt/ml @ 20°C	0.904 to 0.906 gm
Refractive index n_D^{20}	1.5460 to 1.5475

Stablized with 0.001 to 0.002% tert-Butyl Catechol

Flammable, immiscible with H_2O

Explosive vapour air mixture

Harmful vapour

Irritating to skin, eyes and respiratory system

aluminium housing, hydrocarbon storage tank, pressure drop manometer, and tube purge. (See Figure 4.8). The aluminium housing was purged with a continuous flow of nitrogen to ensure an oxygen free atmosphere in the vicinity of the heating elements and tube outlet sampling point. This atmosphere was continuously monitored for oxygen and hydrocarbons. (See Figure 4.9). In the event of a nitrogen purge flow failure, a photo electric cell mounted on the Rotameter would trigger audible and visual alarms. An oxygen meter (Neotronics OTOX90) was used to monitor the oxygen concentration in the aluminium housing. The oxygen meter was set to trigger audible and visual alarms if the concentration of oxygen exceeded 1%. A thermal conductivity meter was used to detect the presence of hydrocarbons in the aluminium housing. The unit was calibrated and set to trigger audible and visual alarms if the nitrogen purge was contaminated by hydrocarbons.

The 34 gal. feed storage tank (27 x 20.5 x 20 in.) of galvanised steel was fitted with an 11.5 ft. vent. The vent outlet was fitted with a flame trap. The liquid level in the hydrocarbon reservoir was monitored to ensure adequate contents. The storage tank was continuously purged with a flow of nitrogen to render the atmosphere inert. The inclusion of a nitrogen supply at the tube inlet allowed for a purge in the event of an emergency shut-down. If this becomes necessary the tube and the water cooled heat exchanger could be purged with nitrogen and the tube cooled.

A hazardous situation could occur in the event of failure of either the feedstock flow to the tube or of the cooling water. The Rotameters in both of these circuits were fitted with photo-electric cells capable of detecting flow failure and

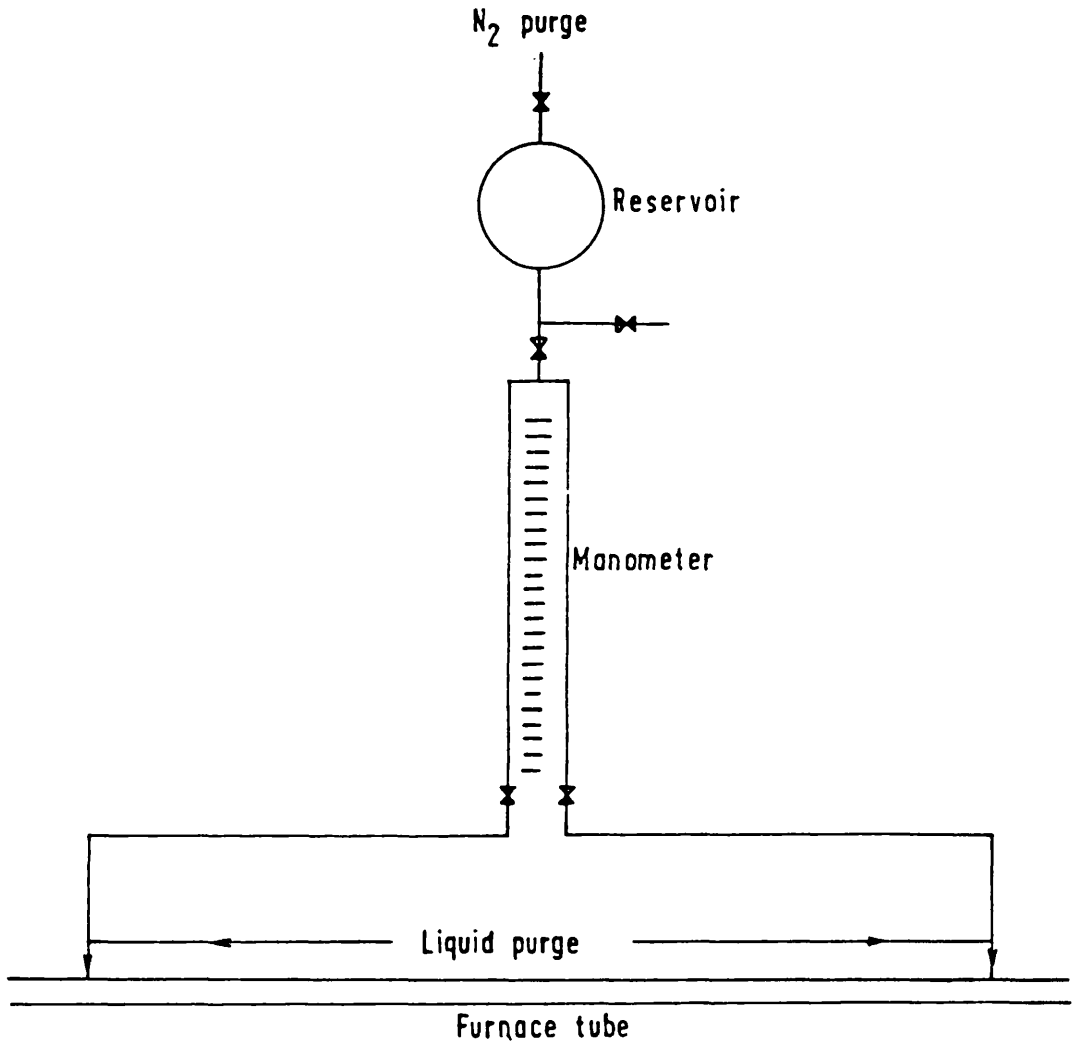

Figure 4.8 Pressure drop measuring circuit

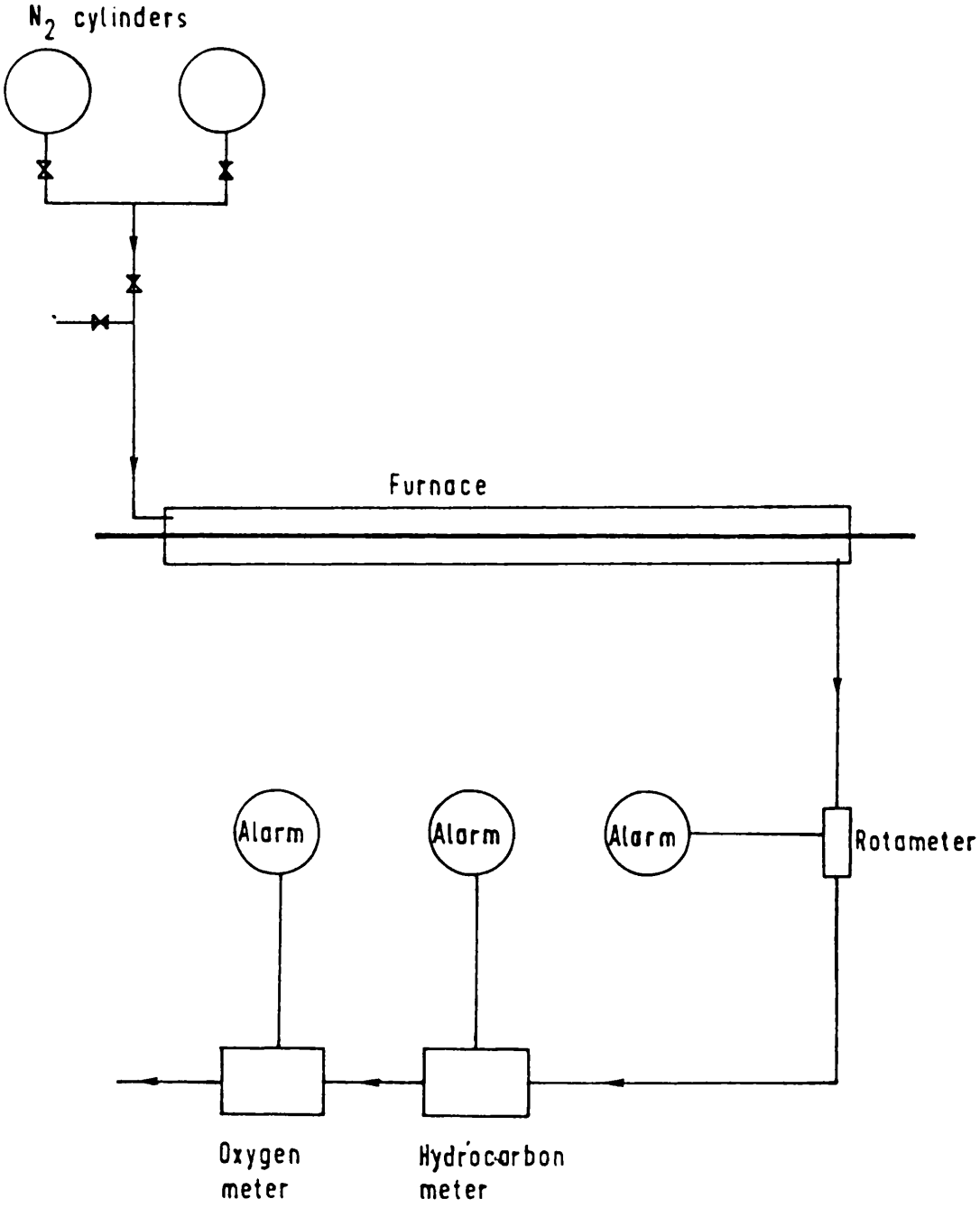

Figure 4.9 Flow diagram to illustrate the N_2 purge system of the aluminium furnace housing.

triggering audible and visual alarms. An additional feature of the heat exchanger cooling water flow failure detection system was a vapour pressure thermometer located in the hydrocarbon outlet line from the condenser. Electrical contacts on the dial enabled the selection of a set point to trigger a high temperature level alarm.

In the event of a blockage in the furnace tube a pressure relief valve in the by-pass header from the pump outlet would open automatically.

An automatic flammable gas monitor was sited in the hydrocarbon reservoir housing to detect the presence of flammable mixtures. To minimize hazards created by the generation of static charges the heat transfer loop was electrically bonded and earthed.

Fire protection was of main concern during the course of the work and fire fighting extinguishers and other equipment were in the vicinity of the apparatus.

4.2 Experimental Procedure

The two feedstock Rotameters were calibrated with the feedstock prior to carrying out the runs. The calibrations are given in Figures C1 and C2. (See Appendix C).

4.2.1 Preparatory Work Prior to a Run

The tube was visually inspected for cleanliness. The feedstock liquid was charged to the storage tank and the flow lines were purged with feedstock. The pressure drop manometer was purged as follows: (See Figure 4.10)

(1) Close all valves, open valves 1_f and 2_f.

(2) Pressurize flow loop by gradually closing valve

2_f until a pressure of 8 psig. is recorded on pressure gauge P_f.

(3) Purge reservoir R with nitrogen by opening valves 4n and 5n, then close both valves.

(4) Purge the pressure tapping purge lines by opening valves 1p, 2p, 3p, 4p, and 5p.

(5) Close valves 2p and 3p. The inlet pressure manometer line is purged by opening valves 6p, 1n, 2n, and 4n, thus charging R with liquid. When bubbles cease to appear in R, close valve 6p and open valve 2_f.

(6) Close 4n and open 5n pressurizing R to 5 psig. The contents of R may be discarded by opening valve 3n or they may be returned to the hydrocarbon flow line by opening valve 6p until the desired liquid level in the manometer is reached at which point valves 6p and 5n are closed.

(7) Close 1n and 2n. Open 6p and 7p. The manometers are then checked to give a zero pressure difference at zero flow.

4.2.2 Start-up of Circulation/Test System

(1) Check auxiliary equipment, availability of tools, nitrogen cylinders, fire fighting equipment, etc.

(2) Switch on alarm circuit.

(3) Start cooling tower fan and cooling tower feed pump.

(4) Switch on equipment power supply.

(5) Start heat exchanger water pump (cancel triggered

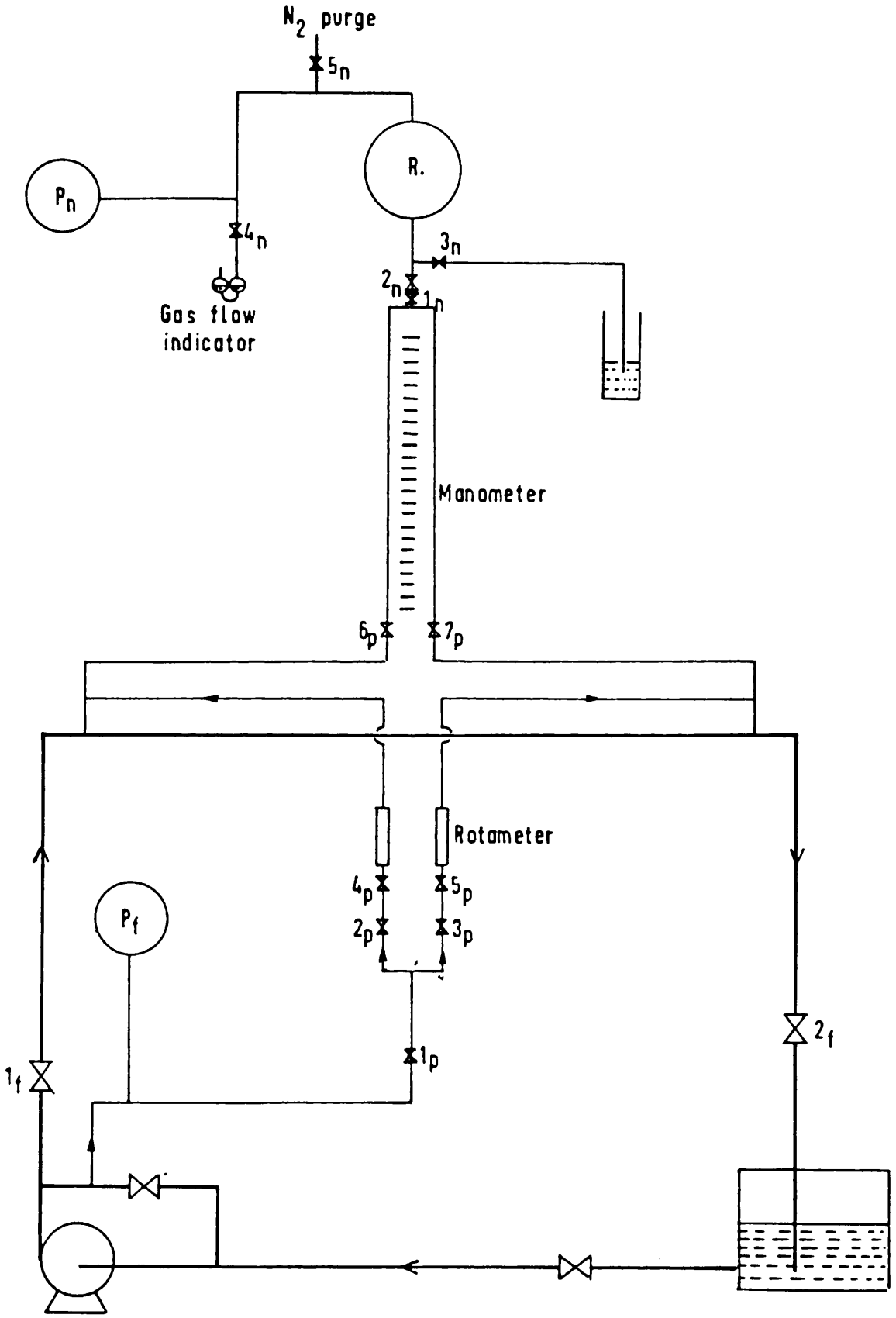

Figure 4.10 Flow diagram of pressure drop measuring lines and purge lines

Table 4.3 Pump specifications.

	TYPE	CAPACITY	SPECIALITY	SUPPLIER
Hydrocarbon	25 WH 161 centrifugal	2 gal/min.octane 20 ft. head	Flame proof	Worthington Simpson Ltd.
Water	32 WJ 160 centrifugal	5 gal/min.water 20 ft. head		Worthington Simpson Ltd.

alarm).

(6) Purge aluminium housing and hydrocarbon tank with nitrogen (cancel triggered alarm).

(7) Start hydrocarbon pump (cancel triggered alarm).

(8) Check flow loop for leaks.

(9) Purge relevant lines with hydrocarbon (pressure lines, by-pass line, etc.) and further check for leaks.

(10) If pressure drop manometer is operational, purge gas space above the liquid with nitrogen.

(11) When the oxygen content in the aluminium housing atmosphere approaches 1% $^{v}/v$, switch on heating elements.

(12) Fill the thermocouple reference container with ice-water slurry.

(13) Allow the equipment to reach steady state before taking experimental measurements.

Operations (1) to (12) took 40 min. A time of between 1.5 and 1.75 hrs. was required before the equipment reached steady state. A very high flowrate was set for the desired heatflux. When steady state was reached the flowrate was reduced to the desired level. The new steady state was reached within 10 min.

4.2.3 Procedure During Runs

Continuous supervision of the equipment was required for safety purposes and therefore the runs were designed to last for 12 hrs. only. The temperatures of the various thermocouples were digitally displayed although some were also re-

corded on charts. Temperature readings and other measurements were made at intervals of ½ hr. for the duration of the experiment. Throughout the experiments the pressure did not exceed 4 psig. Periodically the styrene concentration in the circulating fluid was determined by withdrawing a sample for analysis by gas/liquid chromatography. The styrene concentration was not allowed to fall below 0.96% $^{v}/_{v}$.

4.2.4 Shut-Down Procedure

(1) Switch off heating elements.

(2) Increase hydrocarbon flow to a maximum.

(3) When element temperatures drop to below 100°C shut hydrocarbon flow valve and switch off hydrocarbon pump.

(4) Shut-down water circulation pump, cooling tower air fan and pump.

(5) Close nitrogen purge flow and switch off alarm system.

(6) Switch off power supply.

4.2.5 Inspection and Cleaning of the Tube and Test Section

The hydrocarbon pump outlet valve was kept closed, and the tube was purged with nitrogen. With the nitrogen purge still on, the hydrocarbon pump outlet valve was slowly opened to flush back the hydrocarbon liquid. The necessary panels of the aluminium housing were removed and the required couplings on the tube inlet and outlet were disconnected. The tube was visually inspected. Some of the deposit was scraped out for chemical, spectroscopic and scanning electron microscopic analyses.

The test section was rinsed using an aromatic solvent

pump-around system before and after the mechanical scraping by a long brush and wire tube cleaner. The test section was then left to dry.

The system was purged with nitrogen again and then flushed with hydrocarbon. The hydrocarbon flushing fluid was recovered for further cleaning purposes. The system then was considered to be clean and ready for the next experiment.

5.0 Results

5.1 Single Phase Forced Convective Flow

5.1.1 Pressure Drop

Pressure drop was considered to be a means of detecting significant fouling inside the tube. The loop was filled with 100% kerosene liquid and the pressure drop was measured at various flow rates. The results are given in Figure 5.1. The Reynolds number was calculated from:

$$Re = \frac{4\ G}{\pi d \mu} \tag{115}$$

in which

G = mass flow rate

μ = fluid viscosity

The relationship between Re and G is shown in Figure 5.2.

5.1.2 Tube Roughness Evaluation

To obtain an indication of the tube roughness, a comparison of the experimental friction factor-Reynolds number curve with an established correlation for rough surfaces was conducted. The results are shown in Figure 5.3. The experimental value for the friction factor was calculated from:

$$\Delta p = 4\Phi \frac{L}{d}\ \rho u^2 \tag{116}$$

where

Δp - pressure drop

Φ - friction factor

L - length of test section

d - inside diameter of tube

ρ - fluid density

u - average fluid velocity

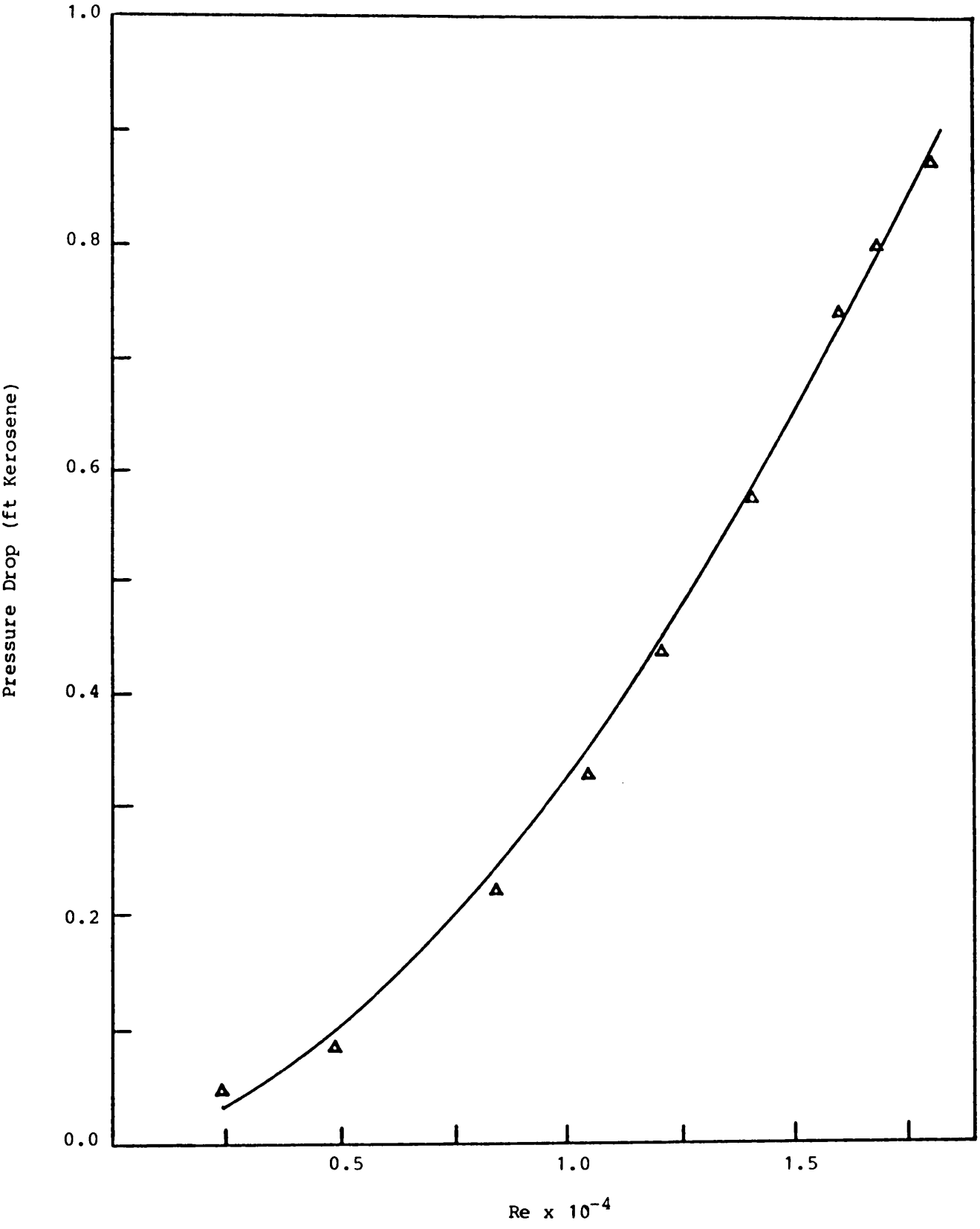

Figure 5.1 A Plot of Reynolds Number Against Pressure Drop for 100% v/v Odourless Kerosene.

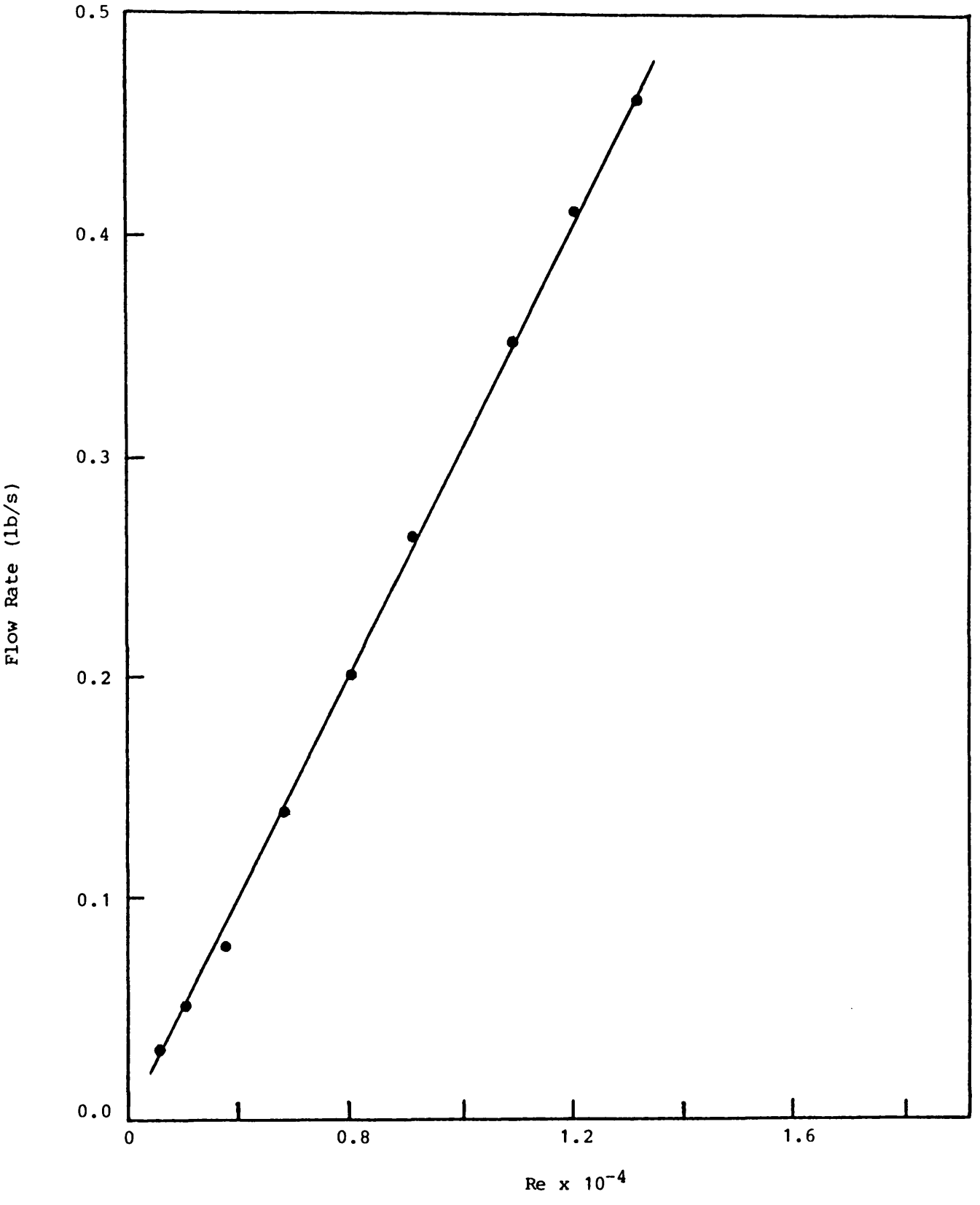

Figure 5.2 A plot of Reynolds Number Against Flowrate for 100% v/v Odourless Kerosene.

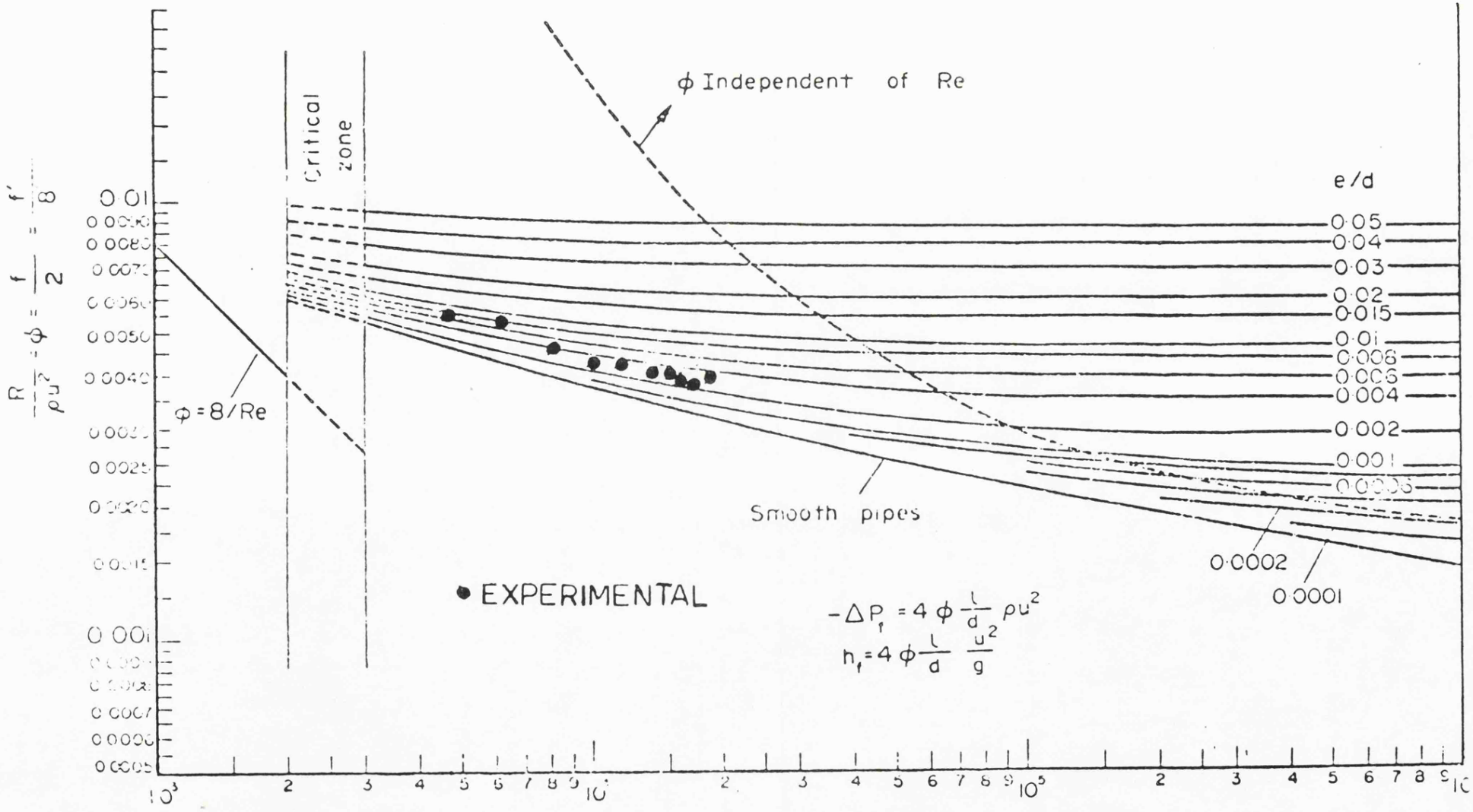

Figure 5.3

Pipe friction chart ϕ versus Re.

An absolute roughness profile was previously measured by Kolaczkowski[114] with a Talysurf. See Figures 5.4, 5.5, and Table 5.1 .

An indication of the surface roughness of the furnace tube was obtained also by Kolaczkowski[114] working with n-Hexane and methylcyclo hexane fluids. His results are shown in Table 5.2 and Figure 5.6.

These results indicate that the average roughness lies between 0.0015 and 0.008 giving protuberance heights on the heat transfer surface of between 0.0012 and 0.0064 ins.

5.1.3 Heat Transfer Evaluation

5.1.3.1 The Determination of the Thermal Characteristics of the Tube

The equipment was started with the maximum flow rate to warm up the system.

The time required for the equipment to reach a thermal steady state from cold was between 1.5 and 1.75 hours. Then the flow rate was decreased to the desired value. The time required to reach the new thermal steady state after the flow rate variation was in the region of 10-15 minutes. One run was carried out each day at a fixed heat flux and fixed flow rate. After a run, the equipment was shut down and the tube was cleaned. A range of heat fluxes was chosen and a series of runs were carried out at each heat flux with various flow rates.

In the manner described by Kolaczkowski[114] the heat transfer efficiency is defined as:

$$\% \text{ efficiency} = \frac{\text{Heat input to process fluid}}{\text{indicated heat output from heating elements}} \times 100\% \quad (117)$$

$$= \frac{Q_I}{Q_O} \times 100$$

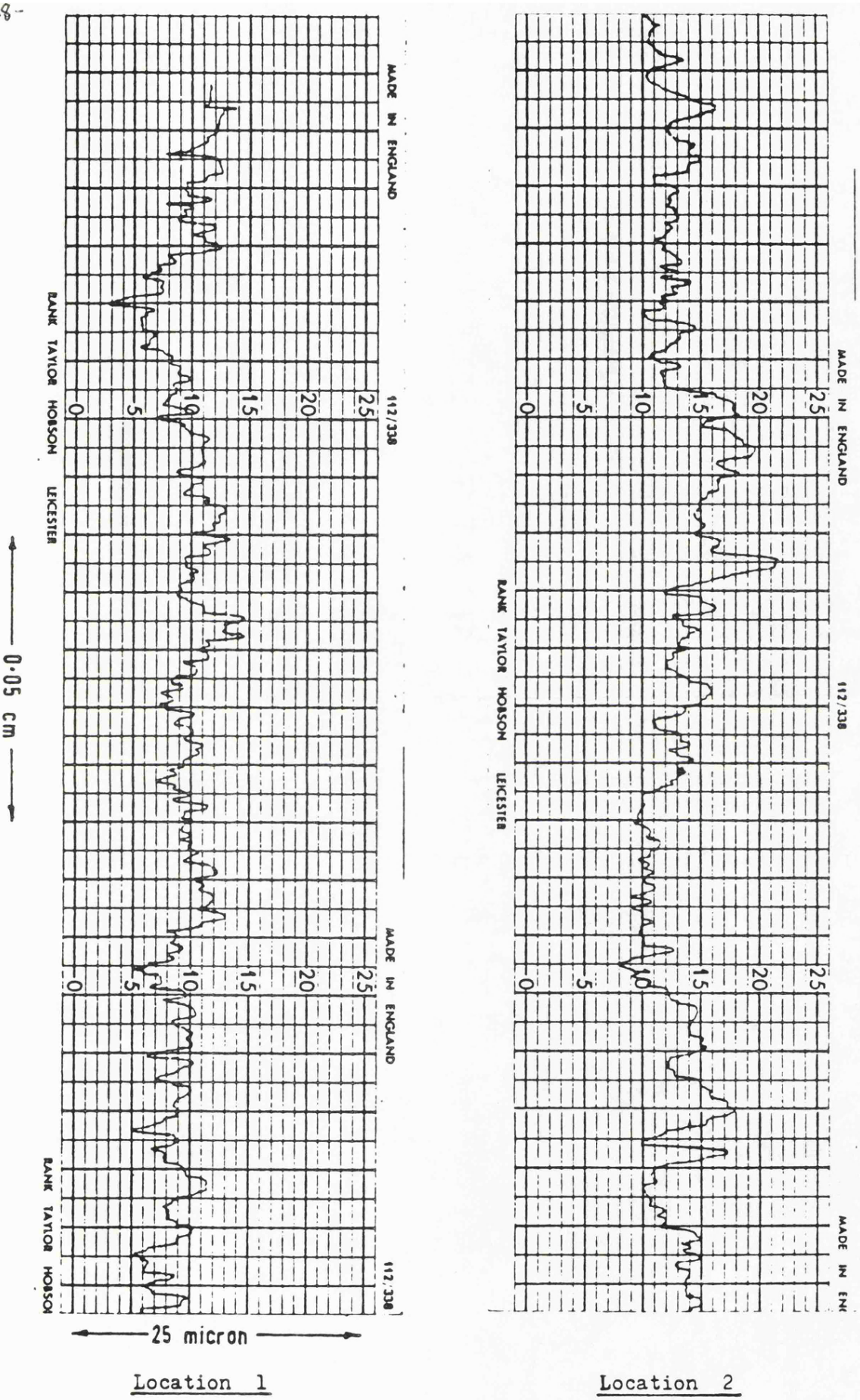

Figure 5.4 Surface profile measurements for a sample of the furnace tube. (114)

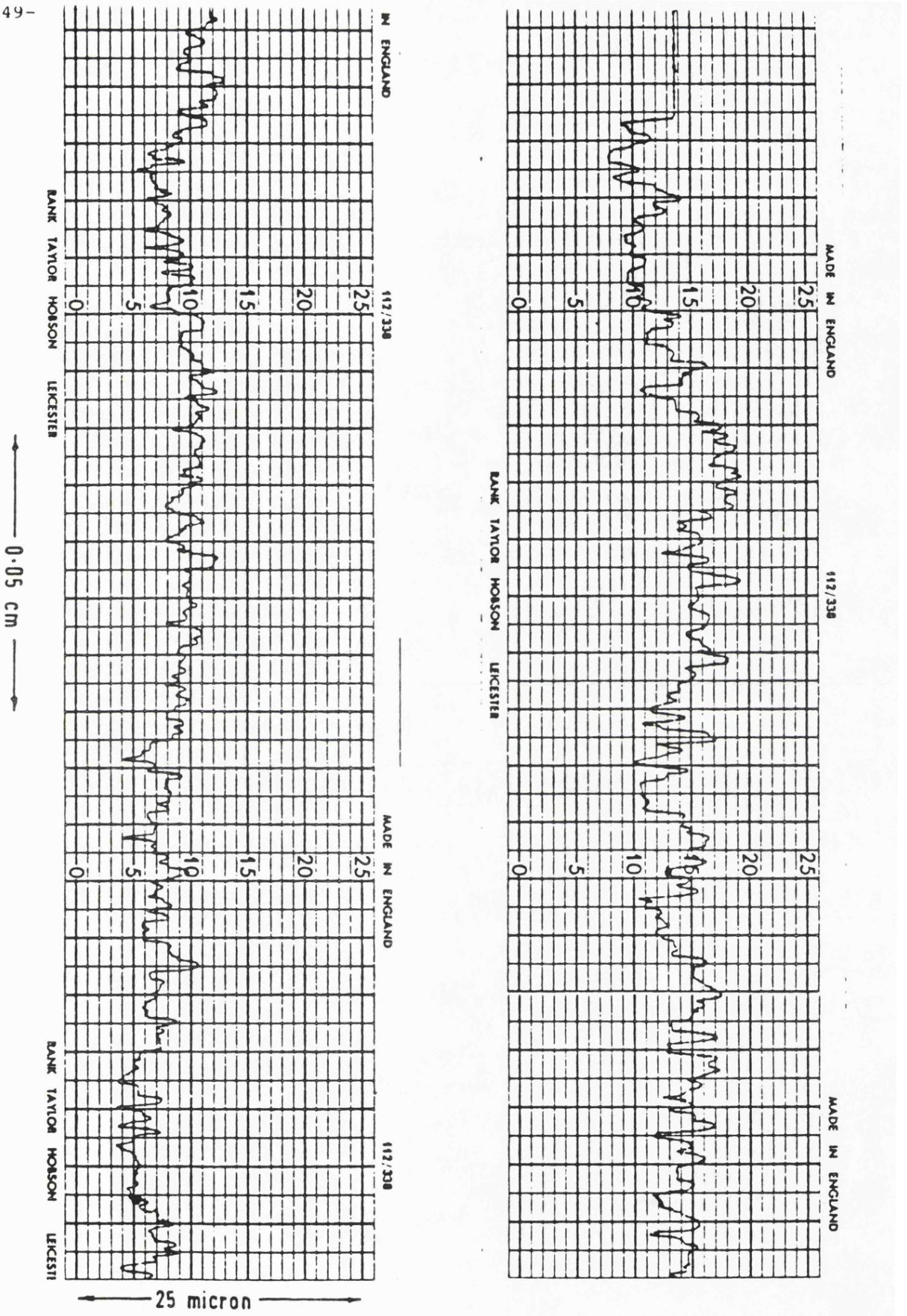

Figure 5.5 Surface profile measurements for a sample of the furnace tube. (114)

Location	Approximate average value (in)	Approximate maximum value (in)
1	0·000048	0·00016
2	0·000056	0·00038
3	0·000046	0·00014
4	0·000058	0·00022

Tube:

I.D. 0·792 in.

O.D. 1·0 in.

Type 321 stainless steel.

Table 5.1 Tube Roughness Measurements.[114]

Table 5.2 Experimental results for hydraulic roughness evaluation.[114]

Flow (lb/m)	Pressure drop (cm of feedstock)	Friction factor	Reynolds number
27.0	30.0	0.0035	23,488
25·5	27·6	0·00363	22,183
23·5	24·15	0·00374	20,443
22·1	21·7	0·0038	19,225
21·0	19·4	0·00376	18,268
19·6	16·9	0·00377	17,050
17·2	13·6	0·00394	14,963
15·1	11·0	0·00413	13,136
12·7	8·1	0·00429	11,048
10·3	5·7	0·0046	8,960
8·2	3·7	0·00471	7,133

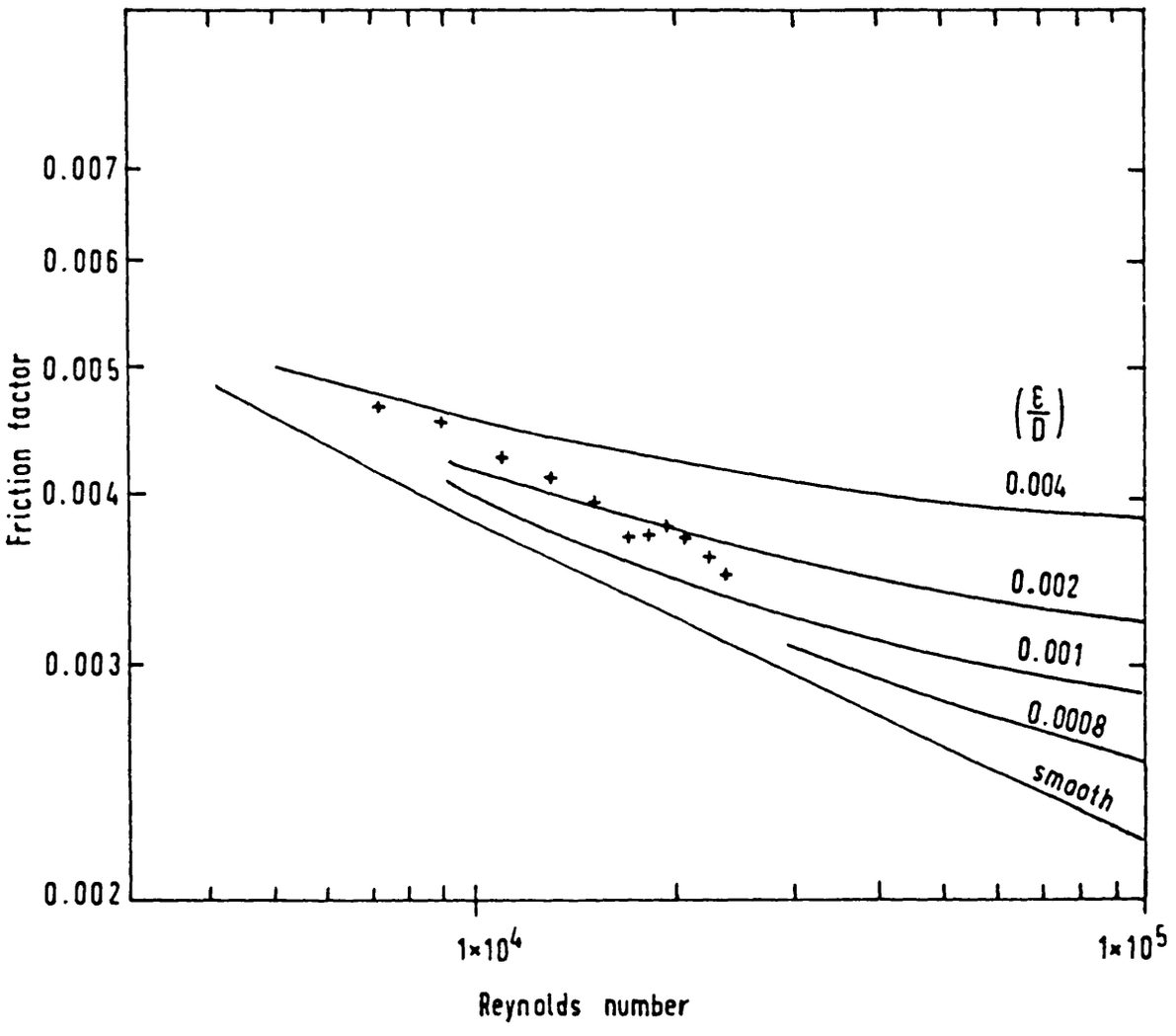

Figure 5.6 Hydraulic roughness determination for the furnace tube.[114]

The indicated heat output from the elements was measured in kilowatts thus:

$$Q_O = Kw \times 3413 \qquad (118)$$

in which

Kw - indicated power output (kilowatts)

Q_O - indicated heat output (Btu/hr)

The heat gained by the process fluid is given by an enthalpy balance:

$$Q_I = G\ (H_O - H_I) \qquad (119)$$

in which

Q_I - heat input (Btu/hr)

G - feed flow rate (lb/hr)

Ho - enthalpy of fluid at outlet from furnace tube (Btu/lb)

H_I - enthalpy of fluid at inlet to furnace tube (Btu/lb)

It was noticed that the efficiency varied on a run to run basis, but not during the run. This was to be expected since the ambient conditions would affect the rate of heat loss from the aluminium housing. Thus it was decided to evaluate the thermal efficiency of the tube on the day of the run at the desired heat flux.

5.1.4 Heat Transfer to Odourless Kerosene (Exsol 200/240°C)

A typical dearomatized, odourless kerosene with relatively stable characteristics (initial boiling point is 201°C) was chosen to be a carrier solvent for the chemical simulation of the fouling process. Before the fouling studies were commenced, it was necessary to obtain the appropriate physical properties of the kerosene over the range of operating conditions (See Appendix E), and to determine the heat transfer characteristics of the kerosene over the ranges

of flow rate and heat flux to be studied. See Figures 5.7-5.12.

The experimental heat transfer coefficient, h_{exp} was evaluated from the overall heat transfer coefficient and the tube wall thermal resistance (See Appendix B).

$$h_{exp} = \frac{d_o/d_i}{1/U - R_{T/C}} \tag{120}$$

where

d_o - outside diameter of the tube

d_i - inside diameter of the tube

U - overall heat transfer coefficient

$R_{T/C}$ - Thermal resistance of the tube wall and of the thermocouple mounted on the wall.

Figure 5.7 shows a rise in the value of the heat transfer coefficient at the end of the tube. This indicates that some bubbles were formed at the wall during this measurement. This is attributed to either dissolved gas, mainly nitrogen used as a purge in the kerosene batch, or to subnucleate boiling taking place in this particular test. This test was a preliminary heat transfer test where styrene was not included in the kerosene batch. However, the temperature at the wall did not exceed the bubble point.

Kolaczkowski[114] also found values of the heat transfer film coefficient greater than the values estimated by the Dittus-Boelter equation[66] for the same tube.

At a constant heat flux, with power in the range 0.2-2.2 KW per element, the effect of flow rate (in the range 200-1800 lb/hr) on the inside and outside wall temperatures and the bulk fluid temperatures was studied. Figures 5.13-5.15 show the variation of these three temperatures with flow rate for one thermocouple

location at the end of the heated section. Superimposed on these graphs are the initial rates of polymerisation of pure, 100% v/v styrene as a function of bulk temperature as given by Roper[168]. These graphs were used to give an indication of suitable operating conditions for the fouling study.

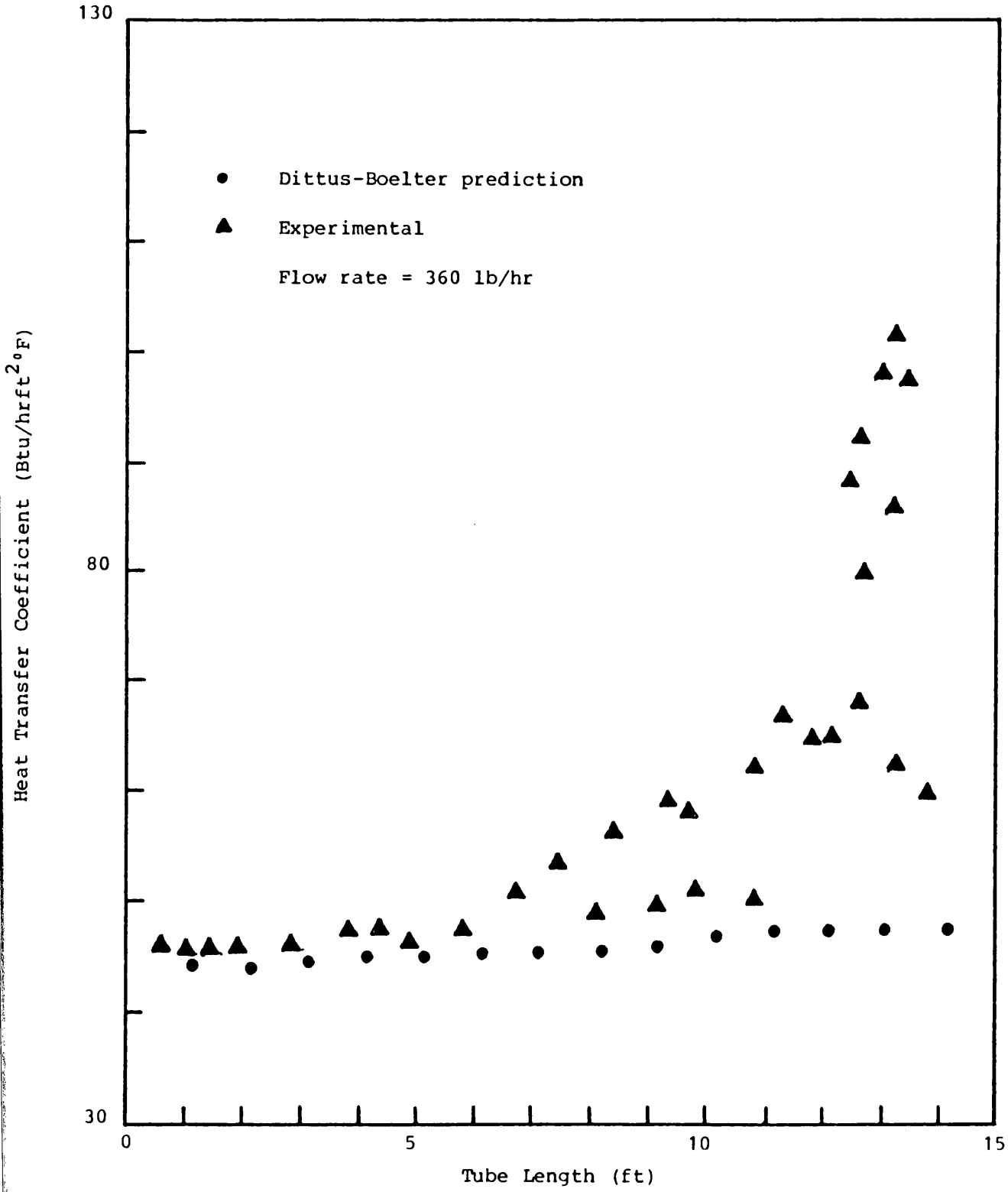

Figure 5.7 Heat Transfer Coefficient Profile. All Liquid 100% v/v Kerosene.

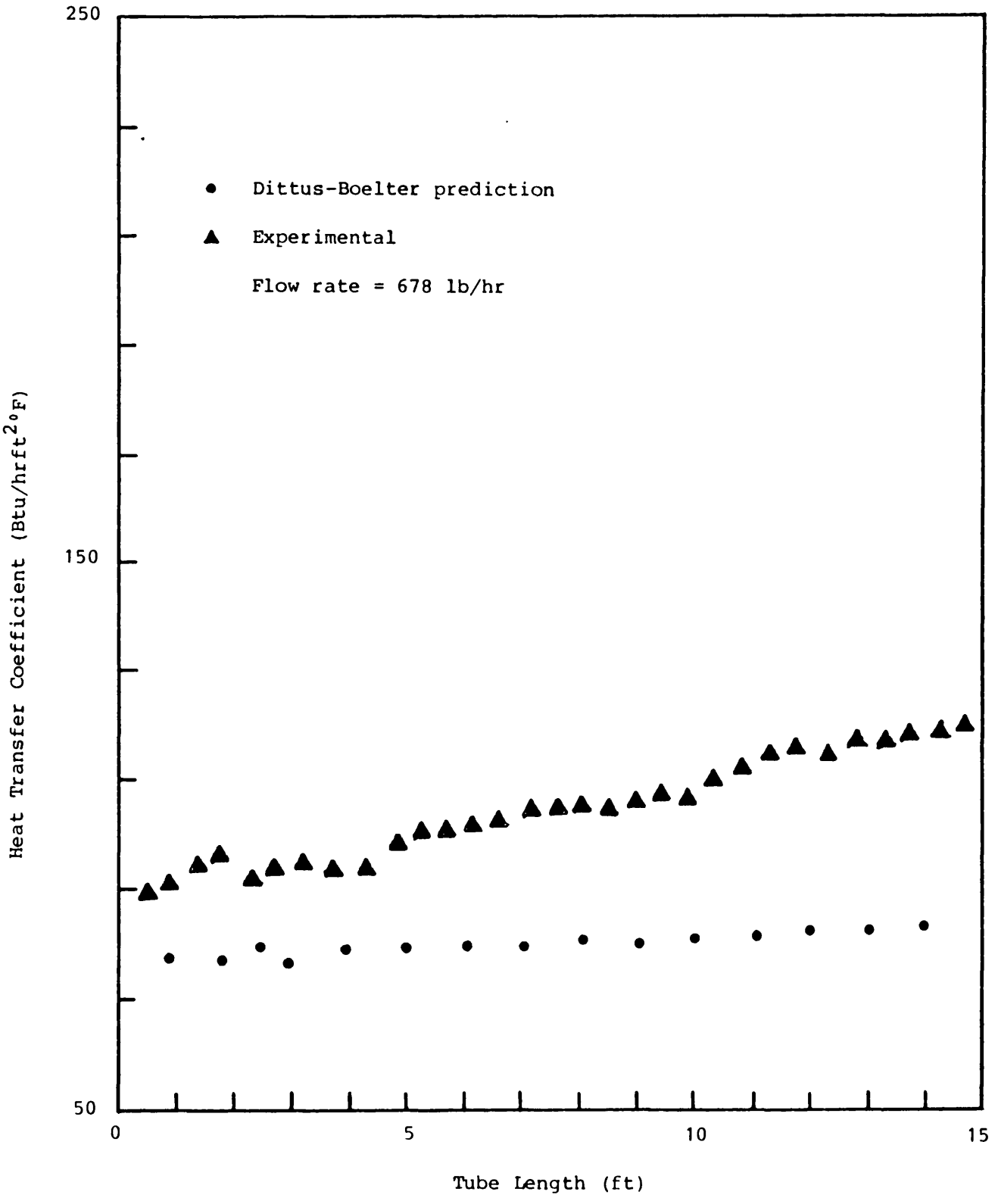

Figure 5.8 Heat Transfer Coefficient Profile. All Liquid 100% v/v Kerosene.

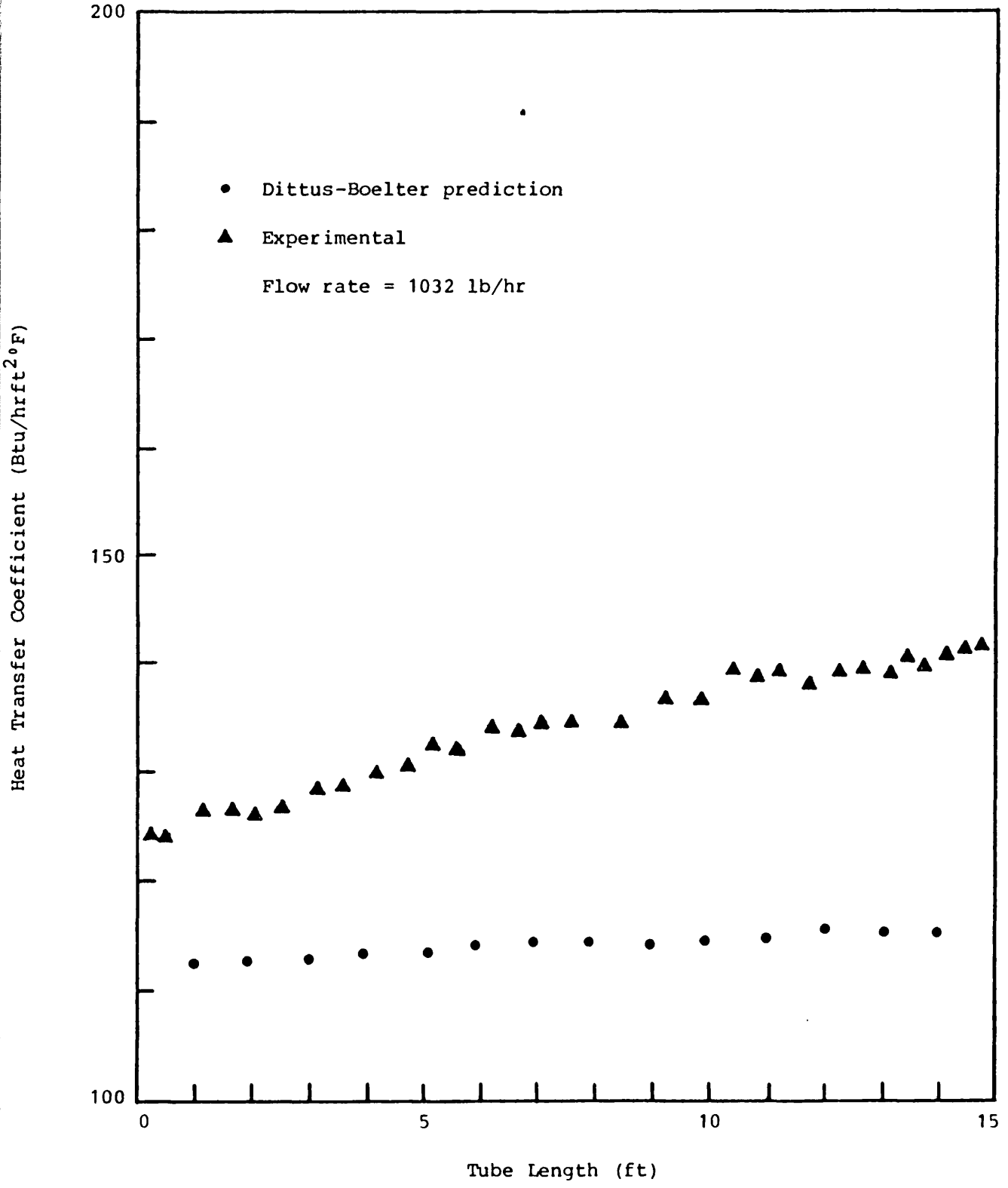

Figure 5.9 Heat Transfer Coefficient Profile. All Liquid 100% v/v Kerosene.

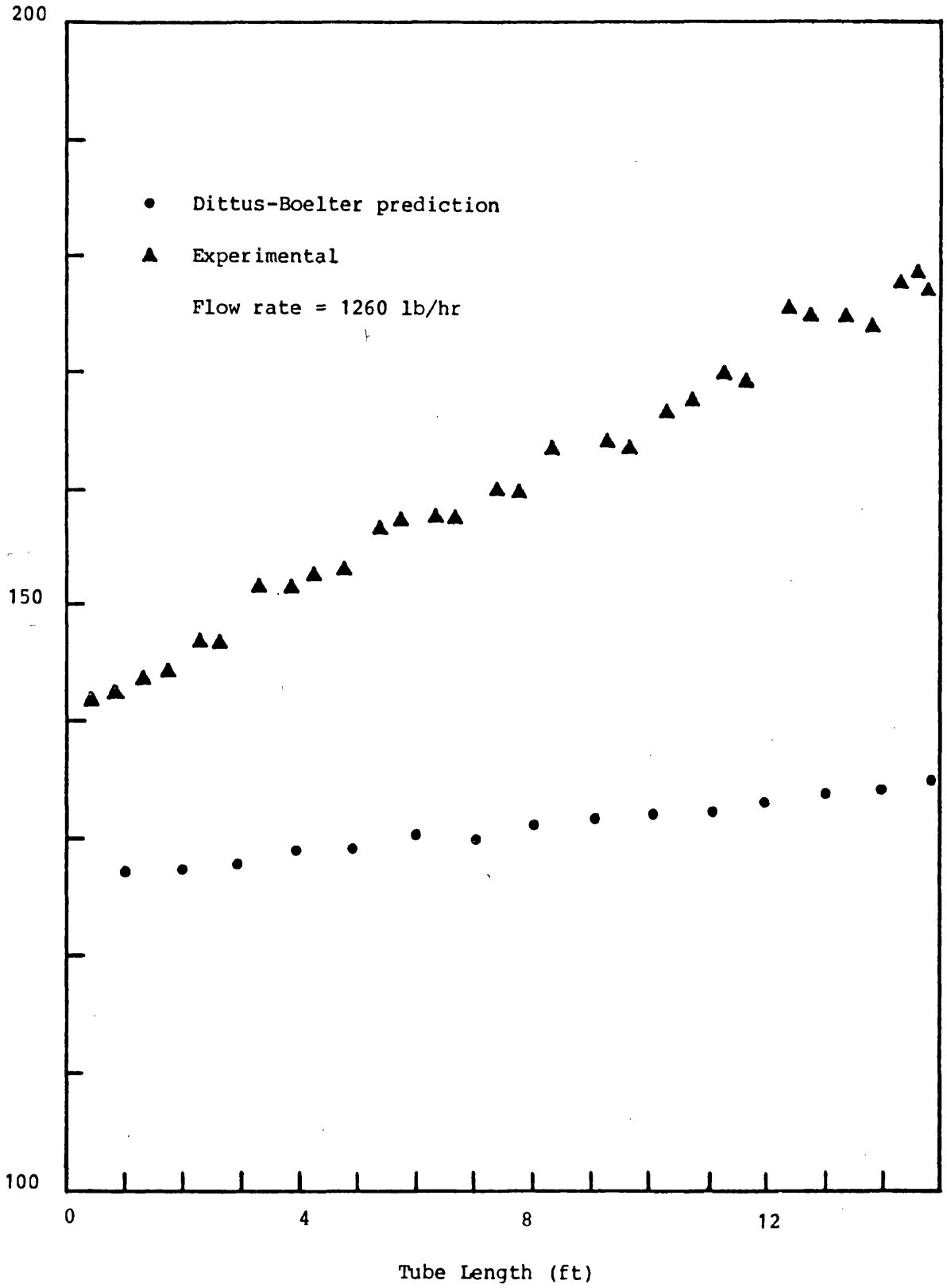

Figure 5.10 Heat Transfer Coefficient Profile. All Liquid 100% v/v Kerosene.

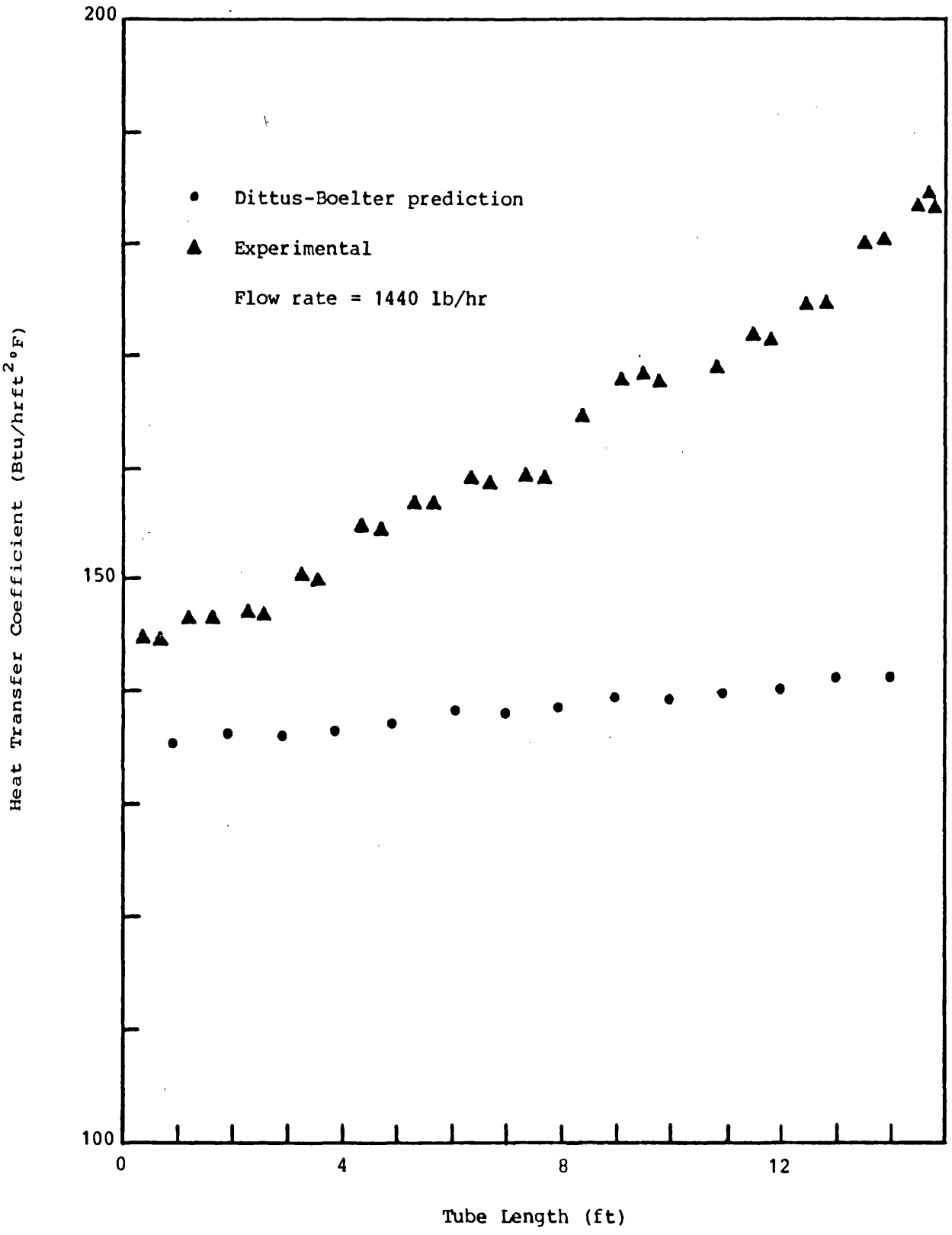

Figure 5.11 Heat Transfer Coefficient Profile. All Liquid 100% v/v Kerosene.

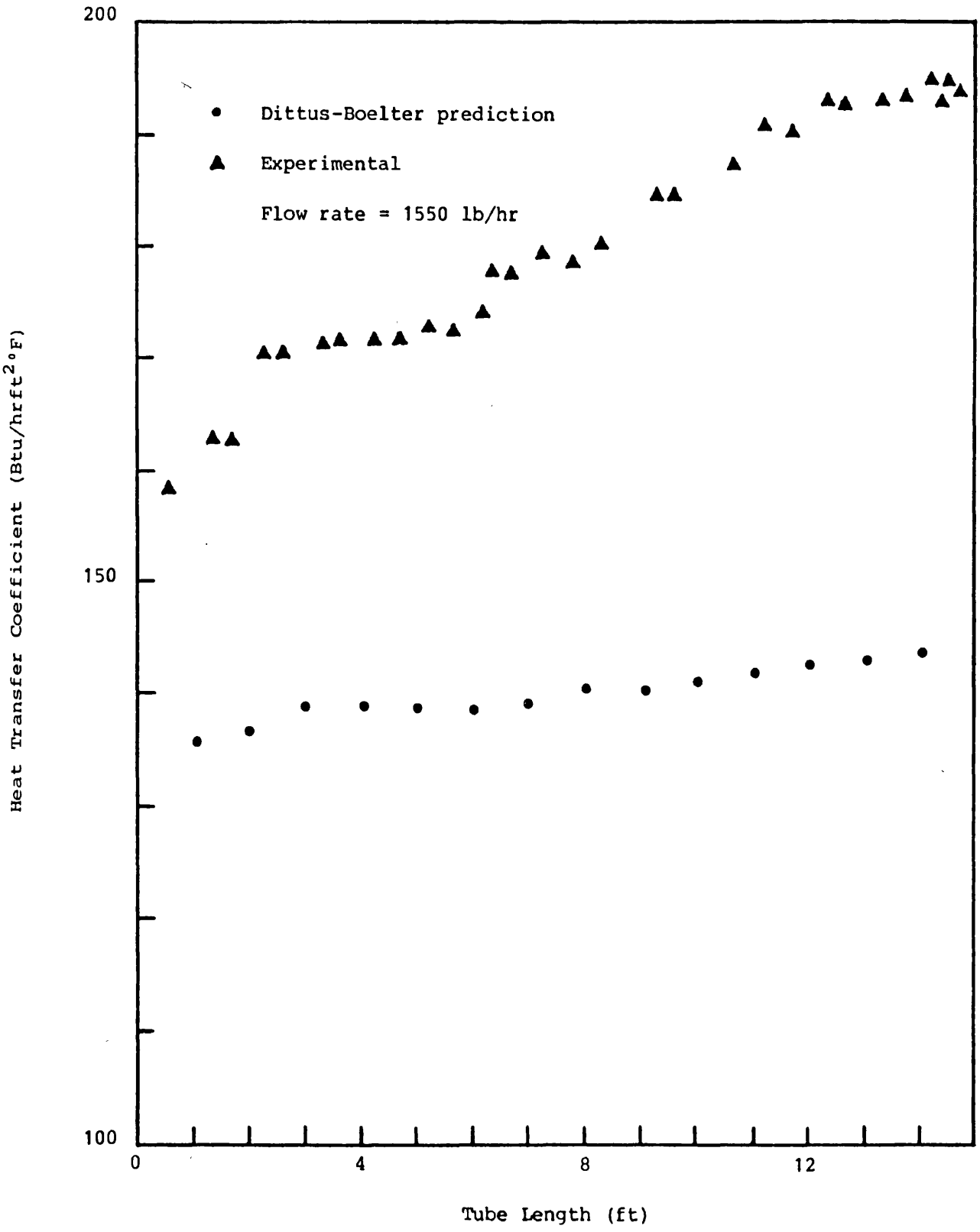

Figure 5.12 Heat Transfer Coefficient Profile. All Liquid 100% v/v Kerosene.

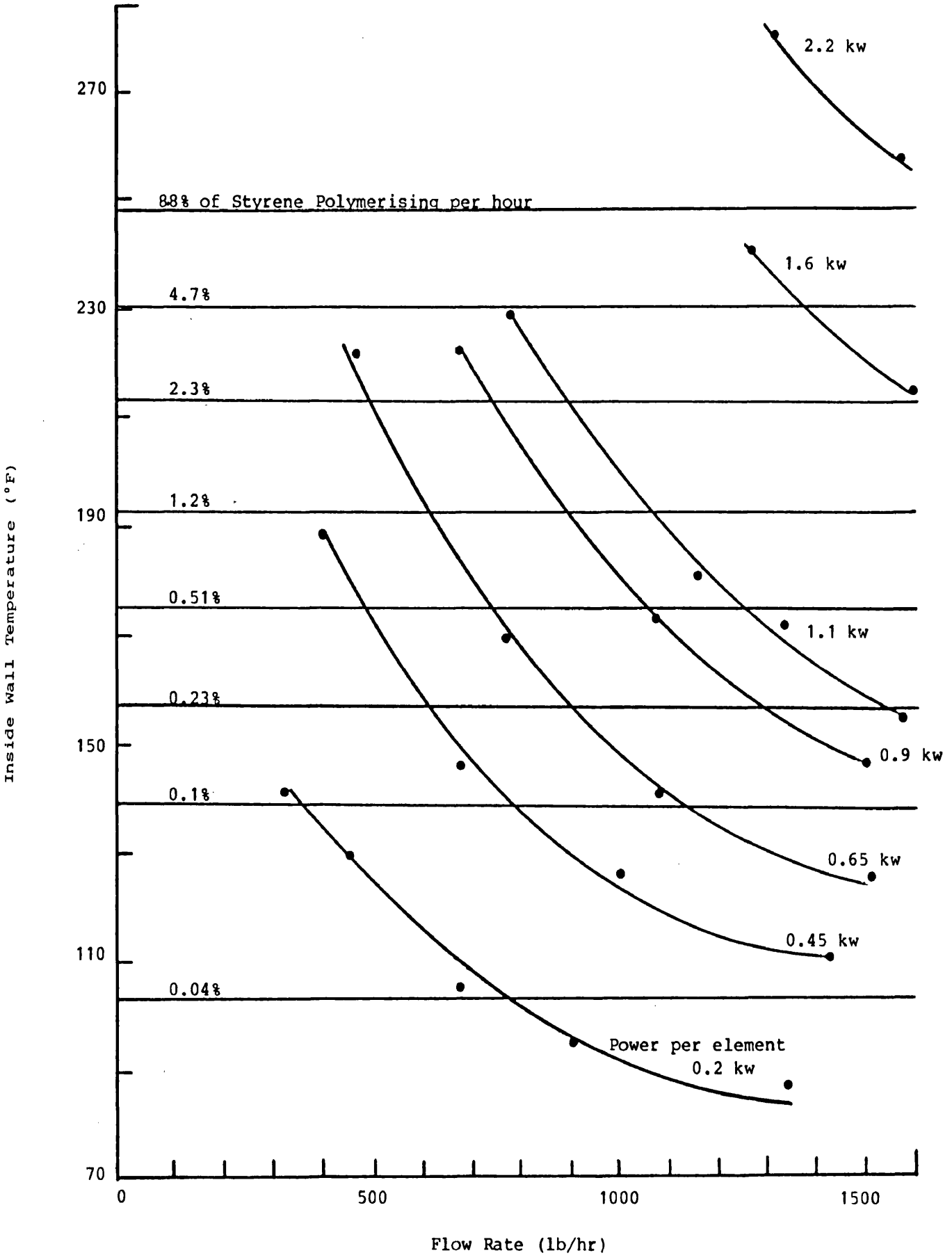

Figure 5.13 Inside Wall Temperature vs. Flowrate. Kerosene System. Element 15, Thermocouple 9.01.

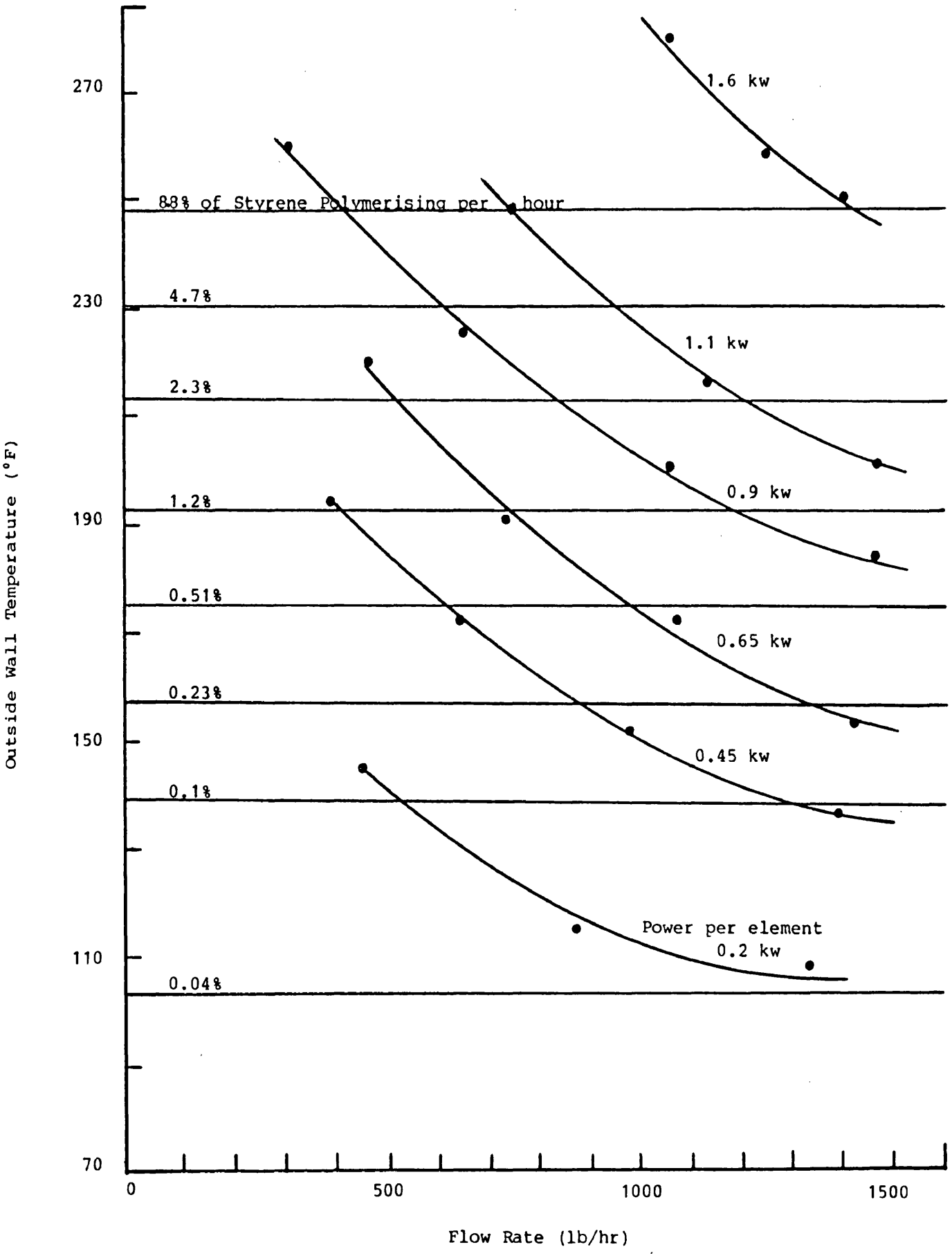

Figure 5.14 Outside Wall Temperature vs. Flowrate. Kerosene System. Element 15, Thermocouple 9.01.

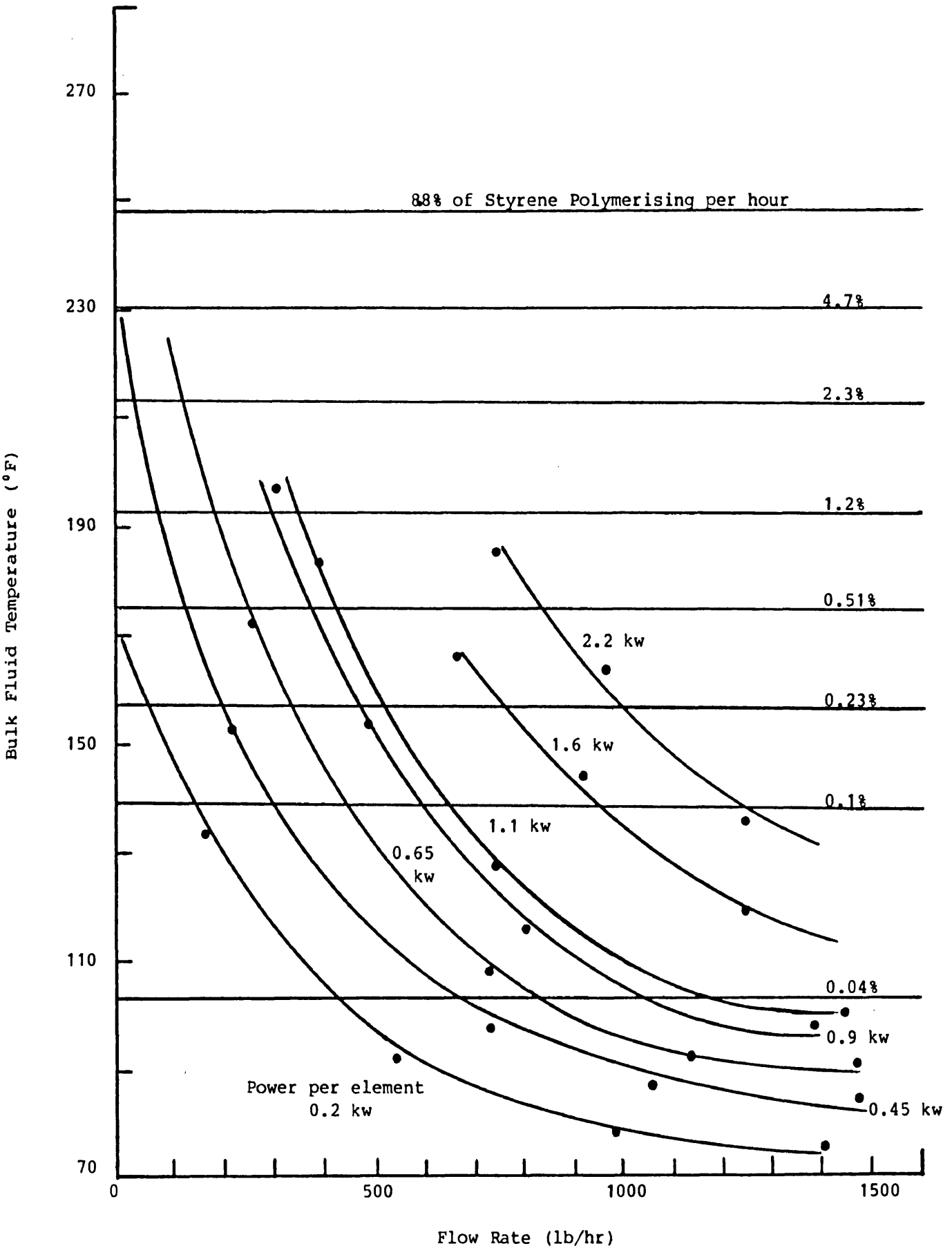

Figure 5.15 Bulk Fluid Temperature vs. Flowrate. Kerosene System. Element 15, Thermocouple 9.01.

5.2 Experimental Fouling Results of 1% v/v Styrene in Kerosene

The variation of heat transfer resistance with time was studied over a range of flow rates and heat fluxes shown in Table 5.3.

5.2.1 Calculation Methods

An outline of the calculation method is presented here. Full details and sample calculations appear in Appendix I.

The fouling resistance at any instant is given by

$$R_f = \frac{1}{U_f} - \frac{1}{U_c} \qquad (121)$$

in which

U_f - instantaneous heat transfer coefficient for fouled conditions

U_c - instantaneous heat transfer coefficient for clean conditions

U is given by

$$U = \frac{\Phi}{T_s - T_b} \qquad (122)$$

where Φ = heat flux

T_s = outside wall temperature at a certain location

T_b = bulk fluid temperature at this location

The heat flux was kept constant during each run and was obtained from the power dissipated in the tube wall. This was equal to the power indicated by the wattmeter multiplied by the efficiency. The heat loss was considered to be uniform along the length of the tube, i.e. the efficiency was considered to be independent of tube length.

Table 5.3 Range of Operating Conditions.

Run	Heat Flux Per Element ($Btu/hr.ft^2$)	Flow Rate (lb/hr)	Initial Inner Wall Temperature (^0F)
1	1851.0	1620	97.6
2	1851.0	1446	104.4
3	1851.0	1278	111.0
4	1851.0	1104	119.0
5	1851.0	936	128.0
6	2424.5	780	167.0
7	2268.1	624	181.0
8	2398.4	480	214.0
9	1851.0	336	225.0
10	4901.2	1620	148.0
11	4901.2	1446	159.0
12	4849.0	1278	167.0
13	4901.2	1104	180.0
14	4849.0	936	196.0
15	4849.0	780	214.0
16	4901.2	624	244.0
17	4901.2	480	286.0
18	4431.9	336	312.0
19	7273.5	1620	170.0
20	6100.4	1446	166.0
21	6022.2	1278	174.0
22	6569.6	1104	193.0
23	7038.9	936	216.0
24	7273.5	780	244.0
25	7430.0	624	278.0
26	7273.5	480	325.0
27	6256.8	336	362.0
28	9802.3	1620	193.0
29	8446.7	1446	193.0
30	9489.5	1278	213.0
31	9698.0	1104	240.0
32	9698.0	936	259.0
33	8551.0	780	277.0
34	9698.0	624	333.0
35	8968.1	480	350.0
36	7403.9	336	388.0
37	12122.6	1620	216.0
38	12122.6	1446	228.0
39	12122.6	1278	241.0
40	12122.6	1104	262.0
41	12122.6	936	285.0
42	12122.6	780	314.0
43	12383.3	624	361.0
44	9254.9	480	387.0
45	9254.9	336	415.0

46	14547.1	1620	225.0
47	14547.1	1446	239.0
48	14547.1	1278	255.0
49	14547.1	1104	281.0
50	14547.1	936	305.0
51	14547.1	780	344.0
52	11105.8	624	370.0
53	14547.1	480	427.0
54	11105.8	336	441.0
55	16971.6	1620	237.0
56	16971.6	1446	252.0
57	16971.6	1278	269.0
58	16971.6	1104	289.0
59	16971.6	936	323.0
60	16606.6	780	362.0
61	13321.8	624	387.0
62	16971.6	480	447.0
63	12956.8	336	451.0
64	19396.1	1620	245.0
65	19396.1	1446	261.0
66	19396.1	1278	278.0
67	19604.7	1104	299.0
68	19187.5	936	341.0
69	19396.1	780	367.0
70	14807.8	624	387.0
71	19396.1	480	461.0
72	14807.8	336	476.0
73	21820.6	1620	250.0
74	22289.9	1446	264.0
75	22289.9	1278	282.0
76	21820.6	1104	305.0
77	21820.6	936	334.0
78	21820.6	780	372.0
79	16658.7	624	393.0
80	21820.6	480	478.0
81	16658.7	336	490.0
82	21638.1	1620	235.0
83	21898.8	1446	250.0
84	22941.6	1278	275.0
85	22420.2	1104	296.0
86	23984.4	936	337.0
87	24245.1	780	378.0
88	23723.7	624	418.0
89	24505.8	480	493.0
90	18509.7	336	501.0

5.2.2 Initial Experiments

From the literature survey it is seen that two of the most important design variables affecting fouling in a heated tube with a given liquid are flow rate and tube wall temperature. Several preliminary experiments were carried out to fix the operating procedure and to select convenient operating conditions. A constant heat flux was applied during each experiment and a constant flow rate was maintained.

Various constant heat fluxes were applied to achieve different wall temperatures. For run length purposes the surface thermocouple temperature was monitored at various flow rates and heat fluxes. It was decided for practical and safety reasons that a run length of 12 hours could not be exceeded. Therefore the results can only be considered to be the initial fouling rates. Over 12 hours with 1% styrene in the feedstock initially and under the most severe conditions it was found that less than 5% of the styrene was consumed. Thus it was considered that the feedstock was of constant composition. Several runs were checked for reproducibility.

It was decided that for all runs the feedstock should have an initial concentration of 1% styrene in kerosene. 1% was chosen as a reasonable trace level contaminant concentration.

5.2.3 Local Fouling Rates

The fouling rate increased along the heated length of the tube. When cleaning the tube, it was noticed that the deposits were thickest at the downstream, i.e. the hottest, end. Each thermocouple measurement enabled the estimation of the local fouling rate at that position. The axial temperature variation of the tube when clean is a clear indication that increased fouling is ex-

pected with increasing heated length. Figures 5.16-5.23 demonstrate this for various flow rates and heat fluxes.

5.2.4 The Effect of Mass Flow Rate and Wall Temperature at Constant Heat Flux

Nine different flow rates in the range 336-1620 lb/hr were used for each of the ten heat fluxes. See Table 5.3. The inside wall temperature range was 554.7-909°R. Thirty-seven surface thermocouple temperatures were used and the extensive set of data is presented in microfische form in Appendix K. For the following fouling resistance-time plots, Figures 5.24 to 5.41, only certain, but typical thermocouples were chosen for different sections of the tube. From the slopes of all the fouling resistance-time plots the logarithm of the initial fouling rate was plotted against the reciprocal temperature ($^{\circ}R^{-1}$) for various flow rates in Figures 5.42-5.50. Detailed computed results are tabulated in Appendix K. The plots of the log initial fouling rate against the reciprocal tube wall temperature (°R) show an Arrhenius type relationship for each particular flow rate. This strong temperature effect suggests that chemical rather than physical processes are important in this kind of fouling. The calculated activation energy using a least squares regression varied between 10.7 and 17.02 K cal/mol.

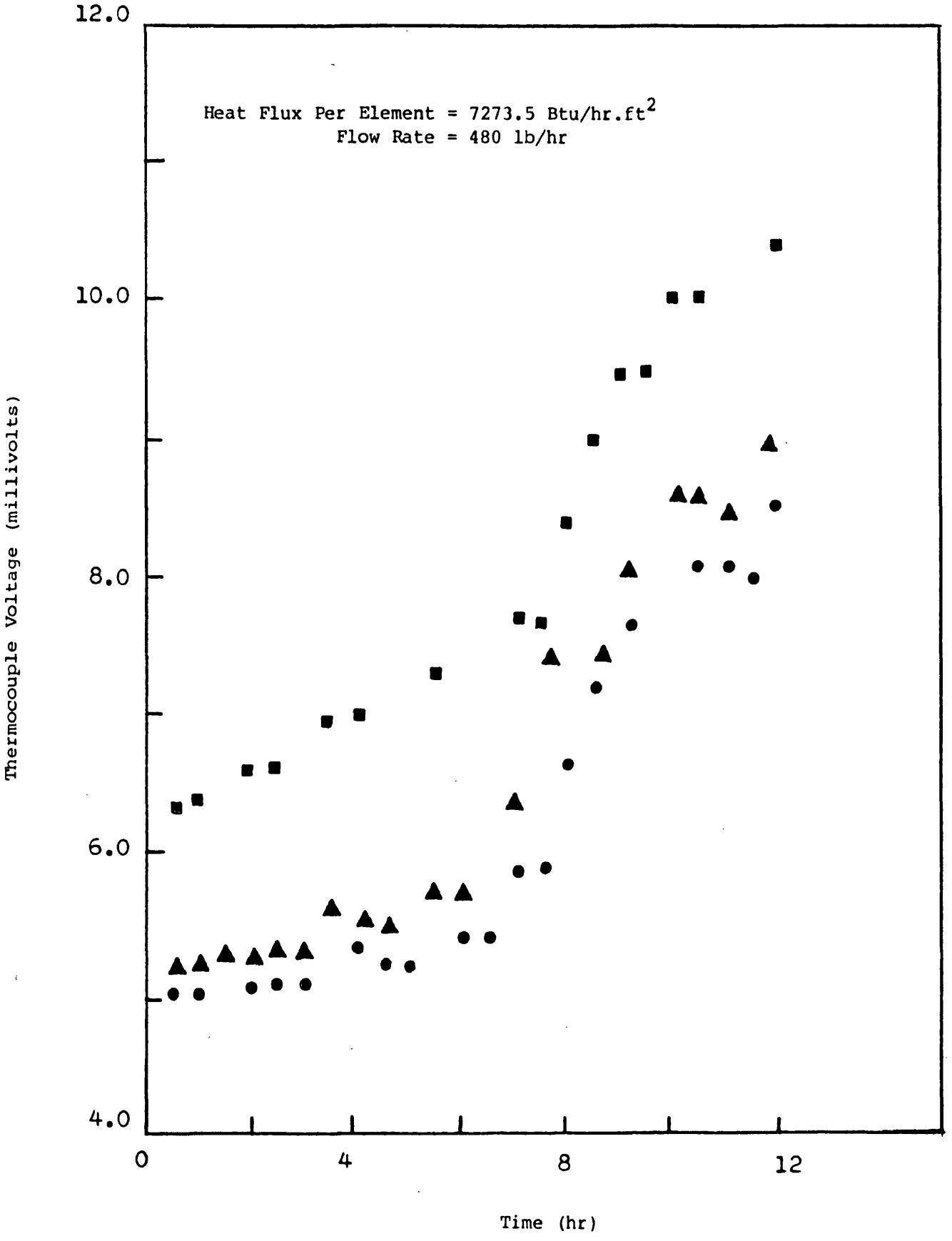

Figure 5.16 Variation of Surface Temperature with Time.
Kerosene System.

T/C ● 5.02, ▲ 8.03, ■ 9.01

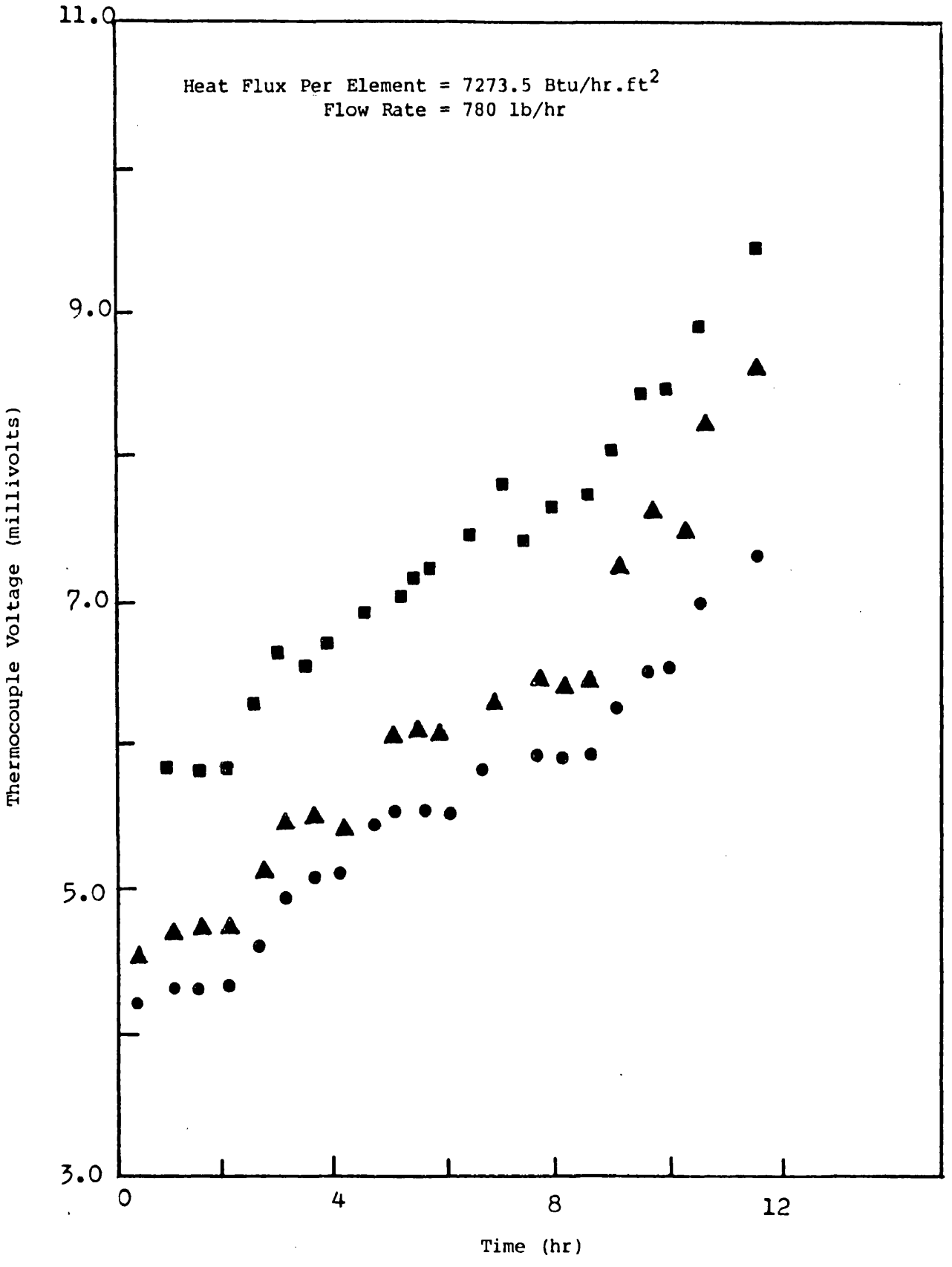

Figure 5.17 Variation of Surface Temperature with Time.

Kerosene System.

T/C ● 5.02, ▲ 8.03, ■ 9.01

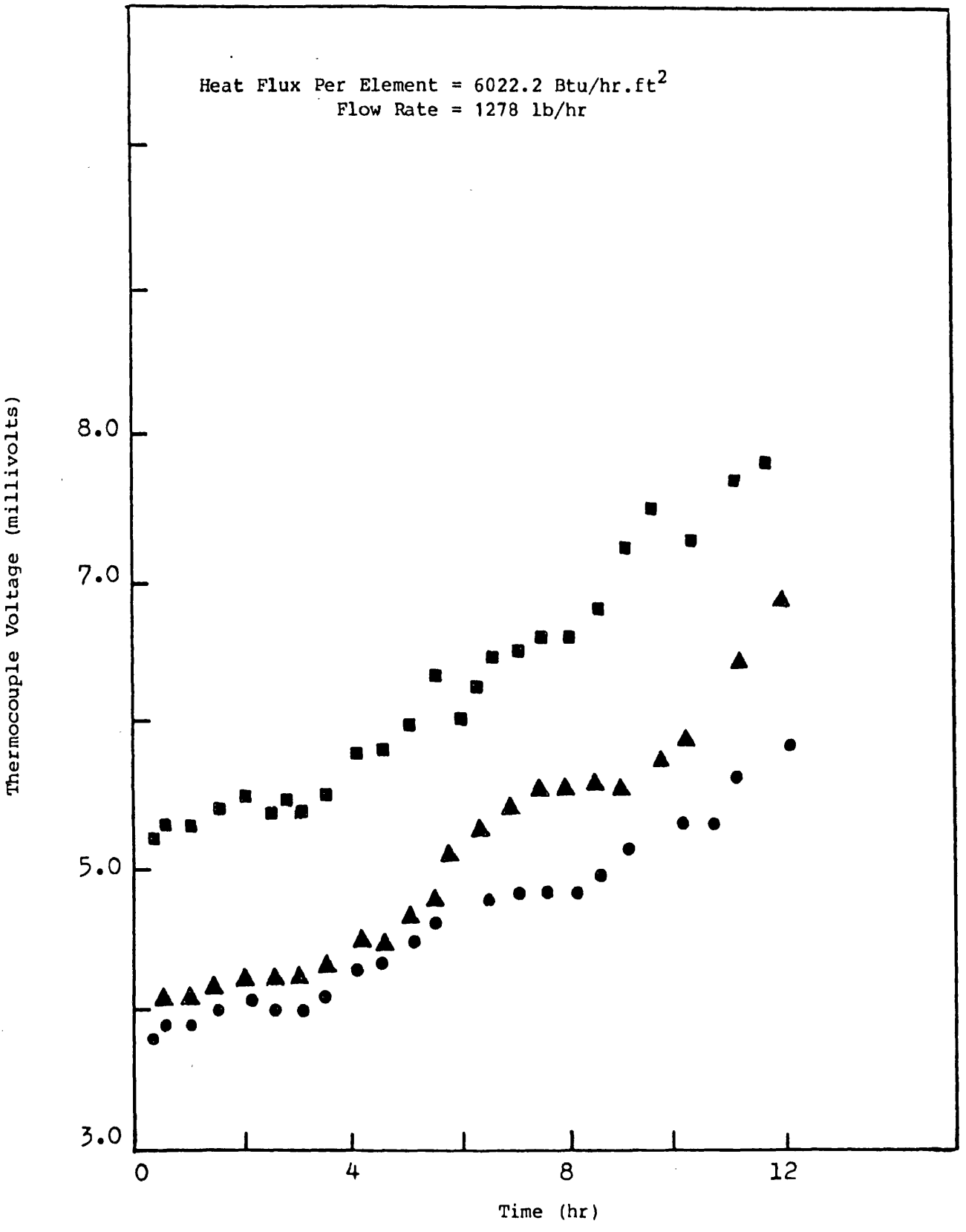

Figure 5.18 Variation of Surface Temperature with Time.

Kerosene System.

T/C ● 5.02, ▲ 8.03, ■ 9.01

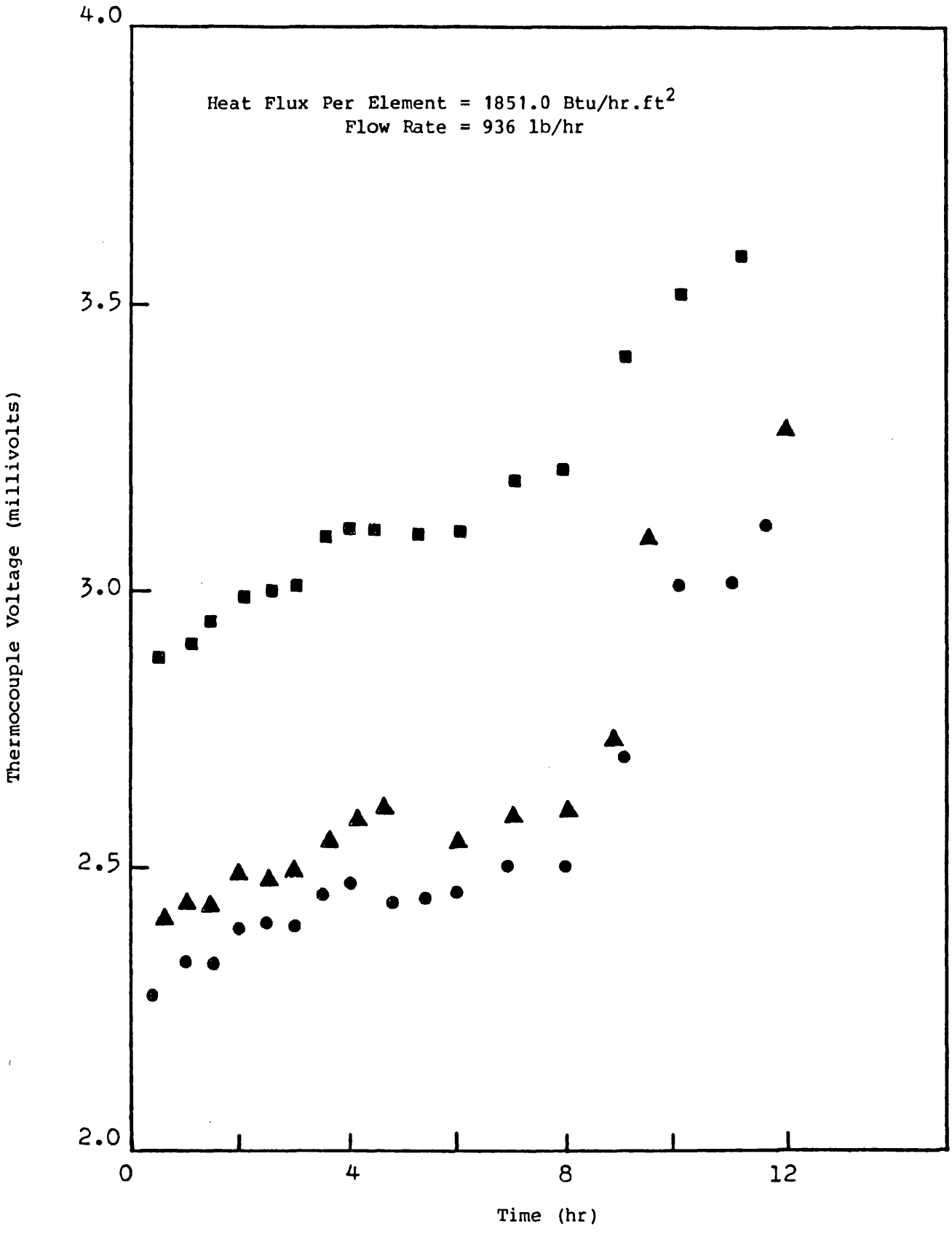

Figure 5.19 Variation of Surface Temperature with Time.

Kerosene System.

T/C ● 5.02, ▲ 8.03, ■ 9.01

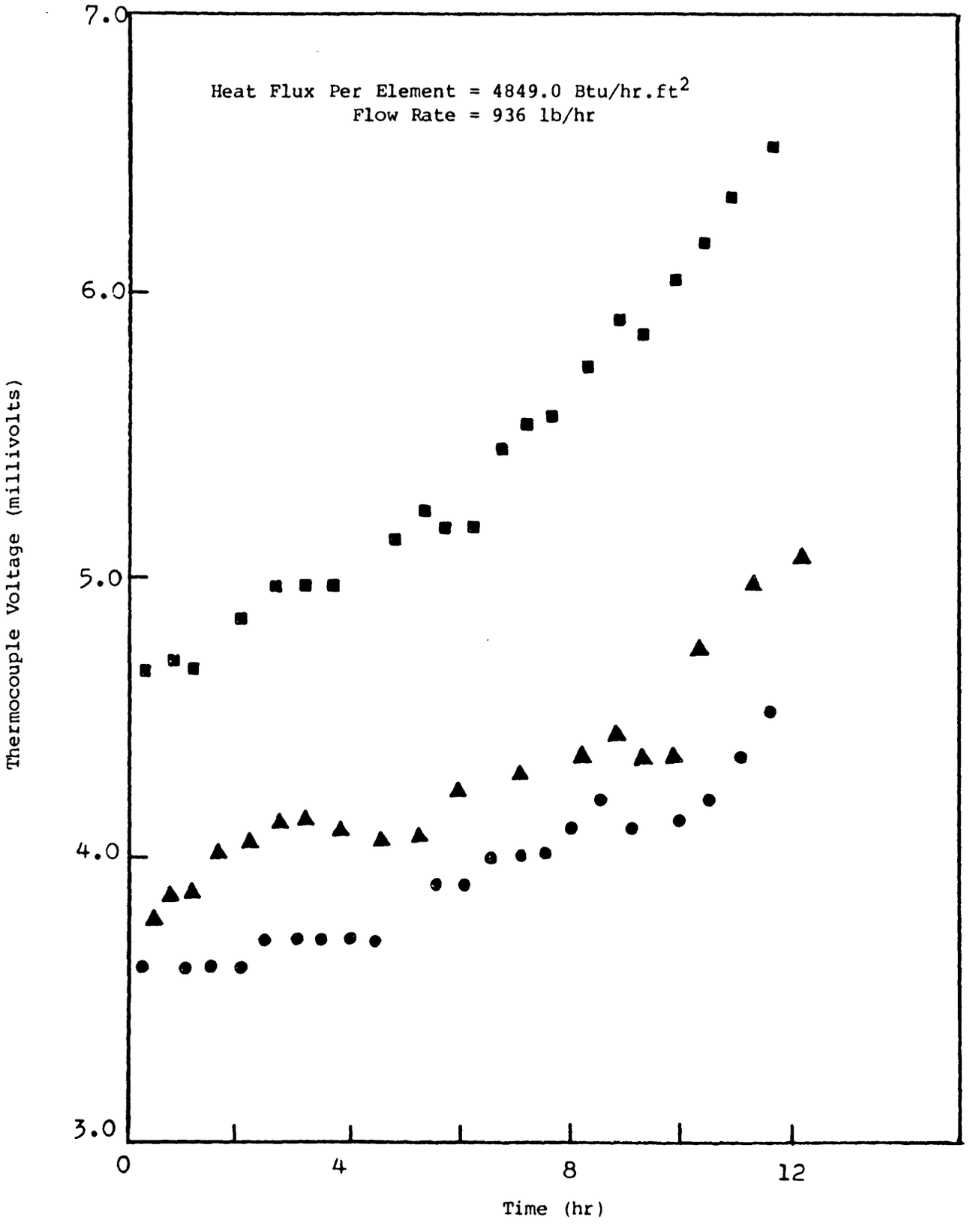

Figure 5.20 Variation of Surface Temperature with Time.

Kerosene System.

T/C ● 5.02, ▲ 8.03, ■ 9.01

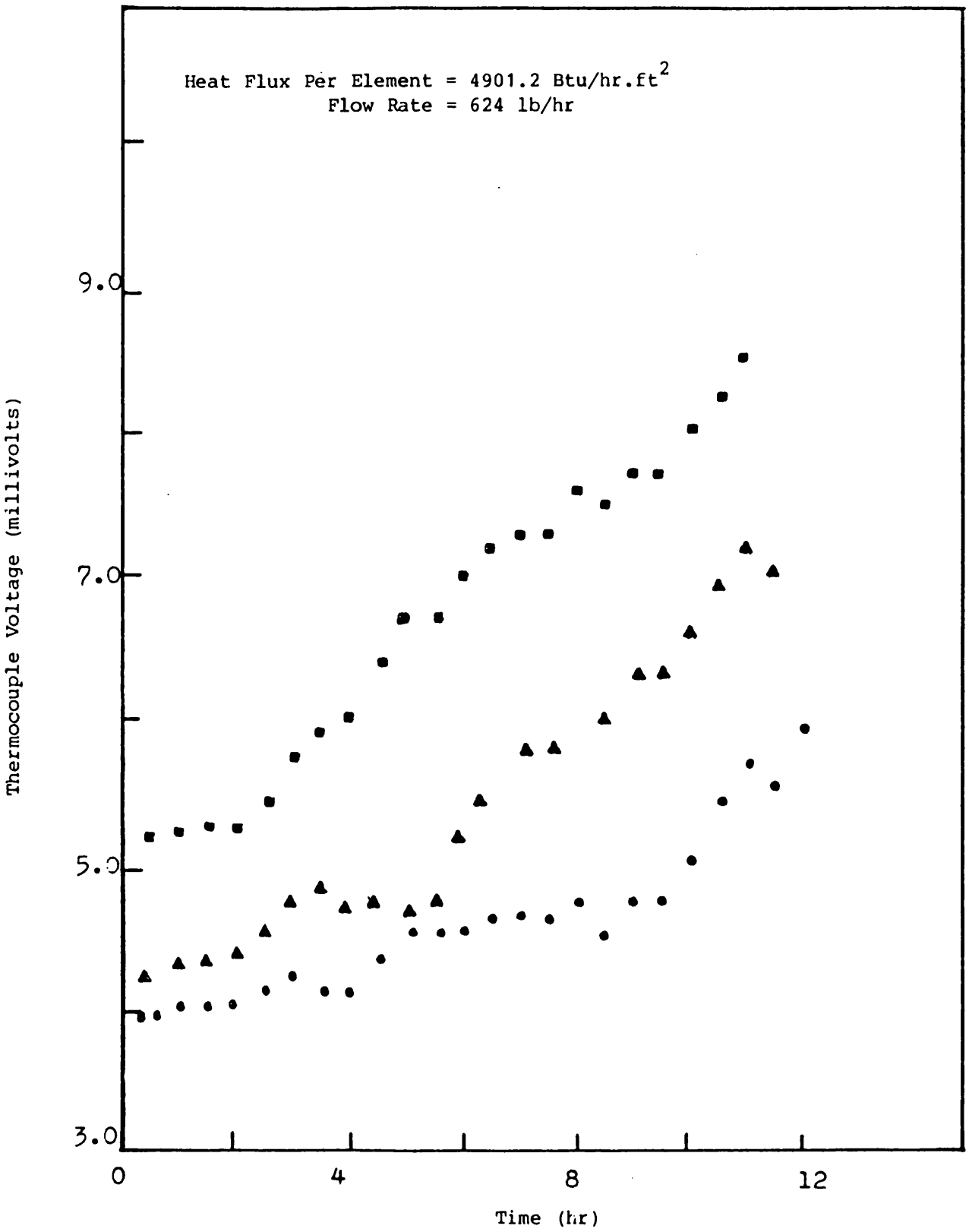

Figure 5.21 Variation of Surface Temperature with Time.

Kerosene System.

T/C ● 5.02, ▲ 8.03, ■ 9.01

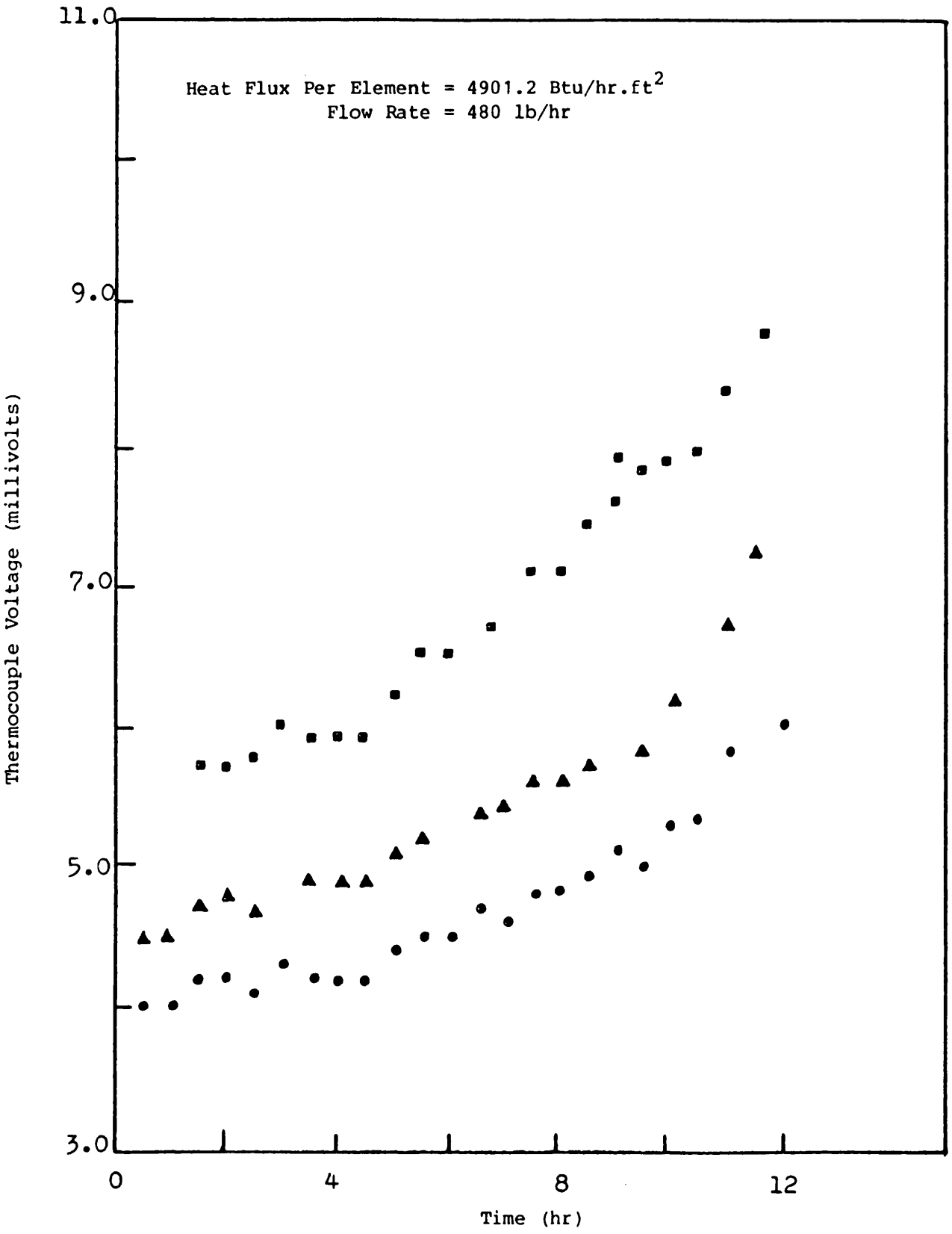

Figure 5.22 Variation of Surface Temperature with Time.

Kerosene System.

T/C ● 5.02, ▲ 8.03, ■ 9.01

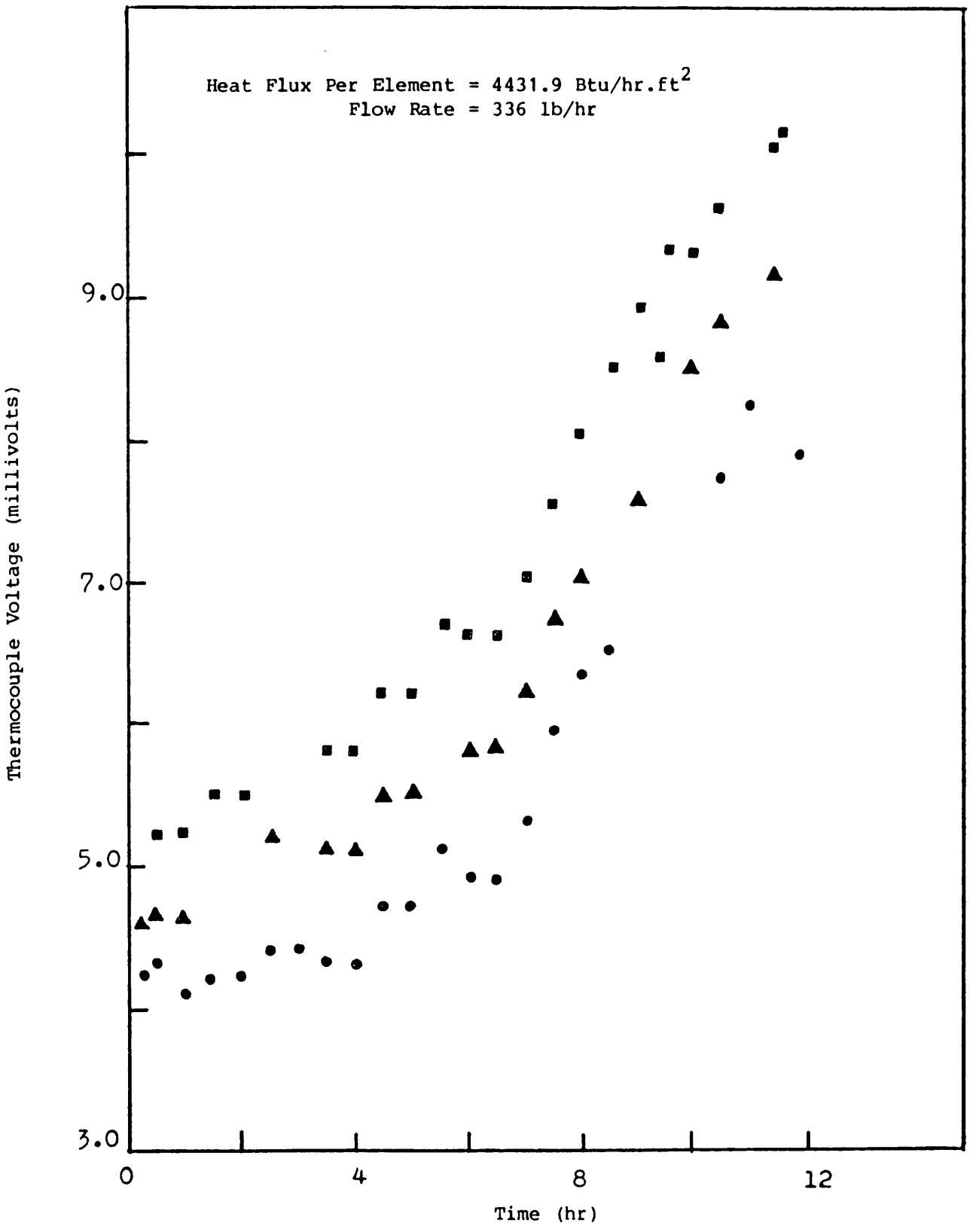

Figure 5.23 Variation of Surface Temperature with Time.

Kerosene System.

T/C ● 5.02, ▲ 8.03, ■ 9.01

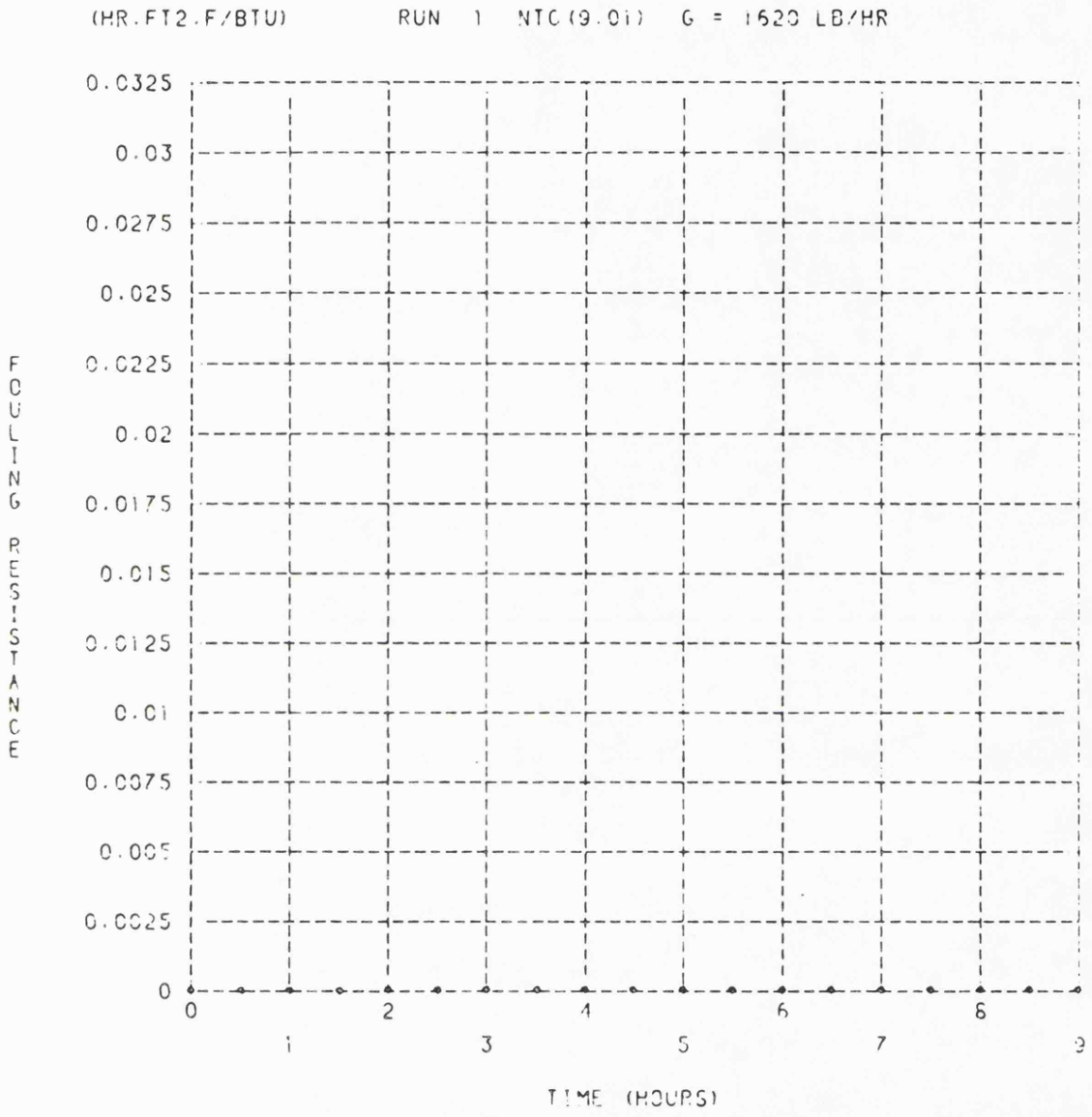

Figure 5.24 Fouling Resistance vs. Time.

Heat flux per element = 1851.0 BTU/HR.FT^2.

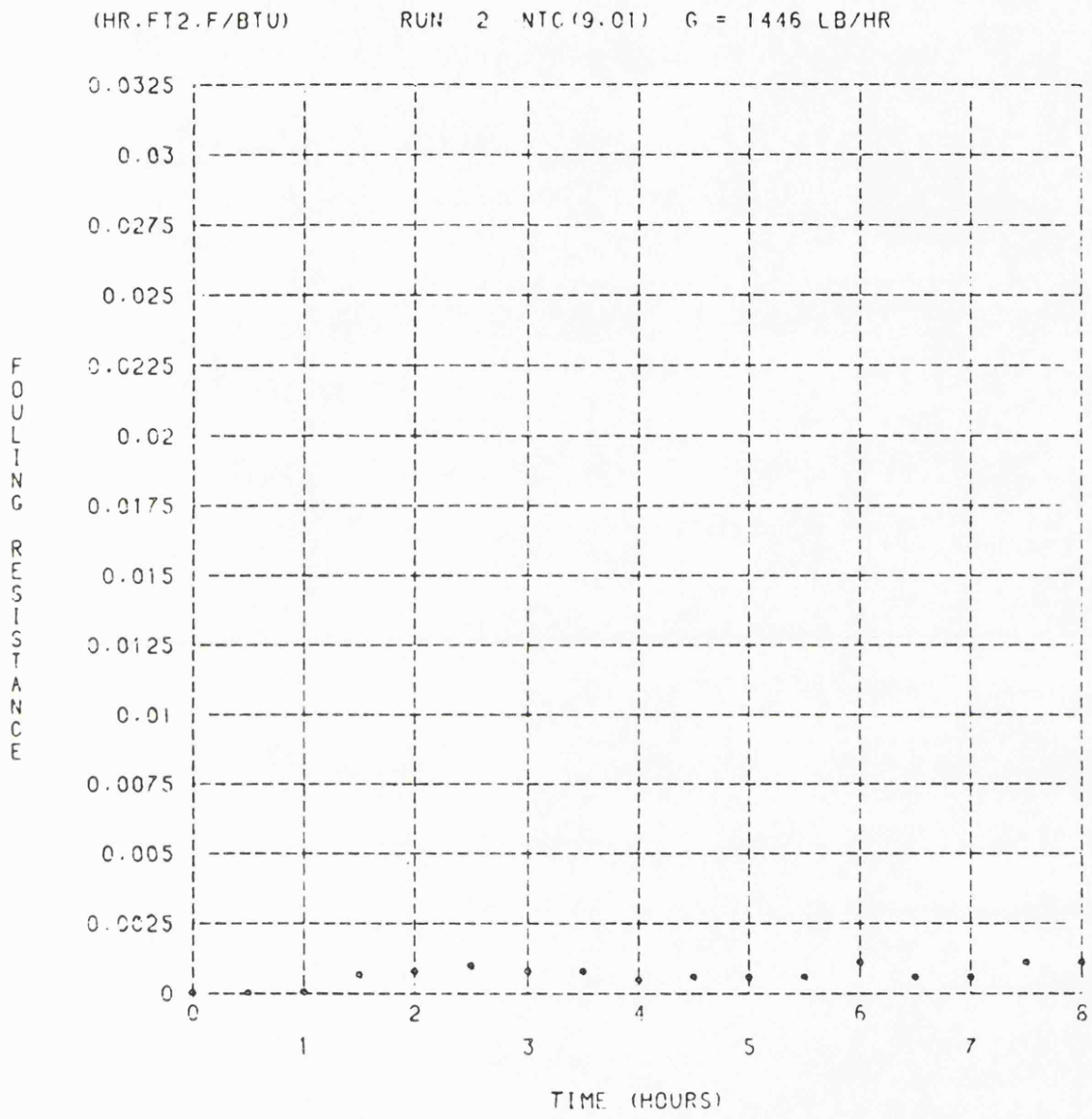

Figure 5.25 Fouling Resistance vs. Time.

Heat flux per element = 1851.0 BTU/HR.FT^2.

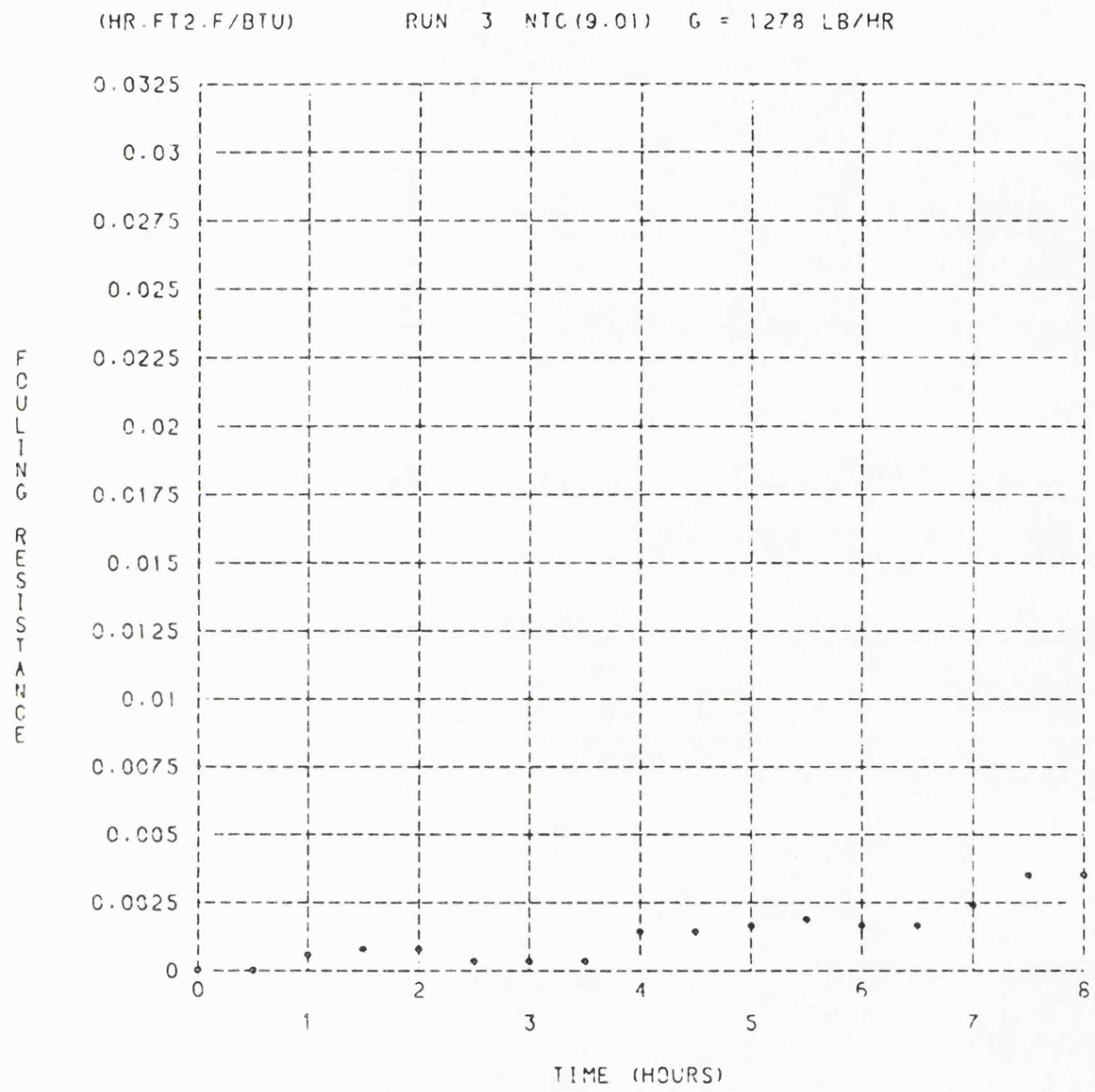

Figure 5.26 Fouling Resistance vs. Time.

Heat flux per element = 1851.0 BTU/HR.FT^2.

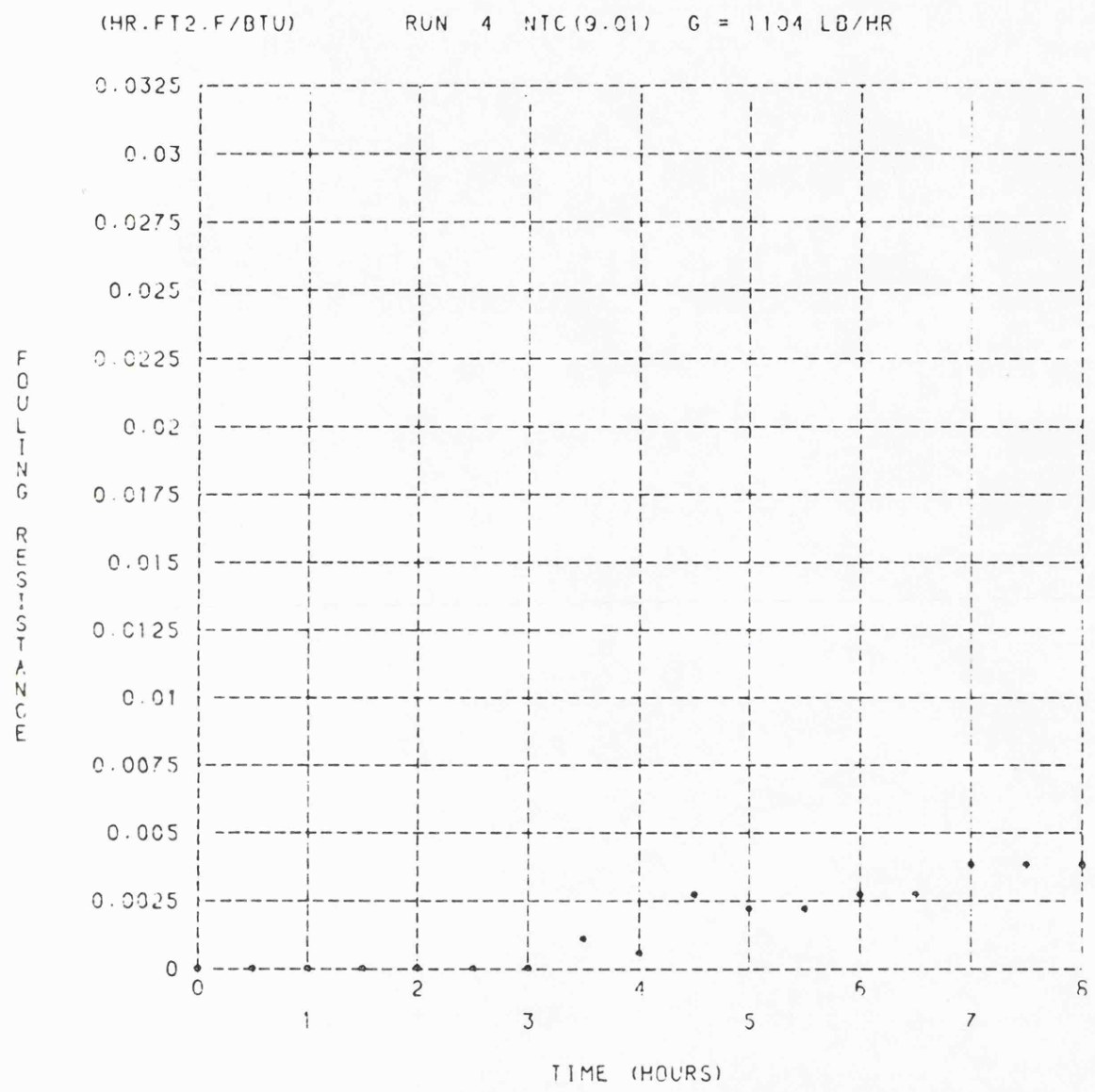

Figure 5.27 Fouling Resistance vs. Time.

Heat flux per element = 1851.0 BTU/HR.FT^2.

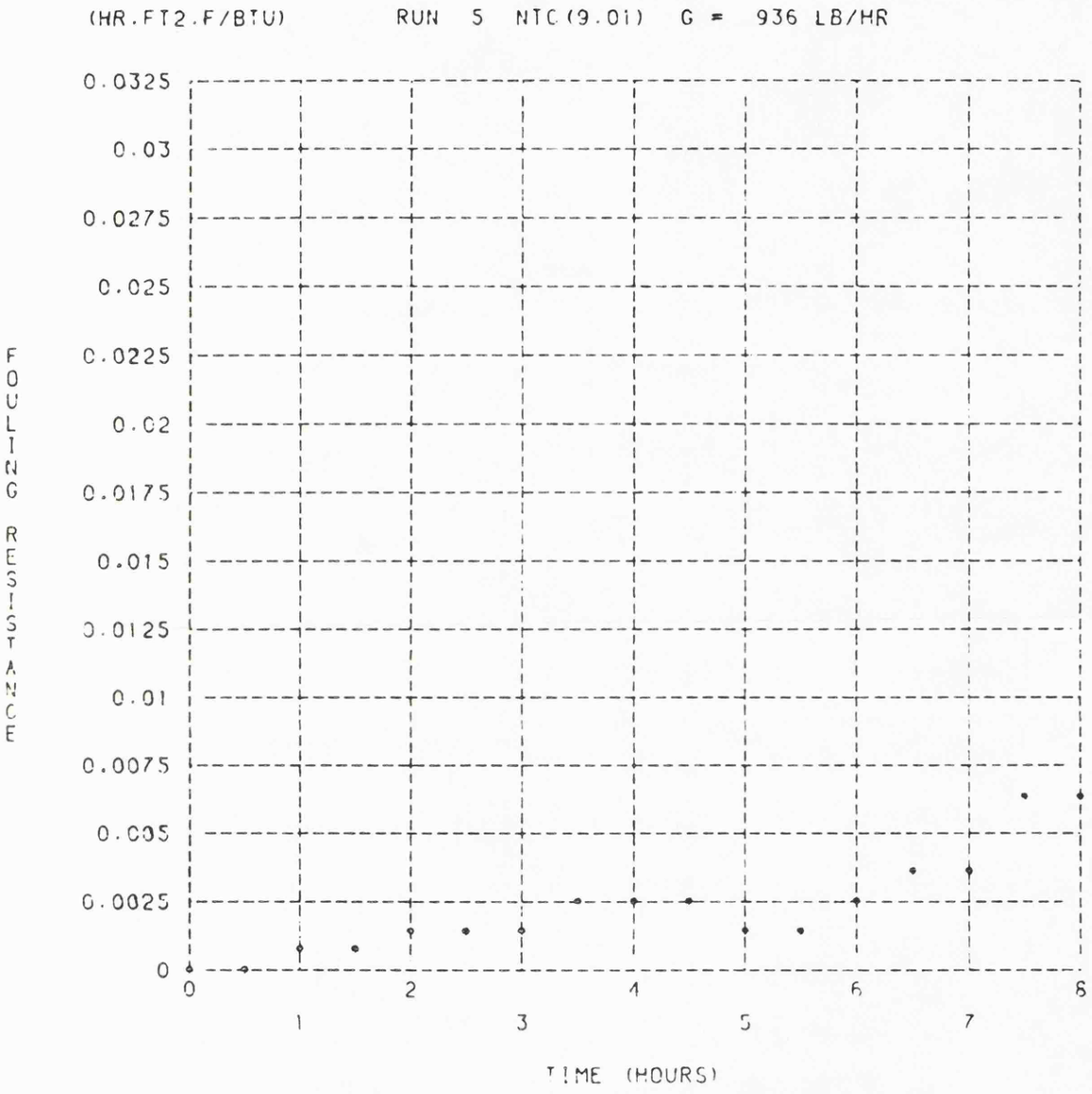

Figure 5.28 Fouling Resistance vs. Time.

Heat flux per element = 1851.0 BTU/HR.FT^2.

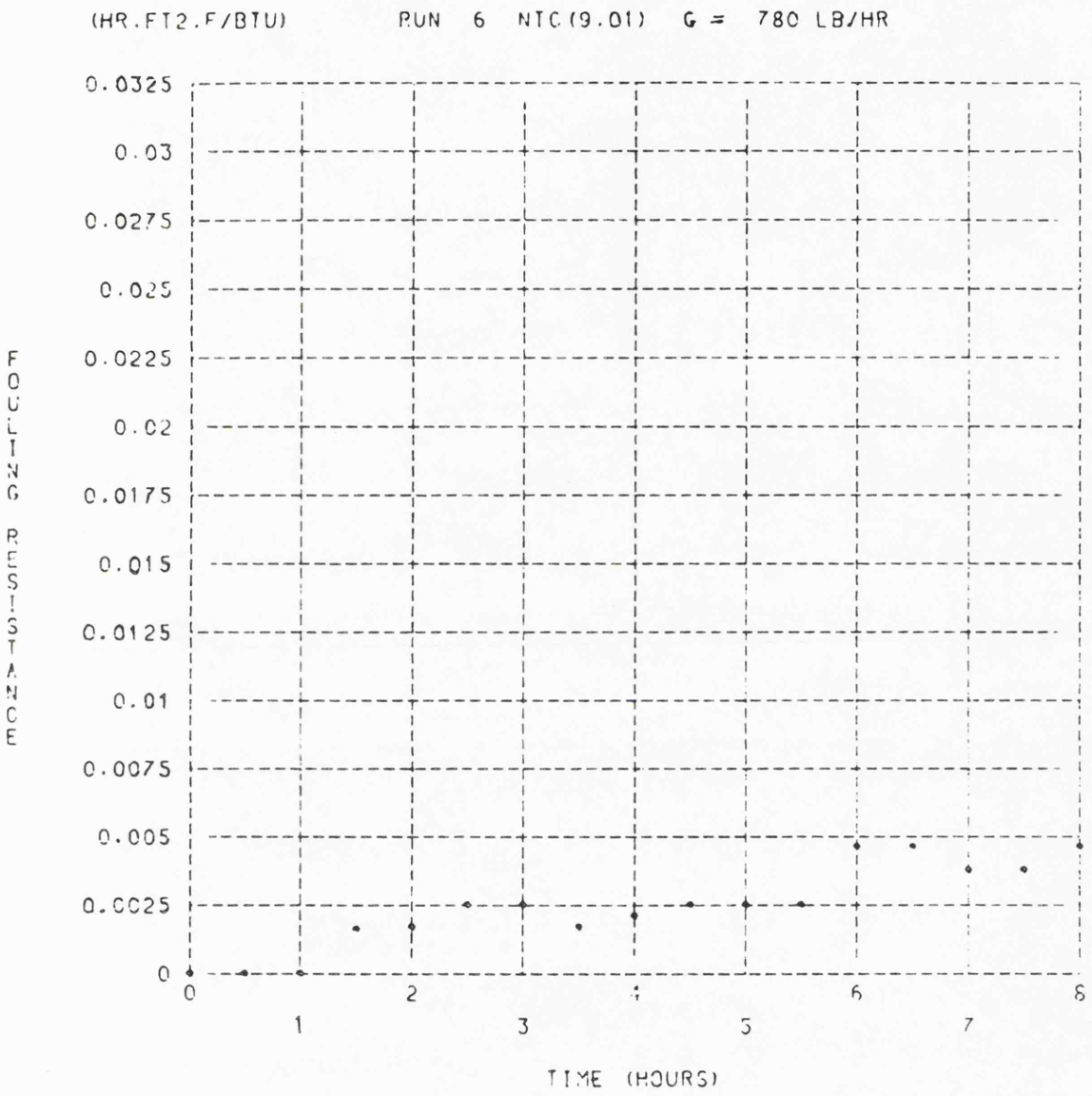

Figure 5.29 Fouling Resistance vs. Time.

Heat flux per element = 2424.5 BTU/HR.FT^2.

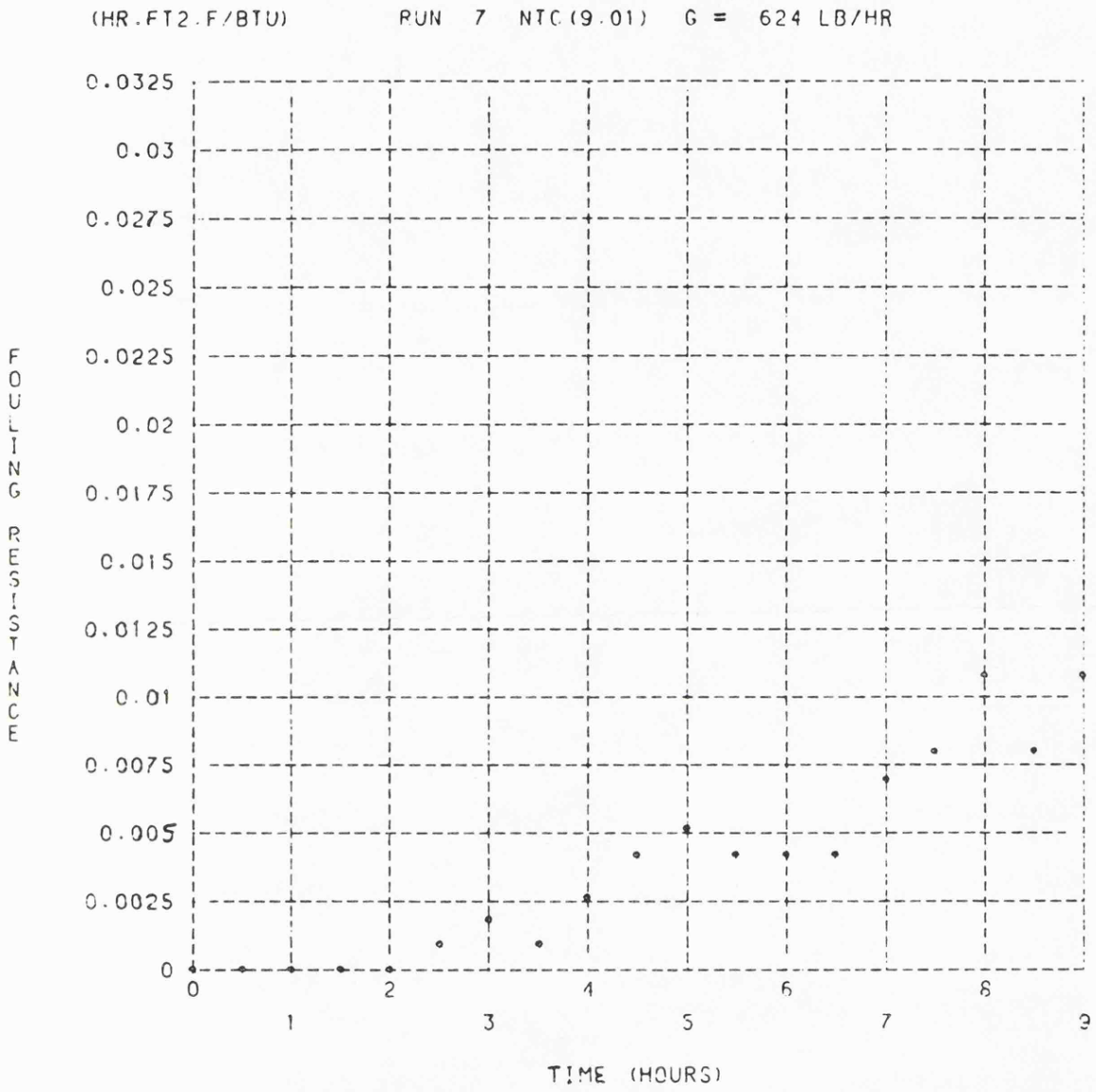

Figure 5.30 Fouling Resistance vs. Time.

Heat flux per element = 2268.1 BTU/HR.FT^2.

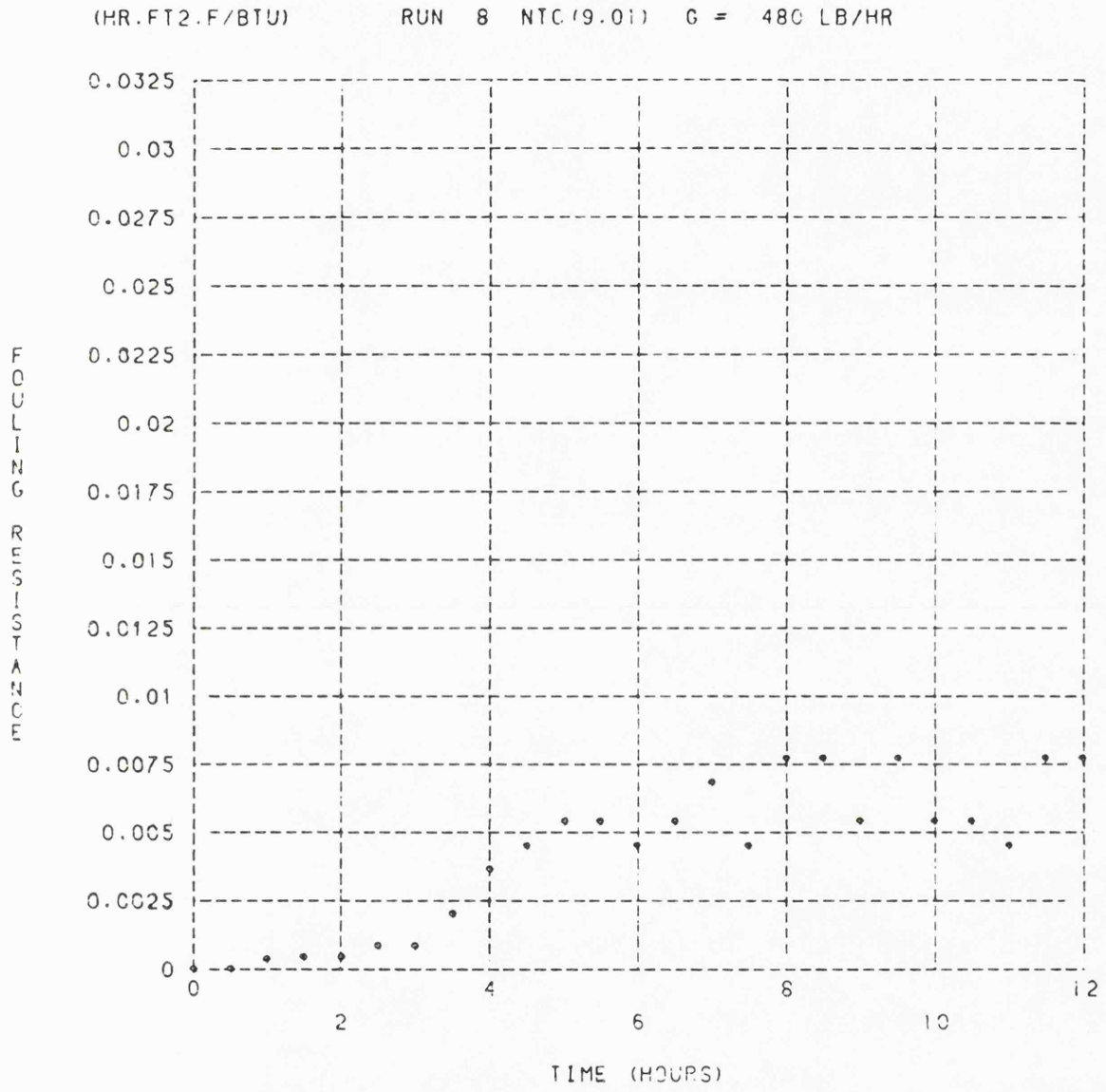

Figure 5.31 Fouling Resistance vs. Time.

Heat flux per element = 2398.4 BTU/HR.FT^2.

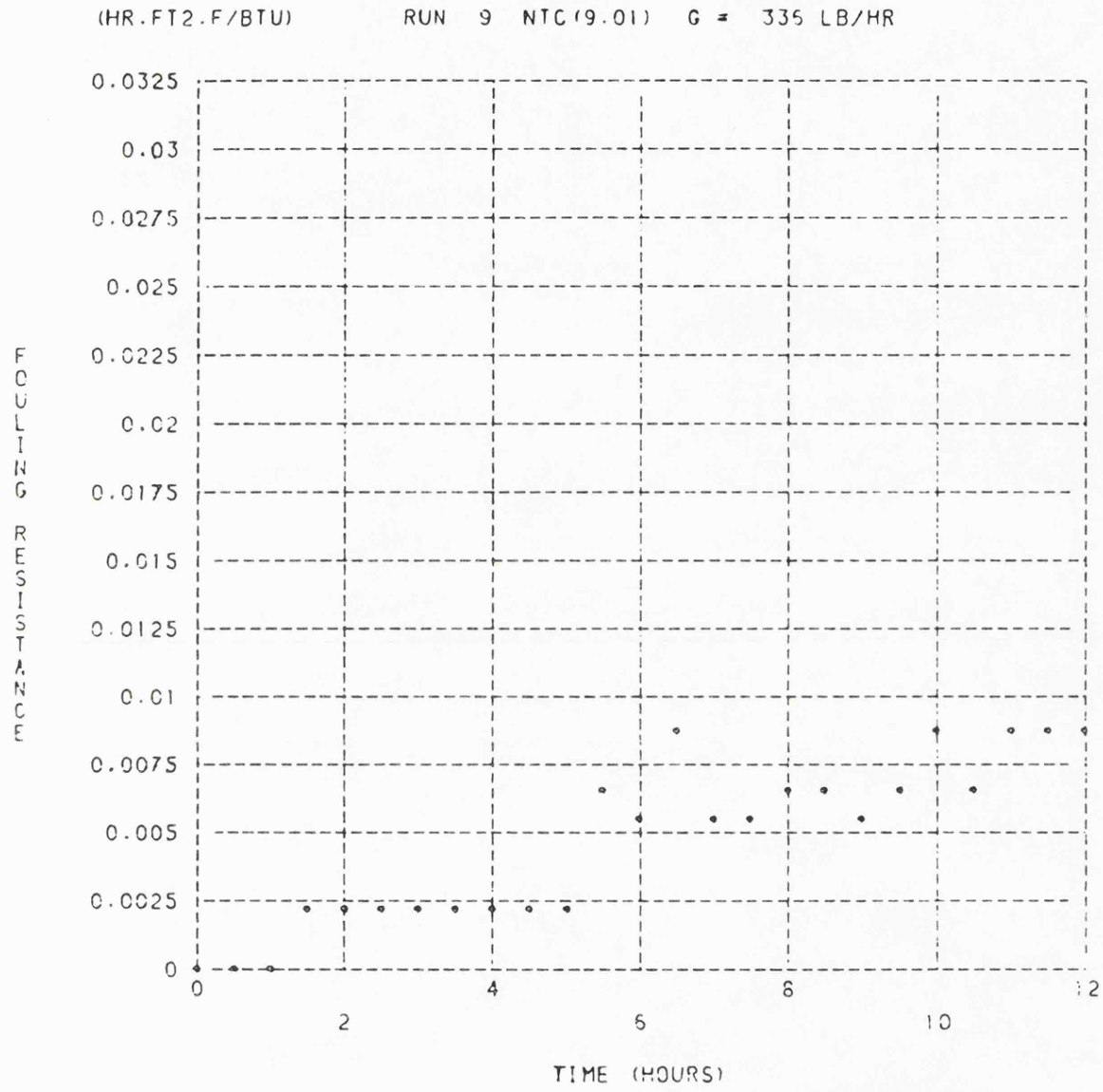

Figure 5.32 Fouling Resistance vs. Time.

Heat flux per element = 1851.0 BTU/HR.FT^2.

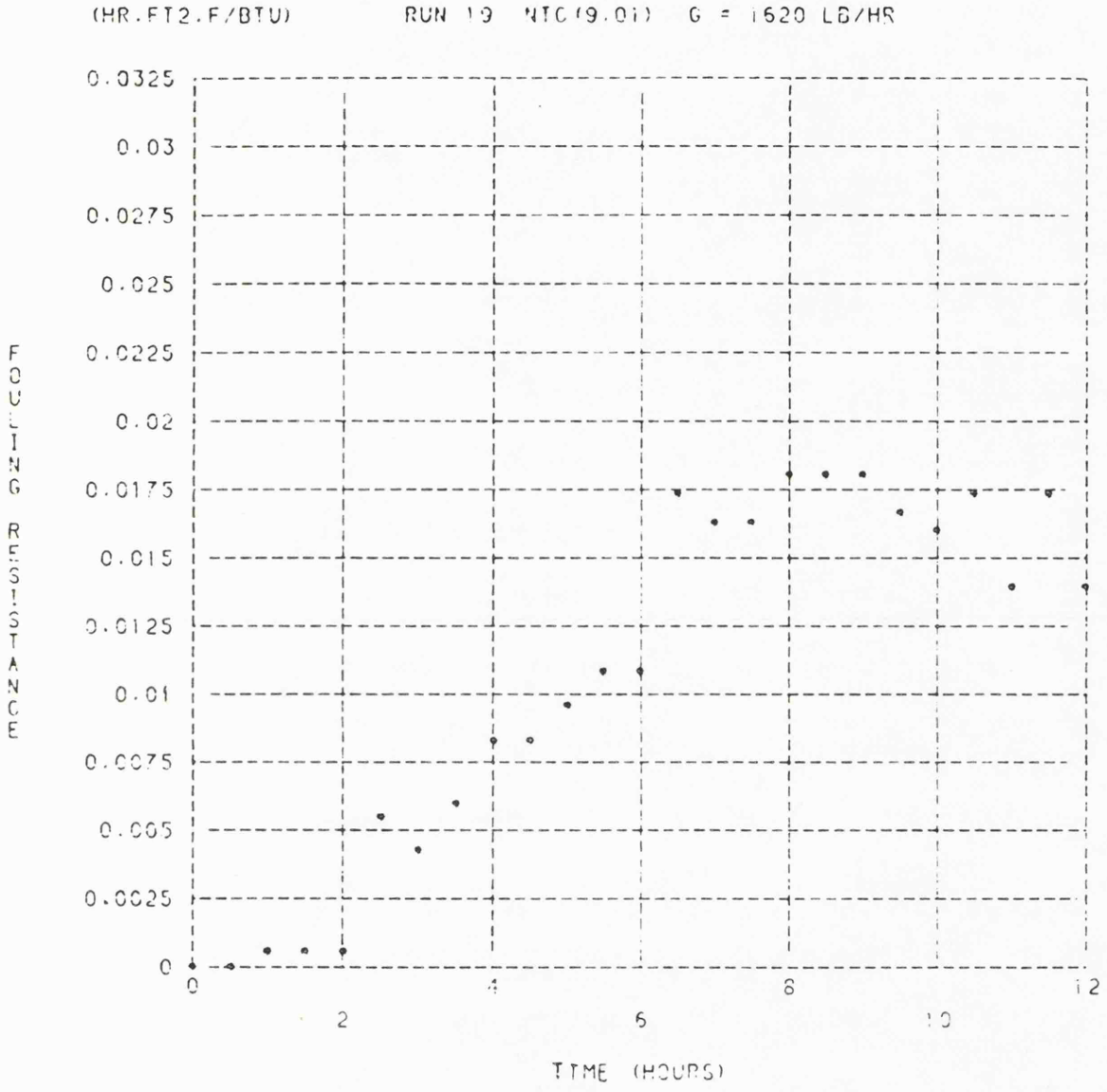

Figure 5.33 Fouling Resistance vs. Time.

Heat flux per element = 7273.5 BTU/HR.FT^2.

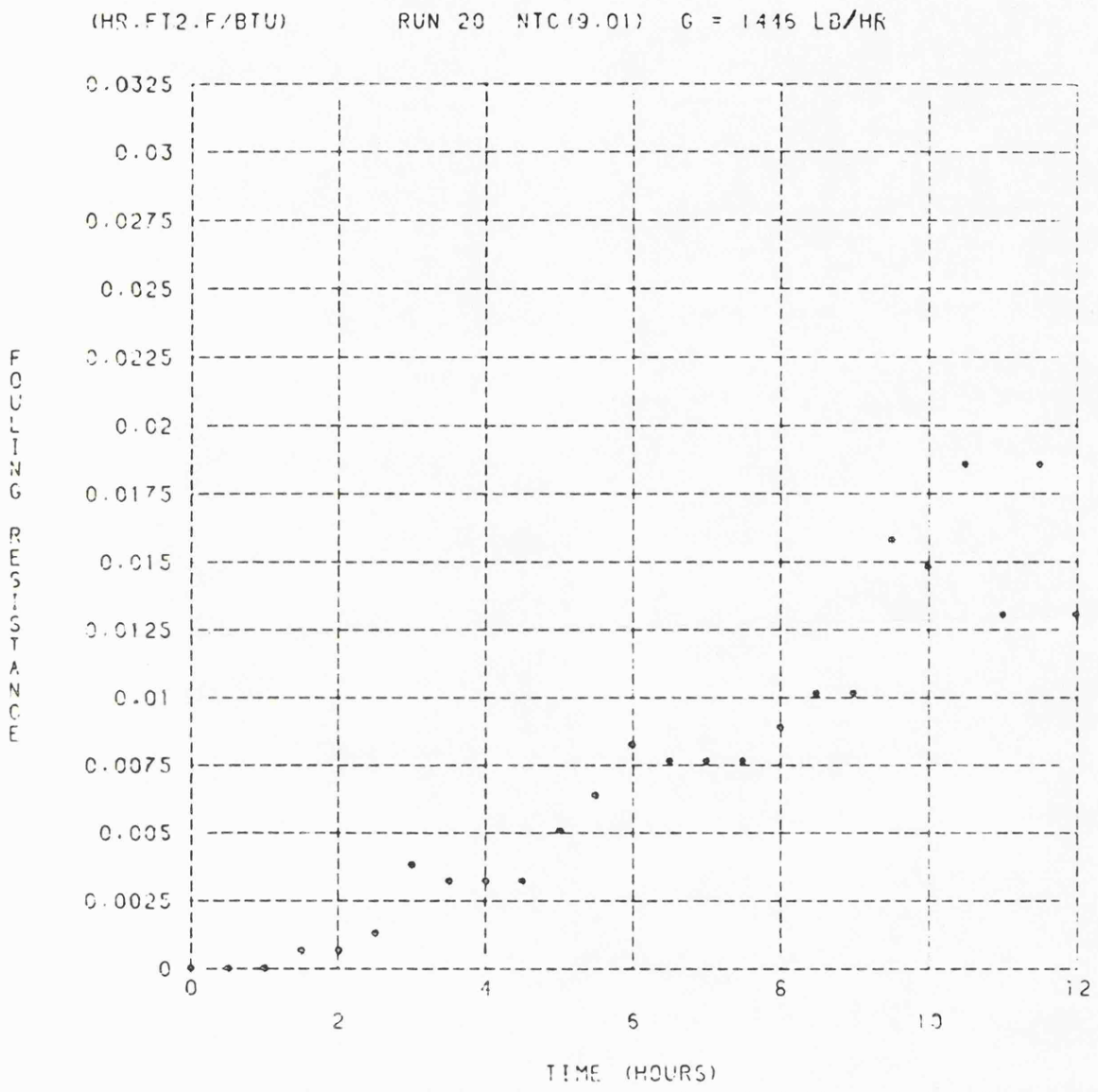

Figure 5.34 Fouling Resistance vs. Time.

Heat flux per element = 6100.4 BTU/HR.FT^2.

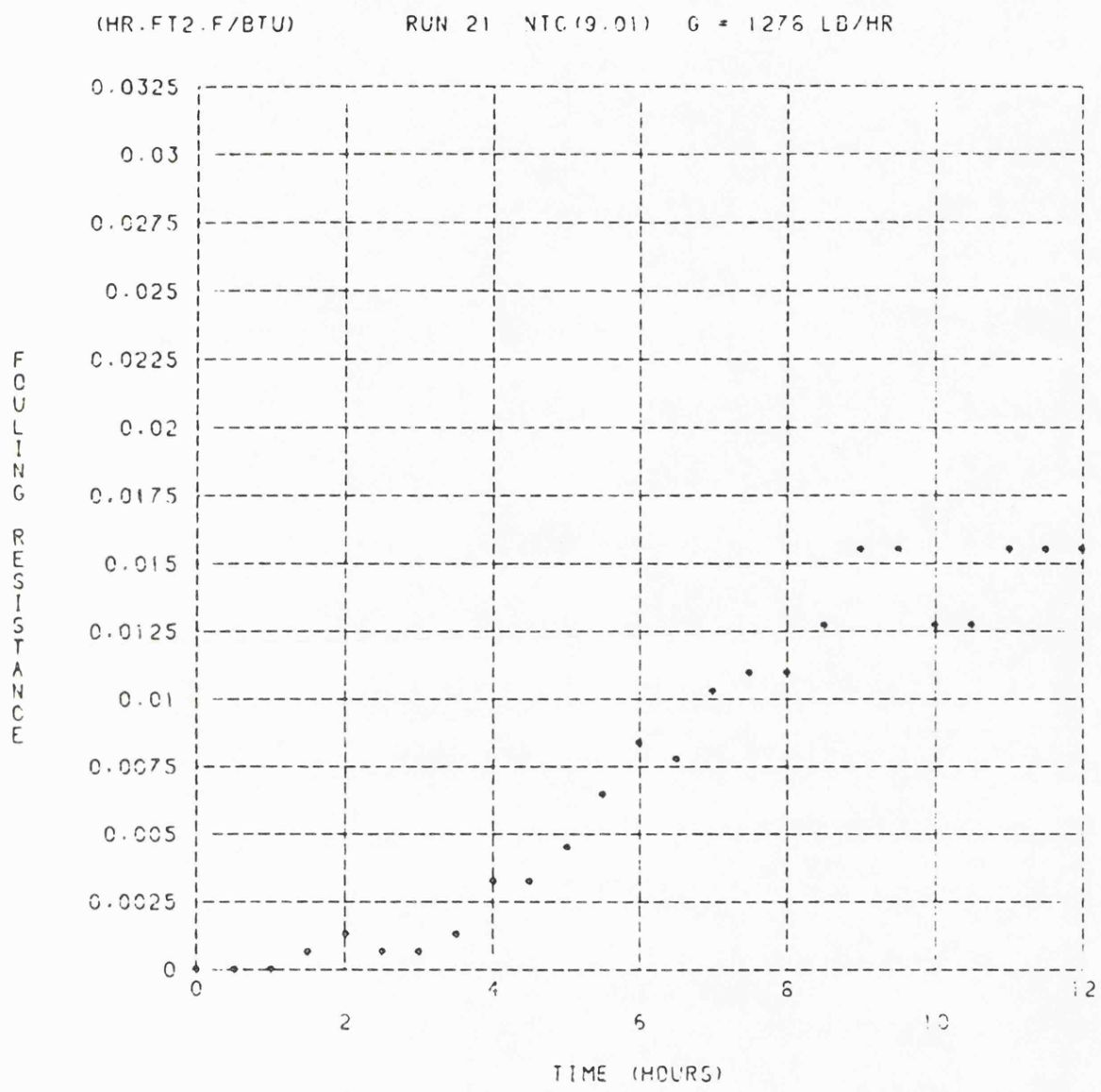

Figure 5.35 Fouling Resistance vs. Time.

Heat flux per element = 6022.2 BTU/HR.FT^2.

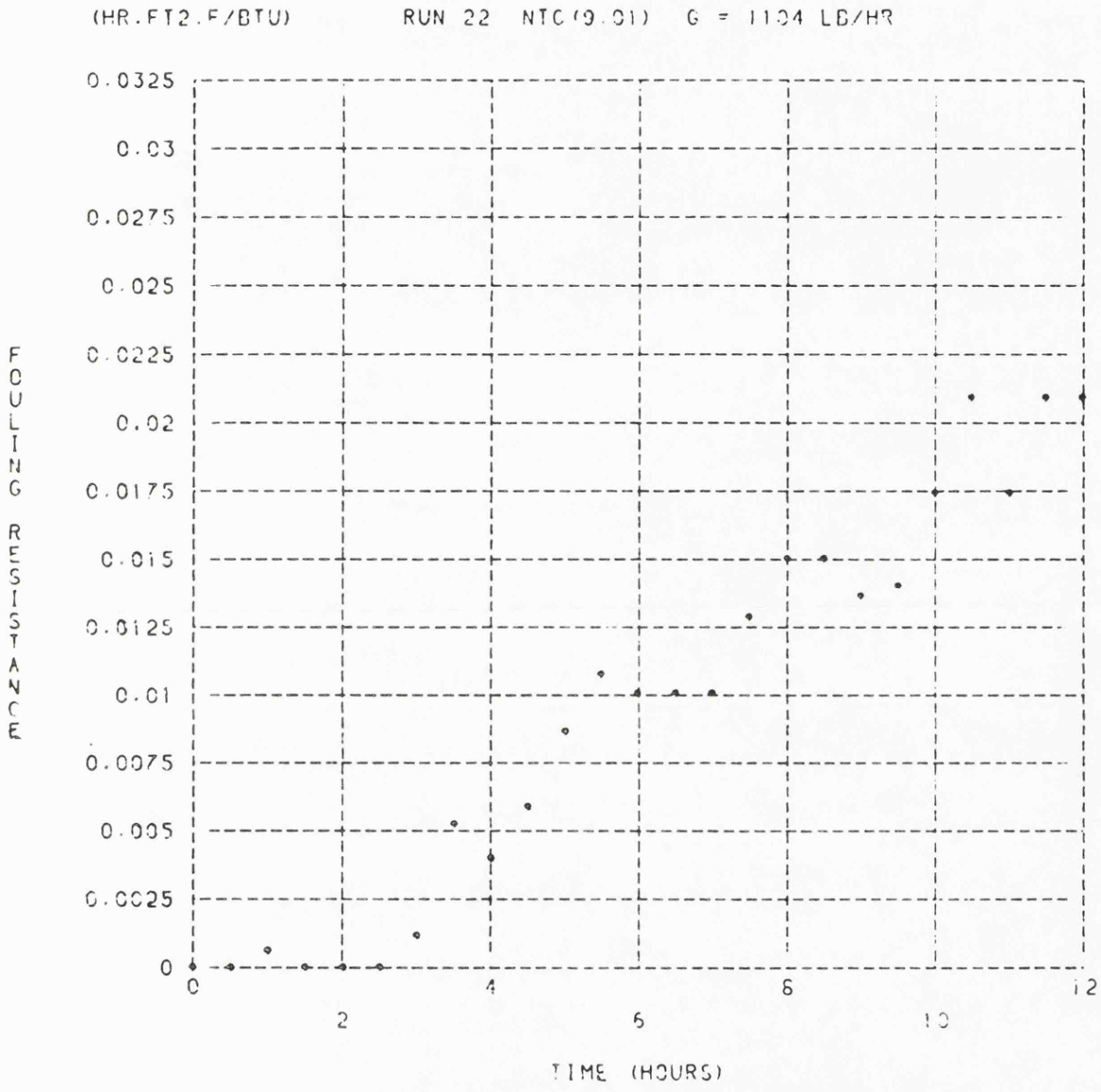

Figure 5.36 Fouling Resistance vs. Time.

Heat flux per element = 6569.6 BTU/HR.FT^2.

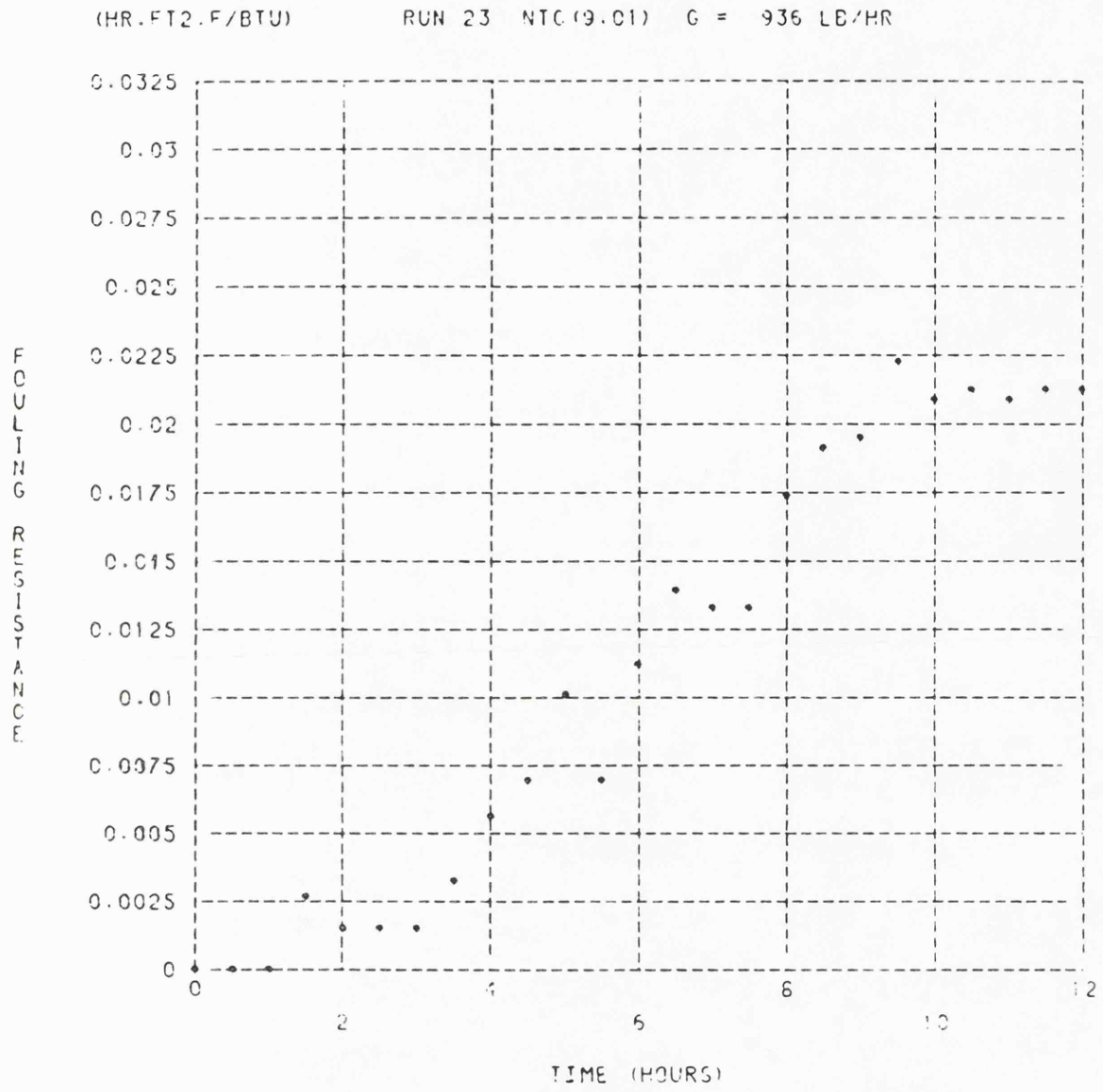

Figure 5.37 Fouling Resistance vs. Time.

Heat flux per element = 7038.9 BTU/HR.FT^2.

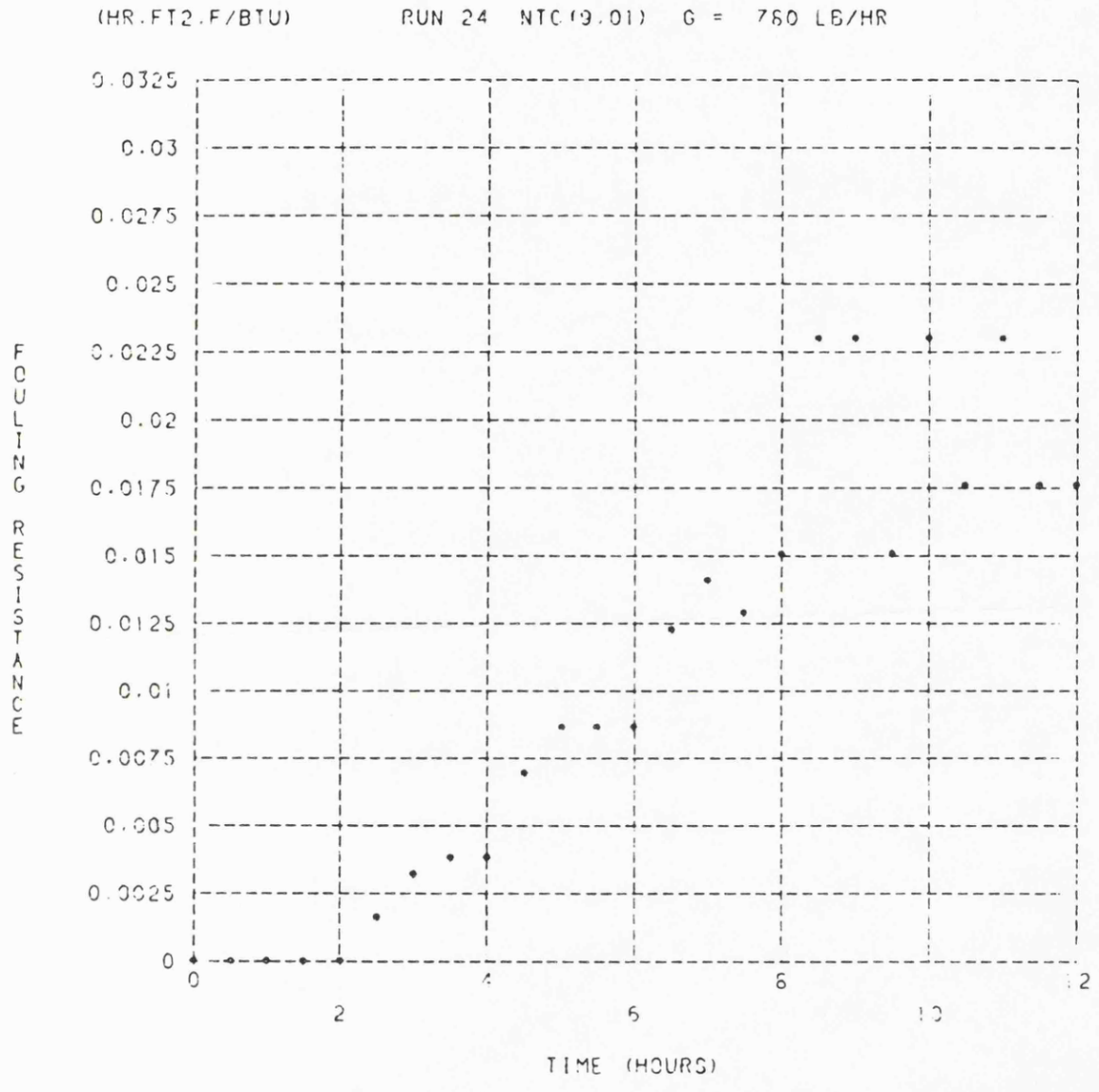

Figure 5.38 Fouling Resistance vs. Time.

Heat flux per element = 7273.5 BTU/HR.FT^2.

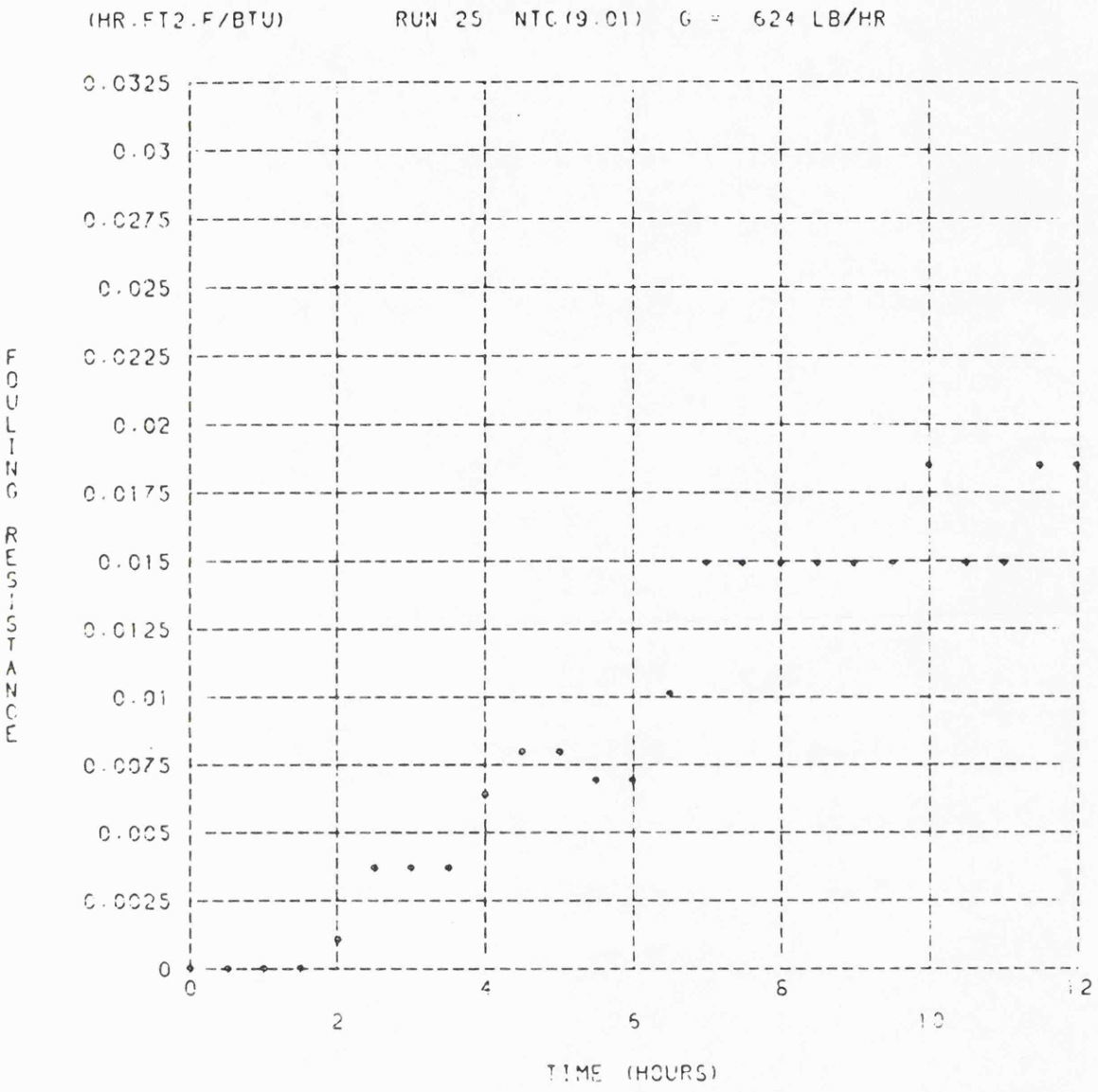

Figure 5.39 Fouling Resistance vs. Time.

Heat flux per element = 7430.0 BTU/HR.FT^2.

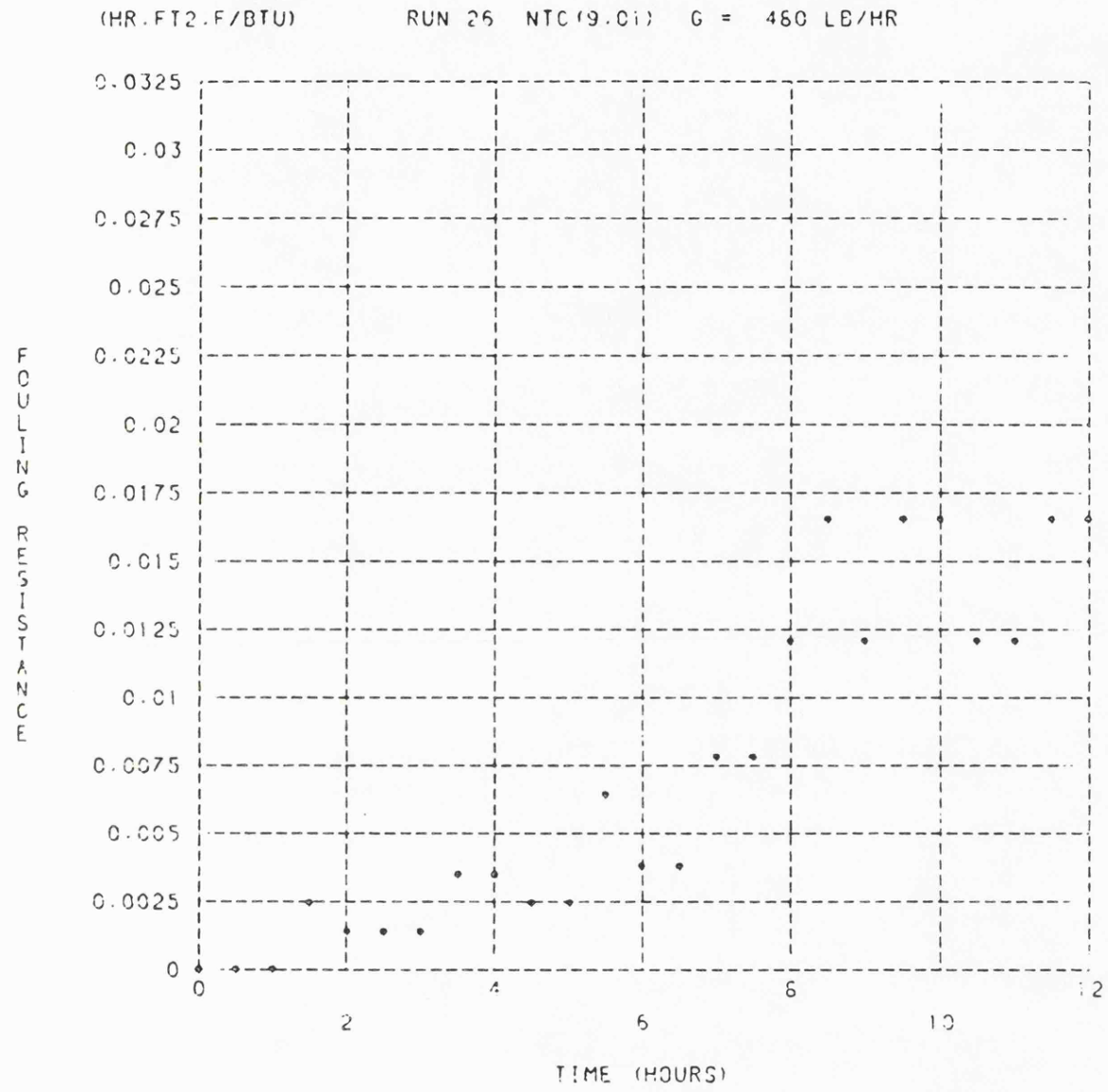

Figure 5.40 Fouling Resistance vs. Time.

Heat flux per element = 7273.5 BTU/HR.FT^2.

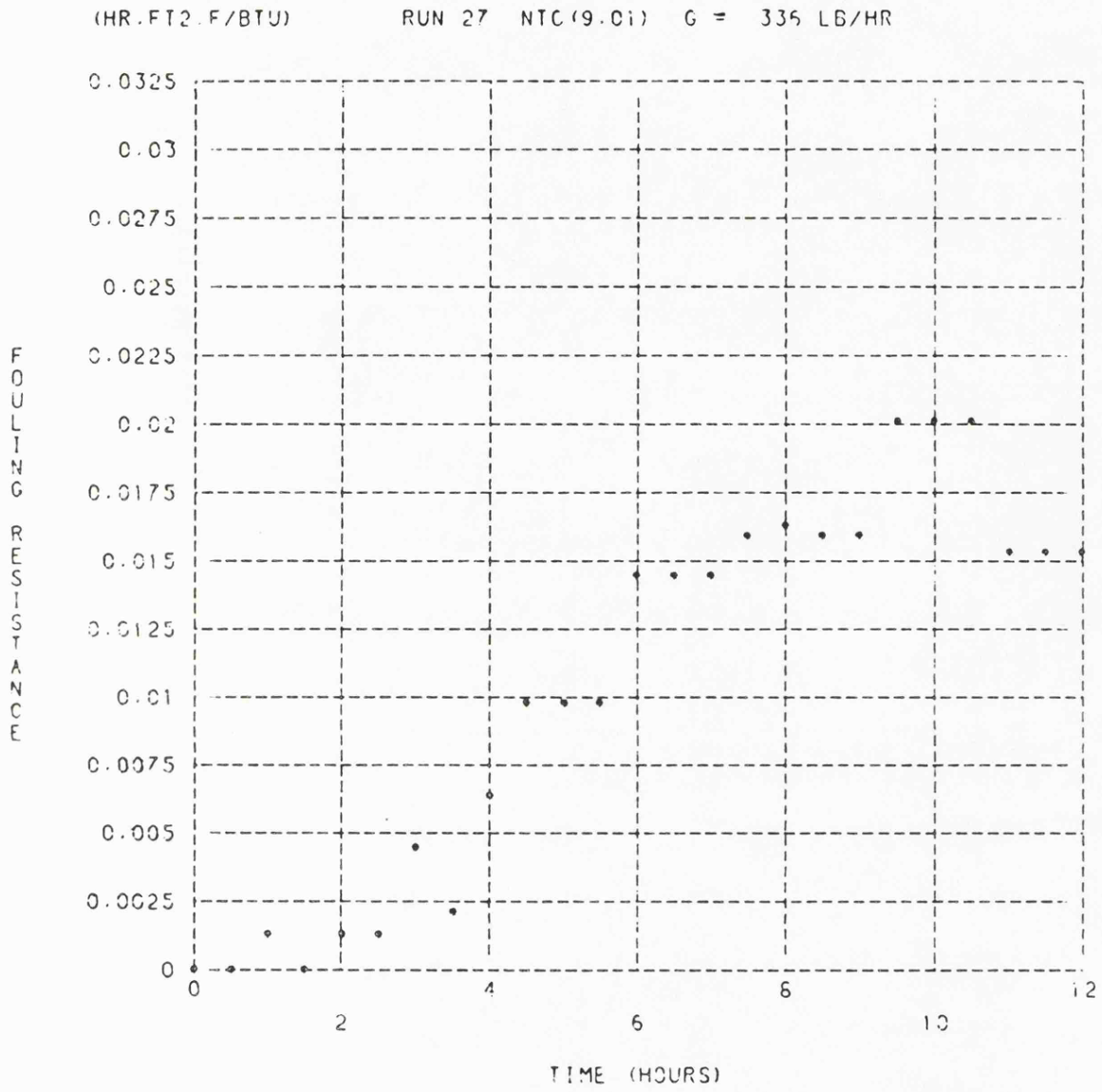

Figure 5.41 Fouling Resistance vs. Time.

Heat flux per element = 6256.8 BTU/HR.FT^2.

5.2.5 Combined Effects of Flow Rate and Temperature

For each set of data shown in Figures 5.42 to 5.50 the best line was obtained by a polynomial (non-linear regression) least squares technique. The equations are given in Table 5.4. These equations then give the effect of temperature on the initial rate of fouling at a specified flow rate. It was noticed from the graphs that the initial fouling rate is not only highly dependent upon temperature but it is also affected by the flow rate. A summary of the results is shown in Figure 5.51.

5.2.6 Cooling Rate

At the end of each experiment the heaters were switched off and the flow rate was increased. Some polymer was recovered downstream of the test section beyond the condenser outlet on the return line filter. Some deposition may have taken place in the test section or in the condenser during cooling. However since raising the flow rate reduces the surface temperature quickly and substantially (Figure 5.52), the additional deposition through chemical reaction was thought to be negligible.

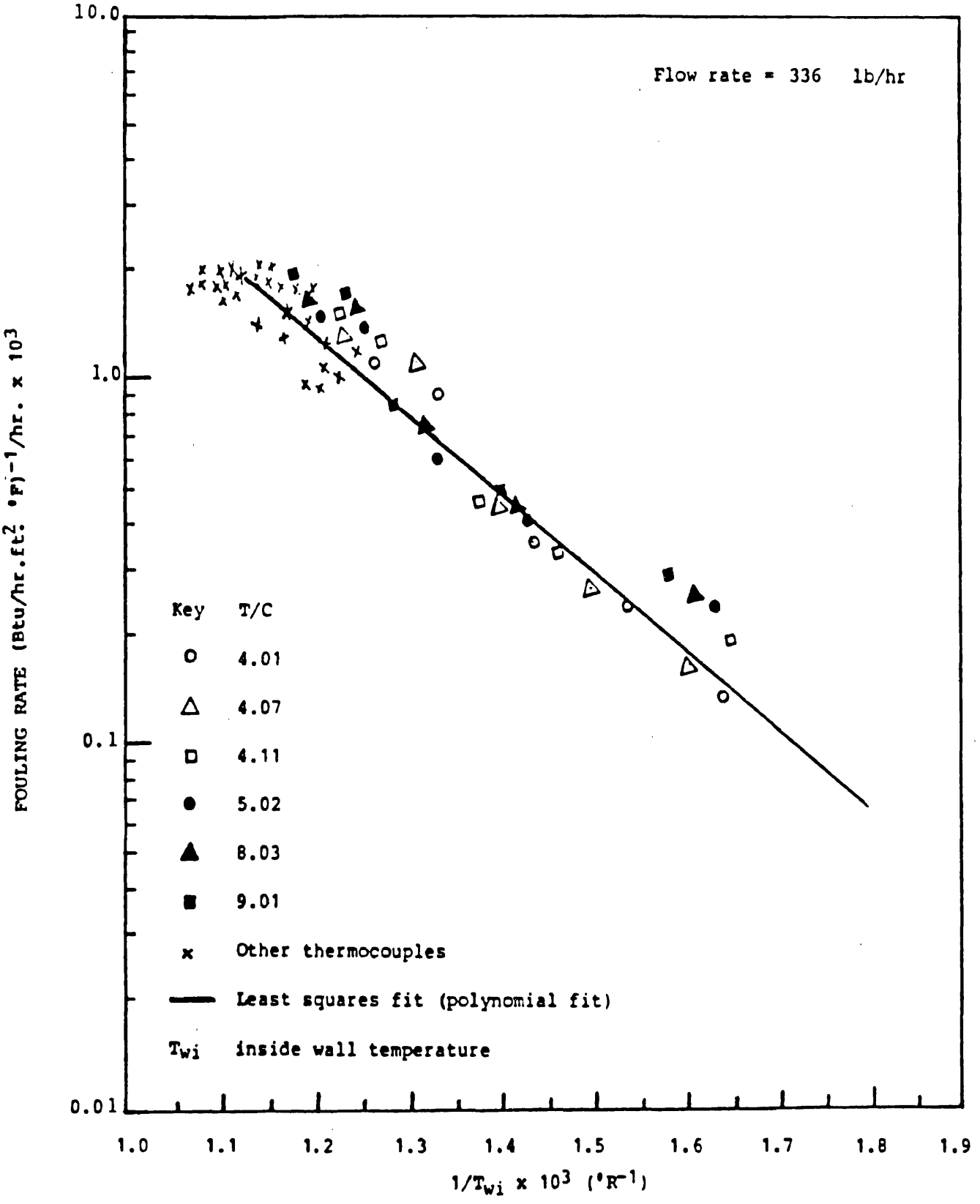

Figure 5.42 Logarithm initial fouling rate against reciprocal absolute temperature

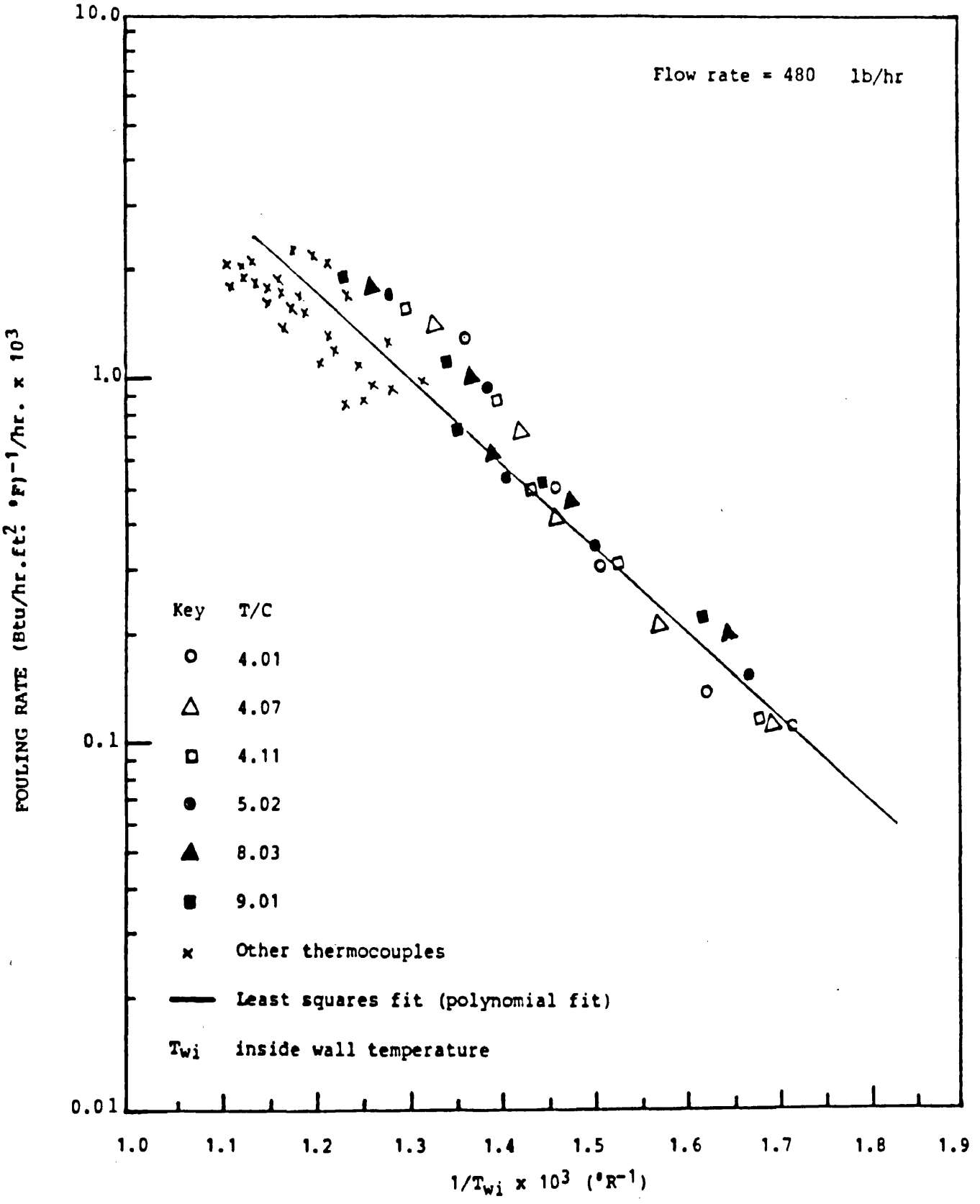

Figure 5.43 Logarithm initial fouling rate against reciprocal absolute temperature

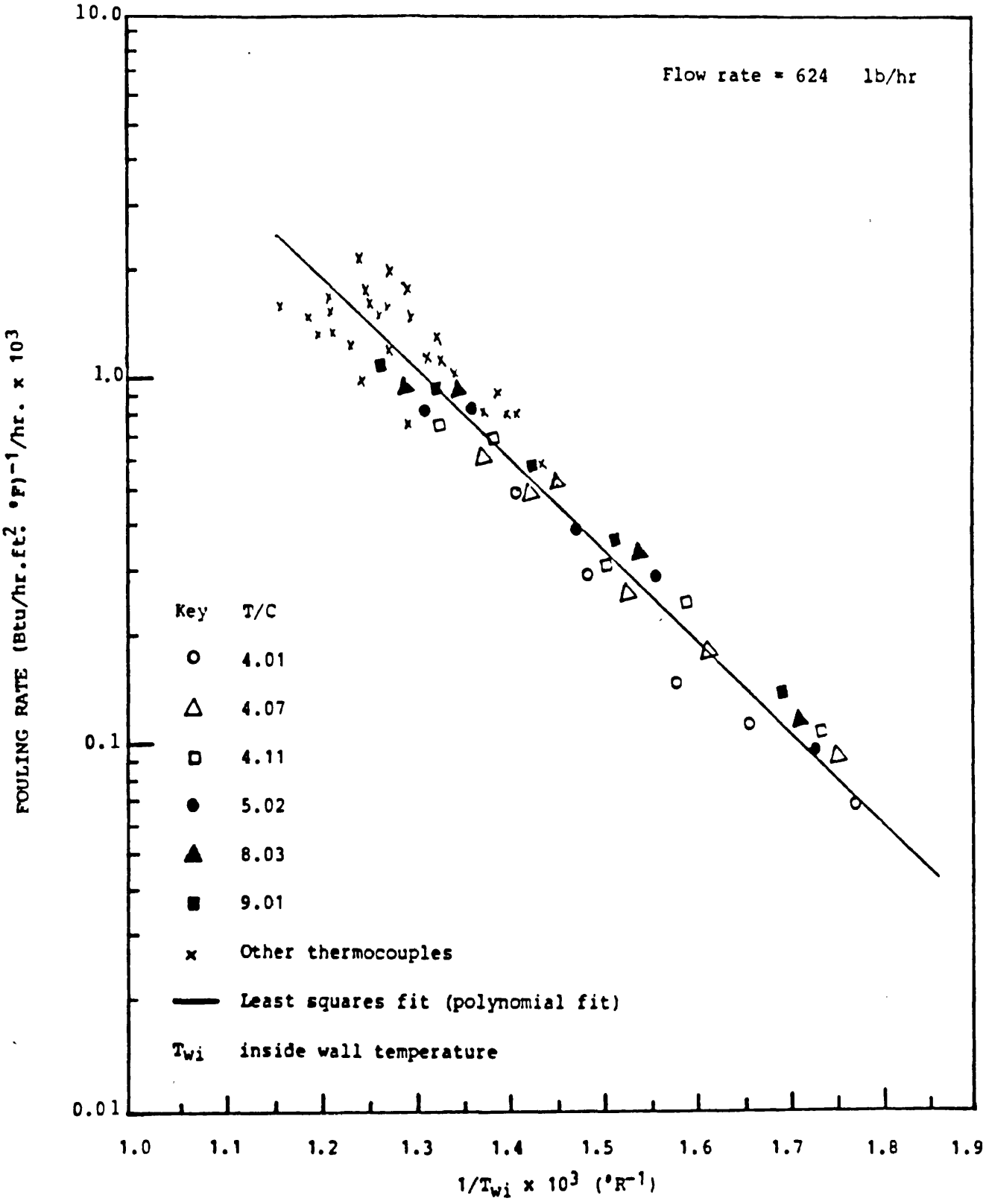

Figure 5.44 Logarithm initial fouling rate against reciprocal absolute temperature

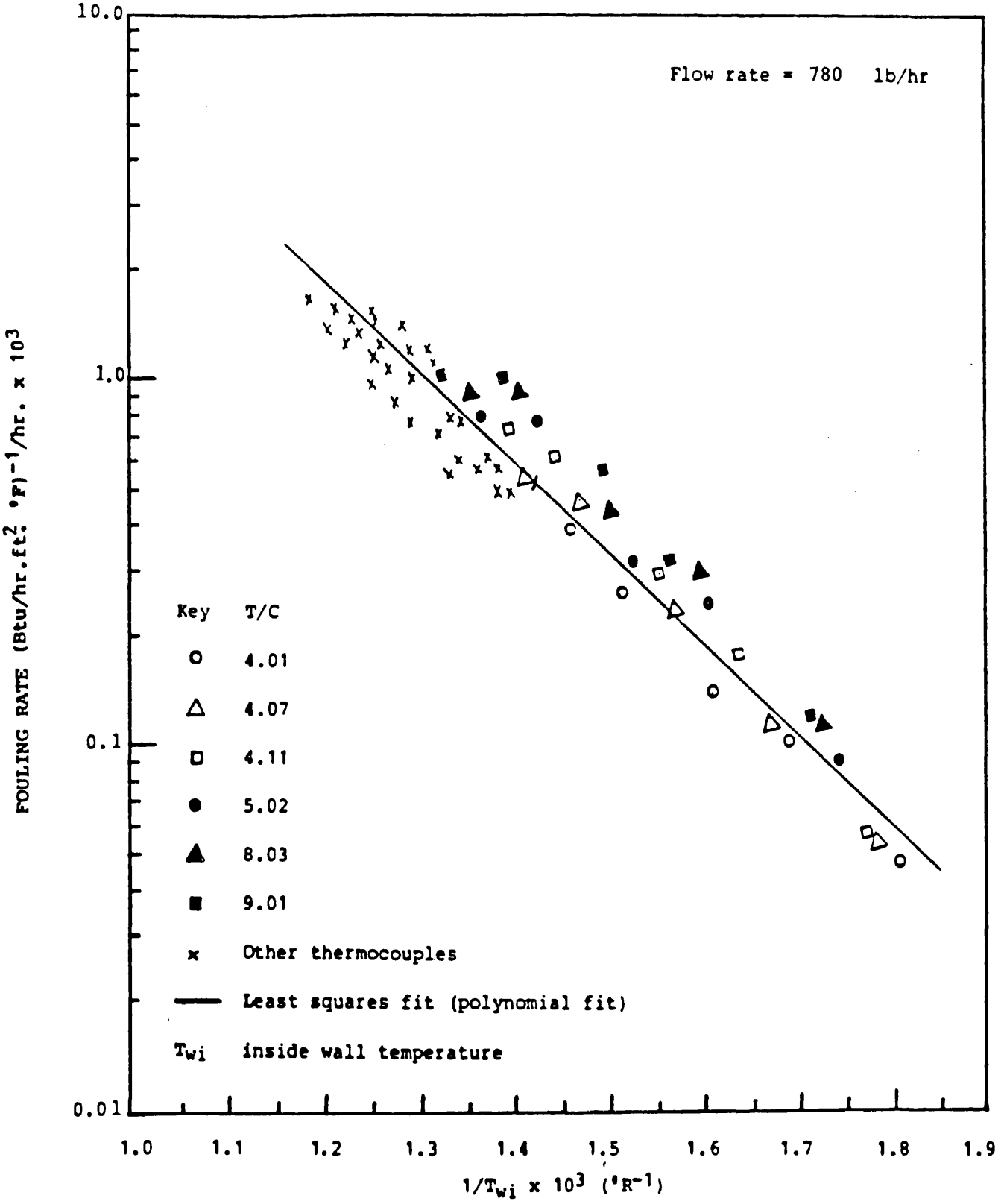

Figure 5.45 Logarithm initial fouling rate against reciprocal absolute temperature

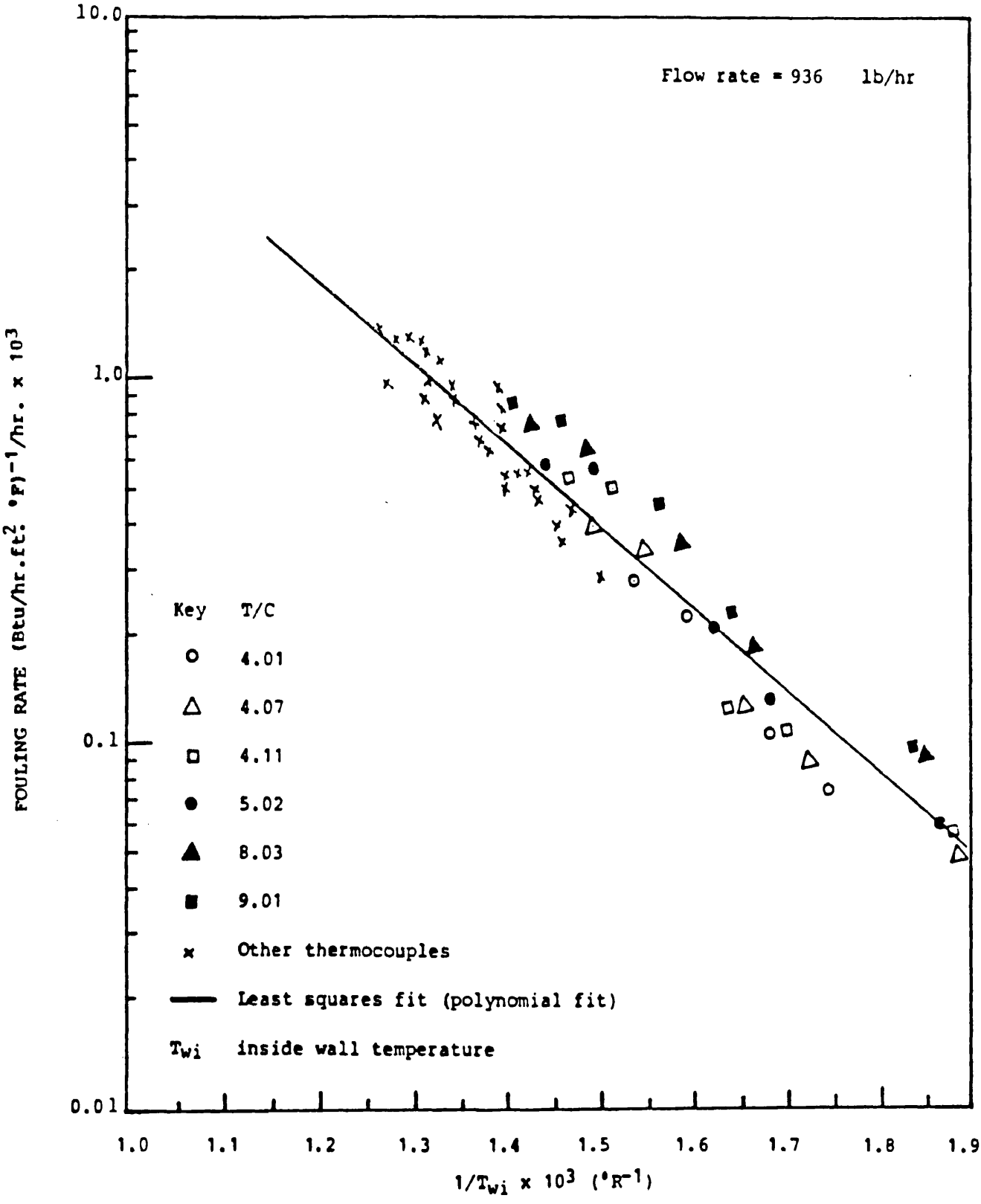

Figure 5.46 Logarithm initial fouling rate against reciprocal absolute temperature

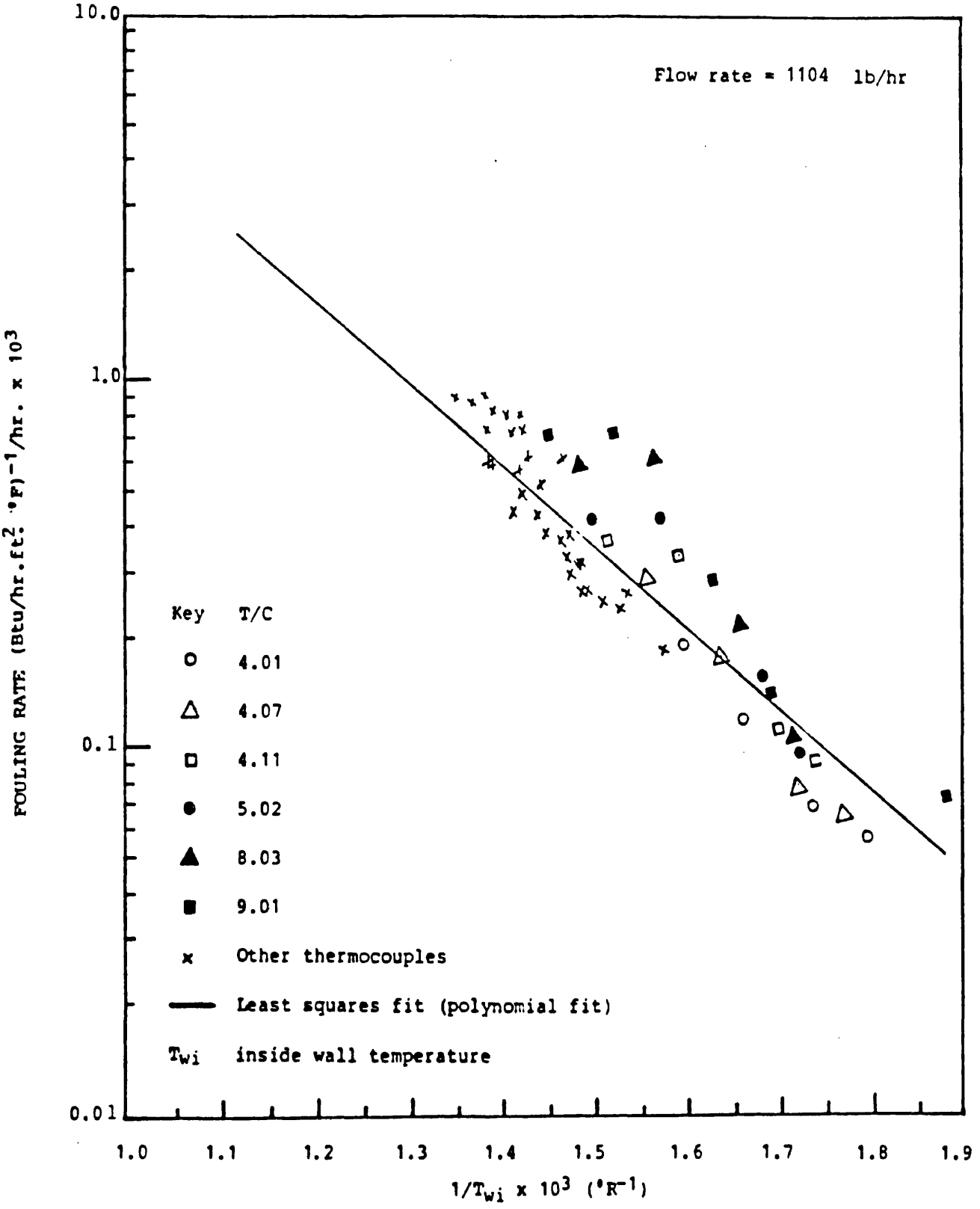

Figure 5.47 Logarithm initial fouling rate against reciprocal absolute temperature

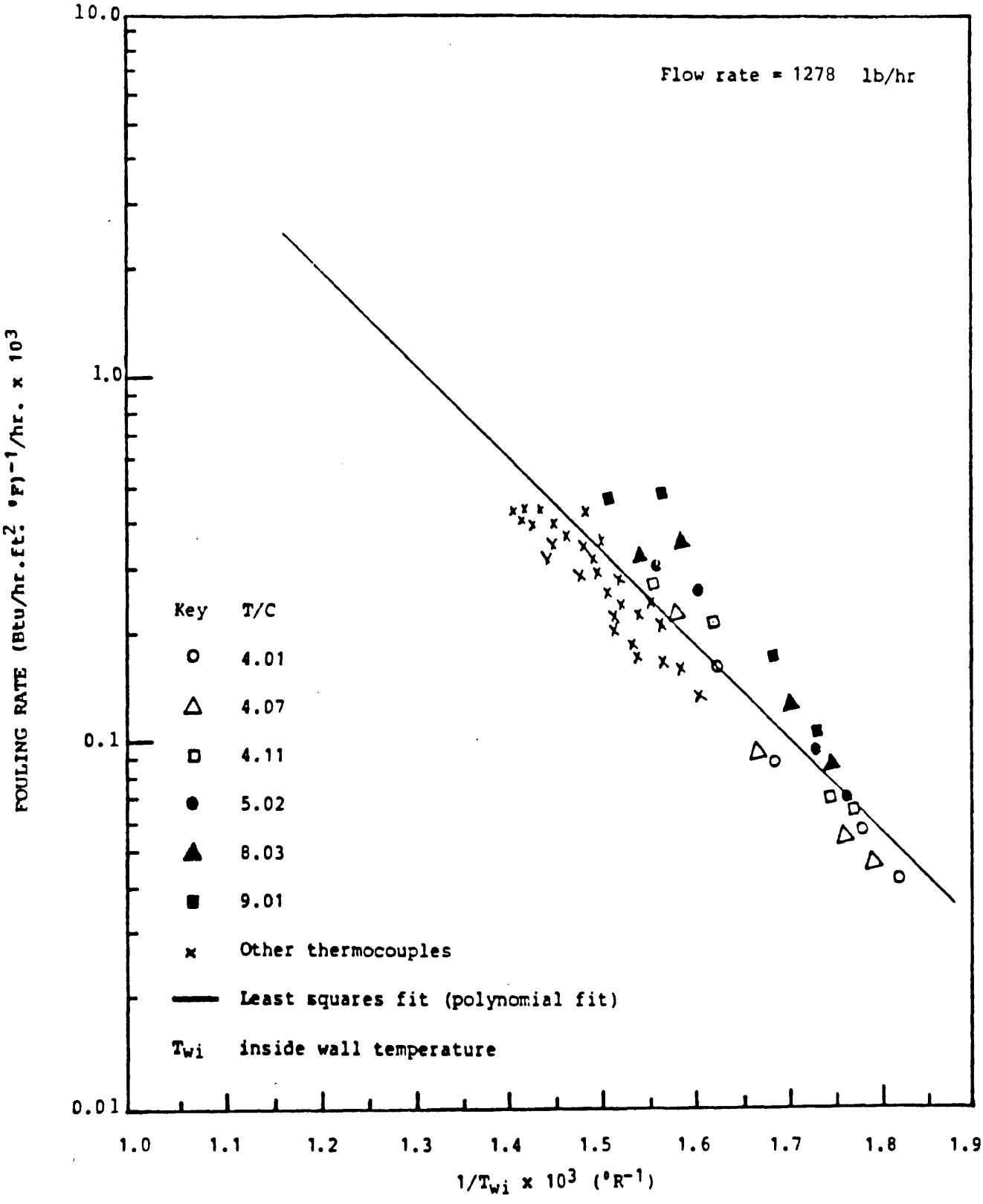

Figure 5.48 Logarithm initial fouling rate against reciprocal absolute temperature

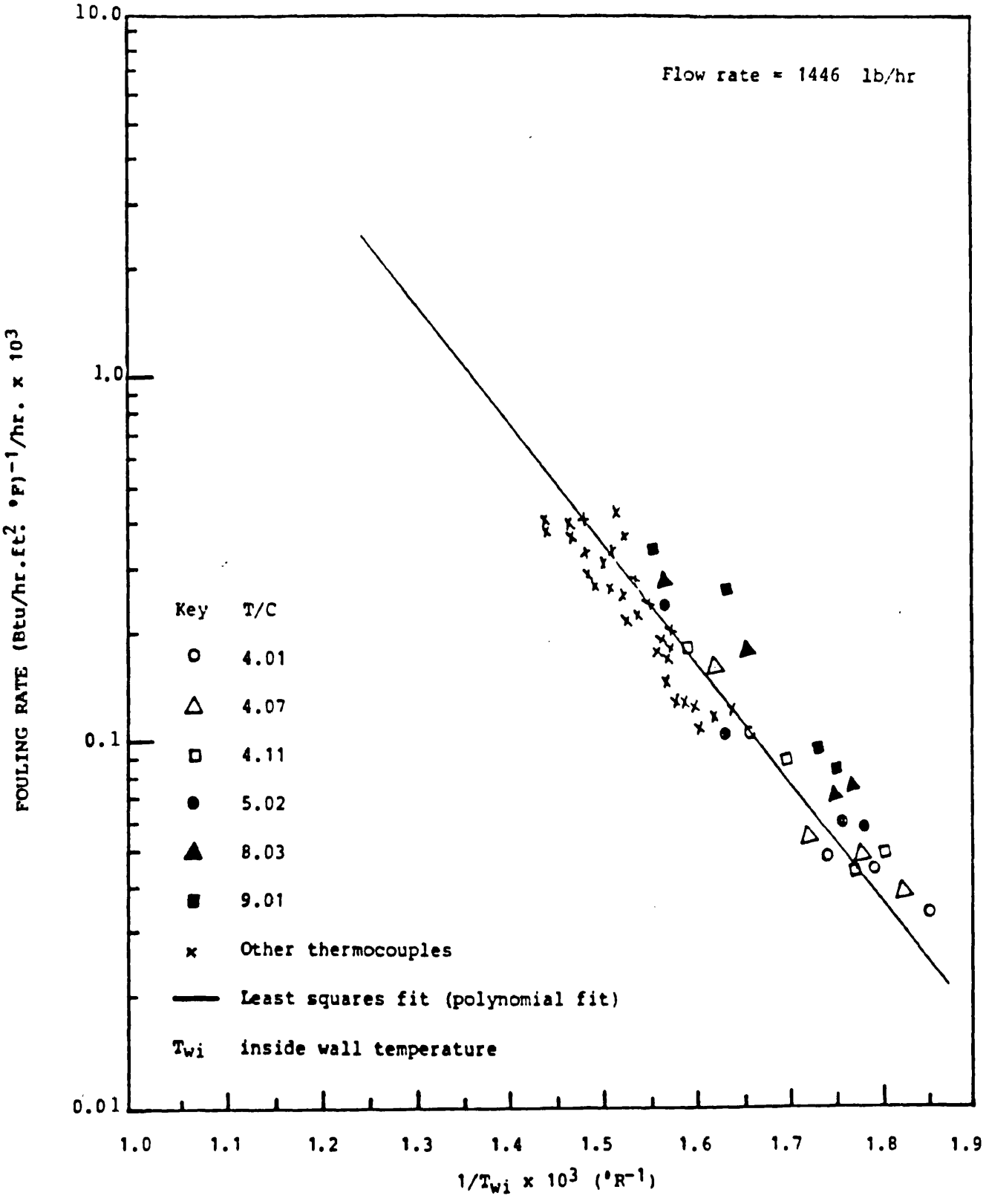

Figure 5.49 Logarithm initial fouling rate against reciprocal absolute temperature

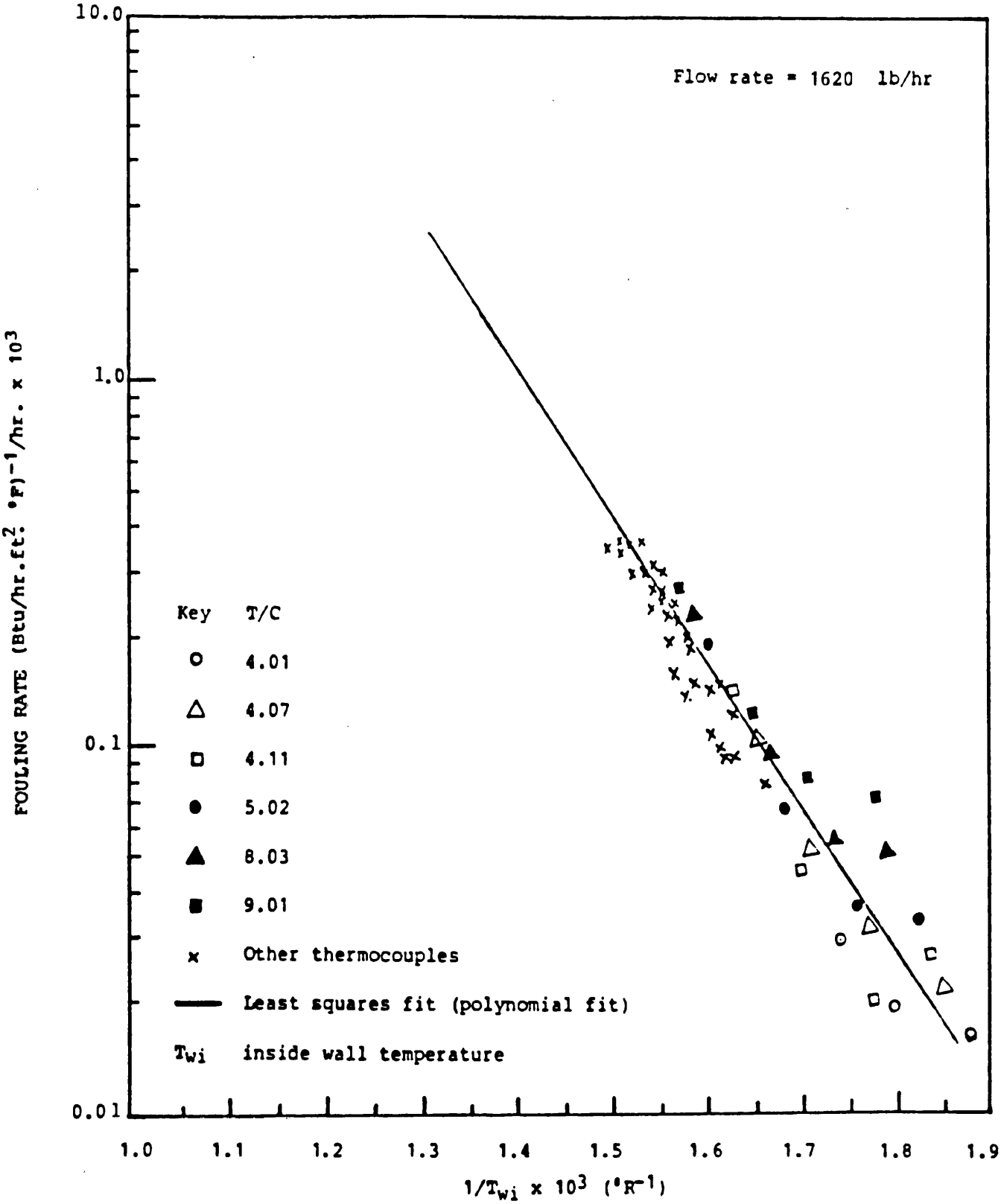

Figure 5.50 Logarithm initial fouling rate against reciprocal absolute temperature

Table 5.4 Equations of the Least Squares Fit to the Plot of the Logarithm Initial Fouling Rate Against Reciprocal of Absolute Temperature.

Equation	Flow Rate (lb/hr)
$\dot{R}_f(0) = 134.71 \exp [(-8.51 \times 10^3)/T]$	1620
$= 28.40 \exp [(-7.51 \times 10^3)/T]$	1446
$= 2.61 \exp [(-5.932 \times 10^3)/T]$	1278
$= 1.15 \exp [(-5.342 \times 10^3)/T]$	1104
$= 0.97 \exp [(-5.184 \times 10^3)/T]$	936
$= 2.05 \exp [(-5.776 \times 10^3)/T]$	780
$= 1.45 \exp [(-5.559 \times 10^3)/T]$	624
$= 0.86 \exp [(-5.278 \times 10^3)/T]$	480
$= 0.89 \exp [(-5.351 \times 10^3)/T]$	336

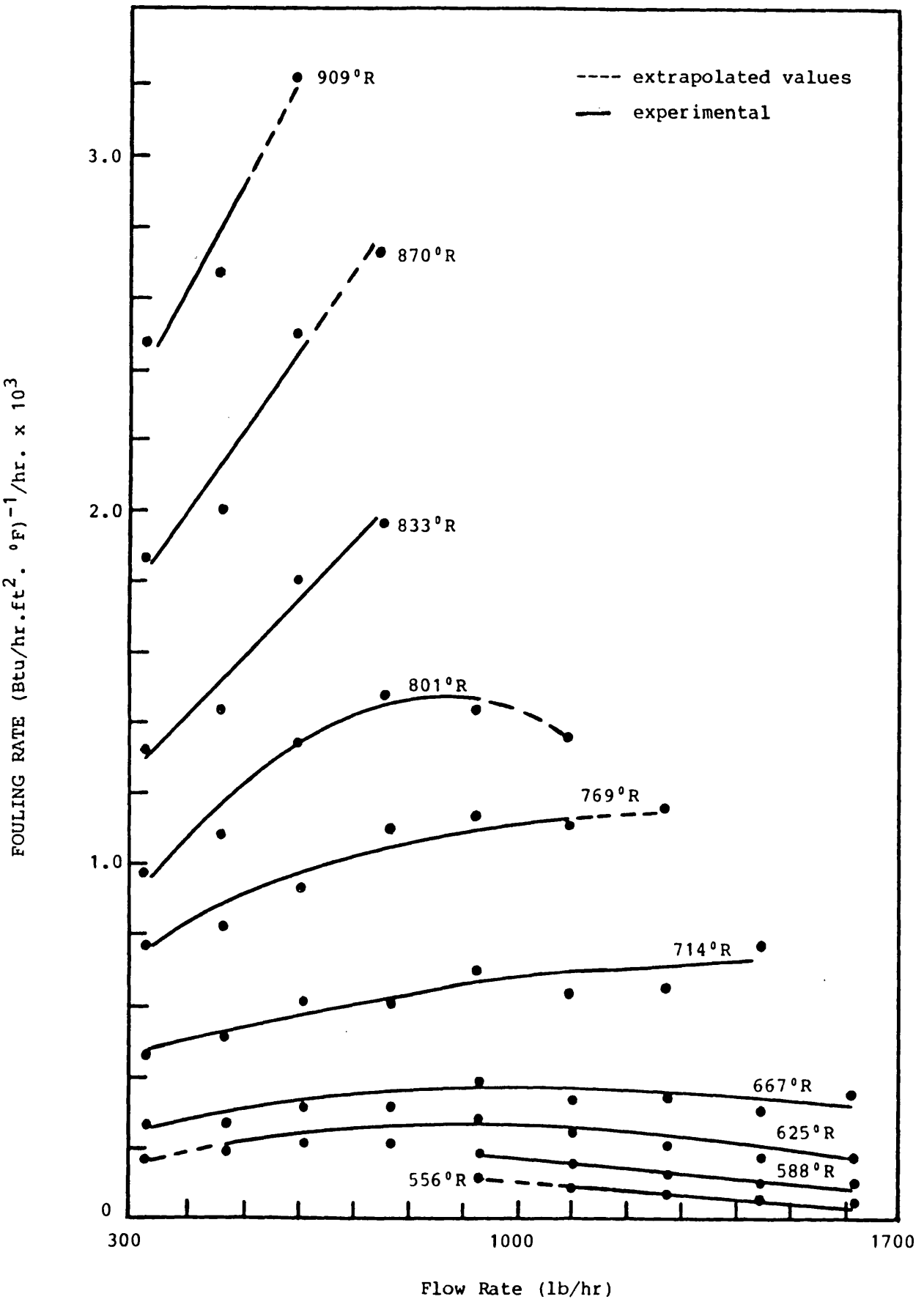

Figure 5.51 Variation of the Initial Fouling Rate Against Flow Rate.

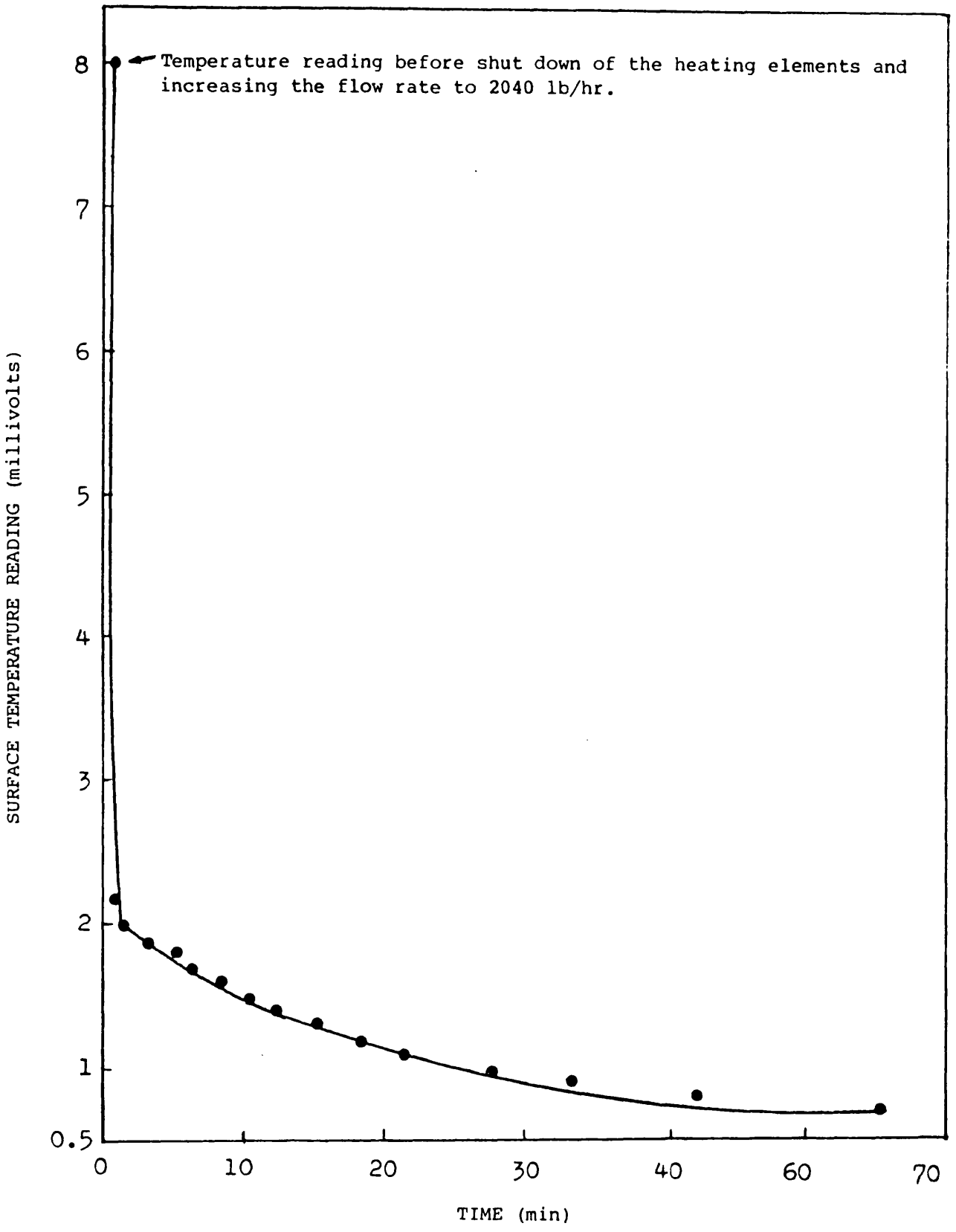

Figure 5.52 Cooling Rate of the Test Section. Variation of the Temperature Drop as a Function of Time. Run Number 43.

5.2.7 Nature of Deposits

Most of the deposits found in the tube were in the form of a soft, pale white film. However some pieces scraped from the film were harder and of a more brittle nature. Spectroscopic analyses showed that the deposit formed is a styrene polymer (Figures 5.53-5.60). Infra red was used to identify the functional groups of the unknown sample and to compare the bands with a synthesised and standard polystyrene sample (Figures 5.53-5.58). Nuclear magnetic resonance was used to confirm the structural characteristics and distribution of the atoms and to prove the identity of the polystyrene formed. The NMR spectrum for the material removed from the tube was compared with a polystyrene standard. This showed that the film formed is of the amorphous atactic form. See Figures 5.59 and 5.60.

A scanning electron microscope was used to inspect the deposit topography. The SEM studies were helpful in showing the deposit film formation and thickness. Also it was possible to see the grooves and seams of the film and tube surfaces. (See Appendix J). It was necessary to gold plate the polystyrene samples for the purpose of generating a sea of electrons on the surface of the sample to respond to the scanner.

Some polystyrene was also recovered downstream of the test section beyond the condenser in the return line filter. This demonstrated:

(1) That some polymerisation could have taken place in the bulk and then condensed upon cooling, or

(2) that some polymer was dissolved in the main bulk fluid in the furnace after being created at the hot surface, or

(3) that some polymer was physically removed from the tube surface by the turbulent action of the fluid.

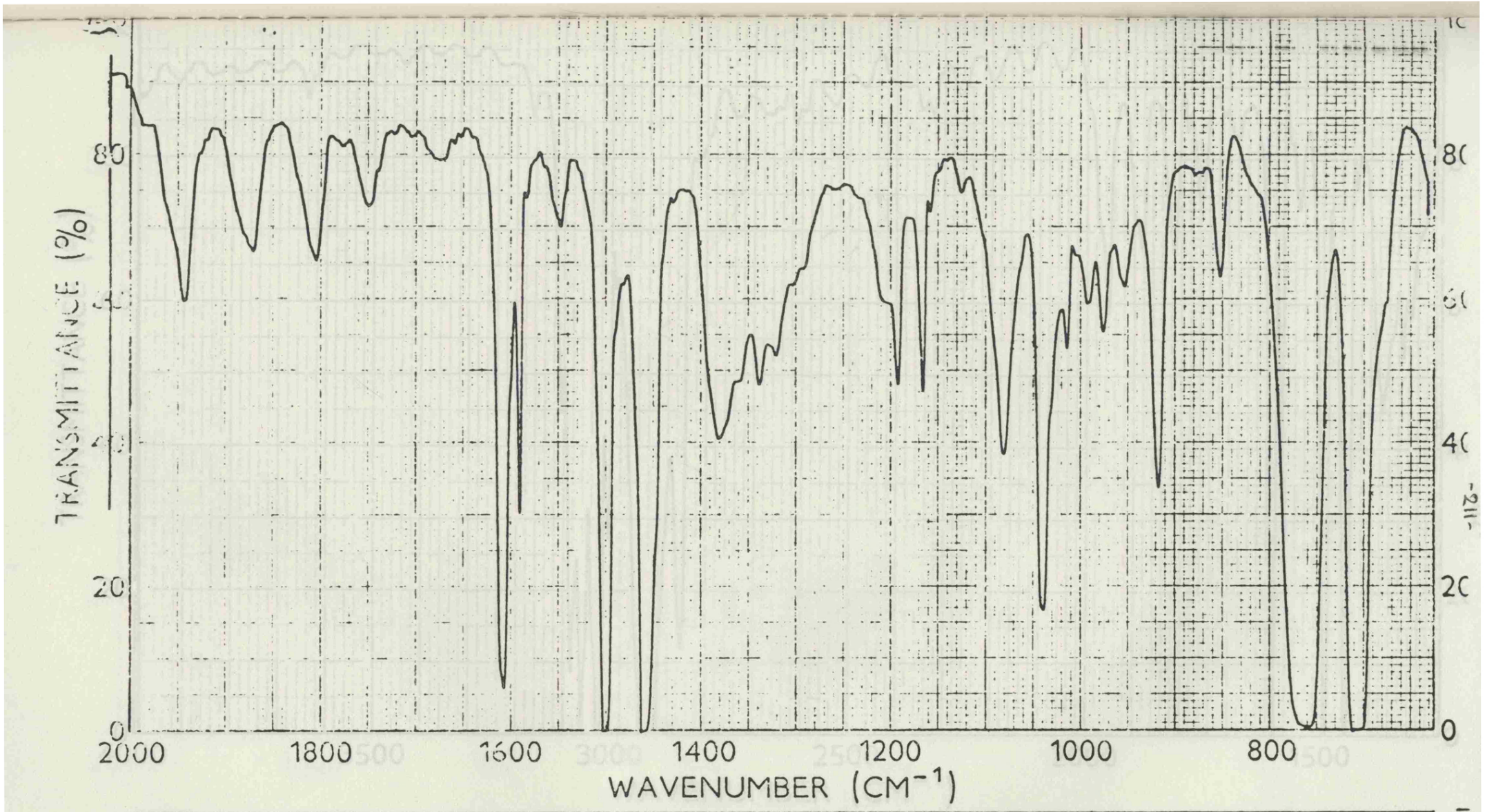

SAMPLE Standard Polystyrene	SOLVENT	SCAN SPEED FAST	OPERATOR RLH
Figure 5.53 Infra Red Spectra	CONC.	SLIT NORM.	DATE 9/12/80
	CELL PATH 0.05 mm.	REMARKS OH-OH	
ORIGIN	REFERENCE Air		

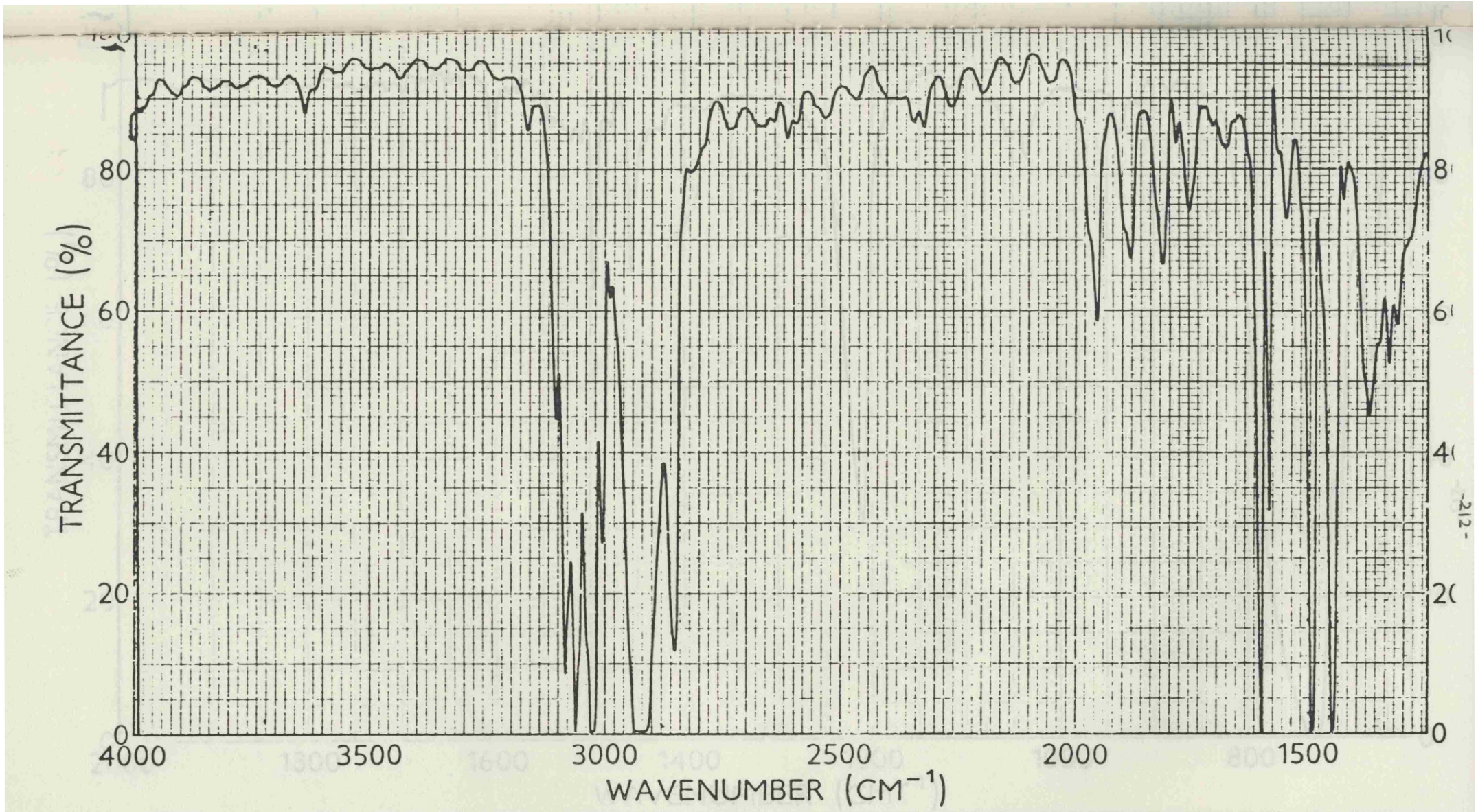

SAMPLE Standard Polystyrene Figure 5.54 Infra Red Spectra ORIGIN	SOLVENT CONC. CELL PATH 0.05 mm. REFERENCE Air	SCAN SPEED FAST SLIT Norm.	OPERATOR RLH DATE 9/12/80 REMARKS OH-OH.

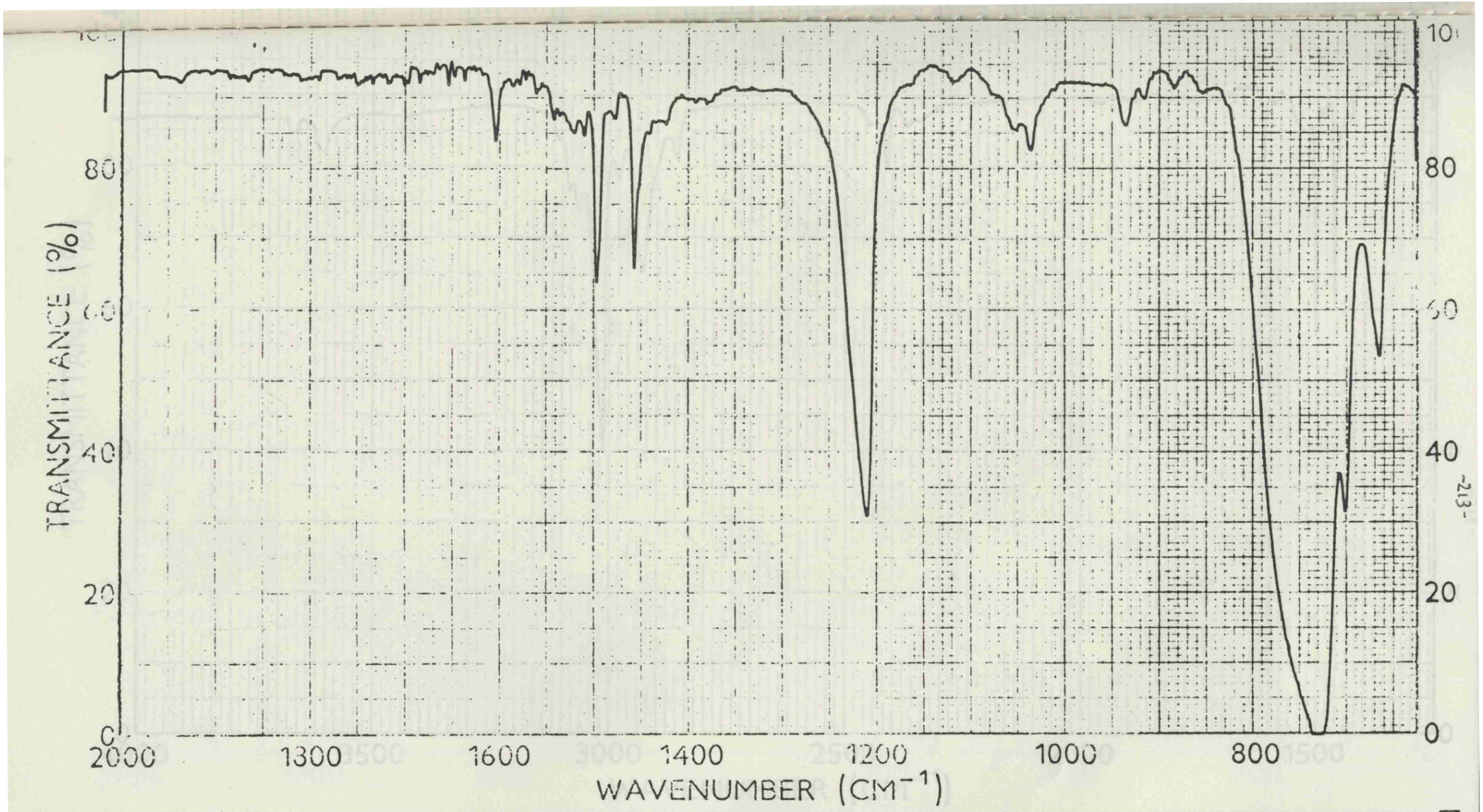

SAMPLE Synthesized Polystyrene	SOLVENT $CHCL_3$	SCAN SPEED Fast	OPERATOR RLH
Figure 5.55 Infra Red Spectra	CONC. 0.0215 gm/ml	SLIT 26	DATE 22/1/87
ORIGIN	CELL PATH 0.1 mm.	REMARKS Perkin Elmer 237	
	REFERENCE $CHCL_3$		

NO.

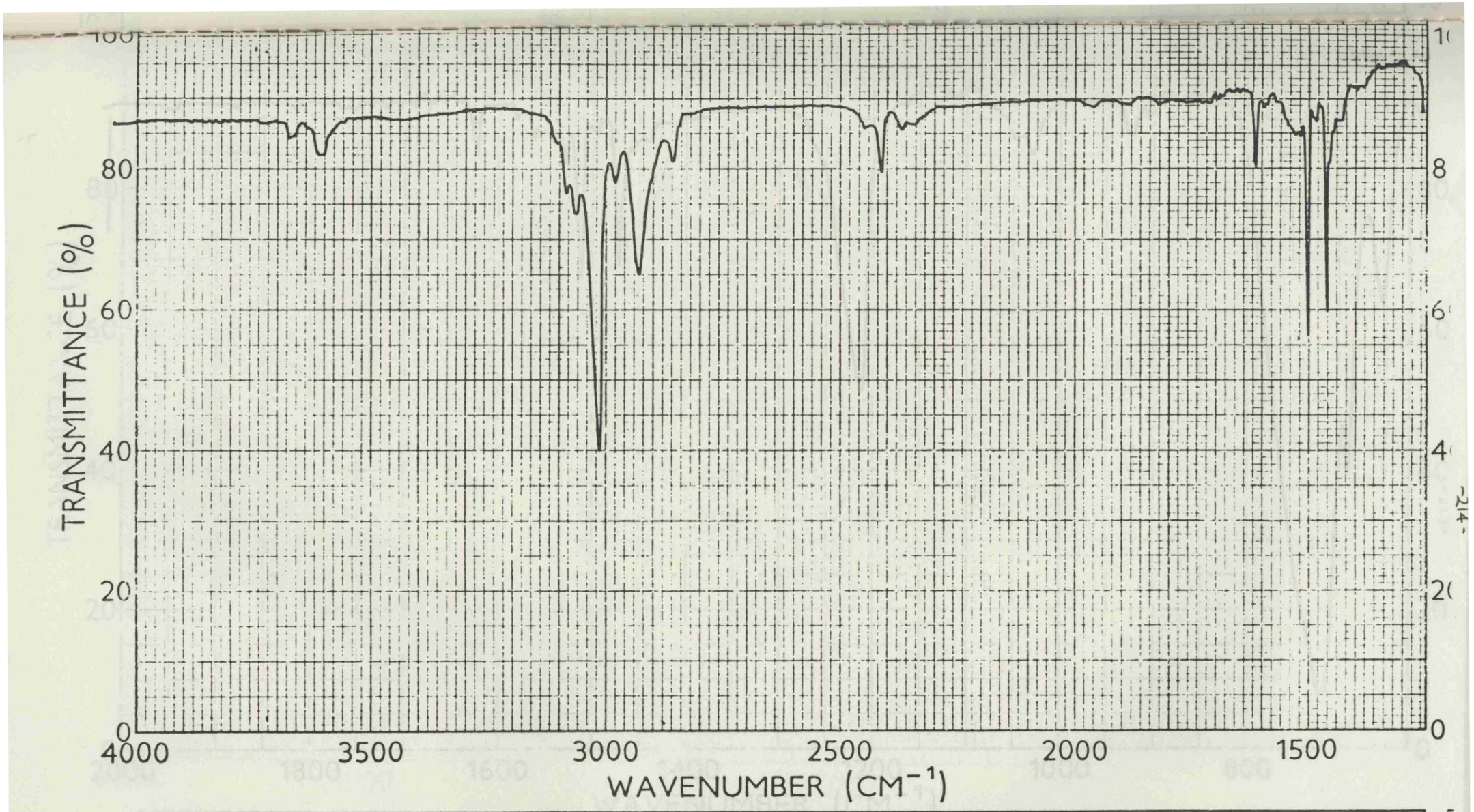

SAMPLE Synthesized Polystyrene Figure 5.56 Infra Red Spectra ORIGIN	SOLVENT $CHCl_3$ CONC. 0.0215 gm/ml CELL PATH 0.1 mm. REFERENCE $CHCl_3$	SCAN SPEED FAST SLIT 26 REMARKS P.E. 237	OPERATOR RLH DATE 22/1/81

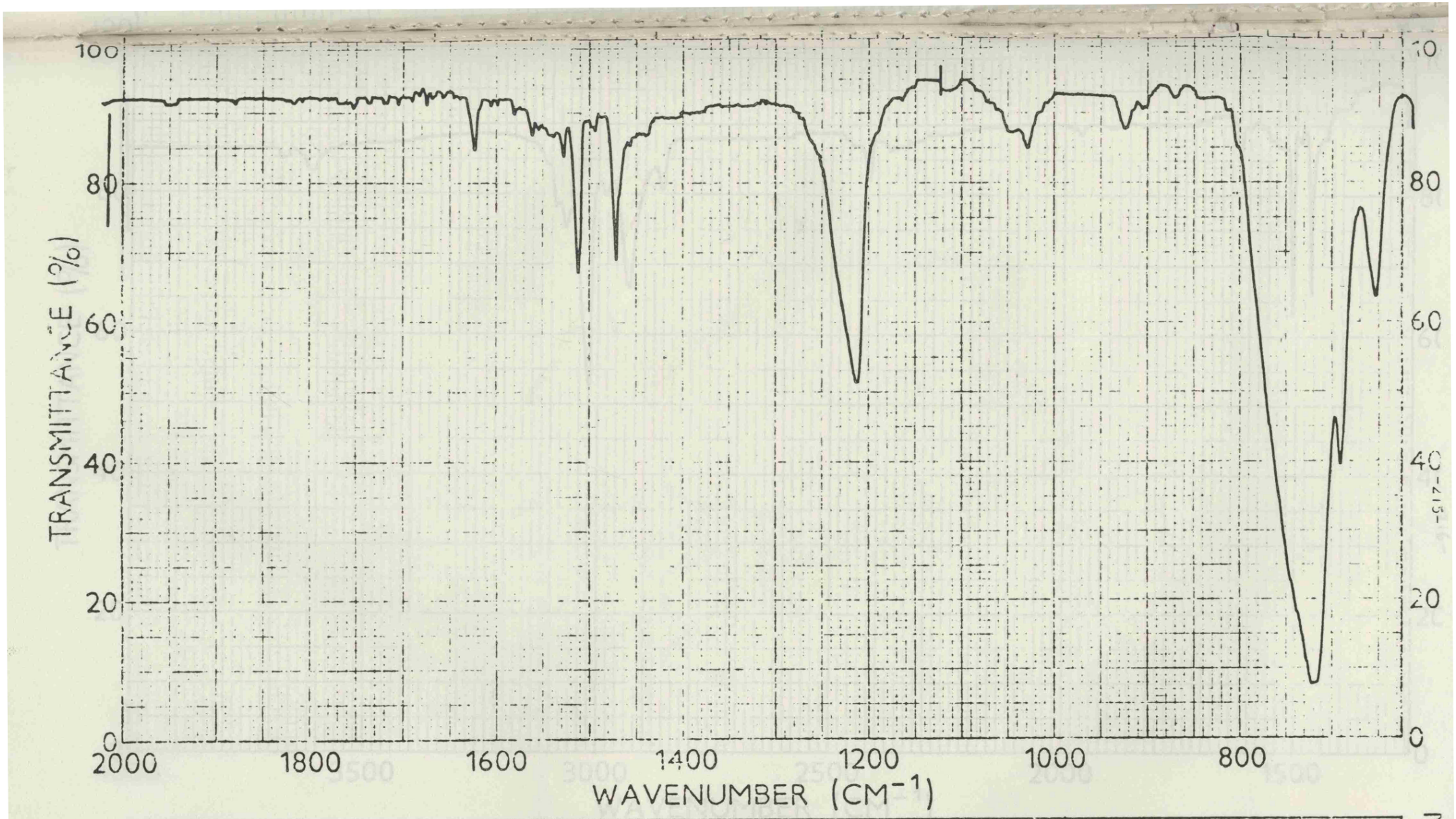

SAMPLE S. Hout Unknown Figure 5.57 Infra Red Spectra ORIGIN	SOLVENT $CHCl_3$ CONC. 0.0196 gm/ml CELL PATH 0.1 mm. REFERENCE $CHCl_3$	SCAN SPEED FAST SLIT 26 REMARKS P.E. 237.	OPERATOR RLH DATE 22/1/81

NC.

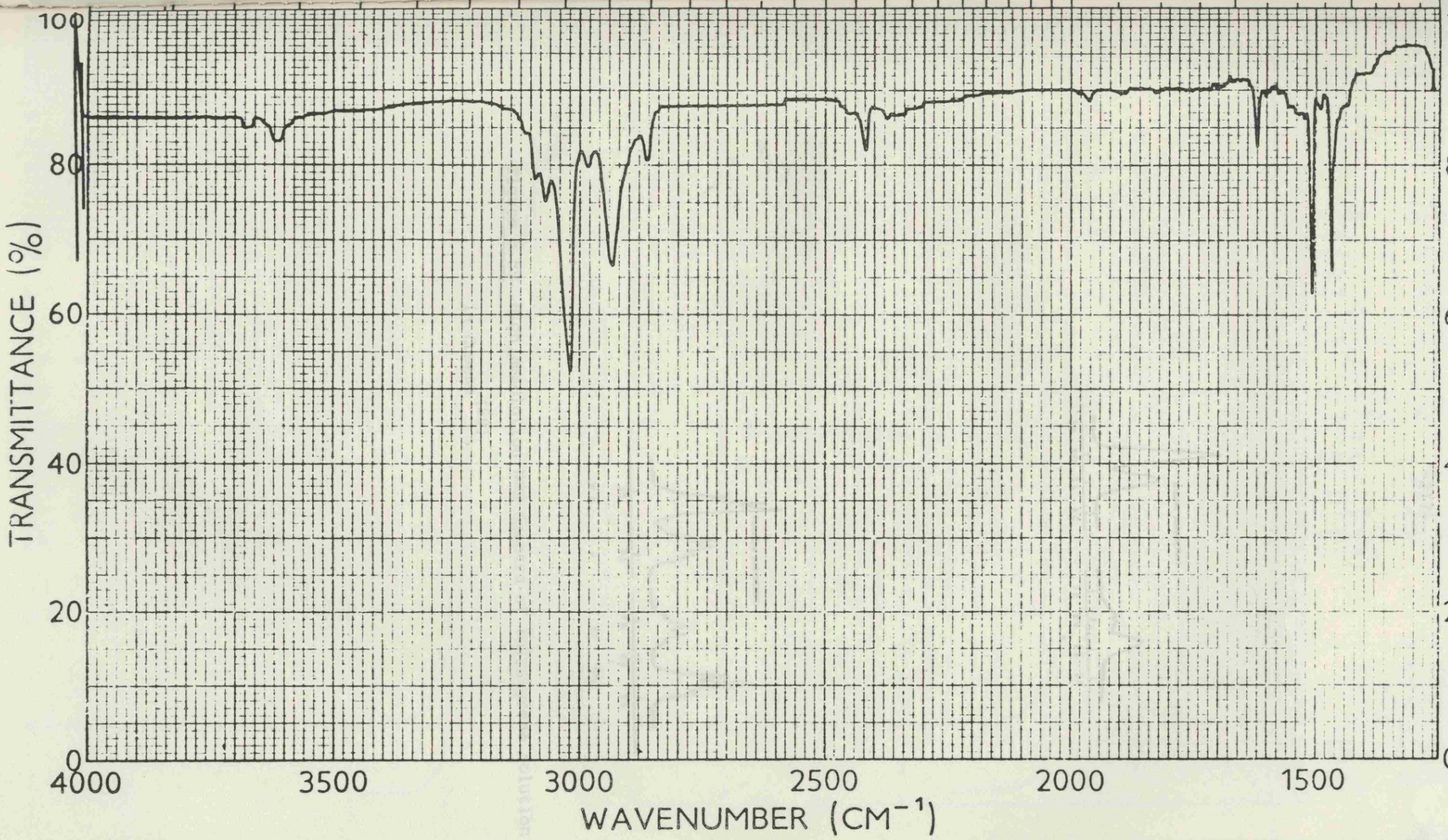

SAMPLE S. Hout Unknown Figure 5.58 Infra Red Spectra ORIGIN	SOLVENT $CHCL_3$ CONC. 0.0196 gm/ml CELL PATH 0.1 mm. REFERENCE $CHCL_3$	SCAN SPEED FAST SLIT 26 REMARKS P.E. 237	OPERATOR RCH DATE 22/1/81

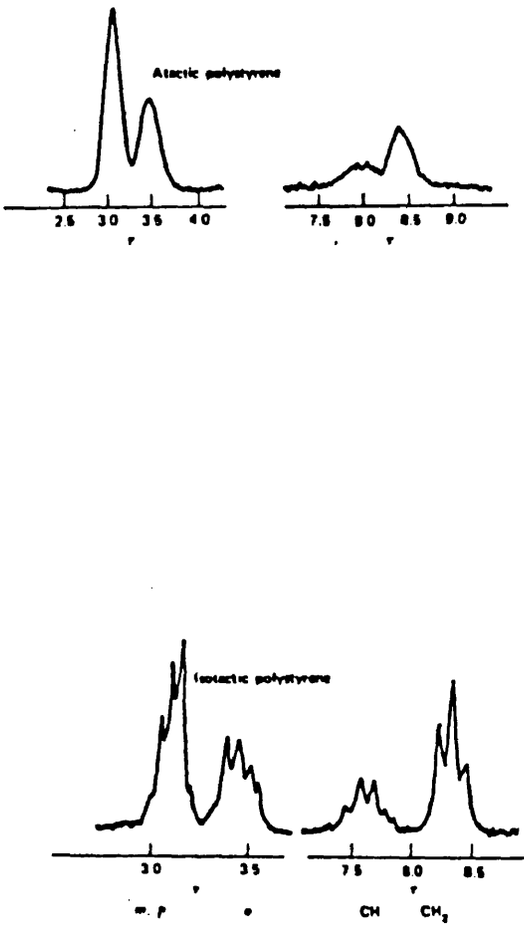

Figure 5.59 High Resolution NMR Spectra of Polystyrene Solution in Cumene[69].

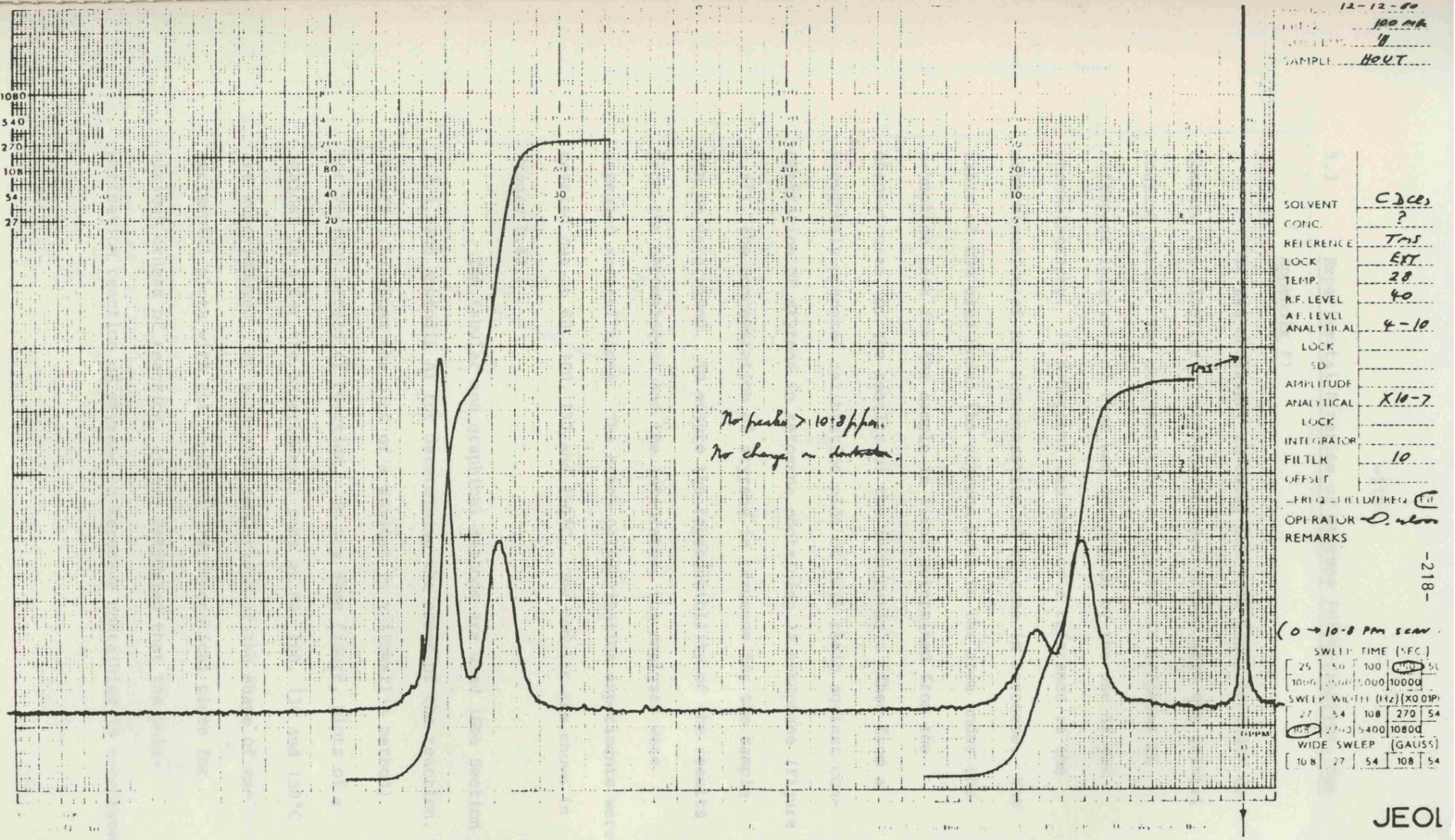

Figure 5.60 NMR Spectra of Unknown.

5.3 Experimental Kinetics of Styrene Polymerisation (See Appendix F)

It was necessary to carry out this study in order to compare the kinetics of styrene polymerisation with the initial fouling rates. The concentration of styrene in kerosene at different intervals of time was determined by the use of gas chromatography. 1% N-heptane was used as a reference in the determination of the concentration of styrene in kerosene. The ratio of the area under the styrene peak to the area under the n-heptane peak for the sample is first determined from the chromatogram (or the results of the integrator). Then from a previously prepared calibration plot of this ratio against concentration of styrene in kerosene containing 1% n-heptane (Figure 5.61), the concentration of styrene in kerosene for the sample can be determined. To ensure the reproducibility of the results from the chromatogram and the integrator, the analyses were repeated several times. The batch polymerisation experiments were carried out at 80, 100, 130 and 150°C. The results are shown in Figure 5.62.

The tabular and graphical methods are used (See Section 3.2.4, and Appendix A) for determining the order of the reaction. Figure 5.63 shows the plot of α against ln τ (Powell's method) for various orders of reaction. On the same figure, plots of α against ln t for the experimental runs at 80, 100, 130 and 150°C are superimposed. By a careful comparison of the shape of experimental plots with the shape of the theoretical plots for various orders of reaction, it was estimated that the polymerisation reaction of styrene in kerosene containing 1% n-heptane

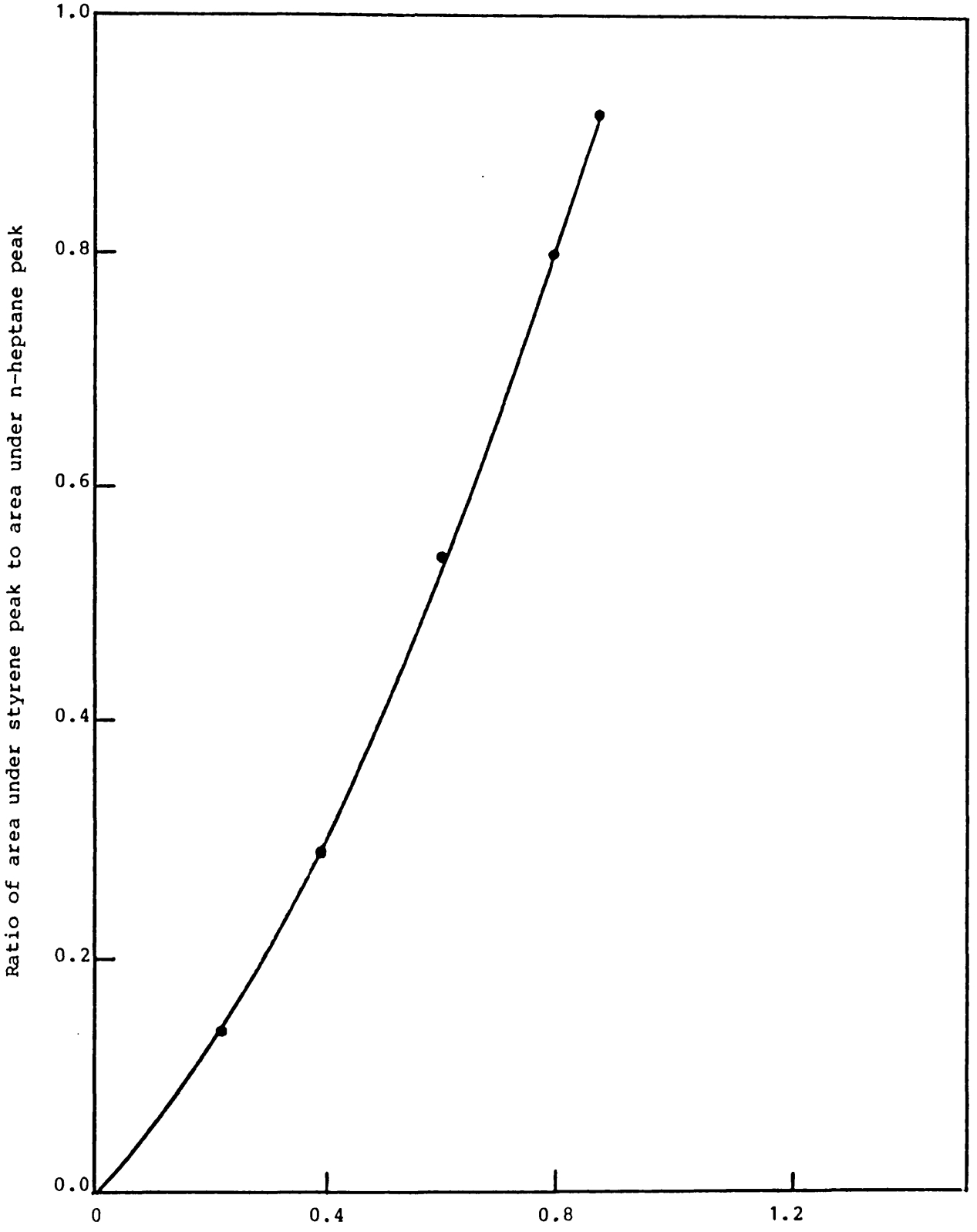

Figure 5.61 A Calibration Plot for the Gas Chromatograph.

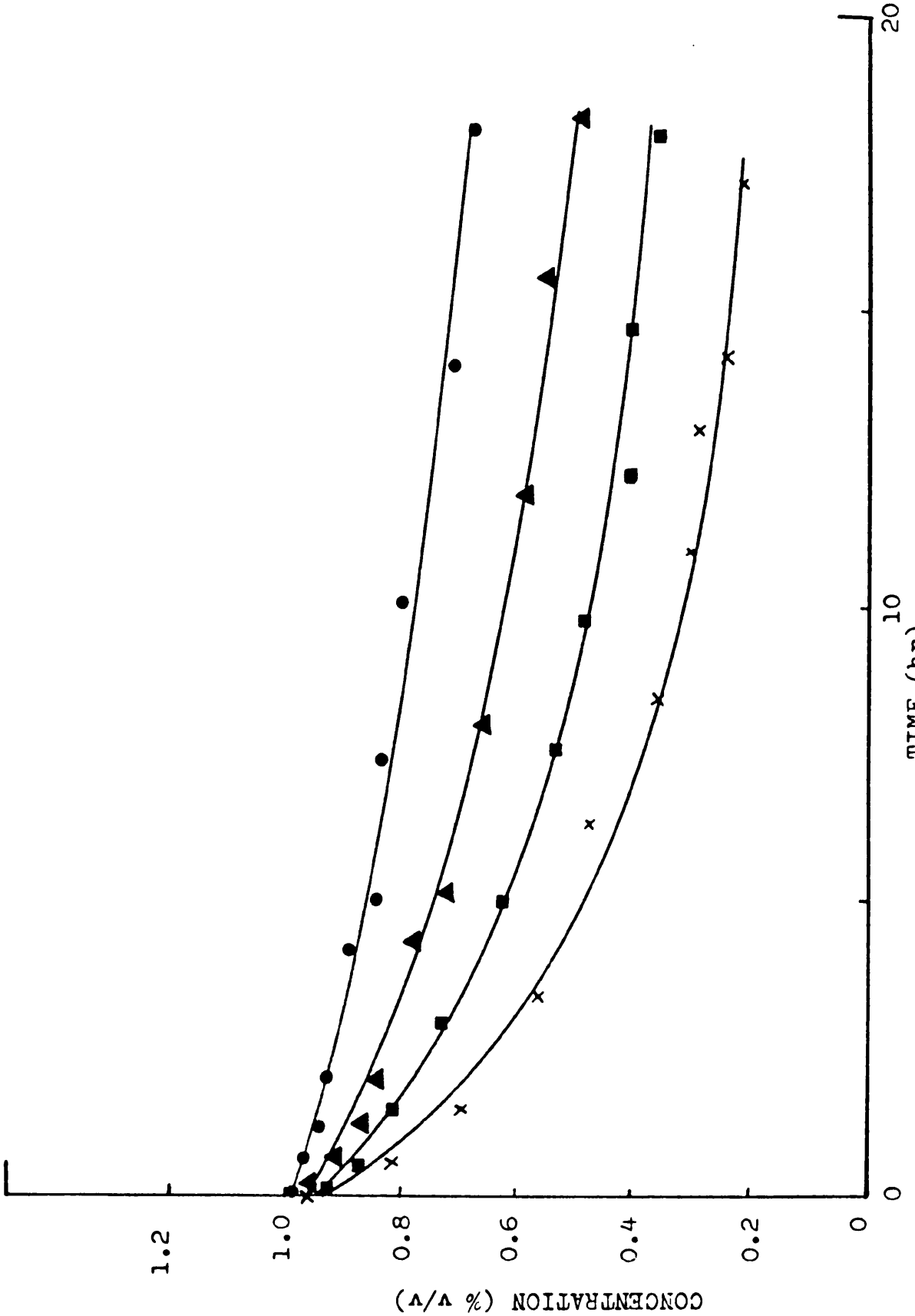

Figure 5.62 A plot of concentration of styrene in kerosene against time for the polymerisation of 1% styrene in kerosene at various temperatures .

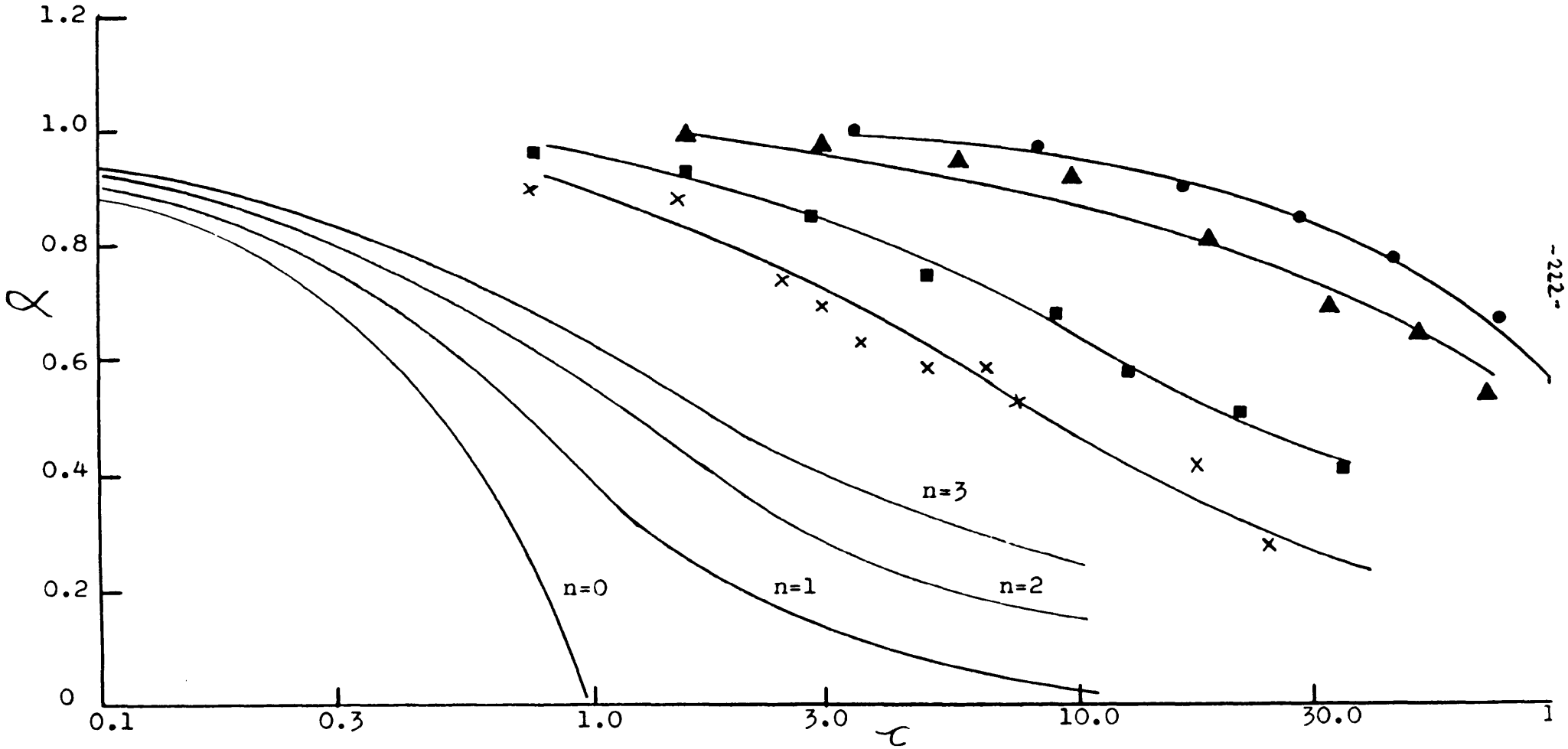

Figure 5.63 A Plot of α Against ln τ for Various Orders of Reaction and the Superimposed Experimental Plots of α Against ln t.

● 80°C ▲ 100°C ■ 130°C × 150°C

is of 5/2 order for the temperature range 80-150°C. This was then confirmed by using the graphical method. Linear curves were obtained by plotting $1/C_M^{3/2}$ against t (See Figure 5.64). C_M is the concentration of styrene in kerosene (% V/v). The linear behaviour was shown over the temperature range 80-150°C. Thus the polymerisation reaction of styrene in the kerosene solvent containing 1% n-heptane was confirmed to be of 5/2 order over the experimental range of temperature.

Figure 5.65 shows a plot of the experimental initial rate of polymerisation as a function of the reciprocal temperature and is compared with literature values reported by Roper[168] for the initial rate of polymerisation of pure styrene. The least squares fit gave a linerar relationship parallel to Roper's plot. An activation Energy of 8.53 Kcal/mol was estimated for the kinetics of 1% styrene in kerosene.

The experimental line of Figure 5.65 is the original plot from which Figure 5.66 was extracted. The initial rate of polymerisation of styrene is converted from % conversion/hr to a fouling rate in $(Btu/hr.ft^2.°F)^{-1}/hr$, as follows:

For the reaction to occur on the surface of the tube only, the reaction rate r is given by

$$r = \frac{yC_bd}{100x4} \quad \text{(lb styrene reacted/ft}^2\text{ surface per hour)} \qquad (123)$$

where

y - % of styrene reacted per hour

C_b - bulk concentration of styrene (lb styrene/ft^3 bulk solution)

$\frac{d}{4}$ - Volume to surface ratio of an element of the tube of inside diameter d. (ft)

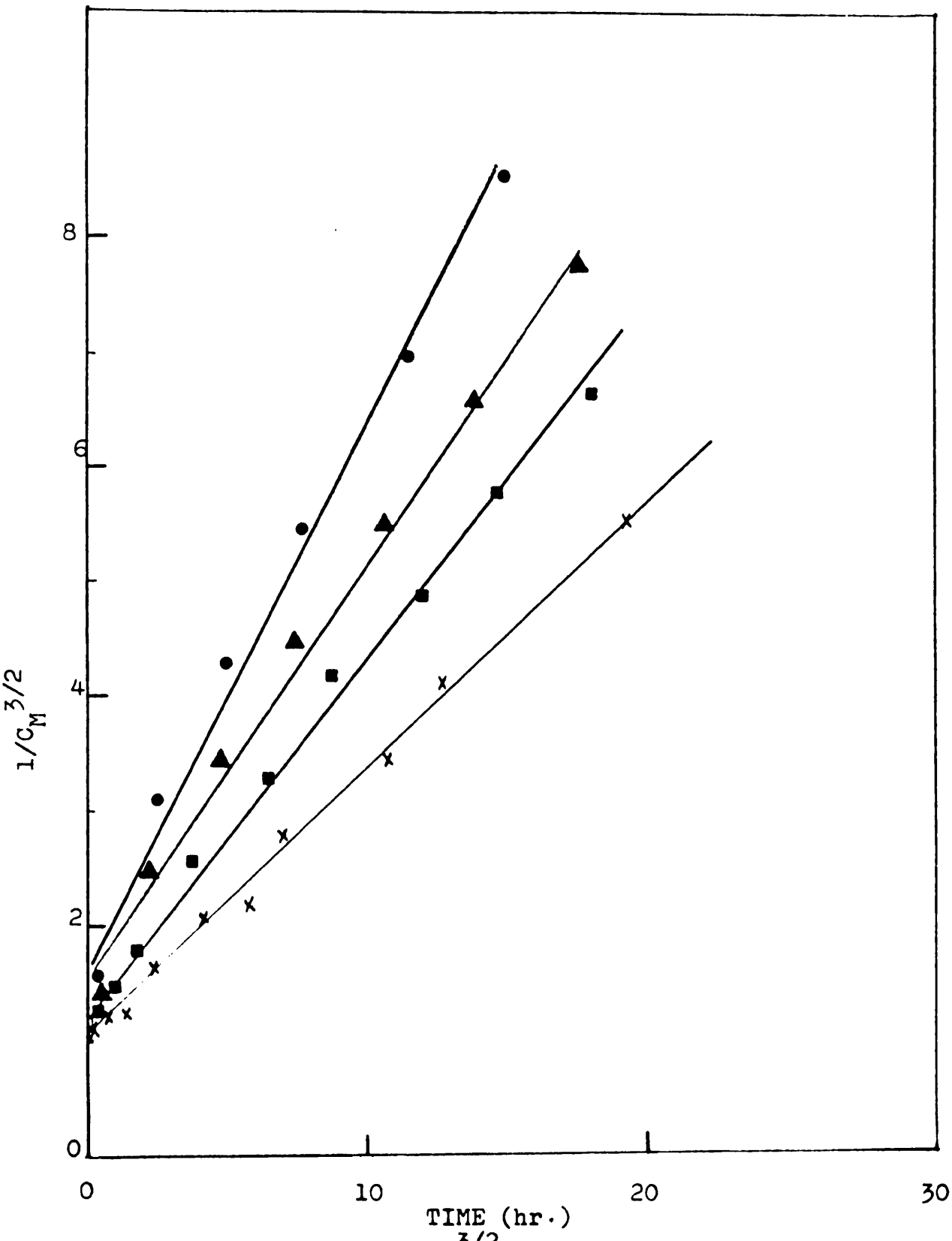

Figure 5.64 A plot of $1/C_M^{3/2}$ against t for the polymerisation reaction of 1% styrene in kerosene at various temperatures. ● 80°C ▲ 100°C ■ 130°C x 150°C

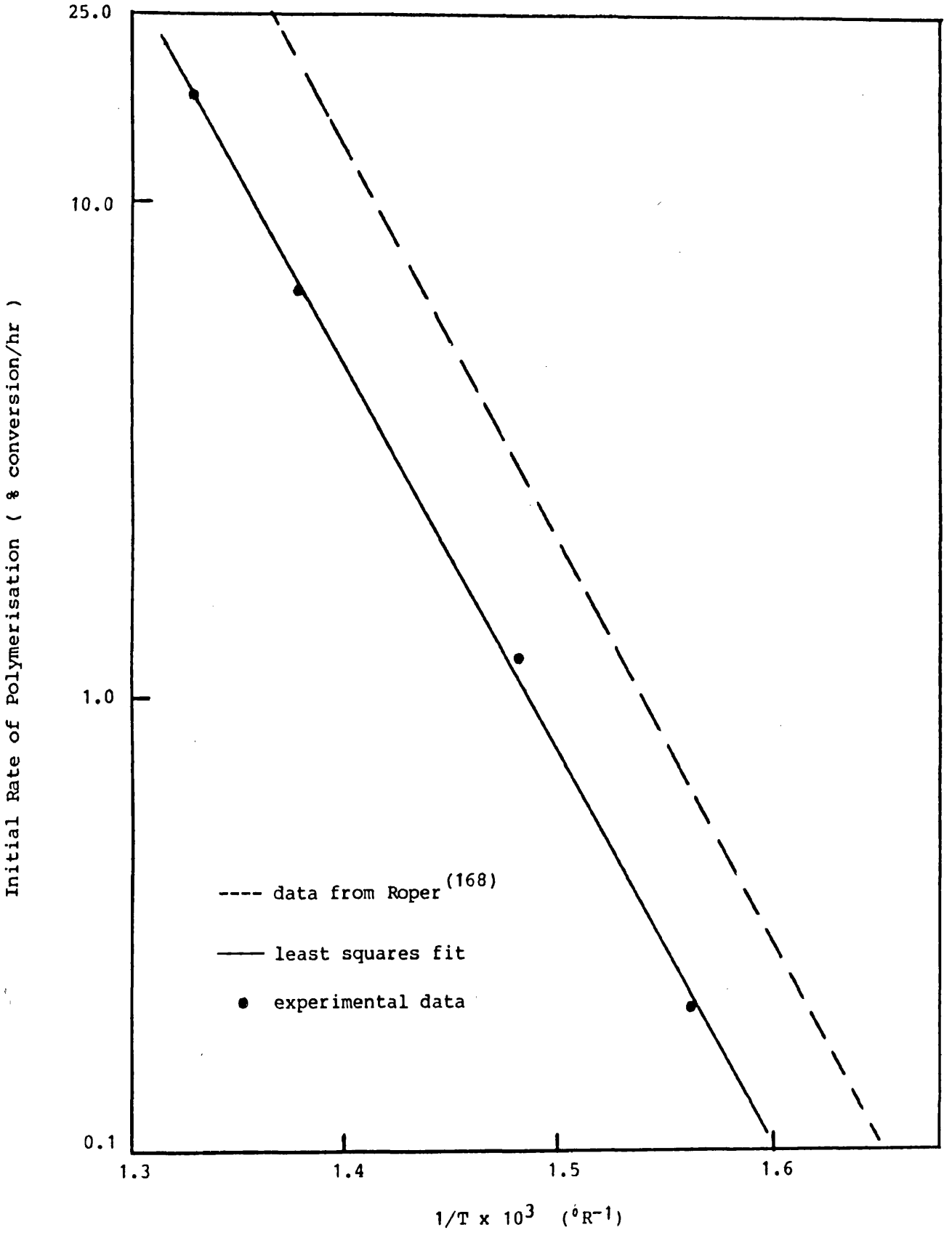

Figure 5.65 Initial Rate of Polymerisation of Styrene as a Function of (temperature)$^{-1}$.

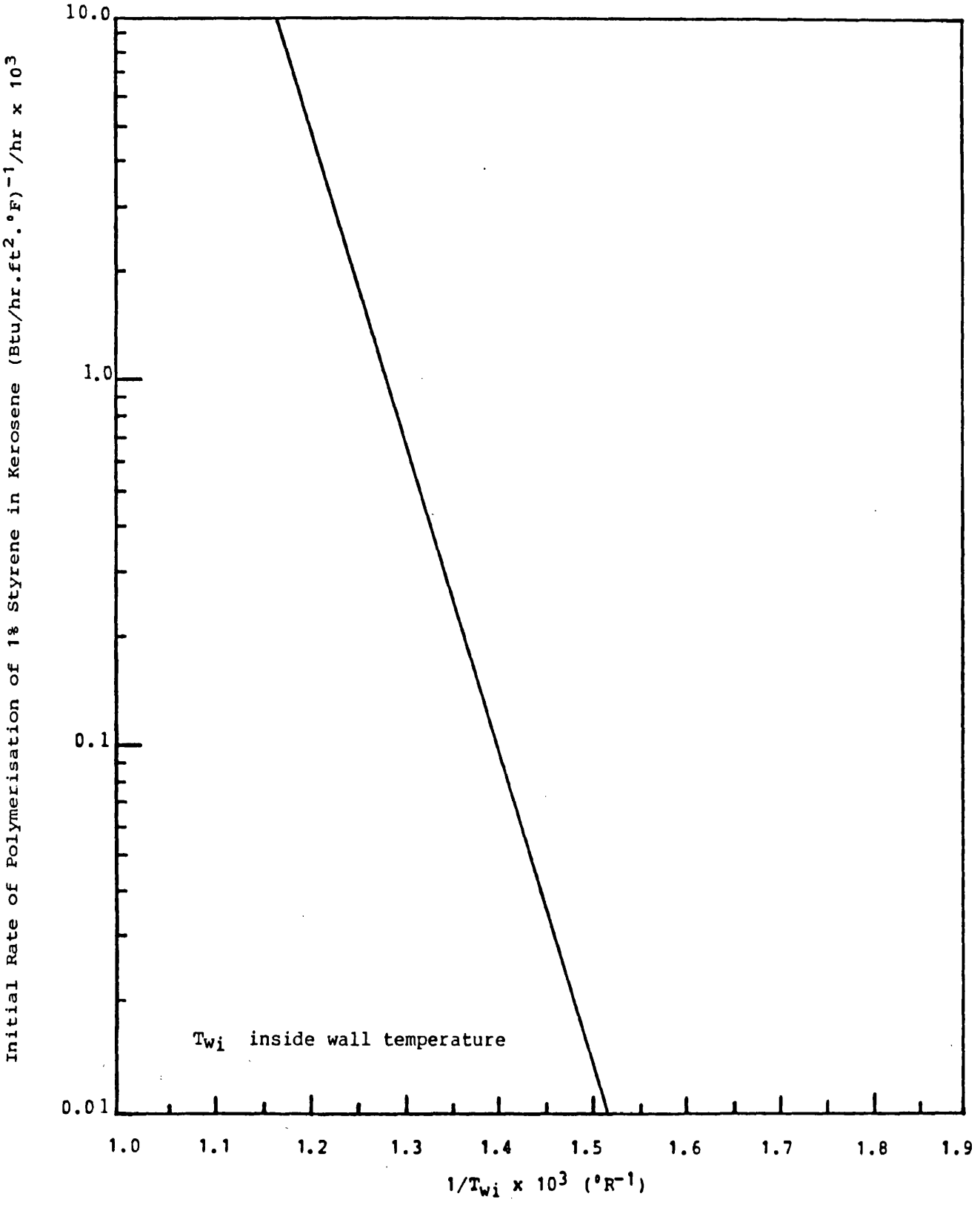

Figure 5.66 Variation of the Rate of Polymerisation of Styrene with the Reciprocal Absolute Temperature.

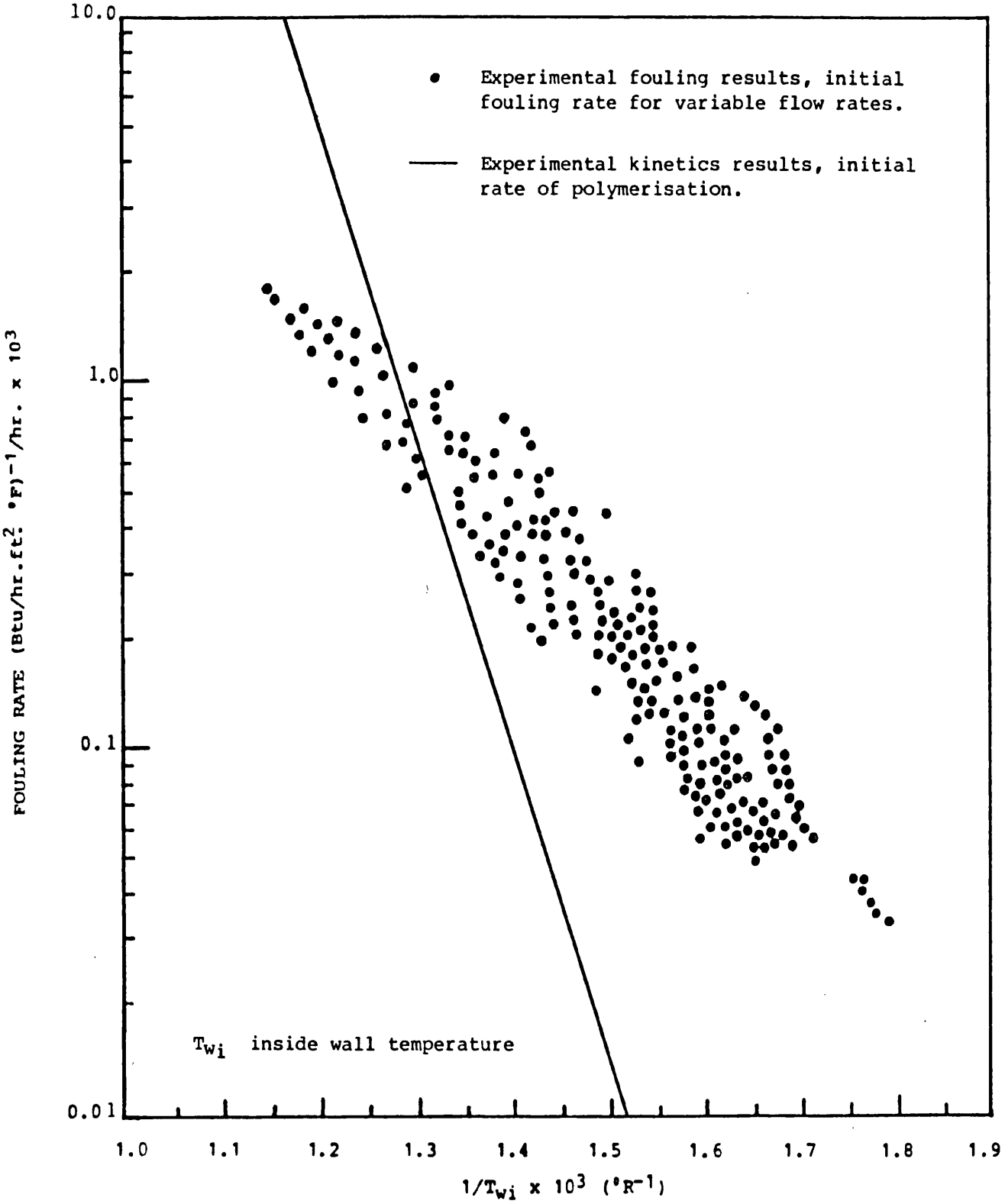

Figure 5.67 Logarithm initial fouling rate against reciprocal absolute temperature

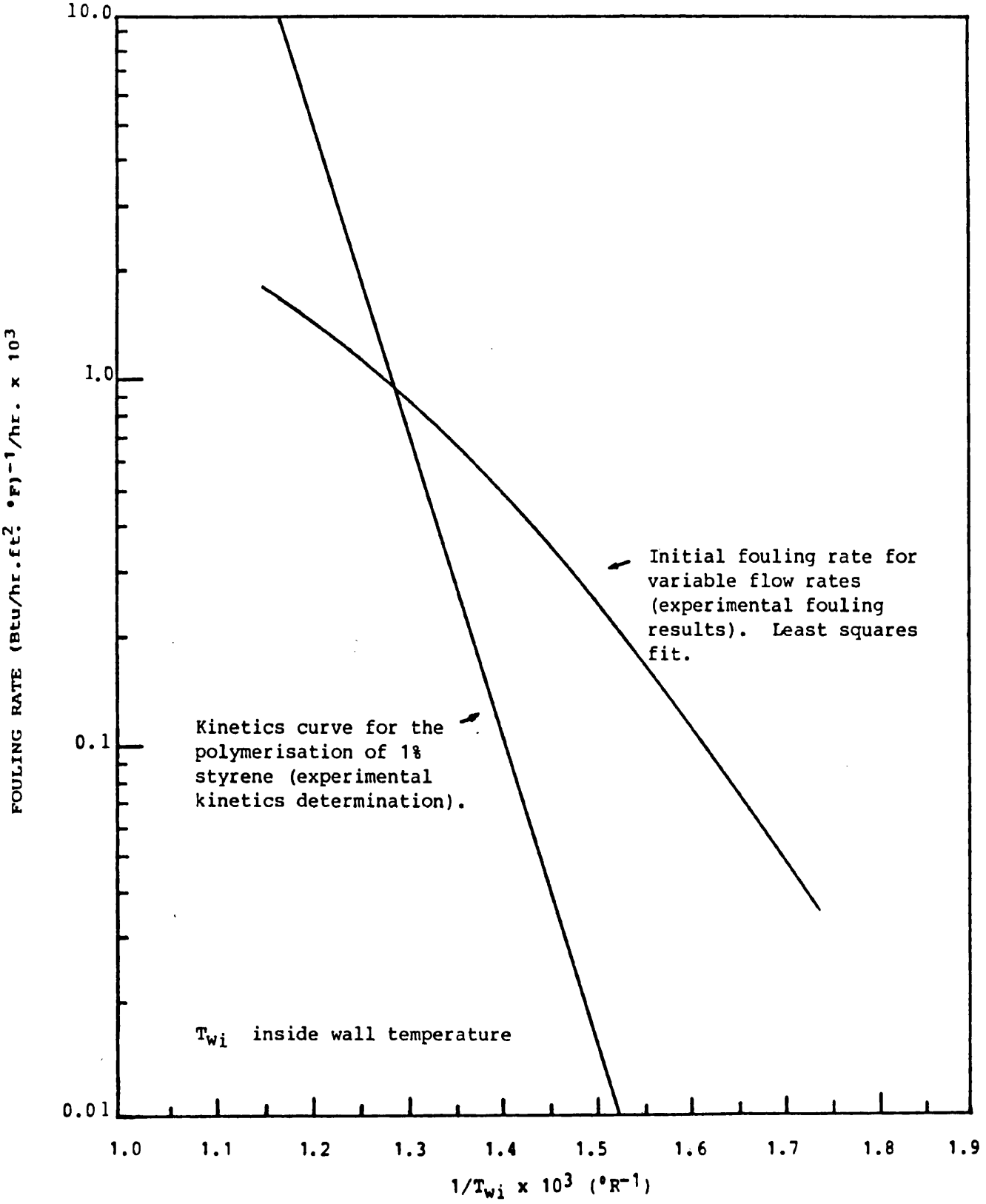

Figure 5.68 Initial Rate of Fouling as a Function of the Reciprocal Absolute Temperature. Styrene/Kerosene System.

The rate of increase in the thickness of the polystyrene layer formed is then

$$\frac{yC_b d}{400\rho_f} \quad \text{(ft polystyrene/hr)} \tag{124}$$

in which

ρ_f - density of polystyrene deposit (lb polystyrene/ft^3 polystyrene)

The initial fouling rate is then given by

$$\dot{R}_f\ (0) = \frac{yC_b d}{400\rho_f Tk_f} \quad (\text{Btu/hr.ft}^2.^\circ\text{F})^{-1}/\text{hr} \tag{125}$$

where

Tk_f - thermal conductivity of the polystyrene deposit (Btu/hr.ft.$^\circ$F)

For polystyrene

ρ_f = 65.55 [69] lb/ft^3

Tk_f = 0.078 Btu/hr.ft.$^\circ$F (See Appendix H)

5.3.1 Comparison of the Kinetics to the Initial Fouling Rate

Figures 5.67 and 5.68 show a comparison between the experimental kinetics of the initial rate of polymerisation of 1% styrene in kerosene and the initial fouling rate at various flow rates and temperatures. At lower temperatures the initial fouling rate is slightly higher than that which would be expected from kinetics control. At higher temperatures however the initial fouling rate becomes progressively lower than the initial rate of polymerisation of 1% styrene indicating an additional resistance to the fouling process, which is a function of mass flow rate.

5.3.2 Effect of 1% Styrene in Kerosene on the Initial Boiling Point of Kerosene

Several experiments were conducted to determine the boiling point of a styrene-kerosene solution at various compositions to study the effect of styrene on the boiling point of kerosene (Appendix K). From the results of these experiments Figure 5.69 was constructed. It was noticed that the existence of styrene in kerosene at 1% concentration had a negligible effect on the initial boiling point of kerosene. All the fouling runs were therefore conducted in the all liquid region.

5.4 Modelling of Results

Figure 5.67 shows that the polymerisation of styrene on the inside walls of the furnace tube, through which a 1% styrene in kerosene solution is flowing, is not controlled merely by the kinetics of the chemical reaction taking place effectively at the surface. It is believed that the mass transfer of reactive species can have an additional effect.

Indeed it is clear from the different forms of the temperature-velocity dependence of the initial fouling rates (Figure 5.51) that the fouling by polymerisation of styrene in kerosene is a complex kinetic and hydrodynamic process. Since the equations of Crittenden and Kolaczkowski[59] (Section 2.2.5.1.8) can predict curves similar to those shown in Figure 5.51, an attempt is made here to fit an extension of their model to the experimental data.

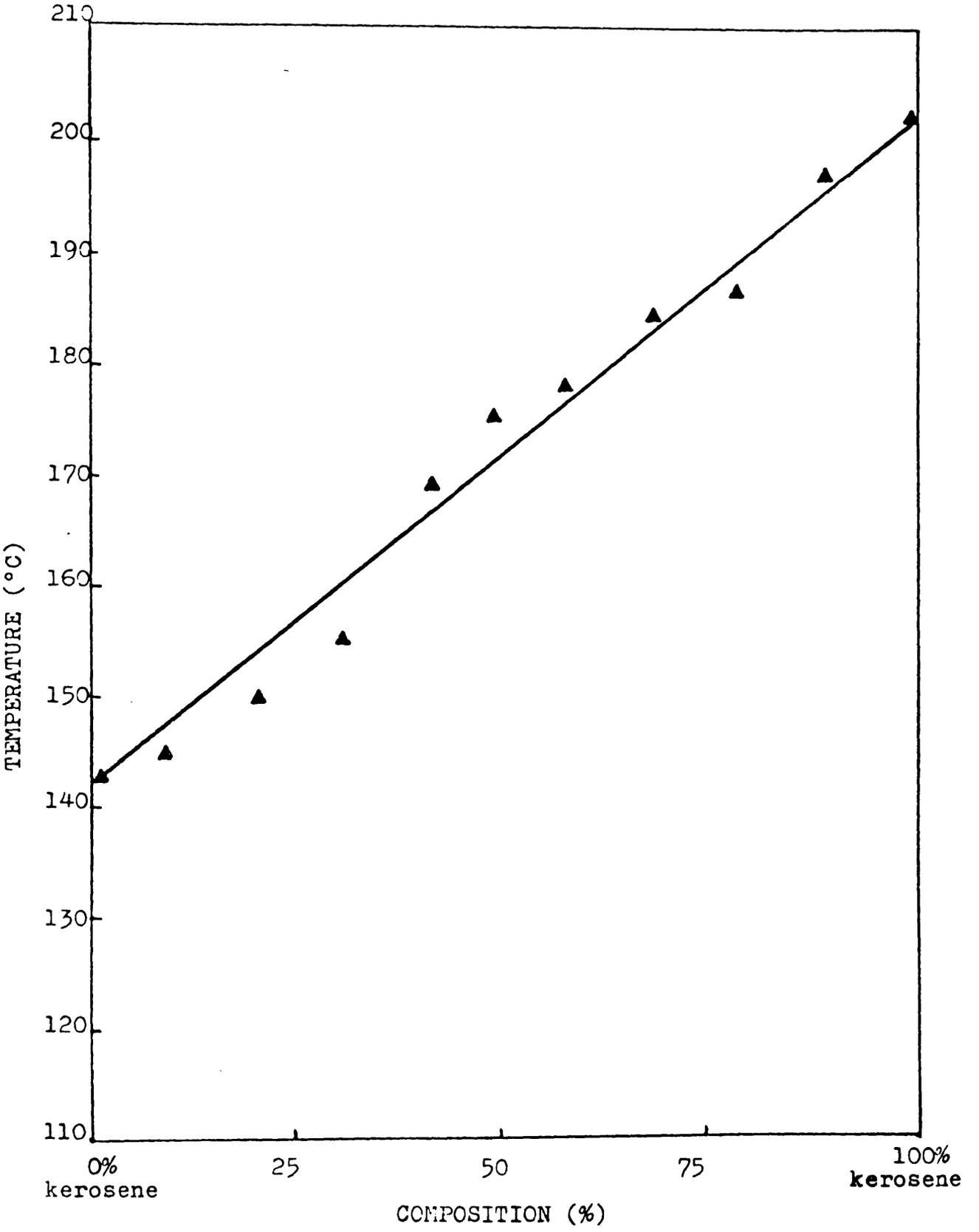

Figure 5.69 Temperature-Composition diagram of Styrene/ Kerosene mixture

5.4.1 Extension of the Crittenden and Kolaczkowski Model to a Reaction Whose Order is Not Equal to One

Assumptions

(1) A concentration gradient (driving force) exists between the fluid bulk and the surface when the reaction consumes the precursors at the fluid-surface interface.

(2) The rate of precursors consumed in the reaction at the surface is equal to the rate of precursors transported from the bulk to the fluid-surface interface or the fluid-deposit interface.

(3) A flux of precursors occurs from the bulk fluid towards the wall. This flux may be written in terms of a mass transfer coefficient and concentration driving force.

(4) Transport of foulant back to the fluid bulk may be by back diffusion and/or fluid shear.

(5) The concentration of foulant in the bulk fluid is zero.

(6) The concentration of precursors in the bulk fluid does not change with time.

(7) The reaction is of n^{th} order.

The rate of fouling was described by Crittenden and Kolaczkowski[58,59]

$$\dot{R}_f(\theta) = \frac{1}{\rho_f T k_f} \left(\begin{array}{l} \text{transport and reaction of} \\ \text{precursors at the transfer} \\ \text{surface to create foulant} \end{array} - \begin{array}{l} \text{diffusion of foulant} \\ \text{back to bulk fluid} \end{array} \right) \quad (126)$$

in which

$\dot{R}_f(\theta)$ is in $(\text{Btu/hr. ft}^2.^\circ\text{F})^{-1}/\text{hr}$

ρ_f = density of foulant (lb/ft^3)

Tk_f = thermal conductivity of foulant (Btu/hr.ft.$^\circ$F)

The rate of reaction at the fluid-surface (fluid-deposit) interface in its most simple form is given by

$$r = k\, C_{p_i}^{n} \tag{127}$$

where

k = rate constant

Cp_i = concentration of precursors at the interface

n = order of the reaction

The rate constant for elementary kinetics can be described by an Arrhenius equation, i.e.,

$$k = A \exp(-E/RT_{wi}) \tag{128}$$

where

A = frequency factor

E = activation energy of the reaction

R = universal gas constant

T_{wi} = inside wall or interfacial temperature

The net initial deposition rate may be described by the difference between the mass flux of precursors approaching the wall and the mass flux of foulant moving away from the wall towards the fluid bulk,i.e.

$$\dot{R}_f(0) = \frac{1}{\rho_f TK_f} (Np - N_f) \tag{129}$$

in which

Np = mass flux of precursors transported to the wall

N_f = mass flux of foulant from the interface to the bulk fluid

The mass fluxes are described by mass transfer coefficients and concentration driving forces,

Thus

$$Np = Kp\ (Cp_b - Cp_i) \tag{130}$$

and

$$N_f = K_f \ (C_{fb} - C_{fi}) \tag{131}$$

in which

K = mass transfer coefficient

p = precursors

f = foulant

C = concentration

b = bulk

i = interface

The concentration of foulant in the bulk fluid is assumed zero, i.e.

$$C_{fb} = 0 \tag{132}$$

Back diffusion of foulant to the fluid bulk may occur as some of the foulant polymer may be dissolved in its monomer and carried by the bulk fluid. The concentration of foulant at the interface, C_{fi} is then equal to the solubility of foulant in the feedstock at local conditions.

Therefore, the mass flux of foulant becomes

$$N_f = K_f \ C_{fi} \tag{133}$$

At pseudo steady state conditions the rate of reaction at the wall must be balanced by the rate of transport of precursors towards the wall, hence

$$r \approx Np \tag{134}$$

Substitute equation (134) in (127), hence

$$Np = k \ C_{p_i}^{n} \tag{135}$$

which gives

$$C_{pi} = [\frac{Np}{k}]^{1/n} \tag{136}$$

Substitute the value of Cp_i in equation (130), therefore

$$Np = Kp\ [C_{pb} - (\frac{Np}{k})^{1/n}] \tag{137}$$

rearrange,

$$C_{pb} = \frac{Np}{Kp} + [\frac{Np}{k}]^{1/n} \tag{138}$$

The value of Np cannot be determined algebraicly when n is not equal to one, therefore a numerical solution of equation (138) is required.

The Colburn-Chilton analogy may be used for non particulate systems to estimate the mass transfer coefficient as a function of velocity[40]

$$Kp,_f = \frac{f}{2} \cdot U_{av} \cdot Sc_{p,f}^{-0.67} \tag{139}$$

in which

f = friction factor

U_{av} = average velocity of the fluid

$Sc_{p,f}$ = Schmidt number pertaining to precursors or foulant

f is given by[151,163],

$$f = \lambda \cdot Re^{-0.2} \qquad 5x10^3 < Re < 2x10^5 \tag{140}$$

in which

λ = a function of roughness

Re = Reynolds number

The average fluid velocity is given by,

$$U_{av} = \frac{Re \cdot \mu}{\rho(d-2x)} \tag{141}$$

in which

μ = viscosity of fluid

ρ = density of fluid

d = inside diameter of tube

x = thickness of deposit

The dimensionless group, $Sc_{p,f}$ is given by

$$Sc_{p,f} = \frac{\mu}{\rho D_{p,f}} \tag{142}$$

where

$D_{p,f}$ = diffusion coefficient of precursors or foulant in the bulk fluid

The mass transfer coefficient for the precursors or foulant then becomes,

$$K_{p,f} = \frac{\lambda Re^{-0.2}}{2} \cdot \frac{Re.\mu}{\rho(d-2x)} \cdot Sc_{p,f}^{-0.67} \qquad (143)$$

$$= \frac{\lambda \cdot \mu \cdot Re^{0.8}}{2 \cdot \rho(d-2x)} \cdot Sc_{p,f}^{-0.67}$$

$$= \frac{\lambda \cdot \mu \cdot \left(\frac{4G}{(d-2x)}\right)^{0.8} \cdot Sc_{p,f}^{-0.67}}{2\rho(d-2x)}$$

then $K_{p,f}$ is given by

$$K_{p,f} = \frac{0.607\lambda\mu^{0.2}G^{0.8}Sc_{p,f}^{-0.67}}{\rho\,(d-2x)^{1.8}} \qquad (144)$$

Substituting equations (133) and (144) into equation (129) gives

$$\dot{R}_f(0) = \frac{1}{\rho_f T K_f}\left(Np - \frac{0.607\lambda\mu^{0.2}G^{0.8}}{\rho(d-2x)^{1.8} \cdot Sc_f^{0.67}} \cdot C_{fi}\right) \qquad (145)$$

The value of the mass flux of precursors transported to the wall, N_p, may be numerically determined from equation (138) by substituting equations (128) and (144) and the values of C_{pb} and n,

$$C_{pb} = Np.\frac{\rho(d-2x)^{1.8}}{0.607\lambda\mu^{0.2}G^{0.8}Sc_p^{-0.67}} + \left(\frac{Np}{A\exp(-E/RT_{wi})}\right)^{1/n} \qquad (146)$$

5.4.2 Testing the Model with Experimental Results

The model is tested by comparing the initial rates of fouling with the experimental data. All experiments were carried out at constant mass flow rate and constant heat flux with time. Therefore, setting the foulant thickness x=o, in equations (145) and (146) at $\theta=0$, gives

$$\dot{R}_f(0) = \frac{1}{\rho_f T K_f}\left(Np - \frac{0.607\lambda\mu^{0.2}G^{0.8}Cf_i}{\rho d^{1.8} Sc_f^{0.67}}\right) \qquad (147)$$

and Np may be numerically determined from,

$$C_{pb} = Np\,\frac{\rho d^{1.8}}{0.607\lambda\mu^{0.2}G^{0.8}Sc_p^{-0.67}} + \left(\frac{Np}{A\exp(E/RT_{wi})}\right)^{1/n} \qquad (148)$$

n = order of the reaction

The parameters of equations (147) and (148) are to be evaluated or estimated whenever they cannot be obtained either experimentally or from the literature. The physical properties are determined as a function of temperature. Cf_i is the solubility of the foulant in the kerosene and therefore will be a function of temperature. Equation (147) may suggest that at high values of G, $\dot{R}_f(0)$ may be negative. This is not actually true, since the function of roughness, λ is not actually constant over a range of flow rates, and as $G \to \infty$, λ decreases and tends to zero (i.e. $\lambda \to 0$).

For the purpose of the analysis, and over the range of flow rates, λ was estimated from equation (140) and the Moody diagram (See Section 5.1.2). Its value will be taken as constant and equal to 5.7×10^{-2} for $4.5\times10^{3} < Re < 19\times10^{3}$. The values for the Arrhenius equation were evaluated, and

E = 33.85 Btu/mol (See Section 5.3)

R = 0.0044 Btu/mol°R

A = 40.5 $(Btu/hr.ft^2.{}^\circ F)^{-1}/hr$ (See Section 5.3.1)

For an isotherm, equation (148) may rearrange to

$$C_{pb} = \frac{\rho d^{1.8} Scp^{0.67}}{0.607\lambda\mu^{0.2}G^{0.8}}\,Np + \left(\frac{Np}{40.5\exp\left(\frac{-33.85}{0.0044T_{wi}}\right)}\right)^{0.4} \qquad (149)$$

for n = 5/2 . (See Section 5.3)

The values of the inside diameter of tube (See Section

4.1.1) and λ are known for all conditions, therefore

$$C_{pb} = \frac{0.066^{1.8}\ \rho\ Scp^{0.67}}{0.607 \times 0.057\ \mu^{0.2} G^{0.8}}\ Np + \left(\frac{Np}{40.5\ \exp\left(\frac{-7693.2}{T_{wi}}\right)}\right)^{0.4} \qquad (150)$$

The concentration of styrene in kerosene was maintained at 1% (C_{pb}=0.564 lb styrene per ft^3 of kerosene) for the duration of each experiment (See Section 4.1.4), hence

$$0.564 = \frac{0.217\ \rho\ Scp^{0.67}}{\mu^{0.2} G^{0.8}}\ Np + \text{constant}\ (Np)^{0.4} \qquad (151)$$

The value of Np may be numerically iterated from equation (151) for various flow rates once the Schmidt number has been estimated.

The molecular diffusivity of the precursors or the foulant can be estimated from the Wilke-Chang relationship[18,163]

$$D_{p,f} = D_{AB} = \frac{7.4 \times 10^{-8} (\Phi M_B)^{0.5} \times T}{\mu_B \times V_A^{0.6}} \qquad (152)$$

where

D = molecular diffusivity (ft^2/hr)

p = precursors

f = foulant

A = solute (styrene or polystyrene)

B = solvent (kerosene)

Φ = association factor (equal to one for styrene/kerosene system)

M = molecular weight

T = temperature

μ = viscosity

V = molar volume @ normal boiling point (ft^3/lb-mol)

Table 3-306 of reference (163) gives the values of V.

For styrene, C_8H_8; $V_{styrene}$ = 148 CC/gm-mol

For polystyrene[69],

$$\left[\begin{array}{l} CH\text{-}CH_2 \\ | \\ C_6H_5 \end{array}\right]_n \quad n \simeq 500 \rightarrow 1000$$

$V_{polystyrene} = 148 \times 10^3$ CC/gm-mol

The Molecular Weight of kerosene was estimated[155] to be approximately 142 gm/mol. Equation (152) may be used with the understanding that there could be deviations of up to 25%[163].

Crittenden suggested[59] that diffusion of foulant back into the bulk fluid may be important when the deposit contains relatively mobile species, i.e. when Sc_f is small. The concentration of the foulant at the interface, C_{f_i} (the solubility of such species in the bulk fluid) is likely to reduce as the molecular weight increases, but increase as the temperature rises. However, higher interfacial temperatures generally tend to further degradation to form higher molecular weight deposits.

The concentration of the foulant,for the initial fouling rate,in the bulk fluid is assumed negligible, i.e. $C_{f_b} = 0$. The value of C_{f_i} may be estimated from

$$\frac{\partial C_{f_i}}{\partial t} = D_f \frac{\partial^2 C_{f_i}}{\partial y^2} \qquad (153)$$

where

∂t = time interval

y = radial direction of the foulant transport by back diffusion

Equation (153) is applicable for a time dependent process. But since quasi-steady state conditions are assumed, hence

$$\frac{\partial C_{f_i}}{\partial t} \rightarrow 0 \tag{154}$$

i.e. C_{f_i} is constant for a given temperature.

therefore

$$D_f \frac{\partial^2 C_{f_i}}{\partial y^2} = 0 \tag{155}$$

i.e.

$$\frac{\partial^2 C_{f_i}}{\partial y^2} = 0 \tag{156}$$

then,

$$C_{f_i} = Ay + B \tag{157}$$

where A and B are constants. The value of C_{f_i} is to be evaluated at y = 0, i.e. C_{f_i} = B. For the purpose of this prediction C_{f_i} may be taken as an adjustable parameter to match up predicted and experimental curves.

The physical and other properties required for equations (147) and (148) have been evaluated and are shown in Table 5.5. These values are used to evaluate the initial fouling rates at the various flow rates and inside wall temperatures. The predicted and experimental results are compared in Figure 5.70.

It is noticed that the model predictions follow the same trend found experimentally. The predicted values were a little lower than the experimental ones.

Good agreement between the postulated model and the experimental results was obtained over the limited range for which data were available. It is believed from these results that mass transfer of species was of a magnitude comparable with

Table 5.5 Variable Properties Used in the Model Equations

Temperature (°R)	ρ * (lb/ft^3)	μ * (lb/ft.hr.)	$D_p x 10^4$ (ft^2/hr)	$Sc_p x 10^{-2}$	$D_f x 10^6$ (ft^2/hr)	$Sc_f x 10^{-3}$	$C_{f_i} x 10^8$ (lb/ft^3)
909	38.4	0.57	3.67	0.41	5.8	2.55	9.57
870	39.7	0.69	2.88	0.60	4.7	3.73	7.69
833	40.9	0.83	2.30	0.88	3.6	5.58	5.94
801	41.9	0.98	1.88	1.24	3.0	7.85	4.95
769	43.0	1.15	1.54	1.74	2.4	10.97	3.96
714	44.4	1.51	1.09	3.14	1.7	19.78	2.81
667	45.6	1.91	0.80	5.22	1.3	32.98	2.15
625	46.7	2.36	0.61	8.31	1.0	52.42	1.65
588	47.7	2.78	0.49	12.01	0.8	75.80	1.32
556	48.5	3.95	0.32	25.23	0.5	159.21	0.83

*See Appendix E

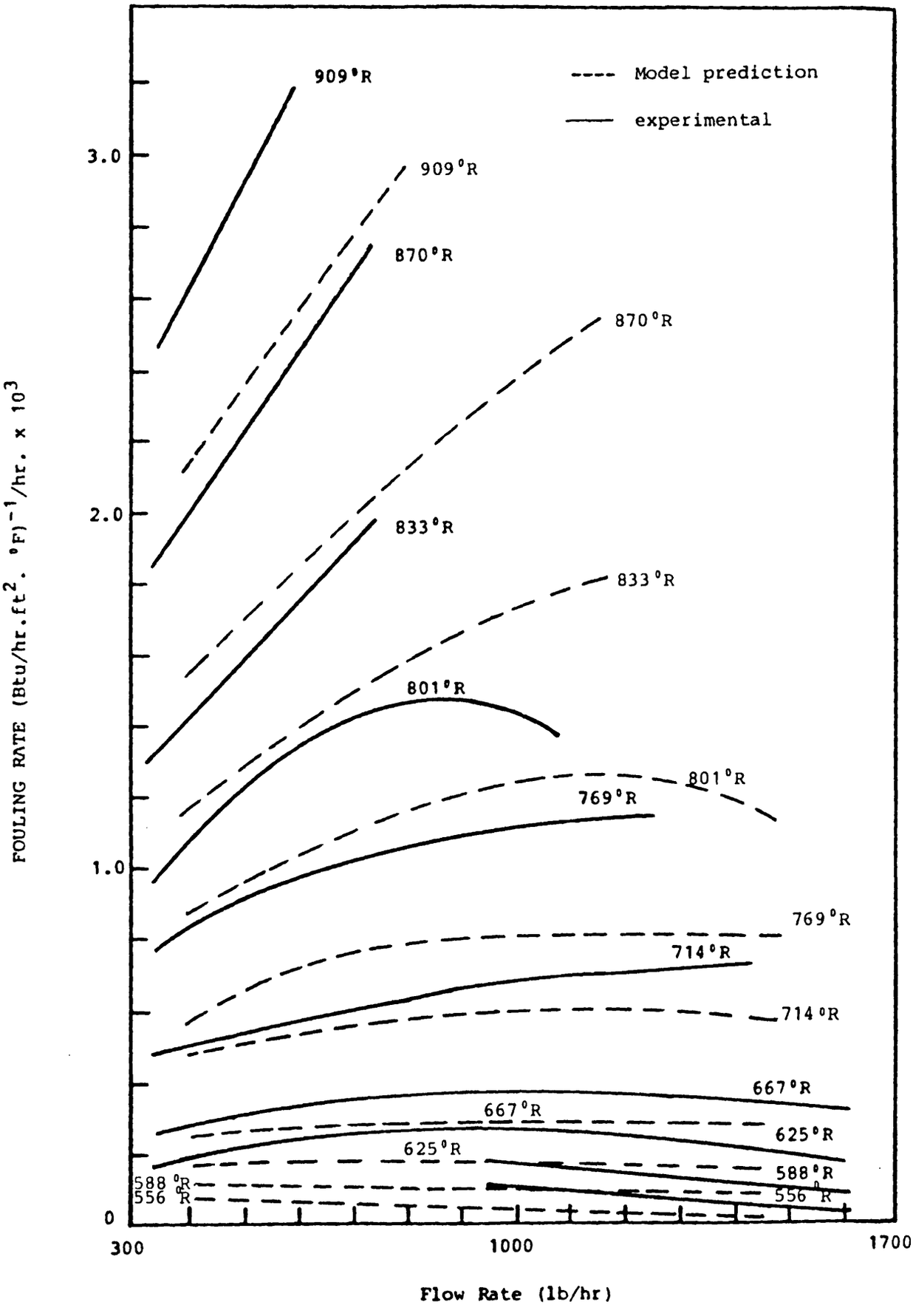

Figure 5.70 Variation of the Initial Fouling Rate Against Flow Rate.

the kinetics of the deposition process. This lends support to the mathematical treatment of Chemical Reaction Fouling as a combination of the two processes namely kinetics and diffusion.

6. Discussion

The literature on fouling shows that deposition from hydrocarbon streams is due mainly to free radical chain reaction processes involving autoxidation-polymerisation, oxidative polymerisation and furthur oxidative dehydrogenation and degradation reactions. The control of process variables can help in controlling fouling, for example, by minimising surface temperatures and pressurizing the system to avoid vaporization of the feed stock where possible. Also, provided that deposition rates are not controlled by mass transfer, the use of higher velocities may be effective in removing deposits.

In this study all experiments were carried out at constant flow rate, constant heat flux and essentially a constant styrene in kerosene concentration.

Over the temperature range 556 - 558°R, the initial fouling rate decreased with increasing flow rate in the range 900 - 1700 lb/hr. Between 625 - 714°R the initial fouling rate showed little variation with flow rate in the range 500 - 1600 lb/hr. For the range of temperature 769 - 801°R the initial fouling rate varied from an increase to a decrease with increasing flow rate in the range 336 - 1100 lb/hr. Finally in the temperature range 833 - 909°R the initial fouling rate increased with increasing flow rate in the range 336 - 800 lb/hr.

This strong but complex dependency of the initial fouling rate on flow rate suggests that mass transfer effects are important in controlling the overall rate of the fouling process. A comparison of the experimental results with an extended mass transfer and kinetics fouling model (Figure 5.70)

suggests that the mass transfer of precursors to the surface and the mass transfer of foulant away from the surface could be important at certain temperatures.

The plots of the initial fouling rate against the reciprocal of the temperature confirm that wall temperature is an important factor in the rate of the deposition process. Generally, an increased temperature increased the initial rate of fouling; this is due to the increase in the chemical reaction rate at the transfer surface.

The solubility of polystyrene, resulting from the polymerisation of styrene at the heat transfer surface, in kerosene was tested and found to be negligible. On the other hand styrene was completely miscible with kerosene and polystyrene was found to be soluble in styrene. The solubility parameter of polystyrene in styrene is negative[69] implying high solubility

$$|\delta_p - \delta_s| = 9.1 - 9.3$$

in which

δ_p - solubility parameter of polystyrene

δ_s - solubility parameter of styrene

This leads to the suggestion that some of the polymer formed may have been dissolved in the 1% styrene/kerosene bulk. Some polymer, recovered downstream of the test section after the cooler on the line filter may have been present in the bulk fluid for this reason; however, some polymerisation may also have taken place in the bulk and the products deposited after cooling.

The fouling resistances measured were in the range of 0.00035 - 0.03 (Btu/hr. ft^2. $^oF)^{-1}$ which are relatively high compared to values found in the literature. It is believed that

such high values are created by the relatively high concentration (1%) of the foulant precursor in the fluid bulk and by the low thermal conductivity of the deposit itself. Normally, precursor concentrations are present in the bulk at trace level concentrations.

7. Conclusions

1. The experimental results show that for a given flow rate the initial fouling rate increases with increasing temperature, the data being well correlated by Arrhenius-type expressions. However, the initial fouling rate increases with increasing flow rate at relatively high surface temperatures and decreases with increasing flow rate at relatively low surface temperatures. At intermediate surface temperatures the initial fouling rate exhibits a maximum with respect to flow rate.

2. The Crittenden and Kolaczkowski mass transfer and kinetics model was extended to account for the experimental results. The initial fouling rate was given by

$$\left.\frac{dR_f}{d\Theta}\right|_{\Theta = 0} = \Phi_p(\text{flux of precursors diffused and reacted}) - \Phi_f(\text{flux of foulant diffused to the bulk fluid})$$

The model includes mass transfer and kinetic mechanisms of fouling and therefore incorporates the important design parameters such as temperature, flow rate, tube diameter and fluid properties. Relatively good agreement was found between the predicted and experimental values.

3. The calculated activation energy for the deposition process was in the range of 10 to 17 kcal/mol for the initial fouling rate. An activation energy of 8.5 kcal/mol was estimated for the kinetics of styrene polymerisation.

4. Experimental single-phase heat transfer coefficients were a factor of 1.2 higher than those predicted by the Dittus-Boelter equation.

8. Recommendations for Future Study

It is recommended that this study be extended in the following ways:

(1) Increase the duration of runs to determine whether the fouling transients remain linear or become asymptotic. A means of keeping the styrene concentration constant will be required.

(2) Vary the styrene concentration in the bulk and correlate results with the mass transfer and kinetic model predictions.

(3) Vary the tube diameter and roughness and correlate results with the mass transfer and kinetic model predictions.

(4) Vaporize the feedstock with and without the added styrene under conditions of forced turbulent convective flow.

NOMENCLATURE

Most of the symbols have been defined in the text and therefore only the fundamental symbols are listed.

A	surface area
A	frequency factor
C	concentration
C_p	heat capacity
d	tube diameter
D	diffusion coefficient
E	activation energy
f	friction factor
G	mass flow rate
Gz	Graetz number
Gr	Grashof number
h	film heat transfer coefficient
H	enthalpy
I	ionic strength
K	thermal conductivity
K_p	mass transfer coefficient
k	reaction rate constant
L	length of section or tube
m	mass of deposit
N	mass flux
n	reaction order
Pr	Prandtl number
P	pressure
Q	quantity of heat
R	resistance

R universal gas constant

Re Reynolds number

R_f fouling resistance

r reaction rate

S sticking probability

Sc Schmidt number

St Stanton number

T temperature

t time

U overall heat transfer coefficient

u average fluid velocity

w flowrate

x film deposit thickness

z charge

GREEK

Δ difference

θ time

β approach to the asymptote

Φ flux

ρ density

μ viscosity

δ film thickness

τ shear stress

λ function of roughness

ψ function of deposit structure

SUBSCRIPTS

b	bulk
c	coke
d	deposition
f	foulant
i	inside
i	interface
m	mean
o	outside
p	precursor
r	removal
s	surface
w	wall
∞	infinity

Conversion Factors to S.I. Units

To convert from:	To	Multiply by
Length		
ft.	m	0·3048
in.	m	$2{\cdot}54.10^{-2}$
Density		
lb/ft^3	Kg/m^3	16·0185
Force		
lb force	N	4·44822
Viscosity		
cp	$N\ s/m^2$	0·001
Enthalpy		
Btu/lb	J/Kg	2326
Heat transfer coefficient		
$Btu/hr\ ft^2\ ^oF$	$J/m^2\ s\ K$	5·67826
Thermal conductivity		
$Btu/hr\ ft^2\ ^oF/ft$	$J\ m/m^2\ s\ K$	1·73073
Thermal resistance		
$(Btu/hr\ ft^2\ ^oF)^{-1}$	$(J/m^2\ s\ K)^{-1}$	0·1761
Heat flux		
$Btu/hr\ ft^2$	$J/m^2\ s$	3·15459
Temperature		
^oF	K	$t_K = (t_F + 459{\cdot}67)/1{\cdot}8$

List of References

1. Allen R.W., Eckert E.R.G. J. Heat. Transfer 86 301 (1964)

2. Anand, L.C., et al, J poly sci, 5, 665 (1967)

3. Angelini C.L., Hopper M., van Rutten F. Euratom Rpt. No. EUR 4235f. (1969)

4. Anon Brit. Chem. Eng. 2 674 (1957)

5. Anon Mater. Prot. 4 70 (1965)

6. Apelblat, A., mass transfer with chemical reaction of the first order, analytic solution. The chemical Engrg. J., No. 2, (1980)

7. API, report of Panel on fouling in process streams, May (1963)

8. API, technical data book, petroleum refining, American petroleum Institute, division of refining (1970)

9. Ashely M.J. Paper 8 Symposium 'Less Common Methods of Heat Transfer' Birmingham (April 1973)

10. Atkins, G.T., Petro/Chem, Eng., 34, (4), 20-25, (1962)

11. Bachman, K.C., heat transfer unit evaluates performance of jet fuels for supersonic aircraft. National aeronautic and space engineering and manufacturing meeting, Los Angeles, Oct. (1965)

12. Baker, L.H., Engineering, 443 (Oct. 1927)

13. Bancroft, A.R., Atomic Energy of Canada ltd., CRCE-1142, Chalk River, Ontario, Mar. (1963)

14. Bartlett, J.W., BNWL-676, UC-80, reactor technology, Richland, Washington

15. Baysal B., and Tobolsky A.V., rates of initiation in vinyl polymerisation, J. poly sci, 8, 529 (1952)

16. Beal S.K. Nuc, Sci. Eng. 40 1 (1970)

17. Benson, P.R. & Martini, W.R. "Measuring the film forming potentials of liquids" Ind. & Eng. Chem. Prod. Res. Dev. 1 No. 1, 7-10, March (1962)

18. Bird, R.B., Stewart, W.E. and Lightfoot, E.N., "Transport Phenomena", John Wiley & Sons, New York, (1960)

19. Boelter, Cherry, Johnson, Martinelli, heat transfer notes (1965)

20. Bott, T.R. "Understand fouling and keep down heat exchanger cost" Process Engineering, 76-81, Nov. (1975)

21. Bott, T.R. and Walker, R.A. (1971). Fouling in heat transfer equipment. The Chemical Engineer, No. 255, pp. 391-395, Nov.

22. Braun, R., Materials Performance, 16, (11), 35-41, (1977)

23. Braun, R. and Hausler, R.H., "Contribution to the understanding of fouling phenomena in the petroleum industry", Paper No. 76-CSME/CSChE-23, 16th National Heat Transfer Conference, St. Louis, Mo. August (1976)

24. Bridgewater, J., crystallisation fouling-a review of fundamentals. Fouling Science or Art? A conf. at the University of Surry, Guildford, England, Mar. (1979)

25. British Standard, B.S. 4937 : Part 4 : 1973

26. Brooks, B.T. The chemistry of gasolines particularly with respect to gum formation and discoloration. Ind. Engng. Chem. 1926. 18, 1198 - 1200

27. Butler, R.C. and McCurdy, W.N., "Fouling rates and cleaning methods in refinery heat exchangers". Transactions of the ASME, 843-847, Oct. (1949)

28. Butterworth, D., unresolved problems in heat exchanger design. Interflow 80, the Institution of Chemical Engineers. Symposium series No. 60 England (1980)

29. Canapary, R.C., "How to control refinery fouling", The oil & gas journal, 114-118, Oct. 9, (1961)

30. Caplan, F. (1974). Nomograph determines design overall heat transfer coefficient. Heat. Pip. Air. Cond., Vol. 46, No. 5, pp. 67-68, May

31. Carberry, J.J., Chemical and catalytic reaction Engineering, McGraw-Hill, New York, N.Y. (1976)

32. Chantry, W.A. and Church, D.M. (1958). Design of high velocity forced circulation reboilers for fouling service. Chem. Engng. Prog., Vol. 54, No. 10, pp. 64-67

33. Charlesworth D.H., Atomic Engergy of Canada Ltd., Chalk River, Ontario, CRCE-1096 (April 1963)

34. Charlesworth D.H. Atomic Engergy of Canada Ltd. Rpt. No. AECL-1761 (1963)

35. Chen J.C., Ind. Eng. Chem. Process Design Development, 5, 322 (No. 3 1966)

36. Chen J., Maddock M.J. Hydrocarbon Process. 52 147 (No. 5 1973)

37. Chen, J. and Vogel, W. Fouling of transfer line exchanger in ethylene service. Proc. 74th National meeting of A.I. Ch. E., New Orleans, 1973, Paper No. 87B

38. Cherington, D.C., and Golan, L.P., fluidized bed combustion for industrial applications - process heaters, A.I. Ch. E., 17th National heat transfer conf., Salt Lake City, U.S.A. Aug. (1977)

39. Cherrington, D.C., et al, industrial application of fluidized bed combustion - single tube heat transfer studies. Proc. 5th Int. conf. on fluidized bed combustion. Washington D.C., U.S.A., Dec. (1977)

40. Chilton, T.H., and Colburn, A.P., Ind. Engng. Chem., 26, 1183-1187, (1934)

41. Cleaver, J.W., Yates, B., "A Sub-Layer Model for the Deposition of Particles from a Turbulent Flow", Chem. Eng. Sci., 30, 983-992, (1975)

42. Cleaver, J.W., and Yates, B., "Mechanism of Detachment of Colloidal Particles from a Flat Substrate in Turbulent Flow", Jnl. Colloid and Interface Science, Vol. 44, No. 3, pp. 464-473, (1973)

43. Cleaver, J.W., Yates, B., "The Effect of Re-entrainment on Particle Deposition", Chem. Eng. Sci., 31, 147-151, (1976)

44. Coggins, J.R. Blocking of naphtha vaporisers - report of gas industry survey. Report No. E.R. 117. The Gas Council, 1968

45. Colburn A.P. Trans, A.I. Ch. E. 26, 166 (1931)

46. Collier, J.G. Convective boiling and condensation. McGraw-Hill, London, 1972

47. Cooper, A.R., and Jeffreys, G.V., chemical kinetics, McGraw-Hill Book Co., London (1971)

48. Cooper, A., Suitor, J.W., and Usher, J.D. (1978). Cooling water fouling in plate heat exchangers. Proc. 6th Int. Heat Transfer Conf., Toronto, Canada, 7-11 August, Vol. 4, pp. 403-406

49. Corino, E.R., and Brodkey, S., J. Fluid Mech., 37, 1 (1969)

50. Cos, M. (1971). Excess exchanger surface for fouling. Nomograph Handbook, reprinted from Hydrocarbon Processing, Gulf Publishing Co.

51. Coulson, J.M., Richardson J.F., Chemical Engineering Vol. 1 Pergamon Press Ltd. (1966)

52. Couper, A.S., and Hamel, F.B. Process side antifoulants in petroleum refineries, NACE Publication T8170. 1970, pp. 29-33

53. Cousins, L.B., Pritchard, A.M., fouling resistance and the designer, Fouling Prevention Research Digest, 2, No. 3, Sept. (1980)

54. Cowan, J.C., and Weintritt, D.J. Water-formed scale deposits. Gulf, Houston, 1976, pp. 366-373

55. Crane Co., Flow of Fluids, technical paper No. 410, U.S.A. (1981)

56. Crawford, J.D. and Miller, R.M., "Refinery process fouling-effect of trace metals and remedial techniques" API, Refining, 28th Midyear Meeting, Philadelphia, Pa. May (1963)

57. Crittenden, B.D., and Khater, E.H. (1979). Economic fouling resistance selection. Int. Conf. Fouling of Heat Transfer Equipment, Troy, N.Y., 13-17 August

58. Crittenden, B.D., and Kolaczkowski, S.T. Energy savings through the accurate prediction of heat transfer fouling resistances. In Energy for Industry (Ed: P.W. O'Callaghan), Pergamon, Oxford, 1979, pp. 257-266

59. Crittenden, B.D., and Kolaczkowski, S.T. Mass transfer and chemical kinetics in hydrocarbon fouling. Paper presented at "Fouling - Science or Art?" conference, Guildford, 1979, pp. 169-187

60. Cross, P.H. (1979). Preventing fouling in plate heat exchangers. Chem. Engng., Vol. 86, No. 1, pp. 87-90, 1 January

61. Dahneke, B. diffusional deposition of particles. J Colloid and Interface. Sci., 48, No. 3, (1974)

62. Dainton, F.S., et al, the heats of polymerisation of some cyclic and ethylenic compounds, trans. Far. Soc., 56, (1960)

63. Davis, H.G., and Farrell, T.J. relative and absolute rates of decomposition of light paraffins under practical operating conditions. Ind. & Eng. Chem. Proc. Des. & Dev., 12, No. 2, (1973)

64. De Bliek, J.L., and Goossens, A.G. Optimize olefin cracking coils. Hydrocarb. Process., 1971. 50, (3), 76-80

65. Denbigh, K. Chemical reactor theory. Cambridge University Press, London, 1965, pp. 159-161

66. Dittus F.W., Boelter L.M.K. Univ. Calif. Pubs. Eng. 2, 443 (1930)

67. Dow's process safety guide, Chem. Eng. Prog., 62, 91 (No. 8 1966)

68. Emanuel, N.M., Denisov, E.V. and Maizus, Z.K. Liquid phase oxidation of hydrocarbons. Plenum, New York, 1967

69. Encyclopedia of polymer science and technology, ed. H.F. Mark et al, 13, John Wiley & Sons, London (1970)

70. Engineering Sciences Data Unit Item No. 66027 (1968)

71. Engineering Sciences Data Unit Item No. 67016 (1967)

72. Epstein, N. (1978). Fouling in heat exchangers. Proc. 6th Int. Heat Transfer Conf., Toronto, Canada, 7-11 August, Vol. 6, pp. 235-253

73. Epstein, N. (1979). Fouling: technical aspects. Int. Conf. Fouling of Heat Transfer Equipment, Troy, N.Y., 13-17 August

74. Fabuss, B.M., Duncan, D.A., Smith, J.O. and Satterfield, C.N. Effect of organosulfur compounds on the rate of thermal decomposition of selected saturated hydrocarbons. Ind. Engng. Chem., Proc. Des. and Dev. 1965. 4, 117-122

75. Fabuss B.M., Kafesjian R., Smith J.O., Satterfield C.N., Ind. Eng. Chem. Proc. Des. Dev., 3, 248 (No. 3 1964)

76. Fage, A. and Townsend, H.C.H., Proc. Roy. Soc., Ser. A135, 656, (1932)

77. Fernandez-Baujin, J.M. and Solomon, S.M., In Industrial and Laboratory Pyrolyses, (Eds: Albright, L.F. and Crynes, B.L.), ACS, Symp. Ser. No. 32, Washington, pp. 345-372 (1976)

78. Fischer, P., Suitor, J.W. and Ritter, R.B. (1975). Fouling measurement techniques. Chem. Engng. Prog., Vol. 71, No. 7, pp. 66-72, July

79. Fitzer, E., Mueller, K and Schaefer, W. The chemistry of the pyrolytic conversion of organic compounds to carbon. In Chemistry and Physics of Carbon, Vol. 7, (Ed: P.L. Walker Jr.), Marcel Dekker, New York, 1971, pp. 237-383

80. Foust A.S., Wenzel L.A., Clump C.W., Maus L., Anderson L.B., Principles of Unit Operations, John Wiley and Sons Inc. (1960)

81. Fraas A.P., Ozisik M.N., Heat Exchanger Design, John Wiley and Sons Inc., Chap. V (1965)

82. Frankenfeld, J.W., Taylor, W.F., deposit formation from deoxygenated hydrocarbons. 4. studies in pure compound systems. Ind. & Eng. Chem. Prod. Res. & Dev., 19, Mar. (1980)

83. Frazier, A.W., Huddle, J.G. and Power, W.R. New, fast approach to reduced preheat-exchanger fouling. Oil Gas J. 1965. 63, (18), 117-122

84. Friedlander S.K., Johstone H.F., Ind. Eng. Chem. 49, 1151 (1957)

85. Froment, G.F., Chemical reaction fouling due to petrochemical feedstocks. Int. Conf. on the fouling of heat transfer equipment. Troy, New York, Aug. (1979)

86. Gallant, R.W., physical properties of hydrocarbons 1 & 2, Gulf Pub. Co., Houston, Texas (1968)

87. Galloway T.R. Int. J.H.M.T. 16 443 (1973)

88. General Electric, corporate research & development, heat transfer and fluid flow, Data Book, N.Y. (1970)

89. Gillespie B.G., Materials Protection and Performance, 10, 21 (No. 8 1971)

90. Gilmour, C.H. (1965). No fooling - no fouling. Chem. Engnr. Prog., Vol. 61, No. 7, pp. 49-54, July

91. Goossens, A.G., Dente, M. and Ranzi, E. Improve steam cracker operation. Hydrocarb. Process. 1978. 57, (9), 227-236

92. Gudmundsson, J.S., "Fouling of Surfaces", Ph.D. Thesis, University of Birmingham, 1977.

93. Gutman, R.G., The Chemical Enger., July (1977)

94. Haluska, J.L., process fouling control by effective antifoulant selection. Corrosion/76. Houston, Mar. (1976)

95. Hasson D., Dech. Monogr. 47, 233 (1961)

96. Hasson D., Avriel N., Resnick W., Rozenman T., Windreich S., Ind. Eng. Chem. Fund. 7 59 (1968), Idem, Desalination 5, 107 (1968)

97. Hasson D., Zahais J., Ind. Eng. Chem. Fund. 9, 1 (1970)

98. Hatch, L.P., Weth, G.G., Office of Saline water R & D Prog. Rpt. No. 571 (1970)

99. Hausler, R.H. New test will show fouling tendency of process streams. Oil Gas J. 1973. 71, (23), 56-63

100. Hausler, R.H. and Thalmayer, C.E., "Fouling and corrosion in feed effluent exchangers: Discussion of a new test method" Preprint No. 06-75, API, Refining, 40th Midyear Meeting, Chicago, Illinois, May (1975)

101. Hazlett, R.N., and Hall, J.M., Chemical aspects of jet fuel thermal oxidation stability. Int. Conf. on the fouling of heat transfer equipment. Troy, New York, Aug. (1979)

102. Howard, J.A., and Ingold, K.U., Absolute rate constants for hydrocarbon autoxidation I. styrene, Can. J. Chem., 43, (1964)

103. Howard, J.A., and Ingold, K.U., The inhibited autoxidation of styrene, part IV. solvent effects. Can. J. Chem., 42, (1964)

104. Howard, R.N., and Simpson, W., the effect of different catalysts on the polymerisation of styrene, trans. Far. Soc., 47, (1951)

105. HTRI Film 'Visualization of Fouling' Heat Transfer Research Inc., Alhambra, California

106. Hui, A.W. and Hamielec, A.E., thermal polymerisation of styrene at high conversions and temperatures - an experimental study. J. appl. Polym. Sci., 16, (1972)

107. Hull, M. Kitchener, J.A., interaction of spherical colloidal particles with planar surfaces. Trans. Far. Soc., 65, (1969)

108. Hutton, J.F., The rheology of lubricants. John Wiley & Sons, N.Y. (1973)

109. Hydrocarbon Processing. hydrocracking handbook (1975)

110. Jackman, A.P. and Aris, R. Optimal control for pyrolytic reactors. Proc. 4th Euro. Symp. on Chemical Reaction Engineering. Pergamon, Oxford, 1971, pp. 411-419

111. Johnson C.E., Thompson W.H., U.S. Pat. No. 2, 908, 624 (Oct. 13 1959)

112. Johnson, C.R., Fink, D.F. and Nixon, A.C. Stability of aircraft turbine fuels. Ind. Engng. Chem. 1954. 46, 2166-2173

113. Johnstone, R.E. and Thring, M.W. Pilot plants, models, and scale-up methods in chemical engineering. McGraw-Hill, New York, 1957

114. Kolaczkowski, S., Ph.D. Thesis, University of Bath, England (1977)

115. Kern, D.Q., Seaton, R.E., "A Theoretical Analysis of Thermal Surface Fouling", Brit. Chem. Eng., 4, (5), 258, (1959), and "Surface Fouling. How to Calculate Limits", Chem. Eng. Prog., 55, (6), 71, (1959)

116. Kern, D.Q. (1963). Heat transfer surfaces for process engineering. Chem. Process Engng., pp. 461-472, August

117. Kern D.Q. Chem. Eng. Prog. 62 51 (No. 7 1966)

118. Idem, Chem. Eng. Prog. 55 71 (No. 7 1969)

119. Kern D.Q., Kraus A.D. 'Extended Surface Heat Transfer' McGraw-Hill, New York (1972)

120. Khater, E.H. (1982). Fouling in a Hydrocarbon Vaporizer Ph.D. Thesis, University of Bath, England

121. Lkine, S.J., Reynolds, W.C., Schraub, F.A. and Runstadler, P.W., J. Fluid Mech., 30, 741, (1967)

122. Knox, J.H., Gas Chromatography, Methuen & Co. Ltd., London (1962)

123. Knudsen, J.G. (1979). Apparatus and techniques for measurement of fouling of heat transfer surfaces. Int. Conf. Fouling of Heat Transfer Equipment, Troy, N.Y., 13-17 August

124. Knudsen J.G., McCluer H.K. Chem. Eng. Prog. Symp. Series 29, 1 (1959)

125. Kos D.D., Tao C.C. Ind. Eng. Chem. Proc. R & D 8, 306 (1969)

126. Kreith, F., principles of heat transfer, Int. Text Book Co., Scranton, Pa. (1969)

127. Laidler, K.J., Chemical Kinetics, McGraw-Hill Book Co. London (1965)

128. Lawler, D. Fouling by crude oil in refinery heat exchangers. Paper presented at "Fouling - Science or Art?" conference, Guildford, 1979, pp. 155-168

129. Lihou D.A., Heaters for Chemical Reactors, I. Chem. E. Services for the Institution of Chem. Eng. (1975)

130. Lihou D.A. Birm. Univ. Chem. Engr. 22, 85 (1971)

131. Lord, R.C., Minton, P.E. and Slusser, R.P. (1970). Guide to trouble-free heat exchangers. Chem. Engng., Vol. 77, pp. 153-160, 1 June

132. Lowrie, R.S., Gas Chromatography, Pergamon press, London (1969)

133. Lowry, J.A., evaluate reboiler fouling, Chem. Engrg. J. 85, No. 4, Feb. (1978)

134. Ludwig E.E., Vol. III Applied Process Design for Chemical and Petrochemical Plants, Gulf Publishing Co., Houston, Texas (1965)

135. Lund, D.B., Chemical reaction fouling due to foodstuffs. Int. Conf. on the fouling of heat transfer equipment. Troy, New York, Aug. (1979)

136. Magaril, R.Z., et al, Int. Chem. Engrg., 8, No. 4, Oct. (1968)

137. Magaril, R.Z., et al, Int. Chem. Engrg., 11, No. 2, Apr. (1971)

138. Marcus, B.D., office of saline water R & D Prog., Rpt. No. 393 (1969)

139. Martens, A.J., Glas, J. and Gaultier, J.L. Test ofefin feed by micropyrolysis. Hydrocarb. Process. 1979. 58, (4), 199-202

140. Maxwell, J.B., data book on hydrocarbons, Van Nostrand, Inc. (1950)

141. Mayo, F.R., Chain transfer in the polymerisation of styrene, J.A.C.S., 75, (1953)

142. Mayo, F.R., Ind. Eng. Chem. 52, 614 (1960)

143. Mayo, F.R., Free-radical autoxidation of hydorcarbons, Accounts of Chemical Research. 1, No. 7, July (1968)

144. McAdams W.M. 'Heat Transmission' 3rd. Edn. McGraw-Hill, New York (1954)

145. McCabe W.L., Robinson C.S. Ind. Eng. Chem. 16, 478 (1924)

146. Meetor, V.V., et al, proc. 6th Int. heat transfer conf. Toronto, Canada, 4, Aug. (1978)

147. Mekler, V. and Brooks, M.E. When is delayed coking worthwhile? Petrol. Refiner. 1959. 38, (6), 169-176

148. Merry, H. and Polley, G.T. (1979). Obtaining valid data on fouling resistance. Int. Conf. Fouling of Heat Transfer Equipment, Troy, N.Y., 13-17 August

149. Metais, B., and Ekert, E.R.G., Forced, mixed and free convection regimes. Trans. ASME, J. Heat transfer, 86, 295 (1964)

150. Mol, A. How various parameters affect ethylene cracker run lengths. Hydrocarb. Process. 1974. 53, (7), 115-118

151. Moody L.F. Trans. A.S.M.E. 66 671 (1944)

152. Morrison, R.T., Boyd, R.N., Organic Chemistry, Allyn and Bacon, Inc. Boston (1973)

153. NACE Publication T8170, Materials Protection, 9, (6), 29-33 (1970)

154. Nelson W.L. Ref. Nat. Gas. Man. 13, 271 (No. 7 1934), 13, 292 (No. 8 1934)

155. Nelson, W.L. Petroleum refinery engineering. 4th Ed. McGraw-Hill, New York, 1969, pp. 547-554, 623-624

156. Nijsing, R. Diffusional and kinetic phenonmena associated with fouling. Euratom Report EUR 543.e, 1964

157. Nijsing R. Euratom Rpt. No. EUR 293e (1963)

158. Palen J.W., Westwater J.W. Chem. Eng. Prog. Symp. Series 64, 77 (1966)

159. Parkins, W.E., "Surface Film Formation in Reactor Systems", Proc. Tripartite Conf. Transport Materials Pressurized-Water Nucl. Systems, Chalk River, Feb. 28-March 1, 1961, edited by G.R. Vavasour, AECL-1265, (June 1961)

160. Patun, R.J., Krueger, R.H. and Starner, K.E. (1979). Fouling studies and heat transfer test stand real time data acquisition system. Int. Conf. Fouling of Heat Transfer Equipment, Troy, N.Y., 13-17 August

161. Pedersen, C.J. Inhibition of deterioration of cracked gasoline during storage. Ind. Engng. Chem. 1949. 41, 924-928

162. Perera, W.G. and Rafique, K. Coking in a fired heater. Chem. Engr. London. 1976, No. 306, 107-111

163. Perry R.H., Chilton C.H., The Chemical Engineers Handbook 5th Ed., McGraw-Hill

164. Potter, R.C., et al, J. poly. Sci., 4, (1966)

165. Randhava, S.S. and Wasan, D.T. Surface catalysed reactions in turbulent pipe flows. In Chemical Reaction Engineering, ACS Series No. 109, Am. Chem. Soc. 1972, pp. 564-568

166. Rankin, B.H., and Adamson, W.L., Desalination, 13, (1973)

167. Reitzer B.J., Ind. Eng. Chem. Process Design and Development, 3, 345 (No. 4 1964)

168. Roper, A.N., polymerisation of styrene, Ernest-Benn Ltd., London (1975)

169. Ruckenstein, E., Prieve, D.C., J. Chem. Soc. Far. II, 69, (1973)

170. Saunders, K.J., Organic polymer chemistry, Chapman & Hall, London (1973)

171. Scarborough, C.E., et al, Chem. Engrg. Prog., July (1979)

172. Schwartz, F.G., et al, Bureau of mines, U.S. Dept. of Interior, Info. circular 8140 (1962)

173. Scully, J.C., The fundamentals of Corrosion, Pergamon press Oxford (1975)

174. Shah Y.T., Stuart E.B., Kunzru D., Ind. Eng. Chem. Proc. Des. Dev., 12, 344 (No. 3 1973)

175. Shah, Y.T., Stuart, E.B. and Sheth, K.D. Ind. Engng. Chem. Proc. Des. and Dev., 15, 518-524, (1976)

176. Sherwood, T.K., Pigford, R.L. and Wilke, C.R., Mass Transfer, McGraw-Hill, New York, p. 168, (1975)

177. Sieder E.N. Oil Gas J. 32, 104 (May 10, 1934)

178. Sieder E.N., Tate G.E. Ind. Eng. Chem. 28 1429 (1936)

179. Smith, J.D. "Fuel for the supersonic transport: effects of deposits on heat transfer to aviation kerosene" Ind. & Eng. Chem. Proc. design & Dev. 8, No. 3, 299-308, July (1969)

180. Smith J.H. Oil Gas J. 48, 46 (Aug. 3, 1950)

181. Smith, J.M., Chemical Engineering Kinetics, McGraw-Hill, (1970)

182. Steele, G.L., et al, Predictive test method for coking and fouling tendency of used lubricating oil. Int. Conf. on the fouling of heat transfer equipment. Troy, New York, Aug. (1979)

183. Suitor, J.W., Marner, W.J., & Ritter, R.B. "The history and status of research in fouling of heat exchangers in cooling service" Paper No. 76-CSME/CSChE - 19, 16th National Heat Transfer Conference, St. Louis, Aug. (1976)

184. Sundaram, K.M. and Froment, G.F. Kinetics of coke deposition in the thermal cracking of propane. Chem. Engng. Sci. 1979. 34, 635-644

185. Szwarc, M., et al, polymerisation initiated by electron transfer to monomer, J.A.C.S., 78, (1956)

186. Taborek, J., Aoki, T., Ritter, R.B., Palen, J.W., Knudsen, J.G., "Fouling: The Major Unresolved Problem in Heat Transfer", Chem. Eng. Prog., 68 (2), 59-67, (Feb. 1972)

187. Taborek, J., Aoki, T., Ritter, R.B., Palen, J.W., Knudsen, J.G., "Predictive Methods for Fouling Behaviour", Chem. Eng. Prog., 68, (7), 69-78, (July 1972)

188. Taylor, W.F., "Deposit formation from deoxygenated hydrocarbon. II. Effect of trace sulfur compounds", Ind. & Eng. Chem. Prod. Res. Dev. 15, No. 1, 64-68 (1976)

189. Taylor, W.F., "Deposit formation from deoxygenated hydrocarbons. I. General Features", Ind. & Eng. Chem. Prod. Res. Dev. 13, No. 2, 133-138 (1974)

190. Taylor, W.F., "Kinetics of deposit formation from hydrocarbons: Fuel composition studies" Ind. & Eng. Chem. Prod. Res. Dev. 8, No. 4, 375-380, December (1969)

191. Taylor, W.F. "Kinetics of deposit formation from hydrocarbons: IV Additive and surface coating effects" J. Appl. Chem. 19, 222-226, August (1969)

192. Taylor, W.F. and Wallace, T.J., "Kinetics of deposit formation from hydrocarbons: effect of trace sulfur compounds" Ind. & Eng. Chem. Prod. Res. Dev. 7, No. 3, 198-202, September (1968)

193. Taylor, W.F., "Mechanism of despoit formation in wing tanks" Paper 680733, SAE Aeronautic & Space Eng. meeting, Los Angeles, October (1968)

194. Taylor, W.F. and Wallace, T.J., "Kinetics of deposit formation from hydrocarbon fuels at high temperatures: general features of the process" Ind. & Eng. Chem. Prod. Res. Dev. 6, No. 4, 258-262, December (1967)

195. Taylor, W.F. Kinetics of deposit formation from hydrocarbons: heterogeneous and homogeneous metal effects. J. Appl. Chem. 1968. 18, 251-254

196. TEMA (1978). Standards of Tubular Exchanger Manufacturers Association. TEMA Inc., 6th edn.

197. Tennison, S.R. coke formation in visbreakers. Conference on gas chemistry in nuclear reactors and large industrial plant. University of Salford, U.K., April (1980)

198. Thackery, P.A., the cost of fouling in heat exchange plant, Fouling Science or Art? Guildford, England, Mar. (1979)

199. Thompson, R.B., Druge, L.W. and Chenicek, J.A. Stability of fuel oils in storage: effect of sulfur compounds. Ind. Engng. Chem. 1949. 41, 2715-2721

200. Thompson, R.B., Chenicek, J.A., Druge, L.W. and Symon, T. Stability of fuel oils in storage: effect of some nitrogen compounds. Ind. Engng. Chem. 1951. 43, 935-939

201. Tong L.S., Boiling Heat Transfer and Two-Phase Flow, John Wiley and Sons Inc. (1965)

202. Trilling C.A. Int. Atomic Energy Agency Tech. Rpt. Series No. 70 (1967)

203. Van Nostrand, W.L., JR., Leach, S.H., and Haluska, J.L. Economic penalties associated with the fouling of heat transfer equipment. Int. Conf. on the fouling of heat transfer equipment. Troy, New York, Aug. (1979)

204. Vranos, A., et al, Determination of coking rate in jet fuel. Int. Conf. on the fouling of heat transfer equipment. Troy, New York, Aug. (1979)

205. Walker R.A., Ph.D. Thesis, University of Birmingham (1973)

206. Walker R.A., Bott T.R., Trans. Instn. Chem. Engrs., 51, 165, (1973)

207. Walters, E.L., Minor, H.B. and Yabroff, D.L. Chemistry of gum formation in cracked gasoline. Ind. Engng. Chem. 1949. 41, 1723-1729

208. Watkinson, A.P., "Particulate Fouling of Sensible Heat Exchangers", Ph.D. Thesis, University of British Columbia, (Sept. 1968)

209. Watkinson, A.P. and Epstein, N., "Gas oil fouling in a sensible heat exchanger", Chemical Eng. Pro. Symposium Series, 65, No. 92, 84-90 (1969)

210. Watkinson, A.P. and Epstein, N. Particulate fouling of sensible heat exchangers. Proc. 4th Int. Heat Transfer Conf. Vol. I. Paris. 1970, paper HE 1.6

211. Watt, J.J., Evans, A. and Hibbard, R.R. Fouling characteristics of ASTM jet A fuel when heated to 700°F in a simulated heat exchanger tube. National Aeronautics and Space Administration Report NASA TN.D-4958, 1968

212. Weiland, J.H., McCay, R.C., and Barnes, J.E. Rates of fouling and cleaning of unfired heat-exchanger equipment. Trans. A.S.M.E. 1949. 71, 849-853

213. Wiseman P., An Introduction to Industrial Organic Chemistry, Applied Science Publishers Ltd. (1972)

214. Wissler, E.H. and Schechter, R.S. Turbulent flow of gas through a circular tube with chemical reaction at the wall. Chem. Engng. Sci. 1962. 17, 937-948

215. Zdonik S.B., Green E.J., Hallee L.P., The Oil and Gas Journal, 96 (June 1967)

216. Zdonik S.B., Green E.J., Hallee L.P., The Oil and Gas Journal, 192 (July 1967)

217. Zdonik S.B., Green E.J., Hallee L.P., The Oil and Gas Journal, 133 (Aug. 1967)

218. Zisman, W.A., effect of chemical constitution, Adhesion and bonding, Wiley-Interscience, John Wiley & Sons, N.Y. (1971)

APPENDIX A

Integration methods for the determination of the order of reaction.

The Tabular Method

Using the integrated form of the chosen differential rate equation, the rate constant is evaluated for each concentration-time experimental observation. The rate constant will be essentially constant for the correct order of reaction, but will change progressively for incorrect orders of reaction.

Graphical Methods

The integrated form of the chosen differential rate equation is rearranged into such a form that a linear plot can be obtained. The experimental results are then plotted according to the rearranged integrated form of the chosen differential equation. If a deviation from linearity is obtained then the reaction under consideration is not of that order.

Another graphical method is Powell's[127] method, which involves the use of dimensionless parameters. Let the dimensionless concentration α be defined as

$$\alpha = \frac{C_M}{C_{Mo}} \tag{A1}$$

The solution of equation (110) (Section 3.2.3) is given by

$$K_n\, t = \frac{1}{n-1}\left[\frac{1}{C_M^{n-1}} - \frac{1}{C_{Mo}^{n-1}}\right] \tag{A2}$$

Equation (A2) gives the rate equation for the n^{th} order reaction where $n \neq 1$. If $n = 1$, then the solution of equation (110) is given by

$$K_1\, t = \ln \frac{C_{Mo}}{C_M} \tag{A3}$$

Rearranging equation (A2) and substituting equation (A1) to eliminate C_M, gives

$$K_n\ t = \frac{1}{(n-1)C_{Mo}^{n-1}}\ [\frac{1}{\alpha^{n-1}}]-\ 1 \qquad (A4)$$

Defining a dimensionless time, τ such that

$$\tau = K_n\ C_{Mo}^{n-1}\ t \qquad (A5)$$

and substituting equation (A5) into (A4) gives

$$(n-1)\ \tau = [\frac{1}{\alpha^{n-1}}]-\ 1 \qquad (A6)$$

If equation (A1) is substituted into the rate equation for a first order reaction given by equation (A3), then

$$K_1\ t = -\ \ln \alpha \qquad (A7)$$

Since from equation (A5), $\tau = K_1\ t$ for a first order reaction, then equation (A7) becomes

$$\tau = -\ \ln \alpha \qquad (A8)$$

Equations (A6) and (A8) do not include C_{Mo} or K; thus for a reaction of a given order, there is a unique relationship between α and τ. Figure (A1) shows a plot of α against τ for various orders of reaction[127], and can be used for the determination of the order of reaction and the rate constant. The procedure is to plot experimental values of α against ln t (not ln τ as this cannot first be determined since n and K_n are unknown). If the reaction is (say) zero order, the experimental plot will match the shape of the theoretical plot for n = o, but will be shifted along the ln τ axis from the theoretical plot for n = o. The amount of shift is seen from equation (A5) to be $-\ln K_n\ C_{Mo}^{0-1}$ where n = o. Since n is now known, K_n can be evaluated.

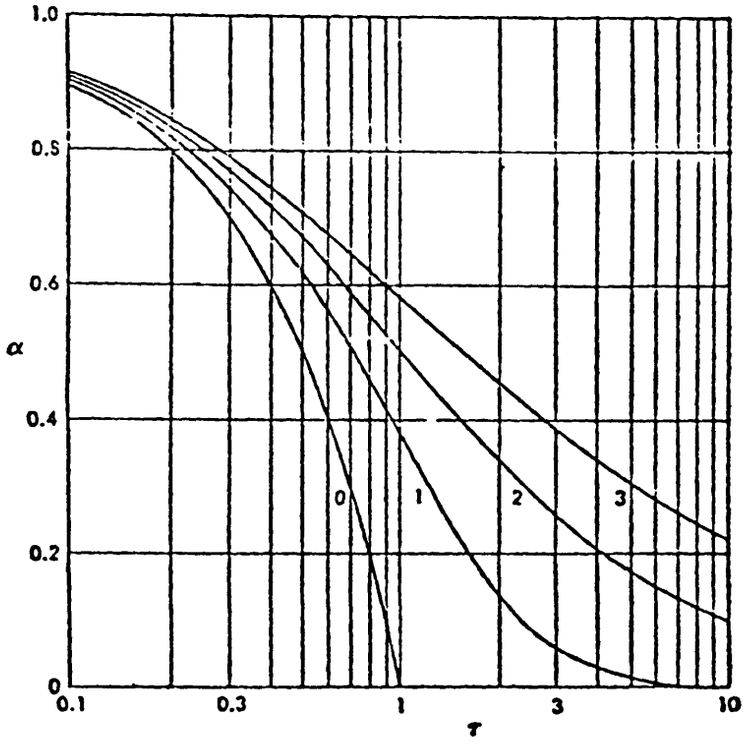

Figure A1[127] A Plot of α Against τ for Various Orders of Reaction.

The Half-Life Method

The half-life of a reaction $t_{\frac{1}{2}}$ is the time taken for the initial concentration of a reactant to be reduced by a factor of two, i.e.

$$\text{at } t = t_{\frac{1}{2}}, \quad C_M = \frac{C_{Mo}}{2} \tag{A9}$$

Applying this to the rate equation for the n^{th} order reaction where $n \neq 1$ given by equation (A2)

$$t_{\frac{1}{2}} = \frac{2^{n-1} - 1}{(n-1) K_n C_{Mo}^{n-1}} \tag{A10}$$

For a first order reaction,

$$t_{\frac{1}{2}} = \frac{\ln 2}{K_1} \tag{A11}$$

Experiments are carried out at two or more different initial concentrations of reactant. If the half-life is independent of the initial concentration, then the reaction is first order. If the half-life varies with initial concentration, then a log-log plot of half-life (See Equation (A10)) against initial concentration will give a straight line of slope -(n-1). Alternatively, the results of two experiments can be expressed in the following form

$$\frac{(t_{\frac{1}{2}})_1}{(t_{\frac{1}{2}})_2} = \left[\frac{(C_{Mo})_1}{(C_{Mo})_2}\right]^{n-1} \tag{A12}$$

from which,

$$n = 1 + \frac{\ln \dfrac{(t_{\frac{1}{2}})_1}{(t_{\frac{1}{2}})_2}}{\ln \dfrac{(C_{Mo})_1}{(C_{Mo})_2}} \tag{A13}$$

APPENDIX B

Calculations

Pressure Drop Calculations

For turbulent single phase internal flow in a tube

$$\Delta P = 4\Phi \frac{L}{D} \rho u^2 \qquad \text{(B1)}$$

in which

ΔP = pressure drop

Φ = friction factor

L = length of tube

D = tube diameter

ρ = density of fluid

u = velocity of fluid = $(Gx4)/\rho x\pi xD^2$

G = mass flow rate

$$\Phi = \frac{f}{2} = \frac{f'}{8} \qquad \text{(B2)}$$

where

f = fanning friction factor

f' = Moody friction factor

$$f = \frac{\tau}{\rho u^2} \qquad \text{(B3)}$$

in which

τ = shear stress

$$Re = \frac{\rho du}{\mu} \qquad \text{(B4)}$$

in which

Re = Reynolds number

μ = viscosity of fluid

The velocity of the fluid is obtained from the measured mass flow rate. Then the Reynolds number is determined from

the velocity of the fluid and fluid properties. The pressure drop is measured and then the friction factor is determined. Plotting the results on Figures B1 or B2 will give an indication of the relative roughness of the tube. When the friction factor is determined the shear stress on the wall can then be determined from Equation B3.

Heat Transfer and Fouling resistance Calculations

The Enthalpy of the fluid was determined at the inlet and outlet of the tube. The quantity of heat gained by the process fluid was determined from

$$Qin = G\ (H_o - H_i) \qquad (B5)$$

where

G = flow rate ($^{lb}/_{hr}$)

$H_{o,i}$ = Enthalpy of fluid at the outlet or inlet of tube ($^{Btu}/_{lb}$)

The quantity of heat dissipated by the heating elements power output is given by

$$Qout = Kw \times 3413 \quad (^{Btu}/_{hr}) \qquad (B6)$$

where Kw = total power output in kilowatts

The heating efficiency was then determined, thus:

$$\% \text{ efficiency} = \frac{Qin}{Qout} \times 100\% \qquad (B7)$$

The test section was divided into differential sections so that the outlet conditions from one section are the inlet conditions to the next one. The outlet temperature from a differential section is determined from

$$T_o = T_i + Qin/(GxCp) \quad (^{\circ}F) \qquad (B8)$$

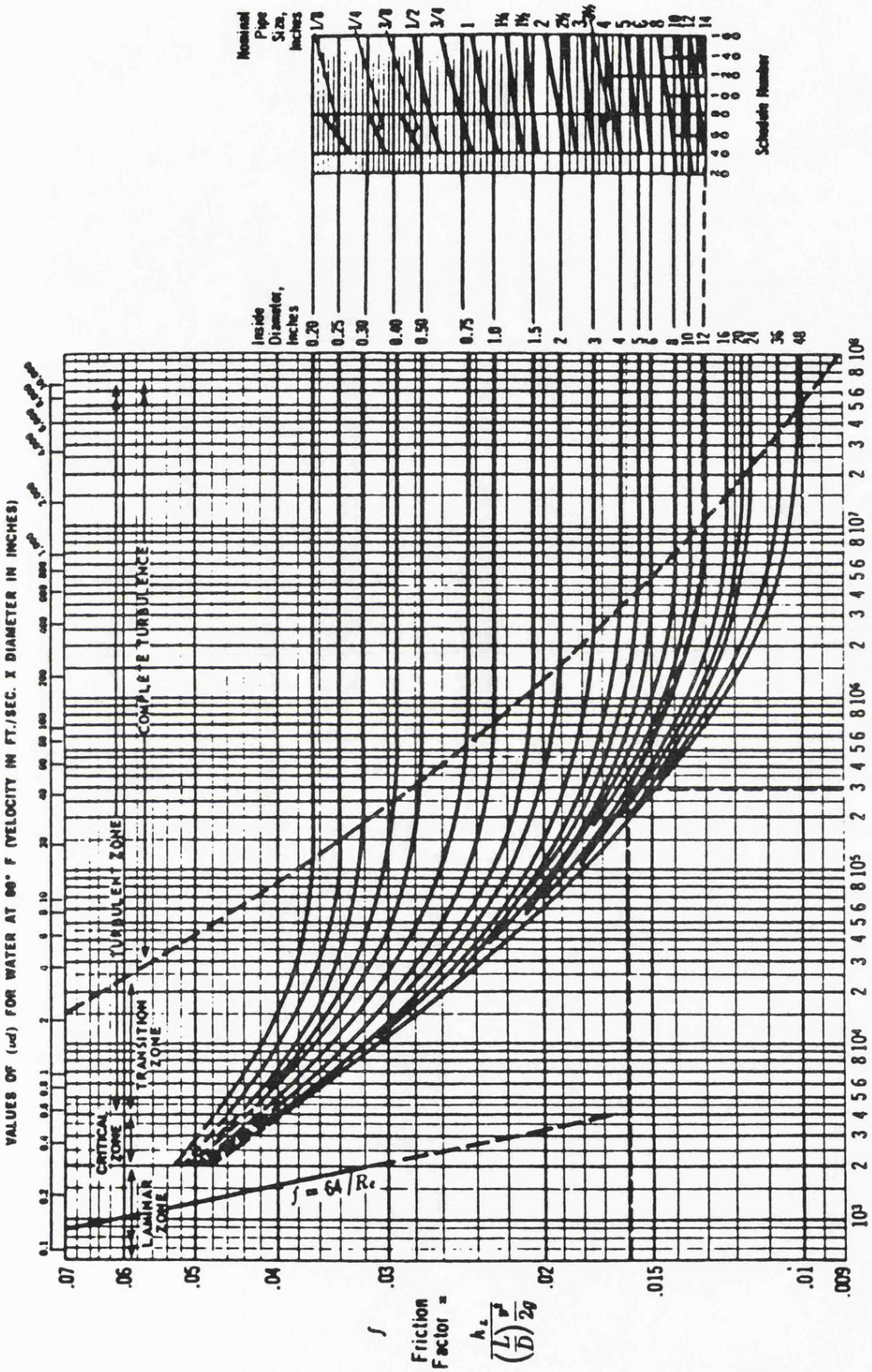

Figure B1(55) **Friction Factors for Clean Commercial Steel Pipe**

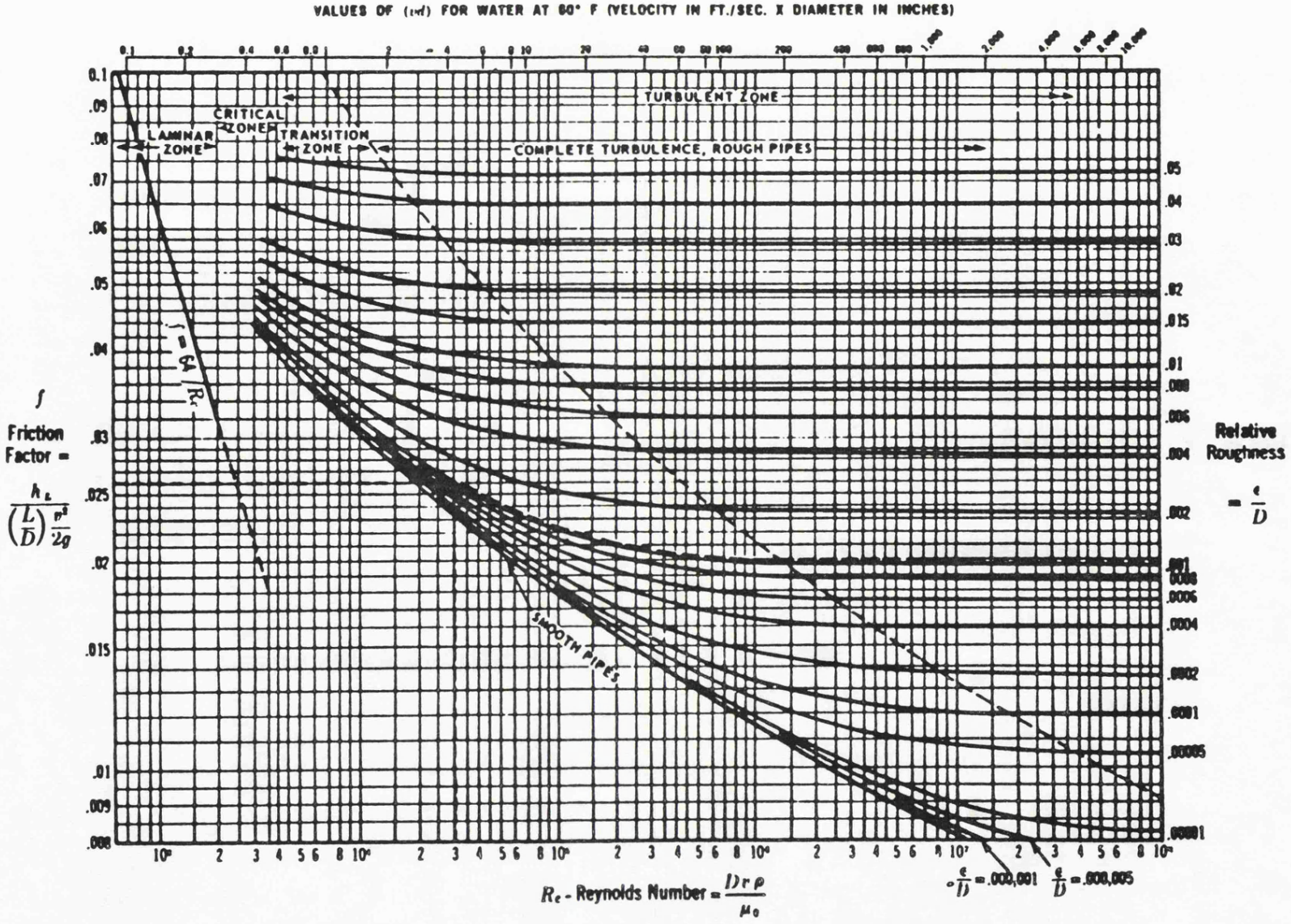

Figure B2 [55] **Friction Factors for Any Type of Commercial Pipe**

in which

T_i = inlet temperature

Qin = quantity of heat gained in that section by process fluid

Cp = Heat capacity of fluid at the entrance to the section

Qin is calculated from Qout for the section multiplied by efficiency. The bulk temperature was then averaged from the inlet and outlet values.

$$T_b = (T_i+T_o)/2 \qquad (^\circ F) \tag{B9}$$

The heat flux to the tube from the heating elements is given by:

$$\Phi = (Kwx3413xEfficiency)/(\pi x d_o x Lx100) \qquad (Btu/hrft^2) \tag{B10}$$

in which d_o = outside diameter of tube

L = section length considered

The overall heat transfer coefficient was then determined

$$U = \frac{\Phi}{T_c-T_b} \qquad (Btu/hrft^{2\circ}F) \tag{B11}$$

in which, T_c = Temperature recorded by a thermocouple.

The variations of physical properties along the tube with temperature were evaluated at the bulk temperature of a specific section of the tube. Then the Reynolds number was determined as follows:

$$Re = (\rho x d_i x u)/\mu \tag{B12}$$

where μ = viscosity of fluid

The Prandtl number was evaluated as follows:

$$Pr = (\mu x C_p)/K \tag{B13}$$

where

C_p = fluid heat capacity

K = fluid thermal conductivity

The Graetz number was evaluated, thus:

$$Gz = \frac{\pi}{4} \times Re \times Pr \times \frac{d_i}{L} \qquad (B14)$$

Then the heat transfer coefficient was obtained either from the Dittus-Boelter equation

$$h_{DB} = \frac{0.023}{d_i} \times K \times Re^{0.8} \times Pr^{0.4} \qquad (B15)$$

or from the ESDU correlation

$$h_{ESDU} = (\rho \times u \times C_p)(\exp(-3.796-0.205\log Re-0.505\log Pr -0.0225(\log P_r)^2)) \qquad (B16)$$

Walker[205] and Kolaczkowski[114] found that the Dittus-Boelter correlation under estimated the heat transfer coefficient and therefore the h_{ESDU} was adopted for the purpose of this calculation. The inside wall temperature is then determined from

$$Tw_i = T_b + \frac{\Phi}{h} \qquad (B17)$$

The Grashof number is evaluated to check for natural convective effects, thus:

$$Gr = \frac{B}{\mu^2} \times g \times d_i^3 \times \rho^2 \times (Tw_i - T_b) \qquad (B18)$$

where

B = coefficient of volumetric thermal expansion

g = gravitational acceleration

The fouling resistance was determined from the variation of the heat transfer coefficient with time

$$R_{fi} = \frac{d_i}{d_o} \left(\frac{1}{U_d} - \frac{1}{U_c}\right) \qquad (B19)$$

in which

R_{fi} = fouling resistance on the inside

$U_{d,c}$ = overall dirty or clean heat transfer coefficient (instantaneous).

Sample Calculation

Kerosene system Run 35

Power input = 0.8 Kw/element

Flow rate = 480 lb/hr

Efficiency = 86%

The heat flux to the test section is given by

Φ = (Power x 3413 x efficiency)/(π x d_o x L x 100)

$$= \frac{0.8 \times 3413 \times 86}{\pi \times \frac{1}{12} \times 1 \times 100} = 8968.2 \quad Btu/ft^2hr$$

The heat transfer coefficient is then determined from

$h = (\rho u C_p) \exp(-3.796 - 0.205 \text{ Log Re} - 0.505 \text{ Log Pr} - 0.0225(\text{Log Pr})^2)$

$= 86.23 \quad Btu/hrft^2{}^oF$

The bulk fluid temperature = 246 °F

hence, $T_{wi} = T_b + \frac{\Phi}{h}$

T_{wi} = 350 °F

The overall heat transfer coefficient is then determined:

Temperature recorded by thermocouple = 390 °F

$$U_c = \frac{\Phi}{T_c - T_b}$$

$$= \frac{8968.2}{390-246}$$

$= 62.3 \quad Btu/hrft^2{}^oF$

The dirty overall heat transfer coefficient was calculated; its value towards the end of the run was 38.23 $Btu/hrft^2{}^oF$. Hence the fouling resistance is determined

$$R_f = 0.792 \left(\frac{1}{U_d} - \frac{1}{U_c}\right)$$

$$= 0.792 \left(\frac{1}{38.23} - \frac{1}{62.3}\right)$$

$$= 0.008 \ (\text{Btu/hrft}^2{}^\circ\text{F})^{-1}$$

It is to be noted that Φ and h can vary slightly with time, leading to a second order variation of the solid-fluid interfacial temperature during a run (see equation B17).

APPENDIX C

Calibration of Rotameter 18E and 24E for 100% v/v kerosene system.

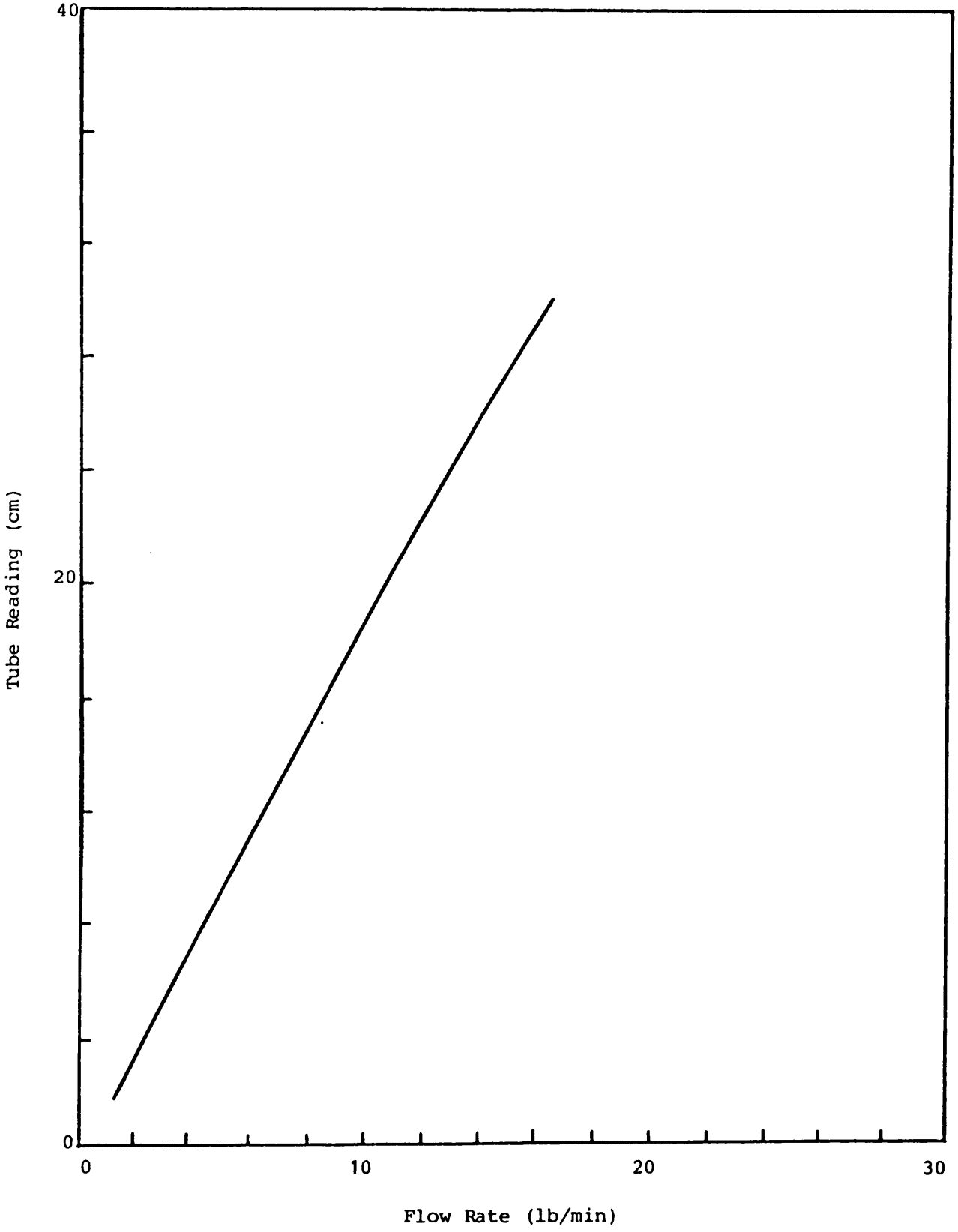

Figure C1 Calibration of Rotameter 18E, 100% v/v Kerosene System.

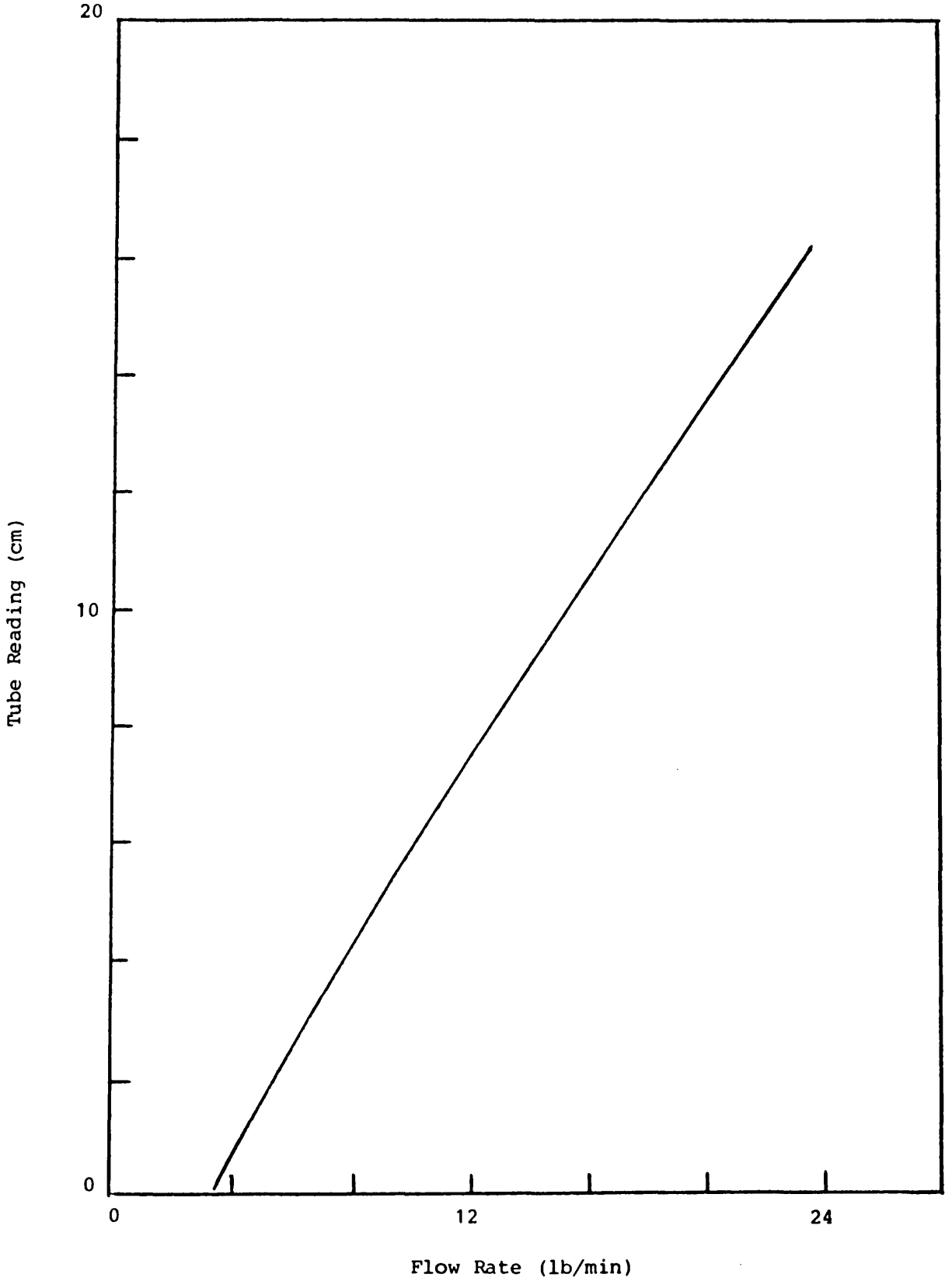

Figure C2 Calibration of Rotameter 24E, 100% Kerosene System.

APPENDIX D

Calibration of the thermocouple voltage output.

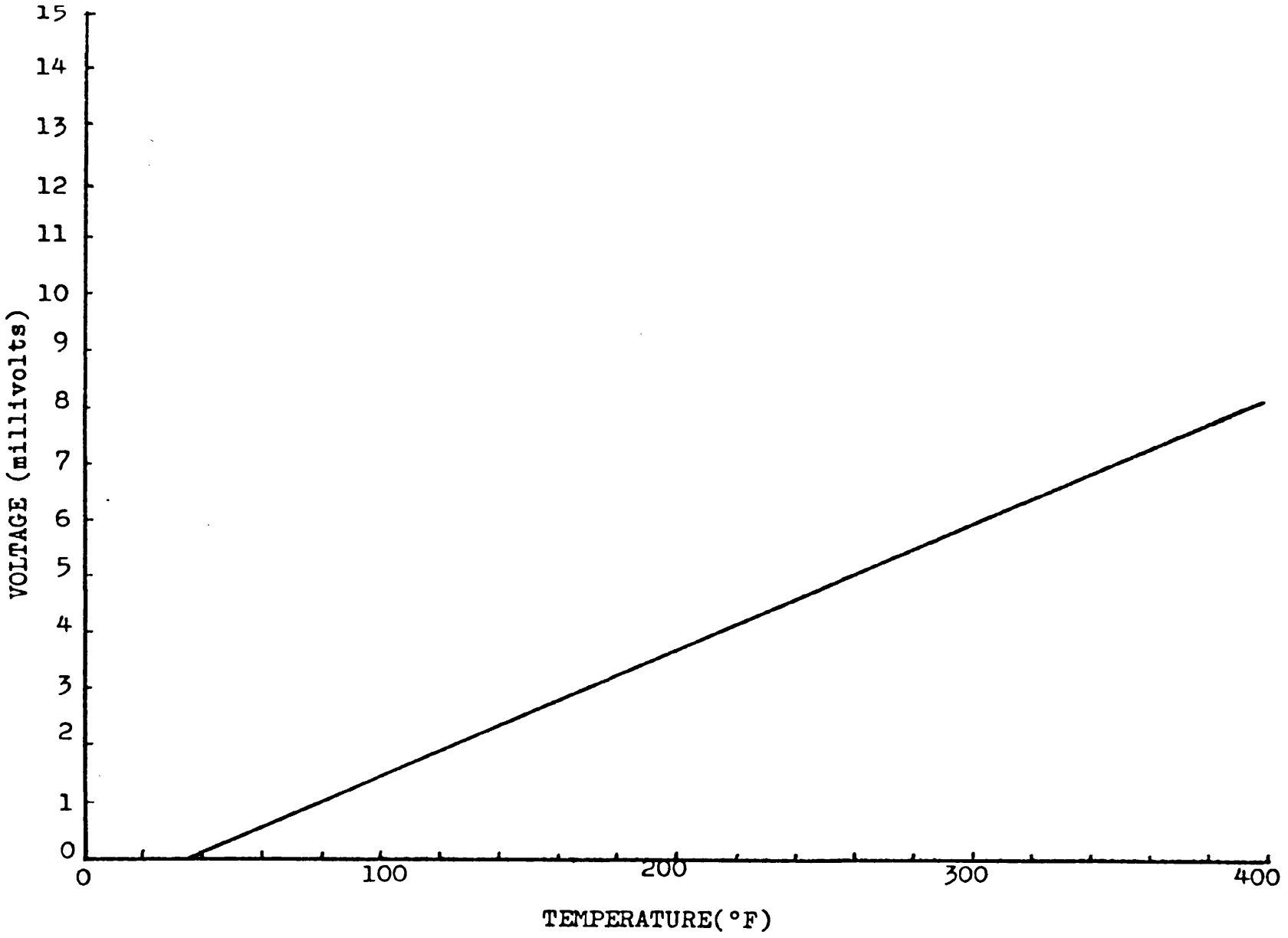

Figure D1 Calibration of the voltmeter .Thermocouple reading output .

APPENDIX E

Physical properties of odorless kerosene (Exsol D 200/240)

The working fluid was supplied by Esso Chemicals, UK, being a saturated petroleum fraction containing 60-70% paraffinic and 30-40% naphthenic hydrocarbons. It was chosen both for its relatively high boiling point and also for its relatively high flash point of 174°F.

Characterization of the Petroleum Fraction

The Watson characterization factor was determined from

$$K = \frac{(Me\text{-}ABP)^{1/3}}{S.g.,\ 60°F/60°F}$$

in which

Me-ABP = mean average boiling point (°F)

S.g., 60°F/60°F = specific gravity

$$K = \frac{(428)^{1/3}}{0.79} = 9.54$$

For kerosene K ranges between 8.5 to 10[155]. For odorless kerosene the indication is that it is paraffinic with naphthenic content and low olefinic content as indicated by the Bromine number (Br No. = 0.09).

The API gravity is given by:

$$\text{API gravity} = \frac{141.5}{S.g.} - 131.5$$

$$= \frac{141.5}{0.79} - 131.5$$

$$= 47.6° \text{ API}$$

From the API handbook[8] the density, enthalpy, heat capacity, viscosity and thermal conductivity were determined at

various temperatures for the kerosene fraction in accordance with the characterization factor. These data were plotted over the temperature range 0-500°F. From the graphs equations were derived to describe the physical property variation against temperature. Subroutines were written to describe these equations.

Enthalpy

$0 \leq T \leq 250°F$

$H = a\ T + b$ (Btu/lb)

$a = \frac{210-80}{250-0} = 0.52$

$b = 80$

Therefore $H = 0.52 \times T + 80$

$250 \leq T \leq 500°F$

$a = \frac{380-210}{500-250} = 0.68$

$b = 0$

Hence $H = 0.68\ T$ (Btu/lb)

Density

$0 \leq T \leq 300°F$

$\rho = a\ T + b$ (lb/ft^3)

$a = \frac{43.2-51}{300-0} = -\ 0.026$

$b = 51$

Therefore

$\rho = -\ 0.026\ T + 51$

$300 \leq T \leq 500°F$

$a = \frac{36.7-43.2}{500-300} = -\ 0.0325$

$b = 53.2$

Hence

$\rho = -\ 0.0325\ T + 53.2$ (lb/ft^3)

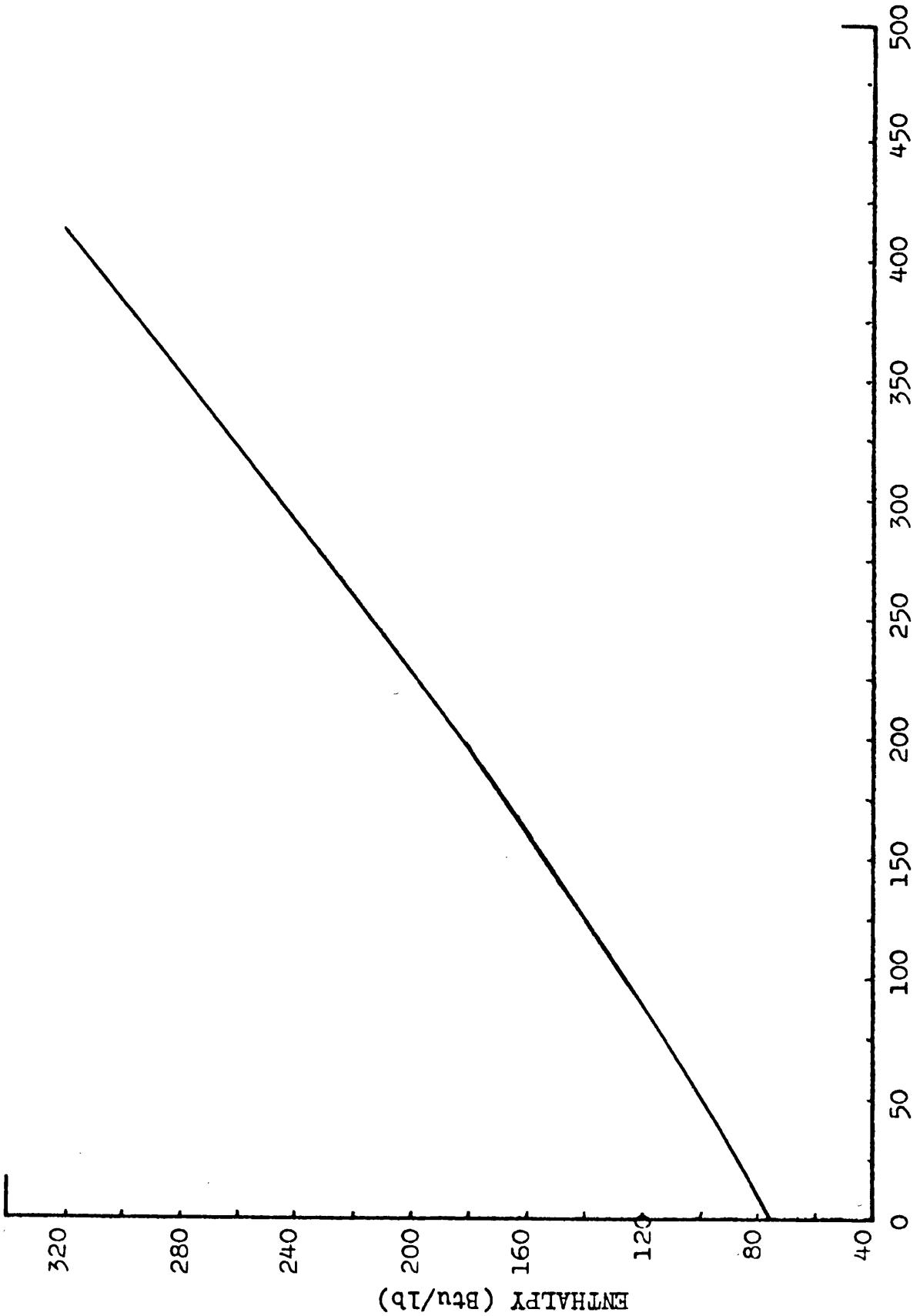

Figure E1 Enthalpy of odorless kerosene against temperature

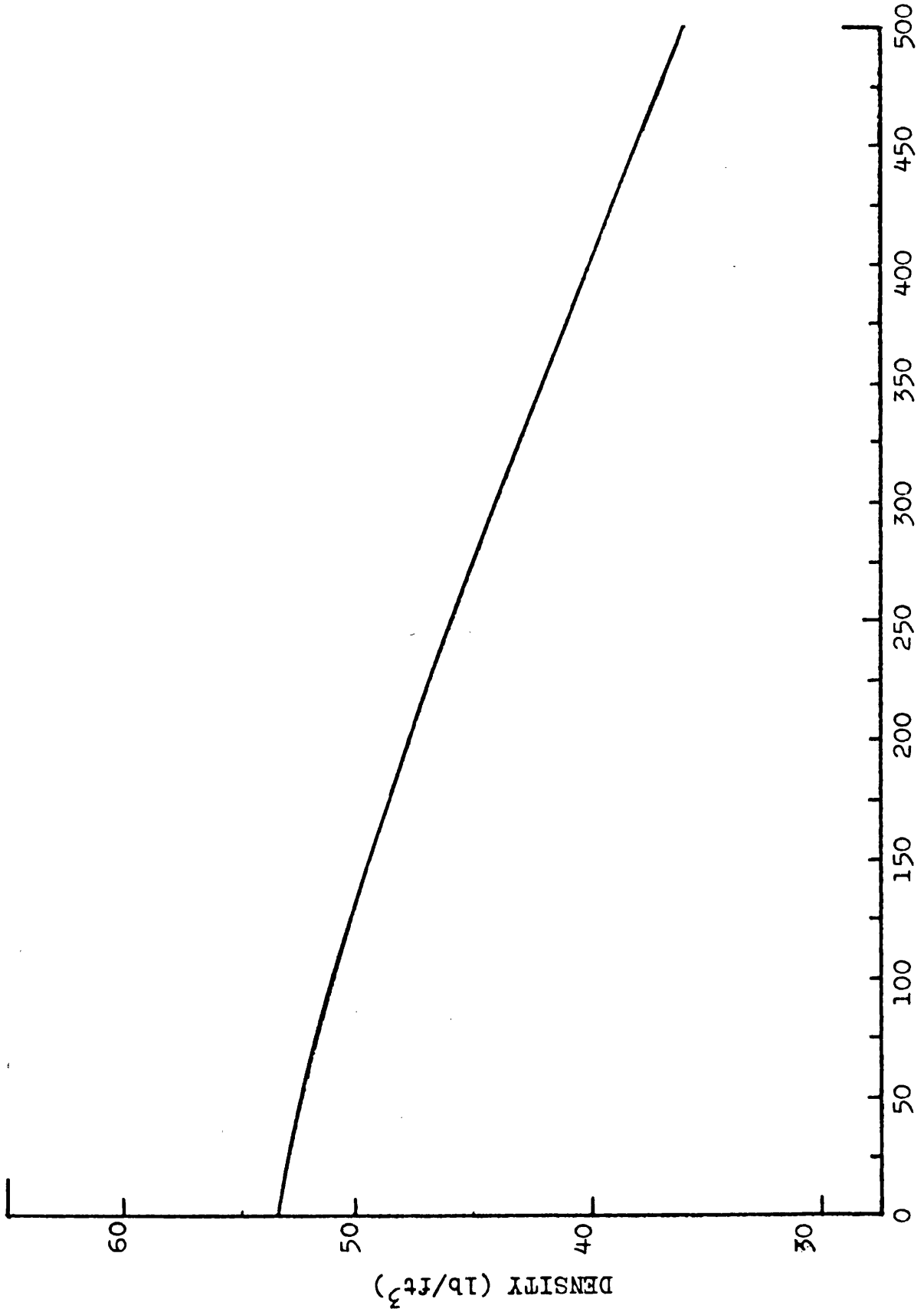

Figure E2 Variation of odorless Kerosene liquid density with temperature

Heat Capacity

$$Cp = a\,T + b \qquad (Btu/lb\,^{\circ}F)$$

$$0 \leq T \leq 500\,^{\circ}F$$

$$a = \frac{0.74-0.45}{500-0} = 0.00058$$

$$b = 0.45$$

Hence

$$Cp = 0.00058\,T + 0.45 \qquad (Btu/lb\,^{\circ}F)$$

Thermal Conductivity

$$K = a\,T + b \qquad (Btu/hr.ft^2.\,^{\circ}F/ft)$$

$$0 \leq T \leq 600\,^{\circ}F$$

$$a = \frac{0.050-0.0754}{600-0} = -4.233 \times 10^{-5}$$

$$b = 0.0754$$

Therefore

$$K = -0.0000423\,T + 0.0754 \qquad (Btu/hr.ft^2.\,^{\circ}F/ft)$$

Viscosity

$$F(x) = Ao\,e^{-BX}$$

$$\mu = \mu_0\,e^{-KT} \qquad (Cp)$$

$$\log_e \mu = \log \mu_0 + \log e^{-KT}$$

$$= \log \mu_0 - KT \qquad K>o$$

plot log μ vs. T

$$0 \leq T \leq 137.5\,^{\circ}F$$

$$-K = \frac{0.05-1.55}{137.5-0} = -0.011$$

$$\log \mu_0 = 1.55$$

Therefore

$$\log \mu = -0.011\,T + 1.55$$

Hence

$$\mu = \exp(-0.011\,T + 1.55) \qquad (Cp)$$

$$137.5 \leq T \leq 400\ F$$

$$-K = \frac{-1.2729-0.05}{400-137.5} = -0.00504$$

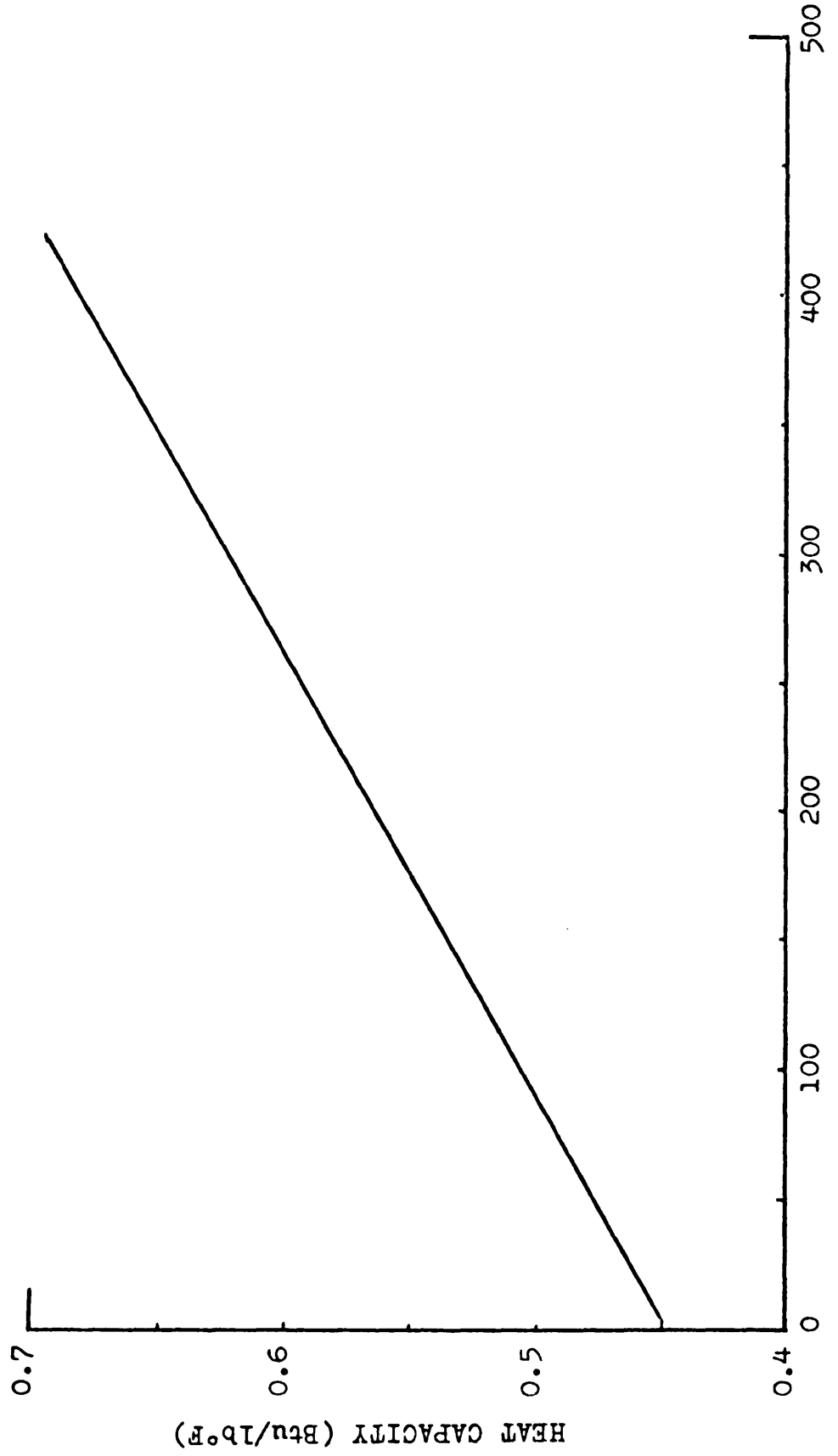

Figure E3 Heat capacity of kerosene against temperature

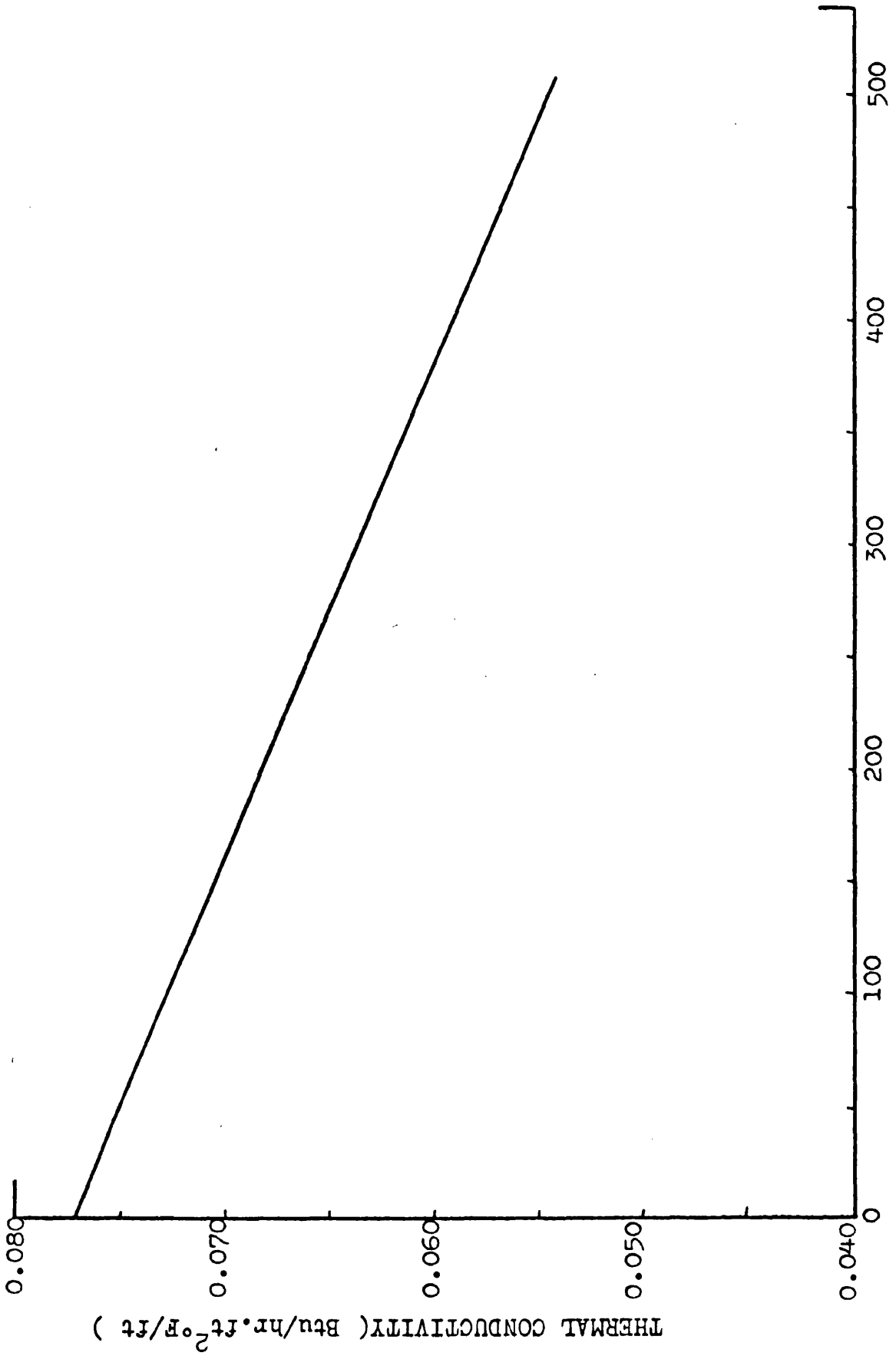

Figure E4 Thermal conductivity of kerosene against temperature .

$$\log \mu_0 = 0.8$$

Therefore

$$\log \mu = -0.00504\ T + 0.8$$

Hence

$$\mu = \exp(-0.00504\ T + 0.8) \qquad \text{(Cp)}$$

Figure E6 shows a chromatogram of pure kerosene. Table E1 gives chemical hazard data of odourless kerosene.

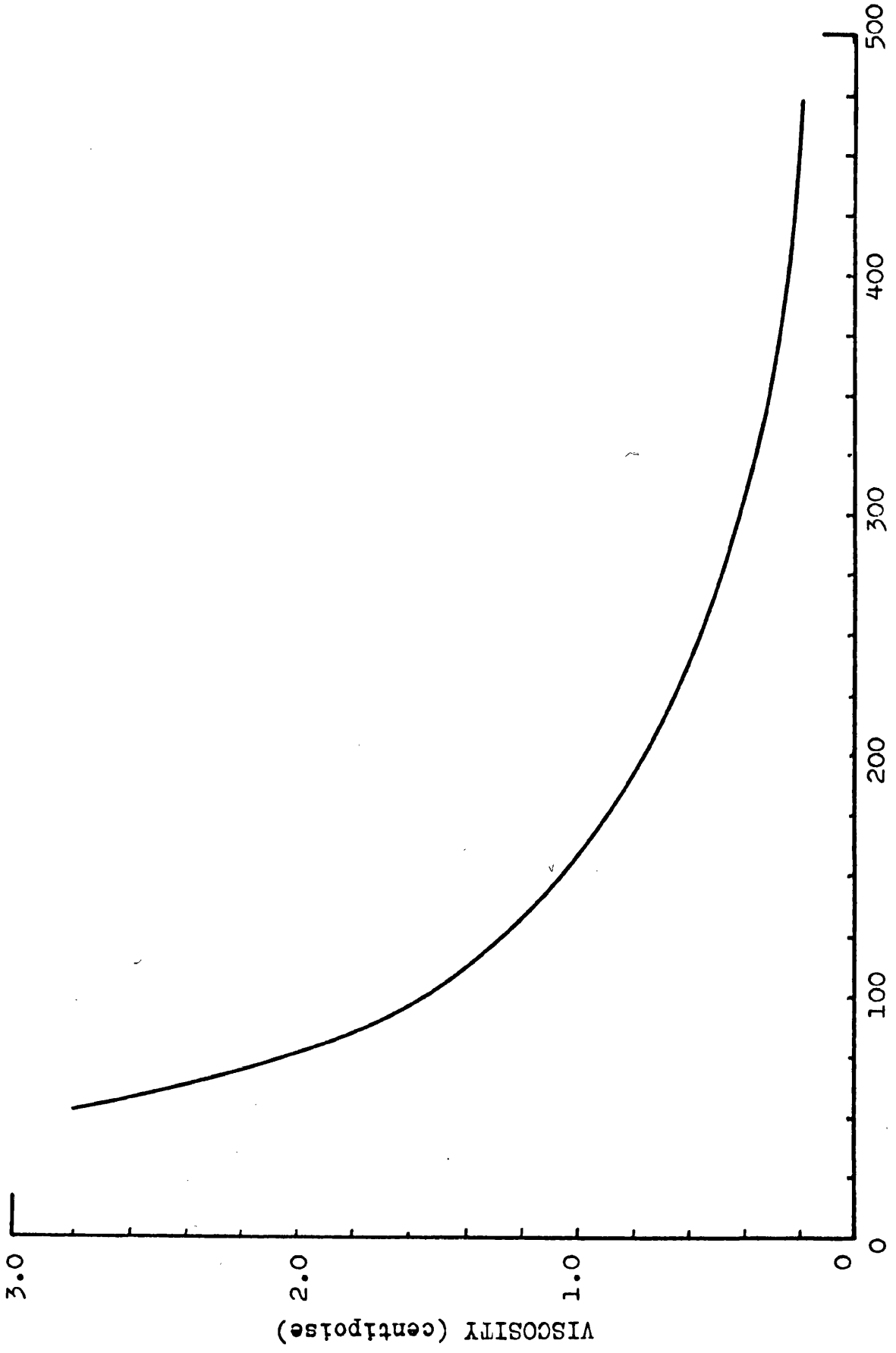

Figure E5 Viscosity of odorless kerosene against temperature

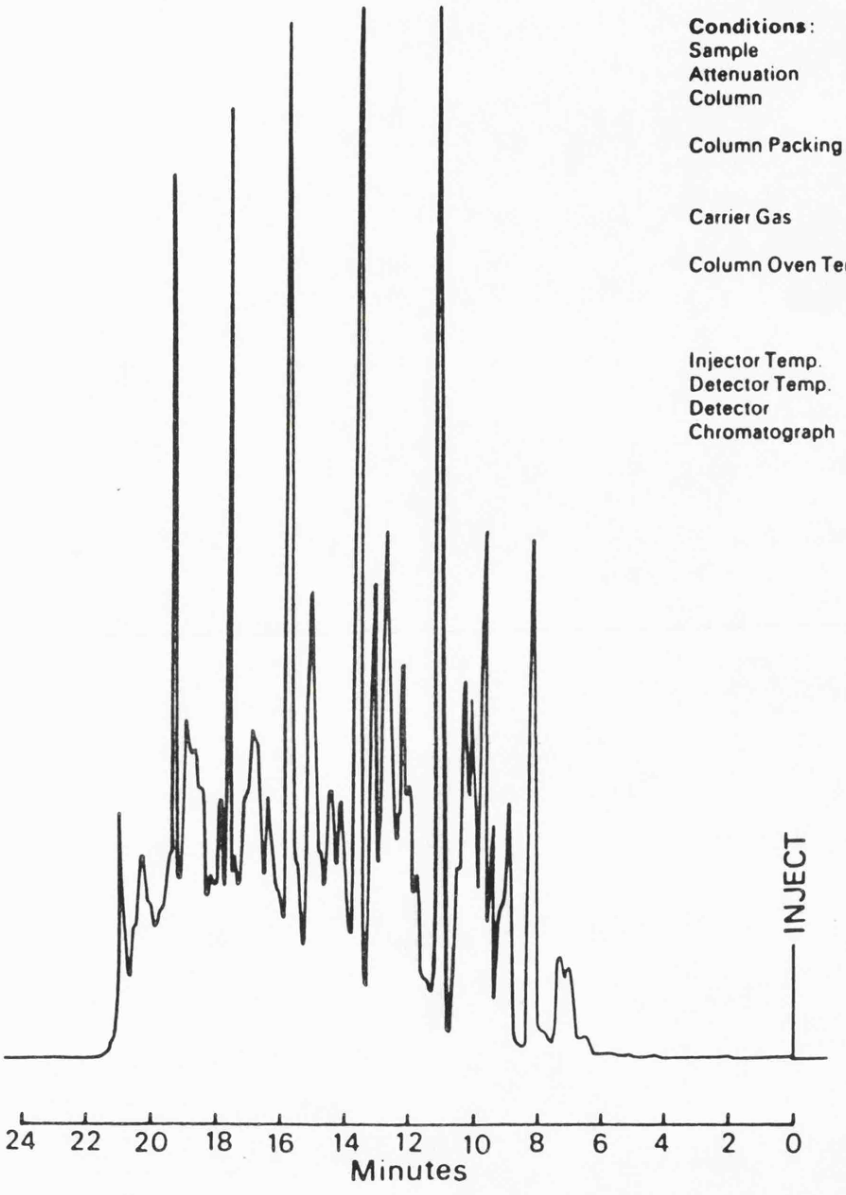

Figure E6 Chromatogram of pure Kerosene .

Table E1

Chemical Hazard Data

ESSO CHEMICALS

PRODUCT NAME		REVISION	DATE	PAGE
EXSOL D 200/240	HDH-C-00630	E 0	Aug. '77	1

I. HEALTH INFORMATION AND PROTECTION

FIRST AID:

Inhalation: Rescuers should wear respiratory equipment. If overcome by vapour, remove immediately from exposure, administer artificial respiration if breathing is irregular or has stopped, keep individual calm and call a doctor.

Eye contact: Flush eyes with plenty of water until irritation subsides.

Skin contact: Remove any contaminated clothing and flush area until irritation subsides.

Ingestion: No hazard by this route in normal industrial use, but if swallowed, do not induce vomiting; keep at rest and call a doctor.

NATURE OF HAZARD:

Inhalation: In high concentrations, vapour is irritating to eyes and mucous membranes and is anaesthetic.

Eye Contact: Slightly irritating, but does not injure eye tissue.

Skin Contact: Low order of toxicity. Frequent or prolonged contact may irritate and cause dermatitis.

Ingestion: Low order of toxicity, but minute amounts aspirated into lungs during ingestion may cause severe pulmonary injury and death.

THRESHOLD LIMIT VALUES (TLV): 300 ppm (recommended by R.E.H.D., Exxon Corp.)

TOXICITY DATA

Inhalation: No data available.

Eye Contact: Direct instillation of test quantities (0.1 ml) of solvent into the rabbit eye would be expected to produce slight to moderate redness and swelling.

Skin Contact: Rabbit dermal LD_{50} would be expected to be greater than 3.0 g/kg.

Ingestion: Rat oral LD_{50} would be expected to be greater than 5.0 g/kg.

SPECIAL PRECAUTIONS:

Observe the recommended TLV. Avoid frequent or prolonged skin contact.

A

Chemical Hazard Data	HDH-C-00630	PAGE 2
PRODUCT NAME EXSOL D 200/240	REVISION E 0	DATE August '77

II. FIRE AND EXPLOSION HAZARD DATA

FLASH POINT (METHOD)
170°F (P.M. closed)

FLAMMABLE LIMITS. VOL. % IN AIR
Approximately 0.6 to 7%

AUTOIGNITION TEMPERATURE
>200°C

FIRE AND EXPLOSION HAZARD, GENERAL

- Low hazard. Material can form flammable mixtures or can burn only upon heating above the flash point.

III. FIRE FIGHTING

FIRE FIGHTING PROCEDURES

- Use water spray to cool fire exposed surfaces and to protect personnel. Shut off "fuel" to fire.
- Use foam, dry chemical powder, or water spray to extinguish the fire. Wrong application of water can cause a boilover.

SPECIAL PRECAUTIONS

- See also Sections I and VI.

IV. SPILL CONTROL PROCEDURE

LAND SPILL

- Keep public away. Shut off source if possible to do so without hazard. Advise police if substance has entered a water course or sewer or has contaminated soil or vegetation. Take measures to minimize the effects on the ground water.
- Contain spilled liquid with sand or earth. DO NOT use combustible materials such as sawdust.
- Consult an expert on disposal of recovered material and ensure conformity to local disposal. Also see Sections I and VI.

WATER SPILL

- Warn other shipping.
- Notify port or relevant authority and keep public away. Shut off source if possible to do so without hazard. Confine if possible.
- Remove from surface by skimming or with suitable adsorbents. If allowed by local authorities and environmental agencies sinking and/or suitable dispersants may be used in non-confined waters.
- Consult an expert on disposal of any recovered material and ensure conformity to local regulations. See also Sections I and VI.

C

Chemical Hazard Data	HDH-C-00630	PAGE 3
PRODUCT NAME EXSOL D 200/240	REVISION E 0	DATE August '77

V. PHYSICAL AND CHEMICAL PROPERTIES

DESCRIPTION Clear colourless liquid	VAPOR PRESSURE < 75 mm of Hg at 38°C
	SOLUBILITY IN WATER, WT.% Insoluble
CHEMICAL NAME Not applicable	IS MATERIAL HYGROSCOPIC? No
CHEMICAL FORMULA Not applicable	MOLECULAR WEIGHT 175
SP. GR. OF LIQUID 0.79	SP. VISCOSITY OF LIQUID, $H_2O = 1$ 1.52 Cps at 40°C
SP. GR. OF VAPOR AT 1 ATM, AIR = 1 6	COEFFICIENT OF THERMAL EXPANSION OF LIQUID Not available
FREEZING POINT < −10°F	EVAPORATION RATE (n. BuAc 1) 0.005
BOILING POINT 201–240°C	HEAT OF VAPORIZATION AT BOILING POINT AND 1 ATM Not available

VI. REACTIVITY DATA

STABILITY	UNSTABLE		CONDITIONS TO AVOID Not applicable
	STABLE	X	

MATERIALS/CONDITIONS TO AVOID (INCOMPATIBILITY)
Strong Oxidizing Agents

HAZARDOUS DECOMPOSITION PRODUCTS
None

HAZARDOUS COMBUSTION PRODUCTS
None

HAZARDOUS POLYMERIZATION	MAY OCCUR		CONDITIONS TO AVOID Not applicable
	WILL NOT OCCUR	X	

VII. HAZARD LABELING INFORMATION

UN HAZARD CLASS NUMBER	US DOT CLASSIFICATION Combustible liquid
US DOT HAZARD INFORMATION NUMBER	EEC DANGEROUS SUBSTANCE CLASSIFICATION
ADR CLASS NUMBER IIIa, Marginal 2301, 4°	EEC SPECIAL RISKS AND SAFETY ADVICE

Chemical Hazard Data	HDH-C-00630	PAGE 4
PRODUCT NAME EXSOL D 200/240	REVISION E 0	DATE August '77

VIII. TRANSPORTATION AND STORAGE

USUAL SHIPPING CONTAINERS Tank cars, tank wagons, barges or drums	ELECTROSTATIC ACCUMULATION HAZARD Yes
	STORAGE/TRANSPORT PRESSURE Atmospheric
STORAGE/TRANSPORT TEMPERATURE Ambient	LOADING/UNLOADING TEMPERATURE Ambient
CEFIC TREMCARD NUMBER TEC(R)-26	VISCOSITY AT LOADING/UNLOADING TEMPERATURE 0.3 to 2.9 cs at 25°C
USCG SUBCHAPTER CLASSIFICATION	

IX. HANDLING AND STORAGE MATERIALS AND COATINGS

SUITABLE	UNSUITABLE
Carbon steel	Natural rubber
Stainless steel	Butyl rubber
Polyethylene	E P D M
Polypropylene	Polystyrene
Teflon	

X. NOTES

Personal Protection

- Ventilation: Use natural, mechanical dilution or local exhaust ventilation as necessary to keep concentration below OEL (TLV). If mechanical use explosion-proof equipment. No smoking or open lights.
- Respiratory Protection: For emergencies involving very high concentrations use self-contained breathing apparatus.
- Eye Protection: Chemical splash goggles or face shield if needed.
- Protective gloves: Chemically resistant gloves if needed to prevent repeated or prolonged skin contact.
- Other Protective Equipment: Chemically resistant apron or other clothing if needed to prevent repeated or prolonged skin contact.

FOR ADDITIONAL INFORMATION, CONTACT:

C

APPENDIX F

Experimental determination of styrene concentration variation with time

The apparatus used for the investigation of the kinetics of styrene polymerisation in kerosene is shown in Figure F1.

Apparatus

A Rota-vapour unit was employed to which a flask was securely attached by means of a PTFE seal. A water cooled condenser was fitted to the flask. The function of the Rota-vapour unit was to rotate the still to give good mixing of the contents. The still was partly immersed in an electrically heated oil bath which was kept at a constant temperature by using a bimetallic strip thermostat.

Procedure

About 300 ml of a test mixture of styrene in kerosene was placed in the still and heated. Before the reaction was allowed to start the oil was checked for constant temperature. An initial sample was drawn and then samples of the test mixture were collected periodically through the course of the experiment. The concentration of styrene in kerosene for each sample collected throughout was determined using the gas chromatograph. Gas chromatographic details are given in Table F1.

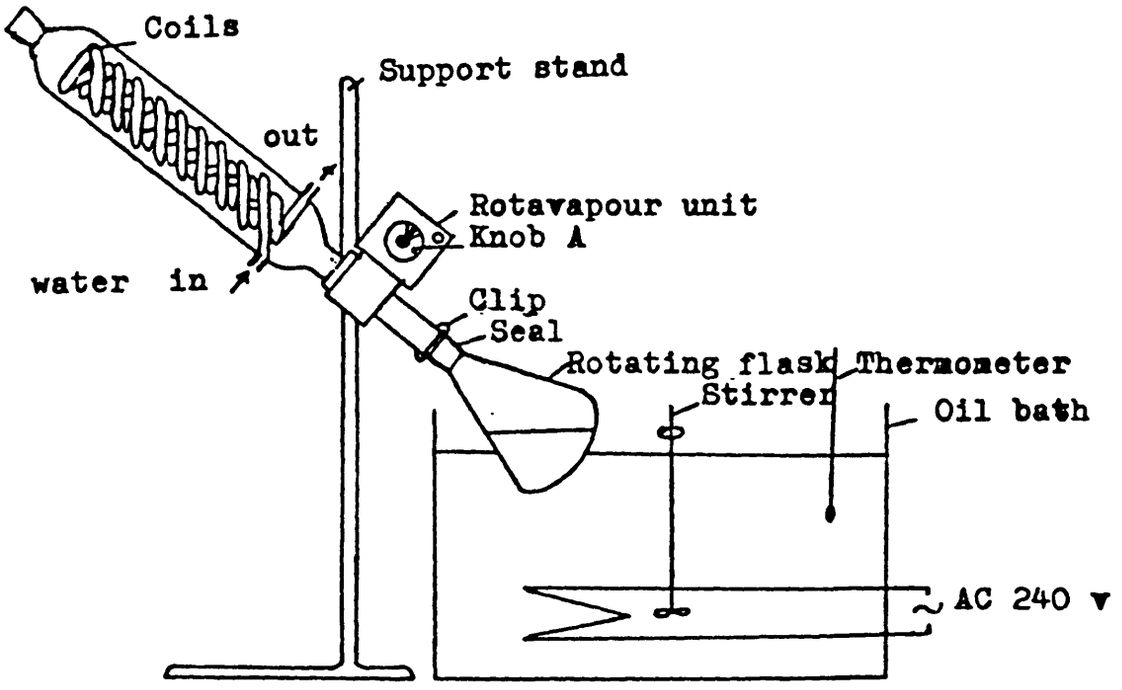

Figure F1 Apparatus used in the Kinetics study of Styrene polymerisation in Kerosene .

Flow rate of Nitrogen through column A = 0.85 ml/s.

B = 0.38 ml/s.

	before ignition	after
Pressure of Hydrogen supply	11 psi	11 psi
Air supply	3-4 psi	11 psi

Oven temperature program	100°C for 6 min
	100°C to 190°C @ 49°C/min
	190°C for 10 min
Wide range amplifier	attenuator = 3200
	coarse back off set +1x
	fine back off set middle range
	polarity set A
Pen chart recorder	chart speed = 1 cm/min
Integrator	Minimum peak width = 15 s
	noise filter = 3
	area print inhibit = 50
	threshold = 10 mv
	event marker attenuation = 1 mv

Table F1 operating conditions of the gas chromatograph.

APPENDIX G

Siwoloboff boiling-point method

The apparatus is essentially the same as for a m.p. determination, but the capillary is replaced by a small tube containing ~ 0.5 cm depth of the liquid. Inverted in this is an empty capillary sealed at one end. Bubbles issue slowly from the lower end as the temperature is raised, but become much more rapid at the b.p.. A second reading is taken as the oil-bath cools and liquid just begins to be sucked back into the capillary. (See Figure G1)

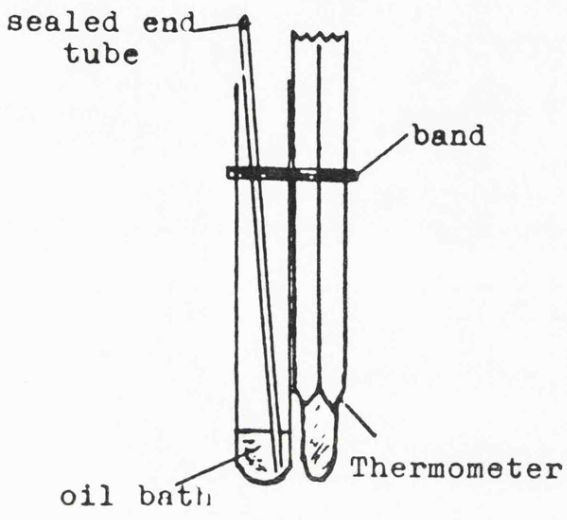

Figure G1

APPENDIX H

Physical properties of polystyrene[69].

Density = 65.55 lb/hr

Melting point = 236.85 °C

Heat capacity = 0.3104 Btu/lb °F

Thermal conductivity = 0.07- 0.08 Btu/ft hr °F

	Type of test	A.S.T.M.	Polystyrene
1	Tensile strength p.s.i.	D638 D651	5000-12000
2	Elongation per cent	D638	1.0-2.5
3	Modulus of elasticity p.s.i. x 10^6	D638	4-6
4	Compressive strength p.s.i.	D695	11500-16000
5	Flexural strength p.s.i.	D790	12000-17000
6	Impact strength ft. lb./in. notch, Izod.	D256	0.2-0.5
7	Hardness (Rockwell)	D785	M65-M90
8	Specific gravity	D792	1.04-1.11
9	Refractive index Nd	D542	1.59-1.60
10	Transparency Clarity	—	Transparent
11	Water absorption %, 24 hr. $\frac{1}{8}$ in. thickness	D570	0.03-0.4
12	Burning rate	D635	Slow
13	Softening point °C	Vicat	82-103
14	Heat-distortion temperature °C	D648	66-96
15	Thermal expansion cm/°C. cm. x 10^{-6}	D696	6-8
16	Thermal conductivity cal. cm./sq. cm. °C. Sec x 10^{-4}	C177	2.4-3.3
17	Specific heat	—	0.32-0.35
18	Dissipation (power) factor 10^6 cycles/sec.	D150	0.0001-0.0005
19	Dielectric constant 10^6 cycles sec.	D150	2.4-3.1
20	Dielectric strength (short time) $\frac{1}{8}$ in. thick, volt mil.	D149	500-700
21	Volume resistivity ohm cm. at 23°C. and 50% R.H.	D257	> 10^{16}
22	Effect of sunlight	—	Yellows slightly
23	Effect of weak acids	D543	None
24	Effect of strong acids	D543	Attacked by oxidizing acids
25	Effect of weak alkali	D543	None
26	Effect of strong alkali	D543	None
27	Effect of organic solvents	D543	Soluble in aromatic and chlorinated hydrocarbons

Table H1 Tests of Polystyrene

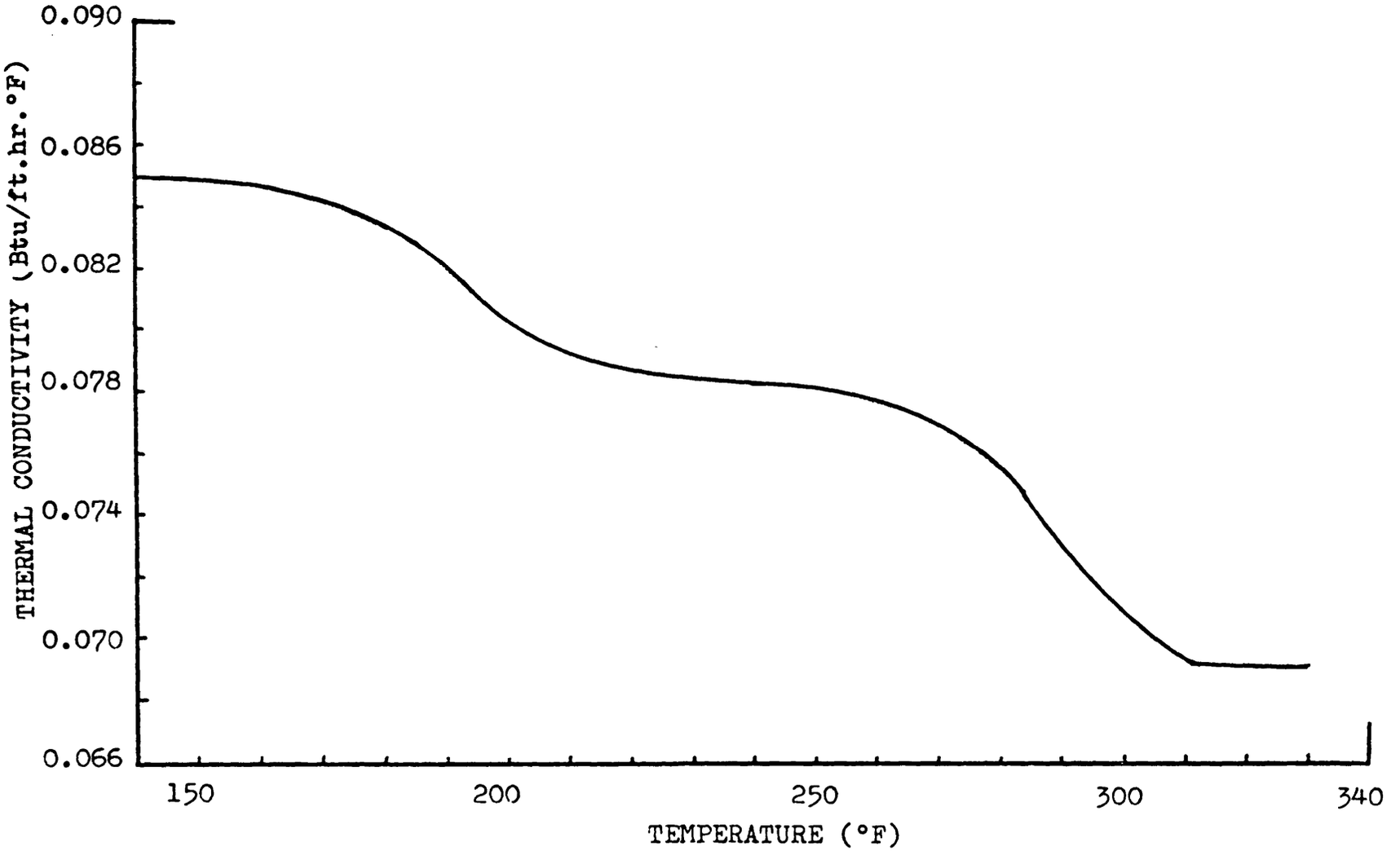

Figure H1 Variation of the thermal conductivity of Polystyrene with temperature .

APPENDIX I

Flow chart and listing of main program and subroutines used in the heat transfer calculations.

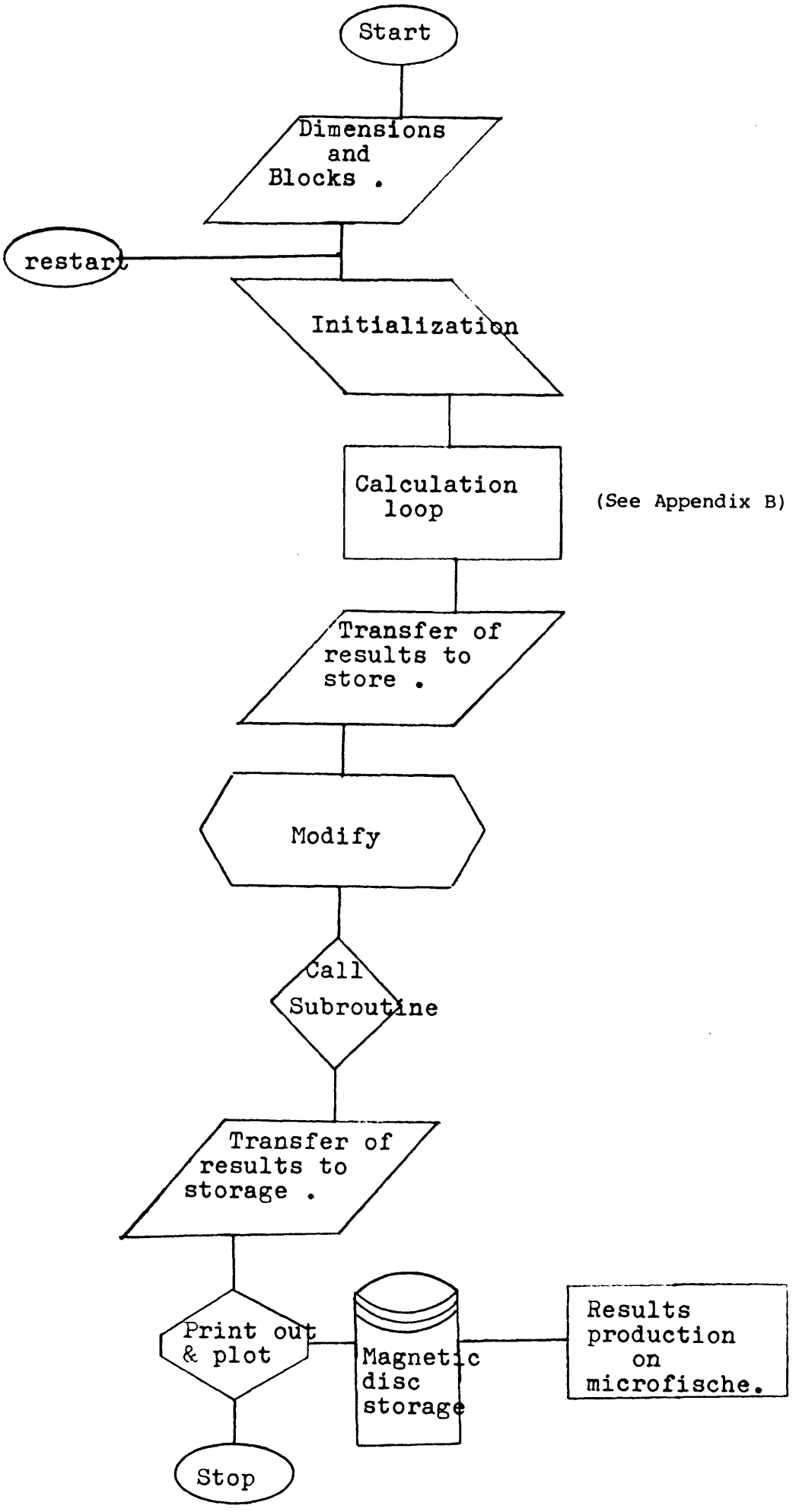

Figure 11 Flow chart of Main program

```
********************   HEAT TRANSFER  PROGRAM   ****************

    ***********   S. A. HOUT   ********************

    FORTRAN************************


*****************************
*****************************
***********   ALL UNITS ARE IN BRITISH STANDARD ENGINEERING UNITS ***

**********NOMENCLATURE************

    TURSCT = TUBE SECTION

    NTC = NUMBER OF THERMOCOUPLE MOUNTED IN A SPECIFIC TUBE SECTION

    T1 = INLET BULK FLUID TEMPERATURE TO A SECTION OF THE TUBE (DEG.F)

    T2 = OUTLET BULK FLUID TEMPERATURE FROM A SECTION OF THE TUBE

    TB = MEAN BULK FLUID TEMPERATURE OF A SECTION  OF THE TUBE

    TC = TEMPERATURE RECORDED BY A THERMOCOUPLE

    U = OVERALL HEAT TRANSFER COEFFICIENT (BTU/HR.FT2.DEG.F)

    X = DISTANCE ALONG THE TUBE (FT)

    NU = NUSSELT'S NUMBER ; DIMENSIONLESS GROUP

    ST-ESDU = STANTON NUMBER;DIMENSIONLESS GROUP,PREDICTED BY THE

    ENGINEERING SCIENCE DATA UNIT CORRELATION,DIMENSIONLESS

    ST-ST = STANTON NUMBER PREDICTED BY SIEDER-TATE CORRELATION

    ST-DB = STANTON NUMBER PREDICTED BY DITTUS-BOELTER EQUATION

    EFF = EFFICIENCY OF THE FURNACE

    G = MASS FLOW RATE (LB/HR)

    TI = INLET TEMPERATURE TO THE FURNACE TUBE

    RF = FOULING RESISTANCE ON THE INSIDE  (HR.FT2.DEG.F)/BTU

    TWI = INSIDE TUBE WALL TEMPERATURE
```

HST = HEAT TRANSFER COEFFICENT PREDICTED BY THE SIEDER-TATE CORRELATION (BTU/HR.FT2.DEG.F)

HDB = HEAT TRANSFER COEFFICIENT PREDICTED BY THE DITTUS-BOELTER CORRELATION

HEXP = HEAT TRANSFER COEFFICIENT MEASURED EXPERIMENTALLY

RTC = THERMAL RESISTANCE OF THE TUBE WALL AND OF THE THERMOCOUPLE MOUNTED ON THE WALL

NUHSN = PREDICTION OF NUSSELT'S NUMBER BY HAUSEN

STHSN = PREDICTION OF STANTON NUMBER BY HAUSEN

HESDU = HEAT TRANSFER COEFFICIENT PREDICTED BY THE ENGINEERING-SCIENCE DATA UNIT CORRELATION

GR = GRASHOF'S NUMBER , DIMENSIONLESS GROUP

GZ =GRAETZ NUMBER,DIMENSIONLESS GROUP

PR = PRANDTL NUMBER ; DIMENSIONLESS GROUP

RE = REYNOLD'S NUMBER ; DIMENSIONLESS GROUP

MUW = VISCOSITY OF THE FLUID AT THE WALL (LB/FT.HR)

MUB = VISCOSITY OF THE FLUID AT BULK CONDITIONS

TK = THERMAL CONDUCTIVITY (BTU/HR.FT.DEG.F)

MU = VISCOSITY

CP = HEAT CAPACITY (BTU/LB.DEG.F)

D = DENSITY (LB/FT.3)

VEL = FLUID VELOCITY (FT/HR)

KW = POWER INPUT IN KILOWATTS

T = TEMPERATURE

H = ENTHALPY (BTU/LB)

I = INLET CONDITION

```
C  O = OUTLET CONDITION
C  F = FINAL CONDITION
C  QIN = HEAT INPUT TO THE PROCESS FLUID     (BTU/HR)
C  QOUT = HEAT OUTPUT FROM THE HEATING ELEMENTS
C  N = STORAGE NUMBER OF THE THERMOCOUPLE CONSIDERED IN A SECTION
C  I,J ,K = DO LOOP PARAMETERS
C  K = RESERVED PARAMETER FOR STORAGE OF VALUES TO BE PLOTTED
C    *******  EQUIVALANCE STATEMENT  USED FOR  STORAGE  PURPOSE
C**********************************************************************
C               MAIN PROGRAM
C  FOULING
C**********************************************************************
      INTEGER TSCT,XG
      DIMENSION TSCT(37),VALS1(37),TSCX(37)
      COMMON/NUBLOCK/NU,UO(37)
      COMMON GZ,GR
      COMMON QIN1, EFF,G,KW,TC,J1
      COMMON RE,PR,MUB,MUW,MV,TIME
      DIMENSION HC(37),HI(37),HCP(37),HIP(37),RF(37),RFP(37)
      DIMENSION HESDU(30),HST(30),HDB(30),HEXP(30)
      DIMENSION XVALS(30),YVALS(30,2)
      DIMENSION X(37),Y(37,6)
      REAL     NTC,KW,T1,T2,MUW,MUB
      REAL NUHSN
      REAL NUDB,NUESDU,NUST,MV
      INTEGER NO,TUBSCT,G
      EQUIVALENCE(YVALS(1,1),HCP(1)),(YVALS(1,2),HIP(1))
      COMMON /K3/ KKK
      COMMON /BL/ TSCT,TSCX,VALS1,XRUN,XG,XKW,XTI,XTF
      COMMON/TFS/TTF,TTFOLD
```

```
      DATA TSCT /4*1,3*2,3*3,4*4,6*5,17*6/
      DATA TSCX /4.0,4.01,4.02,4.03,4.04,4.06,4.07,4.09,4.10,4.11,5.0,
     *5.01,5.02,5.03,6.0,8.01,8.02,8.03,8.04,8.05,8.07,8.08,8.09,8.10,
     *8.11,9.0,9.01,9.02,9.03,9.04,9.05,9.06,9.07,9.08,9.09,9.10,9.11/

         INITIALISATION OF DATA

    1 READ(5,500,END=900)XRUN,XG,XKW,XTI
  500 FORMAT(F7.3,I4,2F5.2)
      TIME=0.0
      XKW=XKW+3.
      IXRUN = IFIX(XRUN+0.5)
      NPTS = 25
      IF ( IXRUN .EQ. 1 .OR. IXRUN .EQ. 7 ) NPTS = 19
      IF ( IXRUN .GE. 2 .AND. IXPUN .LE. 6 ) NPTS = 17
      DO 444 IPLT=1,NPTS
      READ(5,599)XTF,(VALS1(II),II=1,37)
  599 FORMAT(16F5.2)
      KKK=0
      PRINT HEADINGS
      XKW=(XKW-3.)/6
      XXKW=XKW*3413.0
      WRITE(6,401)XXKW
  401 FORMAT(1H1,//////////,20X,'AVERAGE POWER = ',F7.1,
     *' BTU/HR')
      XKW=(6*XKW)+3.
      WRITE(6,601)
  601 FORMAT(1H ,/2X,'TUBSCT',2X,'NTC',4X,'T1',6X,'T2',6X,'TB',6X,'TC',
     *6X,'U',8X,'RE',6X,'PR',6X,'HESDU',5X,'RTC',6X,'HEXP',5X,'HDB',5X,
     *'HST',7X,'TWI',6X,'RF',/16X,'(F)',5X,'(F)',5X,'(F)',5X,'(F)',3X,
     *'(BTU/HR',2CX,'(BTU/HR',2X,'(HR.FT2',2X,'(BTU/HR',2X,'(BTU/HR',1X,
     *'(BTU/HR',5X,'(F)',3X,'(HR.FT2',/46X,'.FT2.F)',20X,'.FT2.F)',2X,
     *'.F/BTU)',2X,'.FT2.F)',2X,'.FT2.F)',1X,'.FT2.F)',11X,'.F/BTU)',/)

      READING  SPECIFIC RUN PARAMETERS

      KKK=KKK+1
      RUN=XRUN
      NO=TSCT(KKK)
      TUBSCT=NO+9
      NTC=TSCX(KKK)
      TC=VALS1(KKK)
      G=XG
      KW=XKW
      TI=XTI
      TF=XTF

      PHYSICAL PROPERTIES CHANGE ALONG THE TUBE DISTANCE PROFILE

      CALCULATION OF THE PHYSICAL PROPERTIES

      MV=TI
      CALL TEMP(MV,T)
```

```
      TI=T
      TTI=TI
      MV=TF
      CALL TEMP(MV,T)
      TF=T
      TTF=TF
      T=TI
      CALL HETCAP(T,CP)
      CPTI=CP*TI
      T=TF
      CALL HETCAP(T,CP)
      CPTF=CP*TF
      QIN1=G*(CPTF-CPTI)
      QOUT=KW*3413.0
      Q=QOUT
      DT=TF-TI
      IF(QOUT-QIN1)5,5,6
    5 T=TI
      CALL ENCPY(T,H1)
      EHI=H1
      T=TF
      CALL ENCPY(T,H2)
      EHO=H2
      T=DT/2.
      CALL HETCAP(T,CP)
      DH=EHO-EHI
      QOUT1=G*CP*DT
      QOUT2=G*DH
      IF(QOUT2-QOUT1)7,7,8
    7 QOUT3=QOUT*(QOUT1/QOUT2)
      GO TO 9
    8 QOUT3=QOUT*(QOUT2/QOUT1)
    9 CONTINUE
      QOUT4=ABS(QOUT3-QIN1)/2.
      QOUT=QIN1+QOUT4
    6 EFF=(QIN1/QOUT)*100.
      CALL FSHANC(TIME,EFF)
      IF(EFF.GT.95.60)GO TO 2
      IF(EFF.LT.70.90)GO TO 3
      GO TO 4
    2 EFF=93.60
      IF(TIME.EQ.5.0)CALL FSHANC(TIME,EFF)
      GO TO 4
    3 EFF=71.74
    4 CONTINUE
      N=2
      T1=TI
      KKK=0
      CALL SCTEMP(2,T1,T2,HC,HI,RF)
      K = 0
```

```
      DO 111 I = 1,2
      K = K+1
      HCP(K) = HC(I)
      HIP(K) = HI(I)
      RFP(K) = RF(I)
111   CONTINUE
      N=2
      T1=T2
      CALL SCTEMP(2,T1,T2,HC,HI,RF)
      DO 112 I=1,2
      K=K+1
      HCP(K)=HC(I)
      HIP(K)=HI(I)
      RFP(K) = RF(I)
112   CONTINUE
      DO 10 J=1,2
      N=2
      T1=T2
      CALL SCTEMP(2,T1,T2,HC,HI,RF)
      DO 113 I = 1,2
      K = K+1
      HCP(K) = HC(I)
      HIP(K) = HI(I)
      RFP(K) = RF(I)
113   CONTINUE
      N=1
      T1=T2
      CALL SCTEMP(1,T1,T2,HC,HI,RF)
      K=K+1
      HCP(K)=HC(1)
      HIP(K)=HI(1)
      RFP(K) = RF(1)
10    CONTINUE
      N=2
      T1=T2
      CALL SCTEMP(2,T1,T2,HC,HI,RF)
      DO 114 I = 1,2
      K = K+1
      HCP(K) = HC(I)
      HIP(K) = HI(I)
      RFP(K) = RF(I)
114   CONTINUE
      N=2
      T1=T2
      CALL SCTEMP(2,T1,T2,HC,HI,RF)
      DO 115 I=1,2
      K=K+1
      HCP(K)=HC(I)
      HIP(K)=HI(I)
      RFP(K) = RF(I)
115   CONTINUE
```

```
      N=4
      T1=T2
      CALL SCTEMP(4,T1,T2,HC,HI,RF)
      DO 116 I = 1,4
      K = K+1
      HCP(K) = HC(I)
      HIP(K) = HI(I)
      RFP(K) = RF(I)
116   CONTINUE
      N=2
      T1=T2
      CALL SCTEMP(2,T1,T2,HC,HI,RF)
      DO 117 I=1,2
      K=K+1
      HCP(K)=HC(I)
      HIP(K)=HI(I)
      RFP(K) = RF(I)
117   CONTINUE
      N=2
      T1=T2
      CALL SCTEMP(2,T1,T2,HC,HI,RF)
      DO 118 I = 1,2
      K = K+1
      HCP(K) = HC(I)
      HIP(K) = HI(I)
      RFP(K) = RF(I)
118   CONTINUE
      N=4
      T1=T2
      CALL SCTEMP(4,T1,T2,HC,HI,RF)
      DO 119 I = 1,4
      K = K+1
      HCP(K) = HC(I)
      HIP(K) = HI(I)
      RFP(K) = RF(I)
119   CONTINUE
      N = 1
      T1=T2
      CALL SCTEMP(1,T1,T2,HC,HI,RF)
      K = K+1
      HCP(K) = HC(1)
      HIP(K) = HI(1)
      RFP(K) = RF(1)
      N = 4
      T1=T2
      CALL SCTEMP(4,T1,T2,HC,HI,RF)
      DO 120 I = 1,4
      K = K+1
      HCP(K) = HC(I)
      HIP(K) = HI(I)
      RFP(K) = RF(I)
120   CONTINUE
```

```
      N = 2
      T1=T2
      CALL SCTEMP(2,T1,T2,HC,HI,RF)
      DO 121 I = 1,2
      K = K+1
      HCP(K) = HC(I)
      HIP(K) = HI(I)
      RFP(K) = RF(I)
121   CONTINUE
      N = 4
      T1=T2
      CALL SCTEMP(4,T1,T2,HC,HI,RF)
      DO 122 I=1,4
      K=K+1
      HCP(K)=HC(I)
      HIP(K)=HI(I)
      RFP(K)=RF(I)
  122 CONTINUE
  *** STORE X VALUES
      X0=0.0
      DELTAX=0.8
      DO 16 I=1,30
      XVALS(I)=X0
   16 X0=X0+DELTAX
      IF(RF.LE.2100.)GOTO  17
      STESDU=EXP(-3.796-.205*ALOG(RE)-.505*ALOG(PR)-.0225*(ALOG(PR))**2)
      STDB=.023*(RE**(-.2))*(PR**(-.6))
      STST=0.023*(RE**(-.2))*(PR**(-.666))*((MUB/MUW)**.14)
      NUDB=STDB*RE*PR
      NUESDU=STESDU*RE*PR
      NUST=STST*RE*PR
      TI=TTI
      TF=TTF
      WRITE(6,603)RUN,TI,TF,G,EFF,GR,GZ,
     *                              STESDU,STDB,STST,NUESDU,NUDB,NUST,TIME
  603 FORMAT(1H ,/2X ,'RUN =',F7.3,/20X,'TI =',F7.2,'    F    ',5X,'TF =',
     *F7.2,'    F    ',//21X,'G =',I4,' LB/HR ',7X,'EFF =',F5.2,' %',30X,
     *'GR =',E12.2,5X,'GZ =',F9.2,//,
     *15X,'ST-ESDU =',F9.2,7X,'ST-DB =',E9.2,5X,'ST-ST =',E9.2,//13X,'
     *NU-ESDU =',F9.2,7X,'NU-DB =',F9.2,5X,'NU-ST =',F9.2,26X,'TIME =',F
     *6.2,' HR')
      GO TO 18
   17 CONTINUE
      NUESDU= ( 1.78 * (( GZ + .0083 * (( GR*PR)**.75))**.33))*
     *         (( MUB/MUW)**.14)
      NUHSN=3.66+(.0668*(.066)*(RE)*(PR))/(1+.04*(((.066)**.66)*(RE**.66
     *)*(PR**.66)))
      NUST=1.86*((RE**.33)*(PR**.33)*(.066**.33)*((MUB/MUW)**.14))
      STESDU=NUESDU/(RE*PR)
      STHSN=NUHSN/(RE*PR)
      STST=NUST/(RE*PR)
      TI=TTI
      TF=TTF
```

```
      WRITE(6,605)RUN,TI,TF,G,EFF,GR,GZ,
     *STFSDU,STHSN,STST,NUESDU,NUHSN,NUST,TIME
  605 FORMAT(1H ,/2X,'RUN =',F7.3,/20X,'TI =',F7.2,'  F  ',5X,'TF =',
     *F7.2,'  F',27X,'HDR= HAUSEN PREDICTION IN THIS CASE'
     *          ,//21X,'G =',I4,' LB/HR ',5X,'EFF =',F5.2,' %',30X,
     *'GR =',E12.2   ,5X,'GZ =',F9.2,//,15X,'ST-ESDU =',E9.2,4X,'ST-HSN
     *=',E9.2,5X,'ST-ST =',E9.2,//15X,'NU-ESDU =',F9.2,4X,'NU-HSN =',F9.
     *2,5X,'NU-ST =',F9.2,26X,'TIME =',F6.2,' HR')
   18 CONTINUE
      X(IPLT)=TIME
      Y(IPLT,1)=RFP(2)
      Y(IPLT,2)=RFP(7)
      Y(IPLT,3)=RFP(10)
      Y(IPLT,4)=RFP(13)
      Y(IPLT,5)=RFP(18)
      Y(IPLT,6)=RFP(27)
      TIME=TIME+.5
      TTFOLD=TTF
  444 CONTINUE
      DO 901 I = 1,1
      J = 2
      IF ( I .EQ. 2 ) J = 7
      IF ( I .EQ. 3 ) J = 10
      IF ( I .EQ. 4 ) J = 13
      IF ( I .EQ. 5 ) J = 18
      IF ( I .EQ. 6 ) J = 27
      WRITE(3,902) IXRUN,TSCX(J),G,Q,NPTS
902   FORMAT('1'/'(HR.FT2.F/BTU)',7X,'RUN',1X,I2,2X,'NTC(',F4.2,')',2X,
     1    'G = ',I4,' LB/HR',2X,'Q = ',F7.1,' BTU/HR'/
     2    'FOULING RESISTANCE'/'TIME (HOURS)'/I2)
      WRITE(3,903) (X(J),Y(J,I),J=1,NPTS)
  903 FORMAT(1P4E15.6)
  901 CONTINUE
      GO TO 1
  900 WRITE(6,604)
  604 FORMAT(1H1,////////////////,5X,'S.A.HOUT')
      STOP
      END
```

```
      SUBROUTINE ENCPY(T,H)
      REAL T,H
      IF(T.LT.250.0) GO TO 10
      H=0.68*T
      GO TO 11
   10 H=0.52*T+80.0
   11 RETURN
      END



      SUBROUTINE HETCAP(T,CP)
      REAL T,CP
      CP=0.00058*T+0.45
      RETURN
      END



      SUBROUTINE DNSTY(T,D)
      REAL T,D
      IF(T.LT.300.0)GO TO 10
      D=-0.0325*T+53.2
      GO TO 11
   10 D=-0.026*T+51.0
   11 RETURN
      END



      SUBROUTINE THCOND(T,TK)
      REAL T,TK
      TK=-0.00004233*T+0.0754
      RETURN
      END



      SUBROUTINE FSHANC(TIME,EFF)
      COMMON/TFS/TTF,TTFOLD
      IF(TIME.EQ.0.0)RETURN
      MV1=(TTFOLD-30.6306)/45.045
      MV2=(TTF-30.6306)/45.045
      EFF=EFF-ABS(MV2-MV1)*TIME/.5
      RETURN
      END
```

```
      SUBROUTINE VSKSTY(T,MU)
      REAL T,MU
      IF(T.LT.137.5)GO TO 10
      MU=EXP(-0.00504*T+0.8)
      MU=MU*2.419
      GO TO 11
   10 MU=EXP(-0.011*T+1.55)
      MU=MU*2.419
   11 RETURN
      END
```

```
      SUBROUTINE TEMP(MV,T)

       PROGRAM TO CONVERT TEMPERATURES FROM MILLIVOLTS TO DEG. F
      REAL MV
      T=45.04504*MV+30.63063
      RETURN
      END
```

```
      SUBROUTINE SCTEMP(N,T1,T2,HC,HI,RF)
      INTEGER TSCT,XG
      DIMENSION TSCT(37),VALS1(37),TSCX(37)
      COMMON/NUBLOCK/NU,UO(37)
      COMMON GZ,GR
      COMMON QIN1, EFF,G,KW,TC,J1
      COMMON RE,PR,MUB,MUW,MV,TIME
      DIMENSION HC(30),HI(30),RF(37)
      DIMENSION HESDU(30),HST(30),HDB(30),HEXP(30)
      REAL MU,NTC,KW,T1,T2,MUW,MUB,MV
      INTEGER NO,TUBSCT,G
      COMMON /K3/ KKK
      COMMON /BL/ TSCT,TSCX,VALS1,XRUN,XG,XKW,XTI,XTF


      DATA TSCT /4*1,3*2,3*3,4*4,6*5,17*6/
      DATA TSCX /4.0,4.01,4.02,4.03,4.04,4.06,4.07,4.09,4.10,4.11,5.0,
     *5.01,5.02,5.03,8.0,8.01,8.02,8.03,8.04,8.05,8.07,8.08,8.09,8.10,
     *8.11,9.0,9.01,9.02,9.03,9.04,9.05,9.06,9.07,9.08,9.09,9.10,9.11/
```

```
      DO 10 I=1,N
      KKK=KKK+1
      RUN=XRUN
      NO=TSCT(KKK)
      TUBSCT=NO+9
      NTC=TSCX(KKK)
      TC=VALS1(KKK)
      G=XG
      KW=XKW
      TI=XTI
      TF=XTF
      QIN=QIN1/12.
      IF(TUBSCT.EQ.15)QIN=QIN/3.

      CALC OF HEAT CAPACITY OF INLET TEMP
      T=T1
      SUBPROGRAM HEAT CAPACITY
      CALL HETCAP(T,CP)


      CALC SECTION OUTLET TEMP FROM HEAT BALANCE
      T2=T1+QIN/(G*CP)
      CALC AVERAGE BULK FLUID TEMP
      TB=(T1+T2)/2.0
      MV=TC
      CALL TEMP(MV,T)
      TC=T
      IF(TC.LE.TB)GO TO 5
      GO TO 6

  TO PROTECT THE CALC. OF OVERALL HEAT TRANSFER COEFF.
  FROM DEFAULT THERMOCOUPLES
  AN AVERAGE NO. HAS BEEN CHOSEN TO COVER UP FOR THE FAULT
5 TC=TB+20.
6 CONTINUE

  HEAT FLUX TO THE FURNACE FROM THE HEATING ELEMENTS
  HETFLX=(KW*3413.0*EFF)/26.18333
  HEATFLUX PER ELEMENT
  HETFLX=HETFLX/12.

  OVER ALL HEAT TRANSFER COEFFICIENT CORRESPONDING TO A SPECIFIC
  THERMO COUPLE
  U=HETFLX/(TC-TB)
  IF(TIME.EQ.0.5)UO(KKK)=U

  CALC OF THE VELOCITY OF THE FLOW
  SUBPROGRAM DENSITY TO EVALUATE THE DENSITY OF THE FLUID AT THE
  BULK TEMP
  T=TB
  CALL DNSTY(T,D)
  VEL=G*4.0/(0.01368655*D)
```

```
      EVALUATION OF THE PHYSICAL PROPERTIES AT THE BULK TEMP OF A SPECIF
      IC SECTION OF THE TUBE
      BASIS 1 FT. SECTION OF THE FURNACE TUBE
      T=TB
      CALL HETCAP(T,CP)
      CALL THCOND(T,TK)
      CALL VSKSTY(T,MU)

      DIMENSIONLESS GROUP TO CORRELATE FLOW RATE
      REYNOLD NUMBER
      RE=(D*0.066*VEL)/MU

      DIMENSIONLESS GROUP TO DESCRIBE HEAT TRANSFER
      PRANDL  NUMBER
      PR=(MU*CP)/TK
      XW=.01733
      TKW=9.166
      RW=XW/TKW
      DIAMO=1.
      DW=.896
      DDW=DIAMO/DW
      PYE=3.1416
      GZ=(PYE/4.)*RE*PR*.066
      B=.0005
      GA=.00000248
      DDD=.066**3
      IF(RE.LE.2100.)GOTO  11

      DITUS BOELTER EQUATION TO CORRELATE HEAT TRANSFER COEFFICIENT
      HDB(I)=0.3484848*TK*(RE**0.8)*(PR**0.4)
      GO TO 12
   11 CONTINUE
      HDB(I)=(3.66+(.0668*(.066)*(RE)*(PR))/(1+.04*(((.066)**.66)*
     *(RE**.66)*(PR**.66))))*(TK/.066)
      HC(I)=HDB(I)
   12 CONTINUE
      CALL DNSTY(T,D)
      CALL HETCAP(T,CP)
      IF(RE.LE.2100.)GOTO 13
      HESDU(I)=(D*VEL*CP)*(EXP(-3.796-.205*ALOG(RE)-.505*ALOG(PR)-0.0225
     **(ALOG(PR))**2))
      HC(I)=HESDU(I)
      GO TO 14
   13 CONTINUE
      TWI=TB+HETFLX/HC(I)
      IF(U.GE.HC(I))GO TO 19
      GO TO 20
   19 UU=HC(I)/(1.+HC(I)*RW*DDW)
      RTC=1./UU-(1./HC(I))
      IF(RTC.LE.0.0)RTC=0.0001
   20 CONTINUE
```

```
      MUB=MU
      GR=(B*GA*DDD*(D**2)*(TWI-TB))/(MUB**2)
      T=TWI
      CALL VSKSTY(T,MU)
      MUW=MU
      HESDU(I)=1.78*((GZ+.0083*((GR*PR)**.75))**.33)*((MUB/MUW))
     *         *(TK/.066)
      HC(I)=HESDU(I)
      IF(U.GE.HC(I))GO TO 14
      RTC=1.0/U-(1.2626/HC(I))
      IF(RTC.LE.0.0)RTC=0.0001
   14 CONTINUE

      THE PROTECTION OF THE CALC. OF THERMOCOUPLE RESISTANCE
      AT LOWER HEATFLUXES.
      IF(U.GE.HC(I))GO TO 7
      GO TO 8
    7 UU=HC(I)/(1.+HC(I)*RW*DDW)
      RTC=1./UU-(1./HC(I))
      IF(RTC.LE.0.0)RTC=0.0001
    8 CONTINUE
      IF(RE.LE.2100.)GO TO 15
      THERMO COUPLE RESISTANCE
      IF(U.GE.HC(I))GO TO 16
      RTC=1.0/U-(1.2626/HC(I))
      IF(RTC.LE.0.0)RTC=0.0001
   16 CONTINUE

      INSIDE TUBE WALL TEMP.
      TWI=TB+HETFLX/HC(I)
   15 CONTINUE

      EXPERIMENTAL HEAT TRANSFER COEFFICIENT
      HI(I)=1.2626/(1.0/U-RTC)
      HEXP(I)=HI(I)


      IF(TIME.EQ.0.0)GO TO 9
      RF(I)=.792*(1./U-1./UU(KKK))
      IF(RF(I).LE.0.0)GO TO 9
      IF(TIME.LT.1.0)RF(I)=.0000
      GO TO 99
    9 RF(I)=0.0000
   99 CONTINUE
```

```
      T=TB
      CALL VSKSTY(T,MU)
      MUB=MU
      CALL DNSTY(T,D)
      CALL HETCAP(T,CP)
      T=TWI
      CALL VSKSTY(T,MU)
      MUW=MU
      IF(MUB.LE.0.0)MUB=.01
      IF(MUW.LE.0.0)MUW=MUB-.003
      IF(MUB.LT.MUW)MUB=MUW+.2
      IF(RE.LE.2100.)GOTO  21
      HST(I)=(D*VEL*CP)*.023*(RE**(-0.2))*(PR**(-.66))*((MUB/MUW)**0.14)
      GO TO 22
   21 CONTINUE
      HST(I)=(1.86*((RE**.33)*(PR**.33)*(.066**.33)*((MUB/MUW)**.14)))*
     *(TK/.066)
   22 CONTINUE
      IF(RE.LE.2100.)GO TO 23
      GR=(B*GA*DDD*(D**2)*(TWI-TB))/(MUB**2)
   23 CONTINUE
      WRITE(6,602)TURSCT,NTC,T1,T2,TB,TC,U,RE,PR,HESDU(I),RTC,HEXP(I),
     *HDB(I),HST(I),TWI,RF(I)
  602 FORMAT(1H ,I4,F6.2,1X,5(F7.2,1X),F9.1,2X,F6.2,2X,F7.2,2X,F8.4,2X,
     *4(F7.2,2X),F7.5)
   10 CONTINUE
      RETURN
      END
```

APPENDIX J

Film deposit and tube surface observation by the scanning electron microscope.

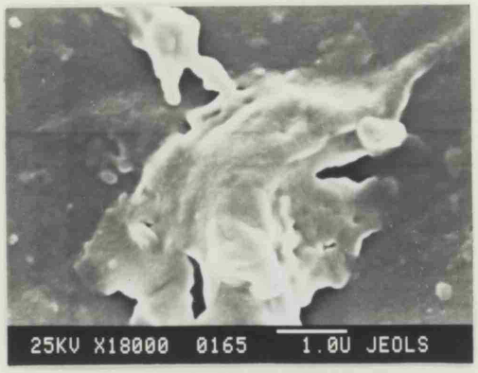

TOP VIEW

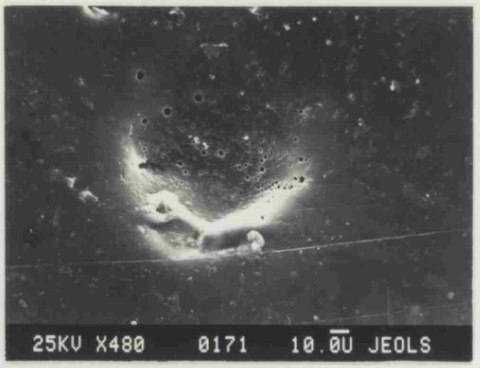

TOP VIEW

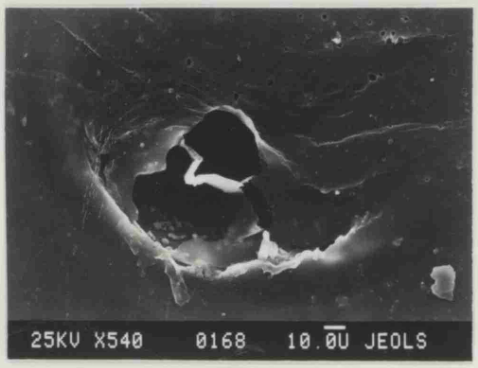

TOP VIEW

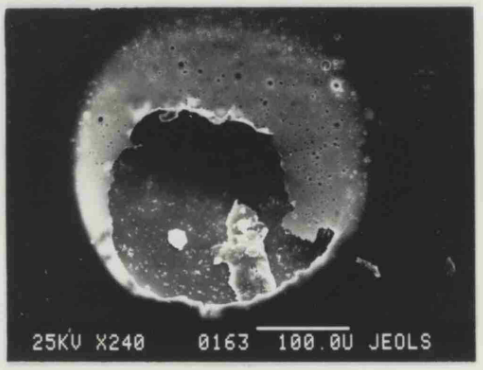

TOP VIEW

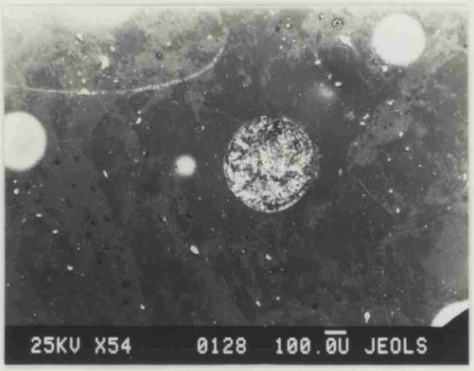

TOP VIEW

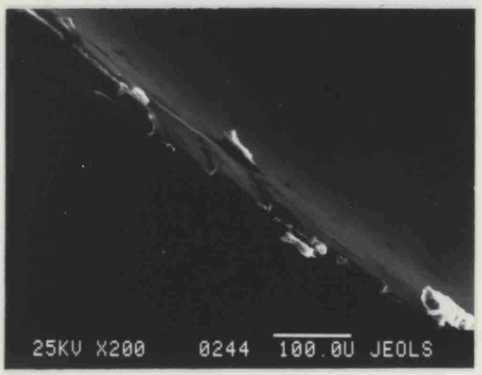

SIDE VIEW

SIDE VIEW

SIDE VIEW

PLATE J1 POLYSTYRENE FILM DEPOSIT AT THE SURFACE OF THE FURNACE TUBE

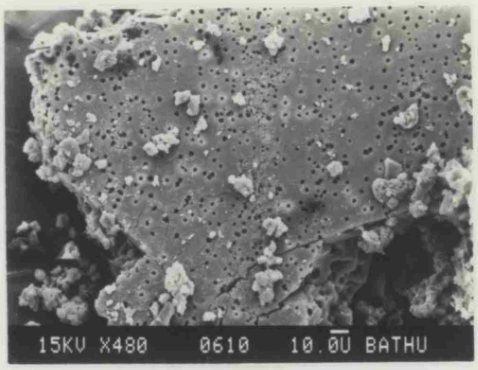

POLYSTYRENE DEPOSITS

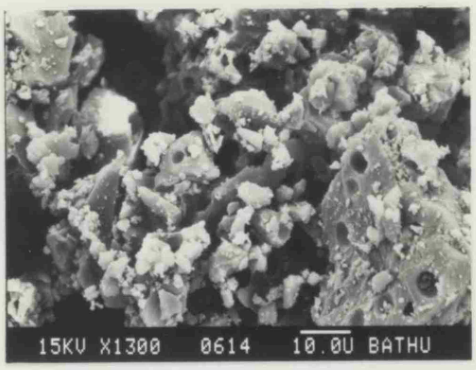

POLYSTYRENE DEPOSITS

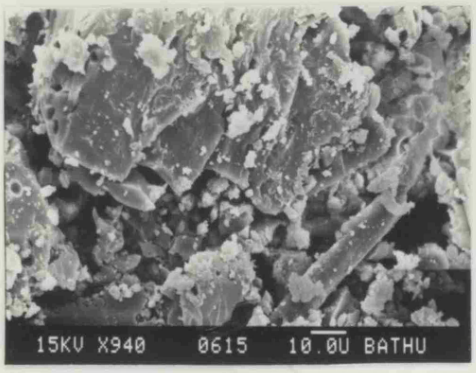

POLYSTYRENE DEPOSITS

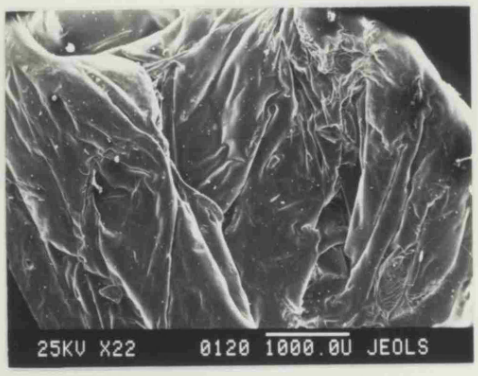

POLYSTYRENE DEPOSIT COLLECTED ON
THE DOWNSTREAM FILTER AFTER COOLING

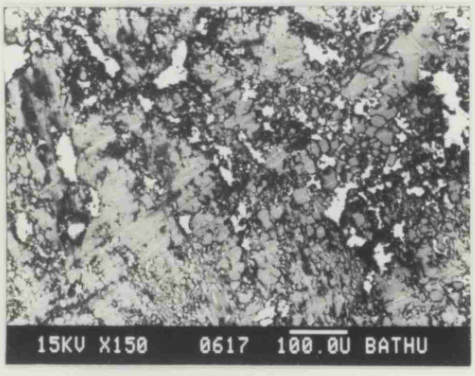

TUBE SURFACE

TUBE SURFACE

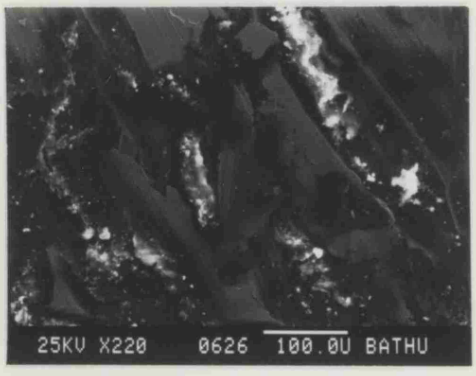

TUBE SURFACE

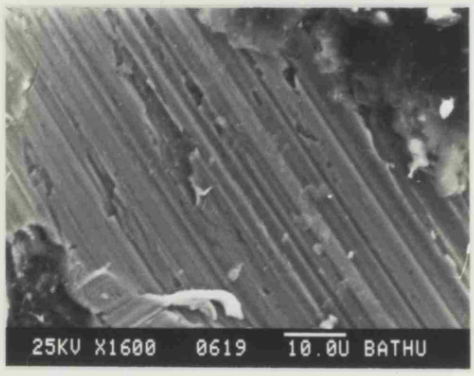

TUBE SURFACE

PLATE J2 POLYSTYRENE DEPOSIT SCRAPED OFF THE FURNACE TUBE SURFACE

APPENDIX K

Microfische computed results

(nine plates)

APPENDIX K

Microfische computed results
(nine plates)